DOWN IS THE NEW UP: MULTIMODAL NEUROIMAGING INVESTIGATIONS OF THE NEGATIVE BOLD RESPONSE

Ross Wilson

A thesis submitted to the University of Birmingham for the degree of

DOCTOR OF PHILOSOPHY

School of Psychology
College of Life and Environmental Sciences
University of Birmingham
March 2018

Abstract

This thesis investigates the negative blood oxygen level dependent response (NBR) to sensory stimulation as measured using functional magnetic resonance imaging. The origin of which is still debated and therefore when found they are difficult to interpret.

We used multi-modal neuroimaging methods to gain a better understanding of the neuronal, vascular and metabolic origin of sensory evoked NBRs both within the sensory cortex stimulated (intra-modal) and in other sensory cortices (cross-modal). We then assessed whether functional/structural connectivity between the PBR and NBR regions were associated with the variability or relative amplitude of the NBR. Lastly, we examined the behavioural relevance of the NBR i.e. whether intra- and cross-modal NBRs are similarly related to levels of neurotransmitter or cortico-spinal-excitability.

We found neuronal, metabolic and vascular components for both intra- and cross-modal NBRs. However, the local Glutamate/GABA balance within a NBR region was only implicated in the origin of intra-modal NBRs. For motor task IM NBRs only, increased structural connectivity was associated with increased variability of NBR with no relationship noted for cross-modal or visual stimuli NBRs. Lastly, no association was found between NBRs and cortico-spinal-excitability in motor cortex. Overall this work increases the interpretability of NBRs during sensory stimulation studies.

Acknowledgements

This was not a one man job….

Many thanks to Dr Steve Mayhew! Who else would have taken me on? Without his wit, intelligence, down to earth manner, never ending patience, and ability to deal with (and laugh at) my confused looks I would still be sat wondering where the hell I was and why never mind putting together a thesis. It was an interesting few years and he was a steady friendly and challenging presence throughout. Thank you to Dr Craig McAllister who was always waiting with one wise crack or another. His attention to detail helped to slow me down when my fingers were running away from my brain. While all the extra work he's managed to throw my way has helped keep me housed (and prevented me living in my car). Thank you as well to Dr Karen Mullinger who's meticulous nature always kept me on my toes!

I also want to thank everyone that has worked in the corridor at one time or another over the last few years. The shared stress and numerous tea (or other) breaks have been essential. It would have been a sad life without you all. I also extend my gratitude to Josie for her generosity letting me stay in her house on the cheap (keeping me from living in my car)!

Finally thank you to the EPSRC for providing me with money over the first 3 years of my study. How incredible to be paid to do something so interesting.

Table of Contents

List of Figures

List of Tables

Abbreviations

ACC: anterior cingulate cortex

ASL: arterial spin labelling

BOLD: blood oxygen level dependent signal

CBF: cerebral blood flow

CBV: cerebral blood volume

CC: corpus callosum

CI: confidence interval

CM: cross-modal

CMRO2: cerebral metabolic rate of oxygen consumption

CoV: coefficient of variability

CSE: cortico-spinal excitability

DMN: default mode network

DMN: default mode network

DTI: diffusion tensor imaging

DWI: diffusion weighted imaging

ECG: electrocardiogram

EEG: electroencephalography

EMG: Electromyography

EPISTAR: echo planar imaging-based signal targeting by alternative radiofrequency pulses

ERD: Event related desynchronization

ERP: event related potential

ERS: Event related synchronization

FA: fractional anisotropy

FAIR: flow-sensitive alternating inversion recovery

FC: functional connectivity

fMRI: functional magnetic resonance imaging

fMRI: functional magnetic resonance imaging

GABA: gamma aminobutyric acid

GLM: general linear modelling

Glx: glutamate/glutamine

HRF: haemodynamic response function

ICA: independent component analysis

IM: intra-modal

iPL: ipsilateral parietal lobule

LOC: lateral occipital cortex

M1: primary moor cortex

MEG: magnetoencephalography

MEP: motor evoked potential

MNS: median nerve stimulation

MRI: magnetic resonance imaging

MRS: magnetic resonance spectroscopy

NBR: negative BOLD response

PBR: positive BOLD response

PCC: posterior cingulate cortex

ROI: region of interest

RSFC: Resting state functional connectivity

S1: primary somatosensory cortex

SC: structural connectivity

SMA: supplementary motor area

SNR: signal to noise ratio

TMS: transcranial magnetic stimulation

V1: primary visual cortex

VCG: vectocardiogram

VE: virtual electrode

VEP: Visual evoked potential

CHAPTER 1

INTRODUCTION

1.1 MRI

Magnetic resonance imaging (MRI) was first used to provide spatially detailed and non-invasive anatomical images of the human body but was soon also found to be a useful method of measuring changes in blood oxygenation in the brain and therefore, indirectly, neuronal activity (Ogawa, Lee et al. 1990). MRI scanners essentially consist of magnetic coils which, when an electrical current passes through them, create a large static magnetic field (B0), gradient coils used to apply spatiotemporally varying small magnetic fields which enable 3-dimensional localisation of the imaging volume, and transmitter and receiver coils required to excite and measure the MRI signal respectively. The way in which these components combine to create an MRI image is described below.

The scanner creates a large static magnetic field (B0: measured in Tesla) creating a net magnetisation (M) in nuclei which have an odd number of protons, mainly hydrogen molecules bound to oxygen in water. This is particularly relevant when imaging biological tissue due to the large percentage of water they contain. Protons have a quantum mechanical property known as angular momentum or ‘spin’, which precess, creating a magnetic moment in the direction of the precession axis (Huettel, Song et al. 2014). Within the same strength magnetic field protons of the same type of molecule precess at the same frequency, known as the Larmor frequency (Rigden 1986). The M of spins aligns to the direction of B0, where each spin

can align either in parallel with the field ('low energy state') or anti-parallel ('high energy state'). As a matter of quantum weirdness, the spins are thought to exist in a supposition of two states and when measured assume one state or the other, with the lowest energy state being the most likely. Interactions between individual spins mean they are not all rigidly locked to the direction of the external magnetic field, however their collective M will be, where the preferable parallel direction of the low level state will dominate. Inside the scanner M is proportional to the number of spins and B0 strength, therefore with greater scanner magnetic field strength there is increased M. It is by taking advantage of these properties that images can be attained with the combination of additional radiofrequency pulses and small changes in magnetic gradient field strength.

Radiofrequency (RF) pulses can be used to excite proton spins in the B0 field. An RF pulse applied at the Larmor frequency will increase the energy of the spins, moving them from low to high energy states, a phenomenon known as resonance. These RF pulses are described in degrees, which is the angle M is moved into (B0 being 0 degrees) after the pulse. A 90^{o} excitation pulse provides enough energy to shift M from the longitudinal plane (in the direction of B0) into the transverse plane where the spins initially precess in phase with one another. However, this change in energy state is temporary and quickly begins to decay with M moving back into the longitudinal plane. The receiver coils of the scanner detect the magnetic flux in the transverse plane, which is strongest immediately after the RF pulse (Figure 1.1). This change in magnetic flux is the MR signal. Full recovery of M to the longitudinal plane is known as T1 recovery (taking milliseconds; see Figure 1.2B). Prior to this recovery, there is decay in the transverse signal as a result of spin-to-spin interactions leading to reduced phase coherence in the transverse plane, this is known as T2 decay and takes only a few milliseconds (see Figure 1.2A). Tiny spatial inhomogeneities in the magnetic field (naturally occurring in biological tissue, particular at boundaries between different tissues) also cause spins to precess at different rates, decreasing the transverse plane magnetisation, known as

T'. T'+T2=T2*, this takes only a few tens of milliseconds to decay, this is the signal utilised for the functional MRI (fMRI) measure of the blood oxygen level dependent (BOLD) signal.

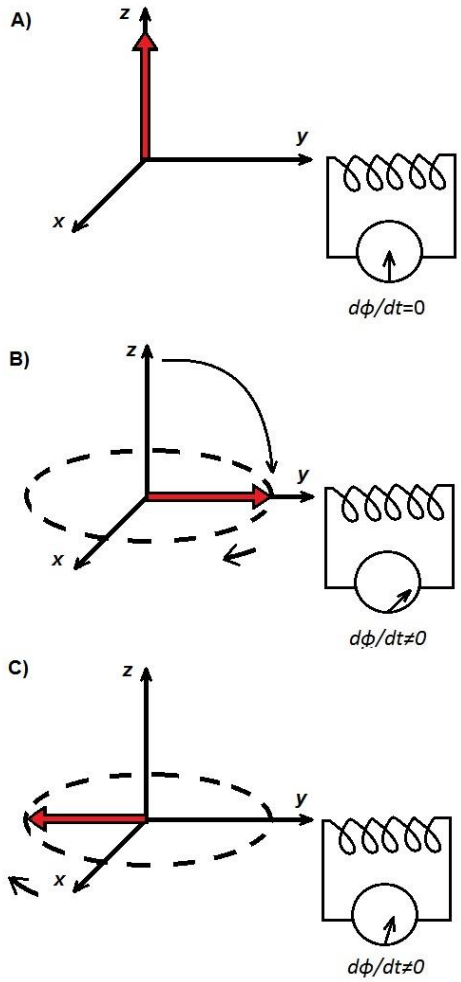

Figure 1.1. Magnetic flux recorded from transverse plane. A) shows the spins net magnetisation in the direction of B_0 prior to a RF pulse, at this time no magnetic flux is measured. After flipping the net magnetisation into the transverse plane via a RF pulse, the spins are in phase and revolve around the z-axis (direction of B_0), the signal changes over time (B and C) which provides the MR signal. Adapted from (Huettel, Song et al. 2014)

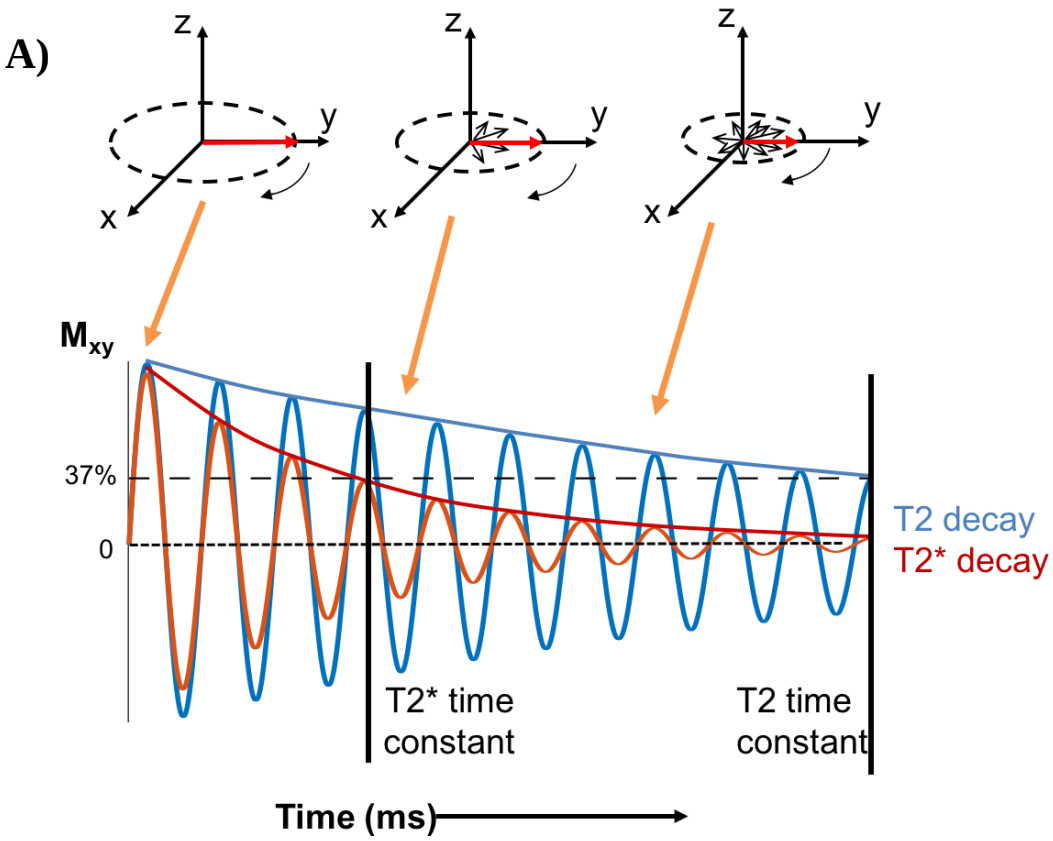
A)
z
y
x
M_{xy}
37%
0
T2 decay
T2* decay
T2* time constant
T2 time constant
Time (ms)

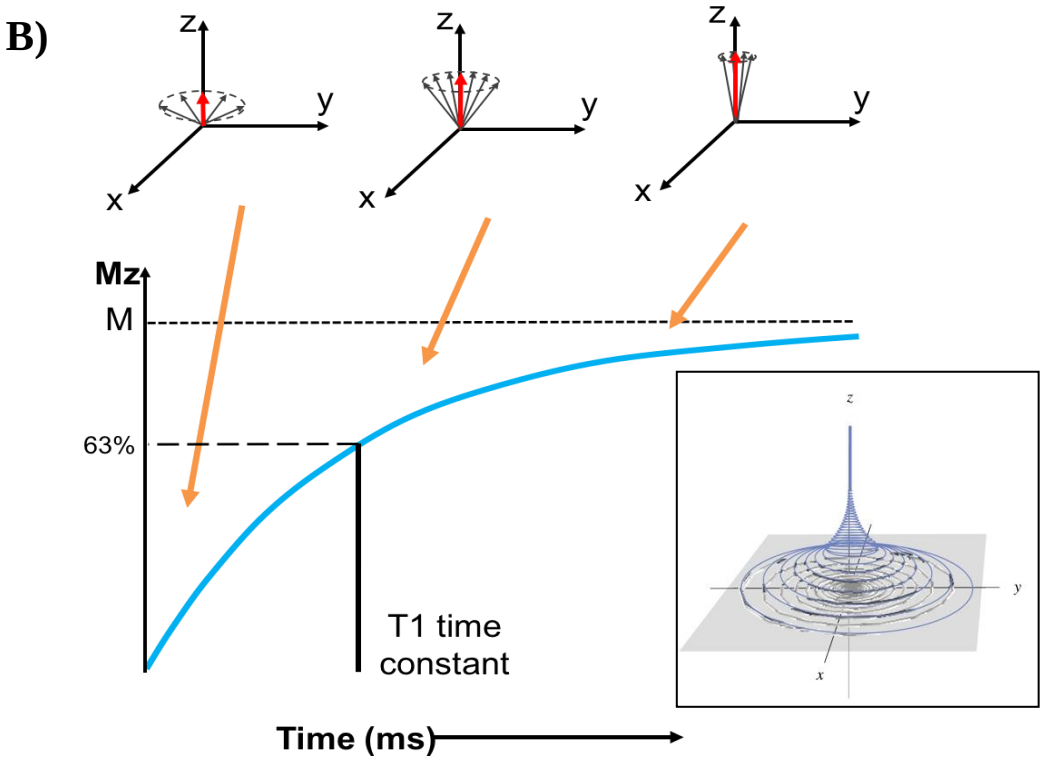
B)
z
y
x
Mz
M
63%
T1 time constant
Time (ms)

Figure 1.2. T2 decay and T1 recovery. A) The top row shows a cartoon representation of the transverse net magnetisation (M; red arrow) after a 90^{o} RF pulse. With B_0 in the z-axis direction, M flips into the transverse plane (xy) with all spins initially in phase. As the spins begin to de-phase (individual spins represented by the black arrows), the MRI signal decreases (as depicted in the second row). The T2 decay (blue line; sinusoidal=M measured, curve=envelope) is a result of the spin-to-spin interactions and is slower to decay than the T2* decay (red line) which is a combination of T2 decay and inhomogeneities in the magnetic field. The time constant for T2 and T2* decay relate to the time taken for the MRI signal to reach 37% of the maximum M value.
B) The top row shows a representation of M as longitudinal relaxation takes place. After T2 decay the spins are out of phase and M starts to increase in the direction of B_0, M actually spirals back to B_0, depicted here as the radius of the precessing spins decreasing around the z-axis (also see inset figure reproduced from (McRobbie, Moore et al. 2017)). The T1 time constant is set at the time taken for the signal to reach 63% of maximum M in the z-plane. Figure adapted from (Ridgway 2010)

In order to create an image, magnetic gradient coils built into the scanner are used to vary the magnetic field in three dimensions within specified regions. Graded variation in the magnetic field relates to graded differences in resonant frequencies (dependent upon the field strength) differ depending upon location, thus providing a method for spatial encoding and a way of distinguishing the origin of the signal. Three gradients are used in x, y and z directions, B_0 being in the z direction. The z-gradient, can be used to vary the magnetic strength and therefore the precession frequency for a certain slice of the object being imaged, a method known as “slice selection”. Using the z-gradient alone would enable only one measurement from each slice, therefore to provide a 3D image the x- and y-gradients are also used to encode 2D measurement positions within that slice.

The z-gradient and RF pulse occur simultaneously while the y-gradient is subsequently applied across the slice producing graded differences in spin precession frequencies therefore changing the T2 decay time in a graded manner across the slice (known as phase encoding). The x-gradient is then applied at the same time as data acquisition, changing the spin precession frequencies in a graded manner in that plane (known as frequency encoding).

Using the y- and x-gradients in this manner along with slice selection, enables the generation of a 3D image.

The most common fMRI sequence is known as Echo Planar Imaging (EPI) which takes advantage of the z- x- and y- gradients (Huettel, Song et al. 2014). It uses slice selection described above and subsequent fast switching of the x- and y-gradients in order to collect data from the full slice using a single RF excitation pulse. The x- and y-gradients are changed consistently in a zigzag manner to take measurements from one volume element (voxel) at a time within the slice and so allow data from each voxel to be measured separately. The acquisition of data is often described as a readout gradient.

There are a large number of parameters for an MRI sequence, which determine the measurement taken. Some basic parameters are the spatial resolution, the temporal resolution, the time at which the MR signal is measured after RF excitation, the flip angle and the field of view (FOV). The spatial resolution or voxel size is the smallest 3D region from which a single measurement is taken. The time taken to acquire a measurement from the entire object (volume) is known as the repetition time (TR) and is related to the number of voxels among other factors. The echo time (TE) is the time at which the measurement is taken after application of the RF pulse. The TE required to measure the BOLD response via a T2*-weighted sequence should be optimised (~30-35ms at 3T) to detect changes in T2* via blood oxygen levels within a voxel described in detail below. The flip angle is the angle at which M is rotated upon application of the RF pulse. The field of view (FOV) relates to the size (in cm/mm) of the imaged slice. These measures are inter-related and therefore all must be taken into account when designing a sequence (McRobbie 2017).

A T2*-weighted sequence is one optimised to measure T2* decay which due to its sensitivity to magnetic field inhomogeneities provides BOLD signal contrast. The iron contained within haemoglobin when bound to oxygen, oxyhaemoglobin, is diamagnetic (creates no distortion of

the magnetic field) whereas when no oxygen is bound to the iron, deoxyhaemoglobin, it is paramagnetic (creates magnetic field distortions). Therefore, regions with high concentration of deoxyhaemoglobin, relative to regions with lower concentration, will cause larger inhomogeneities in the magnetic field leading to faster dephasing of local proton spins which translates to faster T2*-decay and therefore less MR signal (lower BOLD signal). Conversely, larger concentrations of oxyhaemoglobin, lead to less magnetic field inhomogeneities, slower dephasing, slower T2*-decay and greater MR signal (larger BOLD signal). When the BOLD signal is measured in relation to a baseline measure, an increase in signal from the baseline is known as a positive BOLD response (PBR: see Figure 1.3) and a decrease as a negative BOLD response (NBR). The concentration of oxygen within blood (and therefore the BOLD signal) relies upon the coupling between the level of oxygen metabolised in the region and the level of blood flow to the region, known as neurovascular coupling.

1.2 Neurovascular Coupling

At rest the cerebral metabolic rate of oxygen ($CMRO_2$) and cerebral blood flow (CBF) are tightly coupled. However, during task/stimuli induced changes in neuronal activity they become uncoupled, with CBF increasing relatively more than $CMRO_2$ (Fox and Raichle 1986). This uncoupling leads to an increase in oxyhaemoglobin concentration due to an influx of fresh blood (see Figure 1.4) and therefore, as described above, a PBR. It is the ratio between CBF and $CMRO_2$ that determines in large part the concentration of deoxyhaemoglobin in the blood as they act to increase and decrease the oxygen concentration respectively (Buxton, Griffeth et al. 2014). Also important in the generation of the BOLD response is the change in cerebral blood volume (CBV) which is seen to increase in line with increases in CBF although to a lesser extent, see Figure 1.4, (Shen, Ren et al. 2008). This increase in CBV is inherently noted in the veins, in which the deoxyhaemoglobin concentration increases, leading to a reduction in the BOLD signal (Mandeville, Marota et al. 1998). Also of note here is the large increase in

cerebral metabolic rate of glucose (CMR_{gluc}) to neuronal activity, a measure that is coupled with $CMRO_2$ at rest but, in a similar manner to CBF, becomes uncoupled during increased neuronal activity (Fox, Raichle et al. 1988).

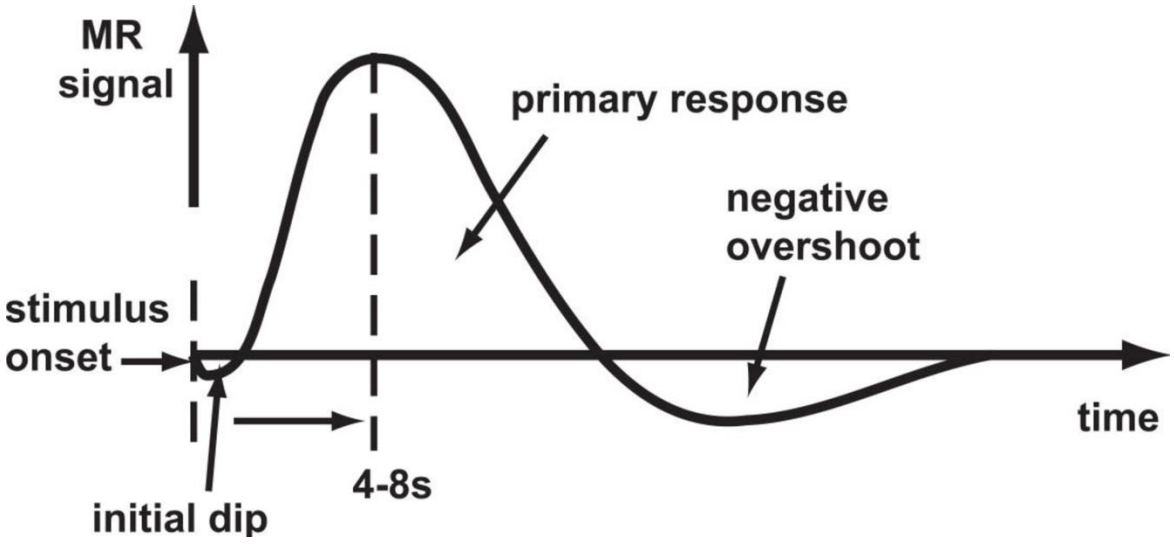

Figure 1.3. The PBR.
The BOLD response is slow to begin, starting 2-4 seconds after the stimulus onset and reaching peak amplitude after 4-8s (Kwong, Belliveau et al. 1992). This response can begin with an initial dip, via a brief signal decrease. This is believed to relate to an initial increase in $CMRO_2$ prior to the large inflow of CBF that follows (Menon, Ogawa et al. 1995, Hu, Le et al. 1997), however it is not consistently reported. The slow onset is a result of the slow change in CBF as described above. After cessation of the stimulus the BOLD signal begins to fall back to the baseline signal level. The duration of the BOLD response peak is dependent upon the stimulus duration. A post-stimulus undershoot is also often found whereby the signal drops below, before returning to, the baseline signal level. It is assumed that the PBR HRF is the same within all voxels, across all brain regions, and across all people. (Figure reproduced from (Kornak, Hall et al. 2011))

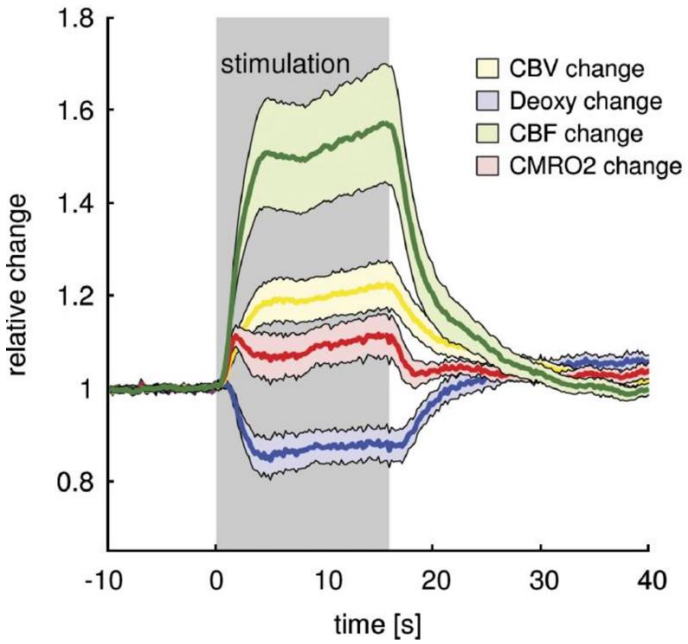

Figure 1.4. CBF, CBV, CMRO2 changes during sensory stimulation. During stimulation the disparity between the relative changes in CBV (yellow), CBF (green) and CMRO2 (red) can be seen. The changes in these three cause decreases in the relative concentration of deoxyhaemoglobin (blue) i.e. an increase in oxyhaemoglobin concentration which is the basis of the PBR. Figure reproduced from (Leithner, Royl et al. 2010)

Glucose is used by cells to produce adenosine triphosphate (ATP), the molecule used as energy 'currency' throughout the body. In neurons it is utilised to reset ionic gradients after activity, for pre- and post-synaptic activity, and glia activity (Attwell and Iadecola 2002). ATP can be created without oxygen (known as glycolysis), producing 2 ATP molecules, pyruvate (which can subsequently be stored as lactate) and nicotinamide adenine dinucleotide (NADH). In the presence of oxygen, pyruvate can go on to be converted to carbon dioxide, water and 30 ATP molecules (a process known as oxidative phosphorylation). The disparity between the $CMRO_2$ and CMR_{gluc} changes during activity, from at baseline, were at first thought to relate to a preference of glycolysis to produce ATP due to the larger apparent uptake of glucose than oxygen and its speed of energy production (Fox, Raichle et al. 1988). However, it is now believed that a greater proportion of ATP is produced via oxidative phosphorylation during neuronal activity, with ATP consumption still dwarfed by the ~4 fold increase in CBF (Lin, Fox et al. 2010). The vascular and metabolic influences on the BOLD response are thought to arise via separate pathways, with metabolic demand not leading directly to increased CBF in a feed-back manner. Instead, CBF increases are thought to be tied to neurotransmitter release (Attwell and Iadecola 2002, Attwell, Buchan et al. 2010), where release of glutamate and Gamma-Aminobutyric acid (GABA: discussed in detail below) during neuronal activation are related to increased CBF (Akgören, Fabricius et al. 1994, Fergus and Lee 1997). Part of this process is hypothesised to be a result of astrocytic signalling (see Figure 1.5), one of a group of non-neuronal glial cells. These neuroglia exist in a ratio to neuronal cells of 1.48 in the cortical grey matter (Azevedo, Carvalho et al. 2009). They are known to synapse ~99% of the vasculature of the cerebral cortex with each astrocyte encircling approximately 140,000 synapses (Agulhon, Petravicz et al. 2008).

Astrocytes function to remove neurotransmitters from synapses after pre-synaptic release, essentially cleaning up the synapse (Agulhon, Petravicz et al. 2008). This uptake of glutamate initiates glycolysis in astrocytes, one product of which, lactate, is shuttled along with glutamate

to the proximal neurons for further oxidative metabolism (Pellerin and Magistretti 1994, Sibson, Dhankhar et al. 1998). CBF is thought to increase as a result of feed-forward pathways relating to some of the shuttled lactate which is lost into the blood causing vasodilation, along with direct astrocytic signalling at astrocyte-vasculature synapses (see Figure 1.5) (Lin, Fox et al. 2010). A similar increase in glycolysis does not occur in the presence of pre-synaptic GABA (Chatton, Pellerin et al. 2003) possibly due to large proportions of GABA being reabsorbed at the pre-synaptic nodule so limiting the astrocytic uptake (Yang, Li et al. 2007). It may therefore be that there is simply a relatively smaller increase in metabolism to GABA than glutamate (Patel, de Graaf et al. 2005). There is however evidence that exogenous GABA can cause vasodilation, and therefore increase CBF, in the hippocampus and cortex (Fergus and Lee 1997). In addition, some GABAergic interneurons are thought to generate and release substances, during activation, to dilate or constrict blood vessels (Price, Cauli et al. 2005) and therefore contribute to CBF regulation.

The information above describes the complexity of the mechanisms which make up the BOLD response. The PBR is the most utilised response feature in fMRI research and contains a distinct temporal profile, the haemodynamic response function (HRF; see Figure 1.3). Given the complex origin of the BOLD signal, having both vascular and metabolic components, multiple measures of neurophysiological responses are required to provide a detailed understanding of its origin. In particular, a measure of CBF can be attained using a method known as arterial spin labelling (ASL) using specifically developed MRI sequences.

1.3 ASL and combined ASL-BOLD measurement

For the measurement of CBF changes, ASL sequences magnetically tag the blood to create an endogenous contrast agent. ASL sequences make use two identical EPI readouts with short TE to measure the MR signal in separate volumes with the first volume also containing an inversion pulse to tag the blood. The tag image is used to magnetically tag spins located in

the water of the blood and then after waiting for a brief period (~1s), to allow for blood perfusion into static tissue, takes a subsequent readout. The perfusion into the tissue reduces the magnetisation of the later by 1-2%. The control image is used to measure the signal without any magnetic tagging. By subtracting the tag sequence from the control sequence a signal proportional to blood perfusion can then be ascertained (Williams, Detre et al. 1992). In order to minimise physiological noise in the signal from the tissue one or more background suppression inversion pulses are often used (Ye, Frank et al. 2000), the timing of which is optimised so that the readout is taken close to the point of null magnetisation (Garcia, Duhamel et al. 2005).

ASL sequences require a specific preparatory phase, location of magnetic labelling of the blood, and a subsequent readout phase, most commonly an EPI sequence. Various methods have been developed for the preparatory phase of an ASL sequence using MRI. Continuous ASL (CASL) was the first method developed, this labels the blood at the neck using a RF pulse and an imaging gradient over a long period of time (Williams, Detre et al. 1992). The long RF pulse used increases the risk of thermal burns due to the rate RF is absorbed: specific absorption rate (SAR). Pseudo–continuous ASL (pCASL) uses a train of RF pulses that create a similar effect to the long duration continuous ASL pulse but decrease SAR. A third ASL sequence uses a short RF pulse over a large area, pulsed ASL (PASL), of which there are a number of specific sequences.

Two main types of pulsed ASL sequences used are EPI-based signal targeting by alternative radiofrequency pulses (EPISTAR) and flow-sensitive alternating inversion recovery (FAIR). EPISTAR uses a slice selection pulse (90^{O}) followed by an inversion pulse (180^{O}) below the slice to tag the inflowing blood. The control scan uses the same slice selection but now followed by an inversion pulse above the slice. The difference between the scans takes into account the perfusion upwards into the slice of interest. FAIR imaging uses an inversion pulse to label the whole brain and a slice selection inversion pulse as a control, the difference

between the two images being the flow of blood into the scan from above or below the slice. These sequences have much lower SAR than CASL and pCASL sequences.

EPI is generally used for the readout of ASL sequences to provide rapid acquisition of data. The TE used to collect the readout for ASL data (~16ms) is much shorter than for BOLD T2* readouts (~30-35ms, at 3T), to increase the sensitivity to the small signal change. Taking advantage of the TE difference allows for the collection of simultaneous ASL and BOLD responses using the same sequence, as the ASL data can be collected prior to the BOLD data. CBF changes can then be related directly to concurrent acquired BOLD changes. The two measures can be used to calculate changes in $CMRO_2$ using a model of BOLD response developed by Davis et al. (Davis, Kwong et al. 1998), see Chapter 3 (Equation 1 for a detailed description).

1.4 Neuronal Activity and the BOLD response

Energy usage is thought to differ between excitatory and inhibitory neurons. Excitatory pyramidal neurons make up 80-85% of the cortical neuronal population, the remaining 15-20% being inhibitory neurons (interneurons) (DeFelipe 1993, Somogyi, Tamas et al. 1998). Excitatory neurons primarily signal using the neurotransmitter glutamate which initiates a fast post-synaptic action potential and subsequently activates the post-synaptic neuron (which can be an interneuron or a pyramidal cell). Interneurons use the inhibitory neurotransmitter GABA. These GABAergic interneurons have synapses located on pyramidal cells in key locations (on dendrites and close to the cell body) for efficient inhibition (Freund and Buzsáki 1996, Koos and Tepper 1999). The prime location of the GABAergic synapses could be linked to synchronisation of pyramidal neuronal firing leading to measurable oscillations of the electric field (discussed further below) (Buzsáki and Draguhn 2004). This apparent efficient nature of GABAergic cells could also relate to a relatively lower metabolic demand than pyramidal cells.

Neuronal activity can be measured on different scales ranging from the smallest, single neuronal recordings, to multi-unit spiking activity recordings (MUA), local field potentials (LFP) and up to the largest scale, electroencephalography (EEG) and magnetoencephalography (MEG). Attempts have been made to correlate recordings at these various levels with the BOLD response in order to understand what aspect of neuronal activity the BOLD response is linked to. By placing an electrode in the extracellular fluid in the cortex, activity of neurons in the region can be recorded, filtering the signal between 300-400Hz produces the MUA while filtering at ~<300Hz produces the LFP (Logothetis 2003). These signals represent different forms of neuronal activity. MUA recordings are believed to relate to the sum of extracellular potential changes (action potential activity) in a particular region, mainly from large pyramidal cells, (a distance of ~140μm from the electrode tip). The LFP signal relates to signal arriving at a region and the processing of that signal within the region (related to pyramidal as well as inhibitory neuronal activity) (Logothetis 2003). It is now generally believed that the LFP is the neuronal measure most closely correlated with the PBR (Logothetis, Pauls et al. 2001, Viswanathan and Freeman 2007). However other work has shown that both MUA and LFP (Heeger and Ress 2002) or a combination of the two (Mukamel, Gelbard et al. 2005) are correlated with the PBR, which could be a result of the difficulty in separating one measure from the other (Kim and Ogawa 2012). The BOLD response however is not simply a direct consequence of neuronal activity, but instead, as described above reflects oxygen levels of the blood, with the link between neuronal activity and changes in oxygen level changes still being teased apart. Recent work has in fact shown that the PBR does not always relate to changes in neuronal activity (Sirotin and Das 2009), with increasing evidence implicating astrocytes as the primary instigators of vascular change (Gordon, Choi et al. 2008), as discussed in detail above.

1.5 Analysing BOLD responses

General linear modelling (GLM) is the most common form of basic fMRI data analysis, providing spatial maps of the brain regions (voxels or clusters of voxels) responding to a stimulus. In an experiment stimuli are presented repeatedly in order to increase the signal measured in relation to noise (signal to noise ratio; SNR). There are two basic fMRI experiment designs: event related design (rapidly presented short stimuli) and block design (long duration stimuli). The block design provides greater statistical power due to the long duration of the stimuli. However, event-related designs are more suited to studies investigating perceptual changes, oddball paradigms, and attentional blink paradigms. Stimuli are separated by periods of no stimulation, “resting baseline”, allowing the BOLD signal to recover back to a baseline level providing accurate response estimation for individual trials.

Prior to statistical analysis, the acquired BOLD data must be pre-processed which reduces any artefactual signal changes that may affect results. Movement during data acquisition can lead to a voxel occupying different locations between volumes which can cause large artefactual changes in BOLD signal intensity. Basic motion correction uses a single volume as a reference image and registers all other volumes to it (Jenkinson, Bannister et al. 2002). The data is also commonly spatially smoothed to increase the SNR using a Gaussian smoothing kernel which averages the signal across surrounding voxels, the size of the kernel mainly dependent upon the voxel size (e.g. 5mm for 3mm voxels). Data can also be corrected for low frequency drifts from physiological noise, magnetic drift, or thermal noise by using a high-pass filter.

As described above, the PBR has a characteristic timecourse (Figure 1.4). In GLM analysis, the BOLD timecourse recorded from each voxel during an experiment is compared to a model (design matrix) of the signal expected. The model is calculated by convolving the timecourse of all stimulation timings with the HRF (see Figure 1.5D). Equation 1.1 represents the linear

regression model, where the data in a single voxel for the entire time course (Y) is modelled by the design matrix (X). The parameter estimate is a scaling factor (β) which is estimated so as to minimise the error of the model (ε). Analysing the data voxel-by-voxel, the GLM produces a map of t-statistics, calculated as β divided by ε. This can then be converted to a Z-statistic and a p-value. Due to the large number of voxels tested within a brain, there is a high chance of type I errors (erroneously finding a voxel significant), which should be accounted for in some form. Strategies exist for such multiple comparison corrections in GLM analysis such as the stringent familywise error rate (FWE), e.g. Bonforroni correction. Cluster thresholds can be used in addition to help decrease type I errors by assuming that the BOLD signal in adjacent voxels will be similar. Alternative to the FWE correction is the false discovery rate (FDR) which attempts to reduce type II errors (false positives).

Equation 1.1: $$\mathbf{Y = X.\beta + \varepsilon}$$

The GLM approach is very useful for finding the location of activity due to a task, but is not the best way of assessing whether regions of the brain are functionally connected. Such functional connectivity can be described as temporally dependent activity between spatially segregated regions. To identify functionally connected regions, fMRI data is often collected during a resting state, i.e. when subjects simply lie in the scanner, awake, with no stimuli/task. Various analyses exist for defining functionally connectivity, the most basic of which is temporal correlation between the BOLD signal from a seed region (voxel or region of ~100 voxels) and the signal from the rest of the brain (voxels/regions) (Friston, Frith et al. 1993). It is thought that connected regions whose temporal signal fluctuates in a similar manner share a mutual exchange of information, although the direction of connection is difficult to determine due to the slow nature of the BOLD response. To analyse fMRI data in this manner the same pre-

processing steps as for GLM analysis are required, with the addition of low-pass filtering (<0.1Hz) and removal of additional confounds (CSF and/or global signal). It is the low frequency fluctuations in the fMRI BOLD signal that have been shown to correlate between regions, providing insight into various functional networks in the brain such as the default mode network (DMN) (Fox, Snyder et al. 2005).

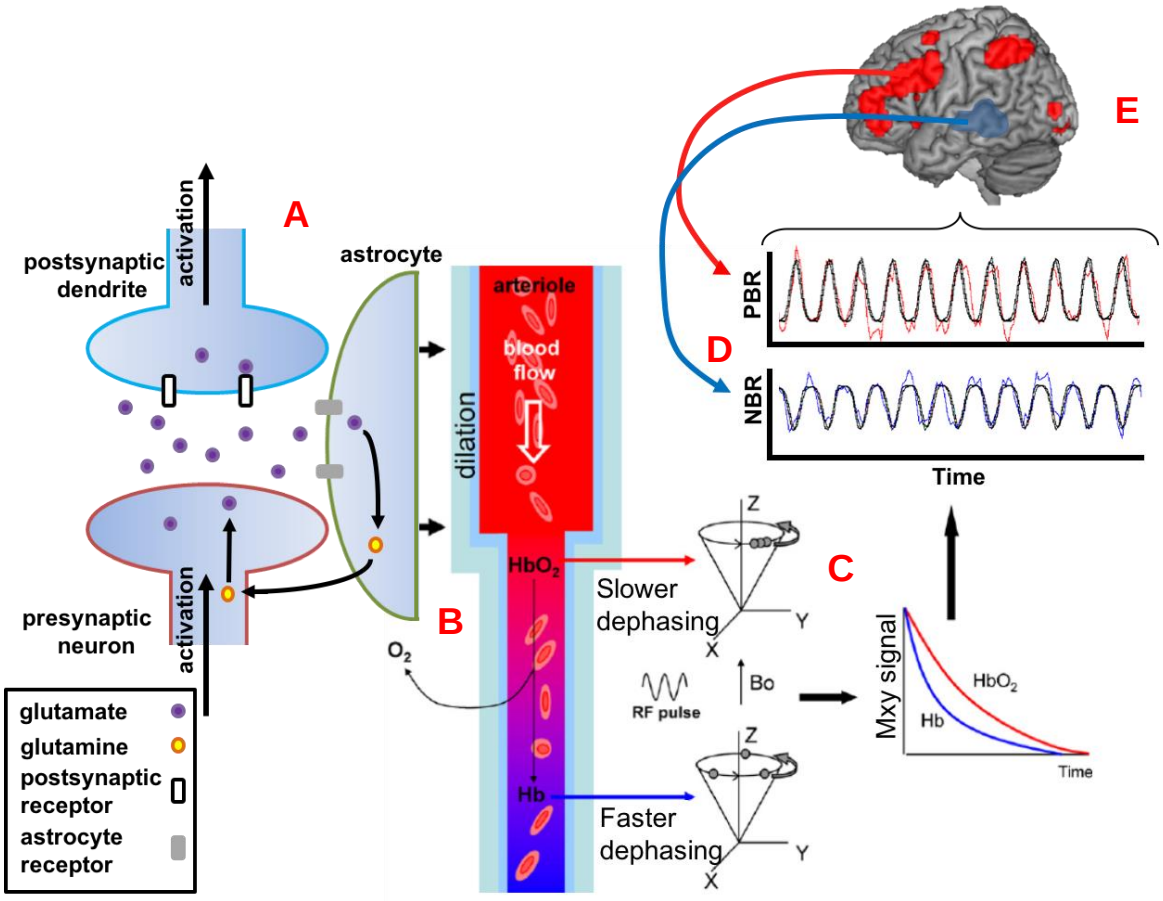

Figure 1.5. BOLD response origin overview.
A) Glutamatergic neuronal activity results in the release of glutamate from the presynaptic neuron into the synapse. Glutamate is taken up by the postsynaptic dendritic bouton, with some also removed by the astrocyte which surrounds the synapse. The uptake by the astrocyte initiates glycolysis and lactate production. Within the astrocyte glutamate is converted to glutamine and, along with lactate, is shuttled back into the presynaptic neuron. **B)** Direct astrocytic signalling and lactate release increases CBF leading to increased oxyhaemoglobin, overriding the uptake of oxygen from the blood. **C)** Regions with Increased oxygen from baseline have slower dephasing spins than those regions with decreases in oxygen from baseline. Slower dephasing leads to larger relative T2* signal. **D)** Voxelwise GLM analysis can then identify those signals which increase or decrease in line with experimental model by convolving the timecourse of all stimulation timings with the HRF **E)** This is used to create a spatial map of BOLD response. Adapted from (Harris, Reynell et al. 2011)

1.6 Negative BOLD responses

As described above, the BOLD response has a complex origin (summarised in Figure 1.5), with PBR most often used in experimental analysis. Often overlooked however are the decreases in BOLD signal from resting baseline, NBRs that are also commonly evoked in response to stimuli. NBRs can be elicited in a variety of cortical regions depending on the paradigm, and can be observed within or outside of the directly stimulated cortex. For example, they are most commonly found either:

1. Within the sensory cortex stimulated but ipsilateral to a unilateral stimulus (IM ipsilateral NBRs) (Allison, Meador et al. 2000, Mullinger, Mayhew et al. 2014).

2. Adjacent to, or surrounding a PBR in the directly stimulated sensory cortex (IM surround NBRs) (Shmuel, Yacoub et al. 2002, Pasley, Inglis et al. 2007).

3. In a sensory cortex other than that directly stimulated, such as observed in auditory cortex during visual stimulation, Cross-modal (CM) NBRs (Laurienti, Burdette et al. 2002, Mozolic, Joyner et al. 2008).

4. Within the default mode network during tasks/stimuli (McKiernan, Kaufman et al. 2003, Buckner, Andrews-Hanna et al. 2008).

5. Proximal to lateral ventricles, overlapping veins, during visual stimuli (Bianciardi, Fukunaga et al. 2011)

Although 1-4 in particular are widely reported, it is currently unknown whether the neuronal, metabolic and vascular origins of these NBRs are comparable to one another. Of these NBRs, only two types, 1 and 2, have been studied in terms of their neurophysiological origins (Shmuel, Yacoub et al. 2002, Mullinger, Mayhew et al. 2014). The fundamental origin of this

signal is increased concentration of deoxyhaemoglobin in the region which, due to the complexity of neurovascular coupling, can result from a number of mechanisms:

1. A decrease in neuronal activity with a small decrease in $CMRO_2$ and larger decrease in CBF (Shmuel, Yacoub et al. 2002, Shmuel, Augath et al. 2006, Mullinger, Mayhew et al. 2014).

2. An increase in neuronal activity leading to an increase in $CMRO_2$ with no concomitant increase in CBF, as seen in the hippocampus during epileptic seizures (Schridde, Khubchandani et al. 2008).

3. A decrease in local CBF due to increases in CBF in other nearby regions (haemodynamic steal) (Harel, Lee et al. 2002, Kannurpatti and Biswal 2004, Puckett, Mathis et al. 2014).

4. An increase in CBV in veins downstream of PBRs evoked during visual stimuli (Bianciardi, Fukunaga et al. 2011)

The main focus of this thesis is studying the IM and CM NBRs to sensory stimuli. Although there are many potential mechanisms in which NBRs can occur, some are unlikely to be involved in the generation of NBRs within sensory cortices to sensory stimuli. Those located in the hippocampus during seizures appear to be specific to that region and circumstance (Schridde, Khubchandani et al. 2008), while the CBV related NBRs are specific to regions which contain large veins close to ventricles (Bianciardi, Fukunaga et al. 2011). The use of multiple neuroimaging measures helps greatly to distinguish between potential origins of NBRs. For example, using multiple MR measurements, e.g. BOLD-ASL such as has been carried out by Mullinger et al. (Mullinger, Mayhew et al. 2011, Mullinger, Mayhew et al. 2014),

allows investigation of the metabolic (Mullinger, Mayhew et al. 2014) vs vascular origins (Schridde, Khubchandani et al. 2008) of BOLD responses (which is the aim of Chapter 3).

Neuronal origins of the NBR can also be examined using corresponding electrophysiological measurements. Seminal studies in primates and rats have shown decreases in gamma frequency (>30Hz) LFP activity (thought to reflect decreased pyramidal activity) in IM surround NBR (Shmuel, Augath et al. 2006) and IM ipsilateral NBR regions (Boorman, Kennerley et al. 2010, Boorman, Harris et al. 2015). These studies of IM NBR form the basis of evidence for the neuronal origin of all NBRs, with over 60% of primate visual IM surround NBR being attributed to decreases in neuronal activity (Shmuel, Augath et al. 2006). Such decreases are thought to result in reduced CBF, accompanied by a proportionately smaller reduction in $CMRO_2$ (mechanism 1), resulting ultimately in the measured NBR. To fully understand and make use of all NBRs observed in human fMRI data, non-invasive studies in humans are vital.

Electroencephalography (EEG; described in detail below) signals provide a high temporal resolution measure of fluctuations in the synchrony of the underlying neuronal activity. Combined EEG-fMRI studies in humans indicate correlations between decreases in neuronal activity and NBRs. In particular, Mullinger et al. (Mullinger, Mayhew et al. 2014) found that increased single-trial IM ipsilateral NBR magnitude (e.g. more negative NBR amplitudes) in primary somatosensory cortex (S1) correlated with increases in the power of S1 alpha frequency neuronal activity (described in detail below), therefore suggesting a link between two measures of decreased cortical activity in this brain region. Further evidence of links between alpha and IM negative BOLD have been observed in visual cortex during photic stimulation (Mayhew, Ostwald et al. 2013, Maggioni, Molteni et al. 2015), however in contrast Yuan et al (Yuan, Perdoni et al. 2011) found only a coupling between alpha and IM PBR during unilateral hand movements. Therefore a comprehensive understanding of the neural activity which most explains each type of NBR is still lacking.

To test the hypothesis that NBRs are related to inhibitory neuronal processes a number of studies have attempted to relate NBR amplitude to the local concentration of GABA using magnetic resonance spectroscopy (MRS; described in detail below). Northoff et al. (Northoff, Walter et al. 2007) found a positive relationship in the anterior cingulate cortex (ACC) of the DMN between the resting level of GABA and the level of NBR during emotional stimulation. Similarly, resting levels of GABA and glutamate were both found to be predictive of NBR in the DMN during working memory tasks (Hu, Chen et al. 2013). The PBRs to basic visual stimuli have been negatively correlated with resting GABA levels in visual cortex (Muthukumaraswamy, Edden et al. 2009), and resting levels of glutamate, have been shown to positively correlate with the level of resting state BOLD activity in visual cortex (Enzi, Duncan et al. 2012). Conversely, Harris et al. (Harris, Puts et al. 2015) studied 5 brain regions and 5 tasks recruiting those areas and found that the PBR evoked was not correlated with the level of GABA. Furthermore, reports suggest that increases in GABAergic neuronal activity lead to local PBRs in rats (Enager, Piilgaard et al. 2009, Pelled, Bergstrom et al. 2009). Therefore, the relationship between BOLD and GABA/glutamate remains contentious.

Whilst evidence mounts for NBRs originating from a local reduction of neuronal activity, it remains unclear how such reductions are initiated, and whether they result from decreased excitatory input to the NBR region or alternatively from increases in local inhibitory neuronal activity. The large size of voxels used in fMRI data collection, relative to the size of neurons, means that there will be a huge number of both GABAergic and many more glutamatergic neurons sampled within each voxel. As described above, GABAergic activity alone is unlikely to explain observed changes in CBF and BOLD signals, to the same degree as glutamatergic activity. The astrocyte based interpretation of BOLD responses suggests that there may be three possible changes which relate to a NBR. They are listed here in order of NBR amplitude evoked (smallest to largest) (Figley and Stroman 2011):

1) a decrease in excitatory input and increase in inhibitory input to the region from baseline; where the activity of the inhibitory neurons is more efficient (less synapses) and would not balance out the decrease in $CMRO_2$ and decrease in CBF seen from the loss of excitatory activity.

2) decrease in excitatory input from baseline; decreasing $CMRO_2$ and CBF

3) decreases in both inhibitory and excitatory inputs from baseline; deceasing both would create large decreases in CBF and $CMRO_2$.

1.6.1 Interhemispheric interaction and NBR

Of particular interest in this thesis are the IM ipsilateral NBR to sensory stimulation which have been widely reported and may be initiated by interhemispheric interactions. Interhemispheric interactions between the left and right hemisphere of the same sensory cortices are known to be facilitated by the corpus callosum (CC) (Bloom and Hynd 2005). Both excitatory and inhibitory connections are known to cross through the CC, however the balance between them and the functional nature of these connections during various tasks is still poorly understood (Bloom and Hynd 2005, van der Knaap and van der Ham 2011). The connectivity of left and right motor cortices has been widely studied, in particular with the advent of transcranial magnetic stimulation (TMS: described below) research and diffusion weighted imaging (DWI; as discussed below).

An early study of motor cortex hemispheric interaction using TMS found that stimulating M1 in one hemisphere decreased the cortico-spinal excitability (CSE: described below) of M1 in the opposite hemisphere, with increased TMS pulse intensity leading to increased duration of inhibition (Ferbert, Priori et al. 1992). Unilateral somatosensory stimulation has also been shown to decrease ipsilateral CSE (Chen, Corwell et al. 1999), as have basic motor tasks (Liepert, Dettmers et al. 2001). This change in CSE of the motor cortex ipsilateral to the stimulus is suggested to be the result of direct interhemispheric interaction (Di Lazzaro,

Oliviero et al. 1999). More physically direct measures of connectivity, such as callosotomy (CC resection) patients, have also increased our understanding of CC interhemispheric connectivity.

Callosotomy patients have been found to show limited or no ipsilateral NBR to unilateral stimuli, which suggests that the NBRs occurrence depends on inter-hemispheric signalling via the CC (Fabri, Polonara et al. 2005, Feige, Scheffler et al. 2005). Work by Genç et al. (Genc, Ocklenburg et al. 2015) measured BOLD responses to a simple unilateral motor task as well as calculating deterministic tractography from DWI data for healthy and callosotomy patients. They found that the mean fractional anisotropy (FA: described in detail below) measured from a sub-region of the CC was positively correlated with the NBR amplitude, which they relate to the level of interhemispheric suppression between the contralateral and ipsilateral motor cortices and that the NBR observed in healthy subjects was not found in the patient group. Although this study directly related FA to the interhemispheric interaction, it did not consider the specific connectivity between the regions of contra PBR and ipsilateral NBR. Such lack of clarity has led to inferences being made via data acquired from monkeys. This monkey research implies that direct inter-hemispheric structural connections don't exist between the specific regions previously found in humans to show IM PBR and IM NBR to median nerve stimulation (MNS) (BA 3b and 1) (Klingner, Hasler et al. 2010), but instead between areas of the somatosensory cortex proximal to them (BA 2 and 5) (Killackey, Gould et al. 1983). As such the interaction between the contralateral IM PBR and ipsilateral IM NBR regions, although perhaps not direct, could involve transcollosal connectivity onto and activation of ipsilateral BA 2/5, and then further intrahemispheric interaction with BA 1/3b (Klingner, Hasler et al. 2010, Schafer, Blankenburg et al. 2012). The interactions between contralateral PBR and ipsilateral NBR regions via this indirect pathway would therefore involve the fibres crossing the CC to terminate onto and excite inhibitory neurons which then act to decrease excitatory neuronal activity in the ipsilateral NBR region (Schafer, Blankenburg et al. 2012).

As with the motor cortex, the two hemispheres of the visual cortex are linked via the CC. The physical attributes of the axons spanning the CC between the visual cortices are such that they are thought more liable to modulate rather than initiate neuronal firing (Tettoni, Gheorghita-Baechler et al. 1998). The extent to which these connections facilitate interhemispheric interactions in the visual cortex is complicated by their dependence on the specific stimulus (Tettoni, Gheorghita-Baechler et al. 1998). The visual interhemispheric connections have been shown to play a role in various functions such as depth perception and binocular vision (Pietrasanta, Restani et al. 2012). However, the relationship between the IM ipsilateral NBRs, contralateral PBRs and structural connectivity within the visual cortex has not yet been studied.

Similarly, research has not investigated CM inhibitory interactions in humans, although work by Iurilli et al. (Iurilli, Ghezzi et al. 2012) in rats, has shown that visual cortex suppression during auditory stimulation resulted from GABAergic inhibition, most likely via cortico-cortical tracts. Connectivity between regions of visual and auditory cortices in humans have been shown to exist (Beer, Plank et al. 2011), however how this relates to the interaction between PBR and NBR regions is unknown.

1.6.3 Functional information provided by the NBR

Whether NBR is related to a functionally relevant change in brain activity, rather than simply arising as a by-product of processing is a key question, but one that remains poorly understood with only a few studies showing evidence of links between NBR and behavioural responses. Kastrup et al. (Kastrup, Baudewig et al. 2008) found that electrical stimulation of the finger elicited a NBR in the S1 ipsilateral hand region, an area found to show an increase in perceptual threshold of electrical stimuli under the same conditions outside of the scanner. Similarly, perceptual threshold noted in the region of MNS IM NBR was found to decrease with increasing NBR across subjects. as a control, the perceptual threshold of hallux electrical

stimulation was found not to change (Schafer, Blankenburg et al. 2012). NBRs have also been shown to be elicited contralateral to sub-perceptual threshold, subliminal, somatosensory stimuli, a finding hypothesized to relate to the prevention of spurious activation (Blankenburg, Taskin et al. 2003). While the location of IM NBRs in the visual cortex have been shown to be specific to the position of visual stimuli (Bressler, Spotswood et al. 2007) (Tootell, Hadjikhani et al. 1998) other findings have shown a distinct lack of specificity, with more widespread NBRs to visual stimuli (Smith, Singh et al. 2000, Smith, Williams et al. 2004).

As well as IM NBRs, CM NBRs located in the auditory cortex were found to be significantly larger during visual imagery than visual stimuli (Amedi, Malach et al. 2005). Increasing CM NBR in the visual cortex were also shown to occur in the presence of increased auditory task difficulty (Hairston, Hodges et al. 2008). NBRs located in the DMN have also been found to scale with difficulty of auditory target detection tasks (McKiernan, Kaufman et al. 2003). This thesis however focusses upon the IM and CM NBRs. Overall these results suggest that the sensory cortex IM and CM NBRs in specific contexts contain functionally relevant information which may relate to neuronal activity and stimulus processing and therefore be useful in the interpretation of fMRI BOLD results.

1.7 Methodologies

Here, the key methodologies used within this thesis will be introduced.

1.7.1 EEG

In order to understand the origin of the EEG signal, a basic comprehension of the neuronal cell biology is required. A neuronal cell is comprised of a cell body (soma), dendrites and a single axon. The cell body and dendrites receive electrical input from other neurons while the axon transmits information to other neurons in the form of action potentials and electrochemical

processes at the synapses, through the release of neurotransmitters such as glutamate (Thompson 2000).

EEG is a non-invasive method of measuring large scale electrical signals (measured in microvolts, μV), arising from large groups of neurons, which propagate to the surface of the scalp where they can be measured using an array of electrodes. Synchronous post-synaptic current flow around the dendrites of pyramidal neurons summates to create an extracellular field which conducts to the scalp. It requires synchrony of neurons within a ~5cm^2 area of cortex for the EEG signal to be measureable at the scalp (Lopes da Silva 1991).

It is the pyramidal neurons which primarily contribute to the EEG signal due to their high synaptic density, as well as their close proximity and perpendicular arrangement to the cortical surface (Speckmann 2005, Lopes da Silva 2013). Activation of pyramidal cells generates extracellular currents where the component parallel to the dendritic tree summates, creating a field measurable at a distance (Speckmann 2005). Although dendritic activity is the main generator of the EEG signal, there are other contributors as well including glial cell activity and calcium and sodium spikes (Cohen 2017).

EEG recording involves placement of electrodes on the scalp, with the impedance of the electrical signal to the electrodes reduced by cleaning under the region with alcohol, lightly abrading the skin and applying conductive gel. The most utilised electrode positons follow the 10-20 international system (see Figure 1.6). The signal from each electrode is amplified and filtered (e.g 0.016-250Hz). The EEG data can then be further analysed.

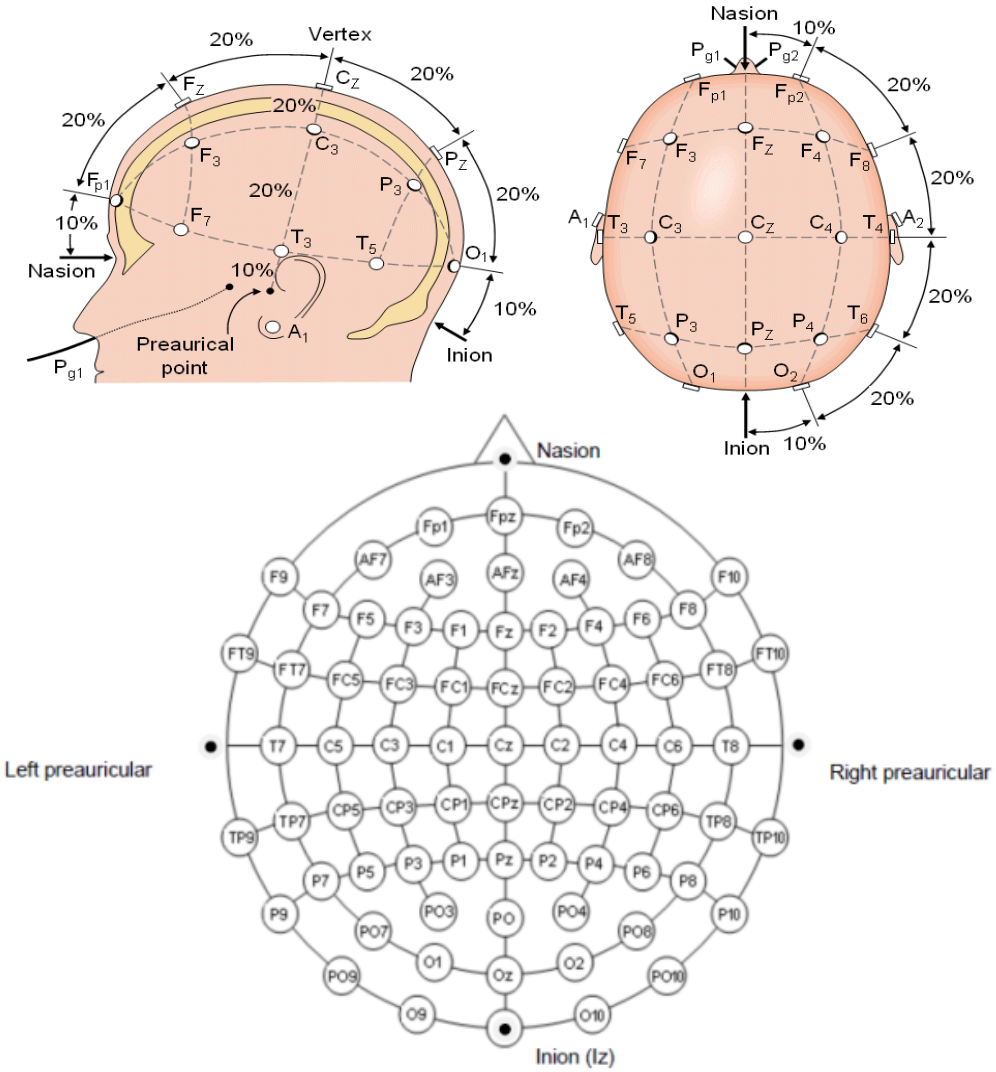

Figure 1.6. The standard 10-20 international system for electrode placement. A) The channel Cz is placed at the vertex: the midpoint between the landmarks, nasion and inion and the periauricular points (left and right). Each electrode is positioned 10% or 20% of the total distance between landmarks from the surrounding electrodes. Recording of the signal requires a ground and a reference channel to be used. The ground (often AFz) is used to reduce noise from the data, while data from all electrodes is measured against the reference electrode (often Fz).

EEG can record many types of neuronal activity but is commonly used to measure rhythmic signals, oscillations, originating from the brain. These oscillations are conventionally separated into specific frequency bands which are thought to influence, or be influenced, during certain types of stimuli. There are five main frequency bands, named in order of their discovery but listed here in ascending frequency: delta (δ, <3Hz), theta (θ, 3-7Hz), alpha (α, 7-13Hz), beta (β, 13-30Hz) and gamma (γ, >30Hz). It is the way in which oscillatory activity of certain frequencies (specifically α and β) change in relation to stimuli and their relation to the NBR which is of primary interest in this thesis.

EEG oscillations provide a high temporal resolution (on the order or milliseconds) measure of fluctuations in the synchrony of the underlying neuronal activity. Of particular interest for this thesis are the low frequency EEG signals, alpha (α) and beta (β), for which event related synchronisation (ERS, an increase in power relative to baseline) is thought to reflect decreased cortical excitability and increased inhibition, required to regulate sensory processing (Pfurtscheller, Stancak et al. 1996, Klimesch, Sauseng et al. 2007, Mazaheri and Jensen 2010) and event related desynchronisation (ERD, a decrease in power relative to baseline) is believed to represent increased excitability and cortical activation (Pfurtscheller, Neuper et al. 1994, Pfurtscheller and Lopes da Silva 2005). To measure these oscillations, they must however travel through the various media from their origin to the electrodes.

From signal to the scalp

The brain, cerebral spinal fluid (CSF), skull and scalp all have particular electrical conductivity values, which along with the various convolutions of the brain lead to difficulties in interpreting the cortical source of a scalp EEG signal. The calculation of how the activity of a source in the brain would be transmitted to the electrodes on the scalp is known as the forward problem. Using anatomical scans of an individual's head, it is possible to segment the scalp, skull, brain and CSF as well as model the convolutions of the brain and so solve the forward problem

(Vorwerk, Clerc et al. 2012). It is more difficult however to solve the inverse problem and calculate the origin of a signal within the brain based on scalp electrode measures,. Theoretically it is possible for the electrode signal to have an infinite number of origins, therefore constraints have to be placed, e.g. restricting the number of locations from which the signal could have arisen which allow estimates of specific types of EEG signal to be localised (Van Veen 1997).

Estimation of the Inverse Problem: Source Localisation

There are three main methods used to estimate the location and magnitude of neural sources: dipole fitting, non-adaptive distributed source imaging, and adaptive distributed source imaging. Dipole fitting attempts to estimate one or more neural current sources, specifically their location and orientation, within the brain. For non-adaptive distributed source imaging thousands of dipoles across the brain are systematically estimated. A grid is created across the brain (lead-field grid: 0.5-1cm lattice) each point representing a dipole. At each of the dipoles, specific electrode weights (known as the lead-field) are calculated by solving the forward problem i.e. how the source would be measured at each electrode given the position of the electrodes relative to the brain. In this manner, multiplying the data at each electrode by the lead-field at each of the dipoles provides an estimate of activity at that dipole.

Similarly, adaptive distributed source imaging also uses a lead-field for thousands of dipoles throughout the brain, with a spatial filter calculated based upon the lead-field and the covariance of the data across time at each electrode (a covariance matrix) (Barnes and Hillebrand 2003, Hillebrand, Singh et al. 2005, Cohen 2014). An assumption is made here that the sources are uncorrelated with partial/full correlation potentially leading to cancellation of the signal (Sekihara and Scholz 1996). Creation of a spatial filter requires that the covariance matrix is inverted which can result in producing a numerically unstable result therefore a regularisation parameter is often used to stabilise this process (Fuchs 2007) which leads as well to a form of smoothing of the final generated source localisation data. Multiplying the data

by the spatial filter at each dipole enables source estimation at each of these locations. Beamforming is the most commonly used adaptive imaging method, it has advantages over the non-adaptive method in that the filters calculated will differ depending upon the data used, which is thought to provide more precise temporal and spatial estimates of activation (Kucukaltun-Yildirim, Pantazis et al. 2006).

There are many types of beamformer, two commonly used are: linearly constrained minimum variance (LCMV) (Van Veen 1997) and dynamical imaging of coherent sources (DICS) (Gross, Kujala et al. 2001). LCMV calculates sources based on temporal changes in the data, while DICS uses frequency domain data (with this technique a cross-spectral density matrix would be calculated instead of a covariance matrix). DICS is primarily used for coherence analyses, i.e. to locate coherent regions (Gross, Kujala et al. 2001). LCMV beamforming is the method utilised in this thesis, it is capable of generating maps of ERS/ERD throughout the brain by filtering data into a frequency band of interest (e.g. α/β) prior to generation of the covariance matrix. Spatial filters generated using frequency specific data can be used to ascertain an estimate of the power at each grid position (also known as a virtual electrode: VE) across time (Barnes and Hillebrand 2003). Maps of ERD/ERS across the brain relating to a stimulus can be calculated at each VE by taking the difference between the estimated power during the stimulus period and a defined baseline, dividing this by the baseline power acts as a normalisation procedure which helps control for source leakage. These maps can be used to locate maximum regions of ERS/ERD and so define a VE from which a timecourse can be extracted for further analysis (see Figure 1.7).

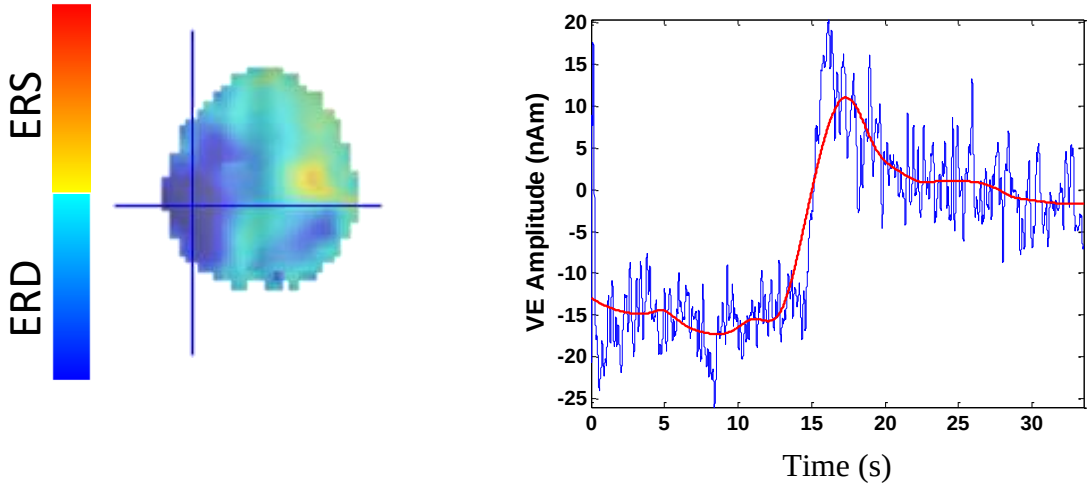

Figure 1.7. Examples of ERD/ERS map and an average VE timecourse. *Left,* a ERD/ERS map generated using an LCMV beamformer from the contrast between a stimulus period (MNS) and a baseline period of no stimulation in between MNS blocks, blue denotes ERD, red to yellow, ERS. The map can be used to find a VE of maximum ERD from the motor cortex region (shown here with a cross hair). *Right*, data extracted from the maximum ERD location is Hilbert transformed and the average power over all trials plotted (baseline corrected). The first 14 seconds relating to the stimulus period and the remaining time a rest period.

1.7.2 Magnetic Resonance Spectroscopy

As described above, understanding links between measures of GABA and Glutamate and the magnitude of NBR can shed light on the physiological foundations of this BOLD response component. It is located in two seemingly distinct neuronal regions, the cytoplasm and the pre-synaptic boutons (Stagg, Bachtiar et al. 2011), having specific roles of metabolism and neurotransmission respectively (Martin and Rimvall 1993). Magnetic resonance spectroscopy (MRS) provides a way of measuring baseline GABA and glutamate, among other macromolecules, levels in vivo. Although various MRS sequences exist, the most popular for measuring GABA is the point resolved spectroscopy (PRESS) sequence. This technique, explained in greater detail below, is unable to dissociate between the cytoplasmic and pre-synaptic GABA, therefore only a single measure of total GABA can be garnered. It is assumed

that the pre-synaptic GABA concentration is correlated with the overall level measured (Stagg, Bachtiar et al. 2011).

The MRS sequence used in this thesis (see Figure 1.8 for overview) uses the same principle of exciting hydrogen nuclei as other MRI sequences (e.g. T2/T1 scans). Protons in different molecules experience different resonant frequencies due to their chemical composition. This is due to the local magnetic field which can be calculated by: B_0 minus the induced and opposing ('shielding') magnetic field from the surrounding electrons. These small differences in resonance frequencies are predictable for specific compounds and are known as chemical shift, measured in relation to a reference standard with their units defined in parts per million (ppm) (Harris, Becker et al. 2008, Puts and Edden 2012). For the quantification of metabolites, a reference concentration value can be used, most often water (Blüml 2013). The spectra from a single MRS voxel is typically analysed using a fitting procedure, based upon the predicted chemical shift, with the area under the curve of the fit providing an estimate of the concentration of each compound (see Figure 1.9).

GABA molecules specifically contain three aspects that have different chemical shifts (2ppm, 2.3ppm and 3ppm: see insert in Figure 1.9) each of which overlap with other metabolites that are found in the brain in greater concentration than GABA: NAA, creatine. Edited MRS sequences use the feature of J-coupling, whereby spins in one molecule affect those in the same molecule, in an attempt to circumvent this issue. An editing RF pulse can be applied that affects signals at 1.9ppm which is linked to one aspect of the GABA molecule but is also J-coupled to the GABA signal at 3.0ppm (Puts and Edden 2012). The implementation of interleaved edit-on and edit-off scans (such as in the PRESS sequence: Figure 1.8) means that by subtracting the edit-on from the edit-off scan the GABA signal at 3.0ppm can be resolved along with glutamate and glutamine at 3.75ppm (Mullins, McGonigle et al. 2014). As glutamine and glutamate have similar molecular structures their chemical shifts are difficult to separate therefore a single measure is taken, referred to as Glx.

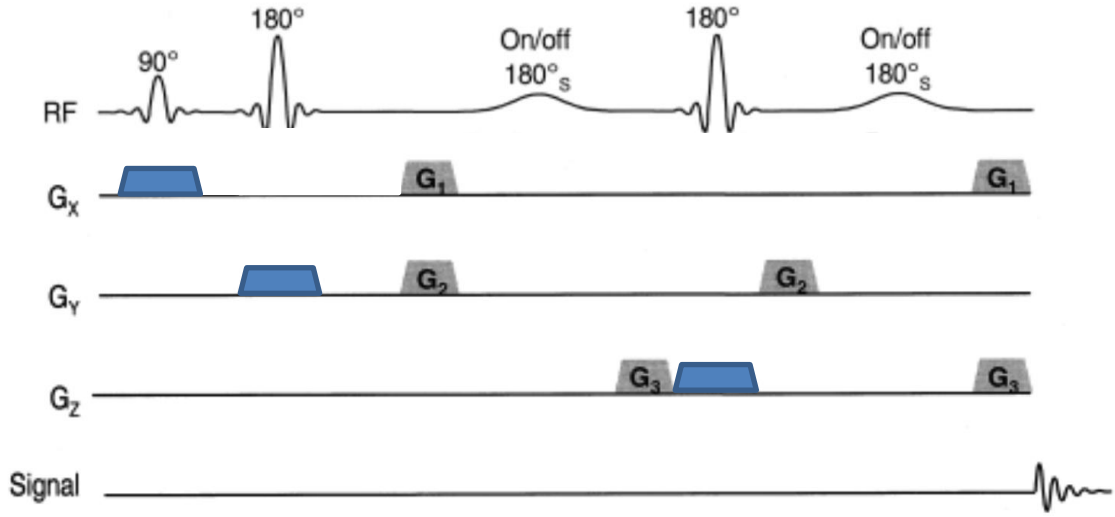

Figure 1.8. MEGA-PRESS sequence overview. This sequence uses consecutive RF pulses of 90º, 180º and 180º (shown on top line), each simultaneous with a gradient change (blue boxes), which are orthogonal to one another (here: x-, y-, and then z-directions). This excites only those spins within the selected voxel of interest. For single voxel MRS no readout gradient is used as no spatial encoding is required, only the frequency. To gather information about the level of a particular molecule e.g. GABA a frequency selective pulse is be applied either side of the last 180º pulse (shown here as On/off 180º pulses). Due to the water signal being much larger than any other signal measured (~40000x GABA levels), water suppression is carried out to prevent swamping the other signals (Mullins, McGonigle et al. 2014). For PRESS sequences, this is most often carried out using additional gradient changes (G1, G2 and G3 boxes), known as MEGA (Mescher-Garwood). The sequence in its entirety is known as MEGA-PRESS. Figure adapted from (Mescher, Merkle et al. 1998)

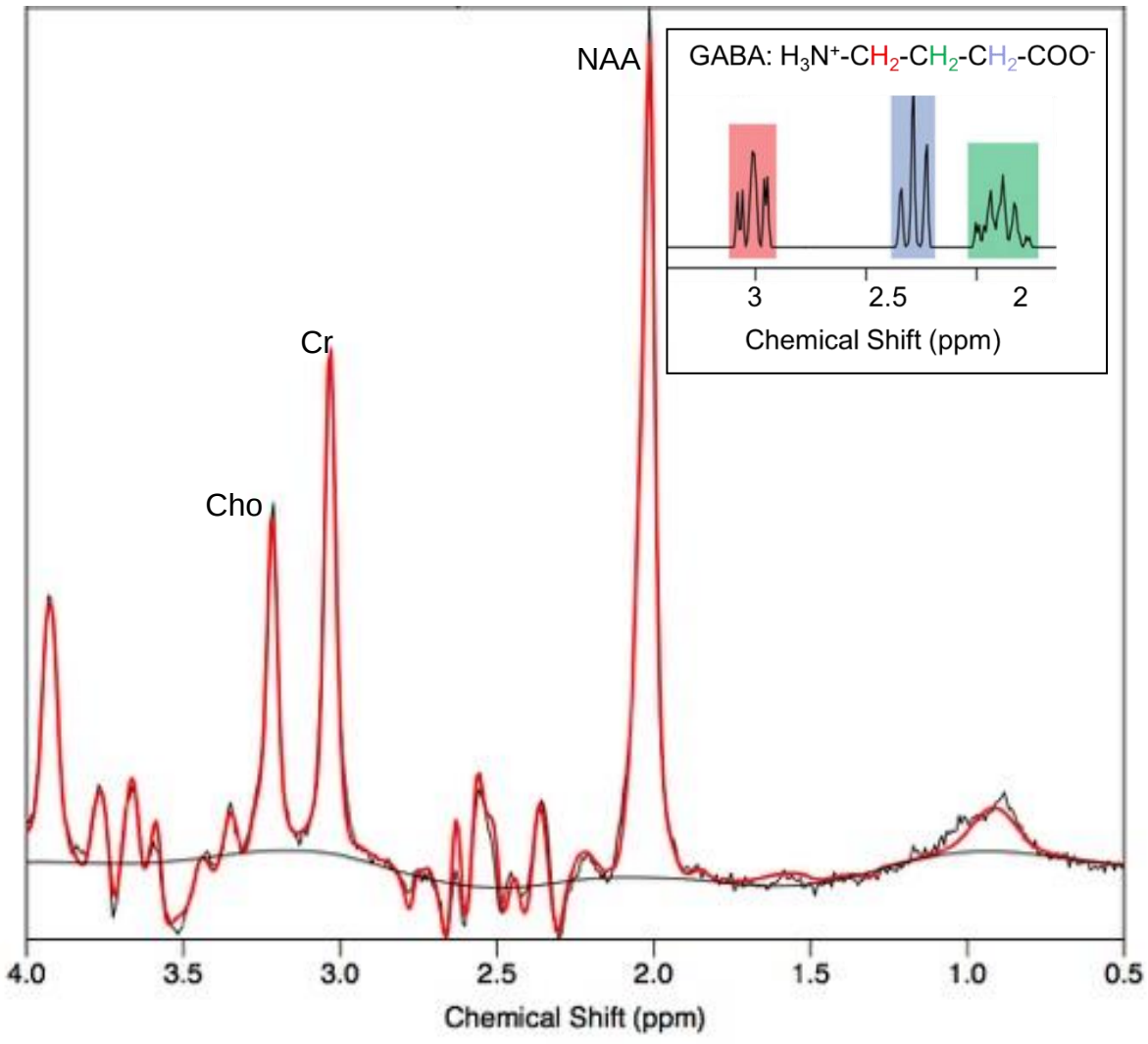

Figure 1.9. An example of MRS spectra data, with fitted line. Following Fourier transform, the raw data is shown as the black line, with a fitted red line over the top. The main peaks, N-acetyl aspartate (NAA), creatine-containing compounds (Cr) and choline-containing compounds (Cho) are highlighted. Inset the chemical structure of GABA is shown, with the regions within the spectra highlighted that match each specific aspect of the molecule where each of these is coupled to one another (J-coupling). The area under the fit of the GABA spectra would correspond to an approximation of the molecular concentration (Inset adapted from (Puts and Edden 2012)).

1.7.3 Transcranial magnetic stimulation

As described above, TMS has been used to study the interactions between left and right motor cortices, in Chapter 5 we use TMS as a measure of cortico-spinal excitability therefore the method is described in detail here. TMS uses the principle of electromagnetic induction to excite cortical neurons. An electric current is passed through a coil of wire enclosed in plastic (often the figure-8 coil) which creates a pulse of magnetic field (~2T), which in turn induces an electric field in the region of the brain directly underneath the coil (Thut and Miniussi 2009). The shape of the coil and strength of the pulse determines how focal the field is and the depth to which the magnetic field will propagate, although the field only penetrates to a maximum of a few centimetres (Thut and Miniussi 2009, Deng, Lisanby et al. 2013). Using a Figure 8 coil the focal point of the magnetic field sits at the central part of the coil, and it is at this region that the largest electric current is generated in the cortex (Hallett 2007, Thut and Miniussi 2009).The electric field generated by the TMS pulse interacts with the neuronal activity already present in the system, generating action potentials in the cortical neurons. The overall outcome of the neuronal response is highly dependent upon the direction of the current generated which is specific to the orientation of the coil on the scalp and also its distance from the scalp (Walsh and Cowey 2000).

Although TMS pulses can be applied repetitively, in this thesis single pulse TMS is used. Single-pulse TMS is often utilised for studying various aspects of cortical physiology, especially in the motor system. This is possible because specific regions of the primary motor cortex (M1) send outputs to specific muscles via the spinal cord. Stimulating specific regions of M1with pulse intensities above a subject's motor threshold level leads to contraction of the corresponding muscle measurable using electromyography (EMG; which measures electrical activity in a muscle) as a motor evoked potential (MEP; see Figure 1.10). The MEP is widely seen as a measure of CSE: the excitability of the entire circuit, from the cortex through the spinal cord and into the muscle (Rothwell 1997, Di Lazzaro, Oliviero et al. 2004, Chen, Cros et

al. 2008). As such this is a complex physiological measurement, the peak to peak amplitude (P2PA) of which captures a summation of repeated descending cortico-spinal volleys which at present cannot be dissociated using single pulse TMS (Bestmann and Krakauer 2015). A TMS pulse results in large scale activation of both excitatory and inhibitory neurons of the cortex at pre- and post-synaptic regions, with MEP amplitude being a result of both this activity and the excitability of spinal neurons. Increasing TMS pulse intensity over the motor cortex relates to an increase in the number of descending volleys measured at the spinal cord (Di Lazzaro, Ziemann et al. 2008) a summation of which are required to increase the membrane potential of the spinal cord above threshold and subsequently initiate an action potential in the muscle to induce a motor evoked potential (Groppa, Oliviero et al. 2012). The descending volleys are generated by different regions of the motor cortex, with early direct-waves (D-waves) a result of activation of fast conducting pyramidal neurons (Patton and Amassian 1954) while slower indirect-waves (I-waves) are a result of, first, the activation of cortico-spinal pyramidal tract neurons and later they are generated from intra- and trans-cortical activation (Fisher, Nakamura et al. 2002) with supplementary motor area (SMA) connectivity playing a potential role (Ziemann and Rothwell 2000).

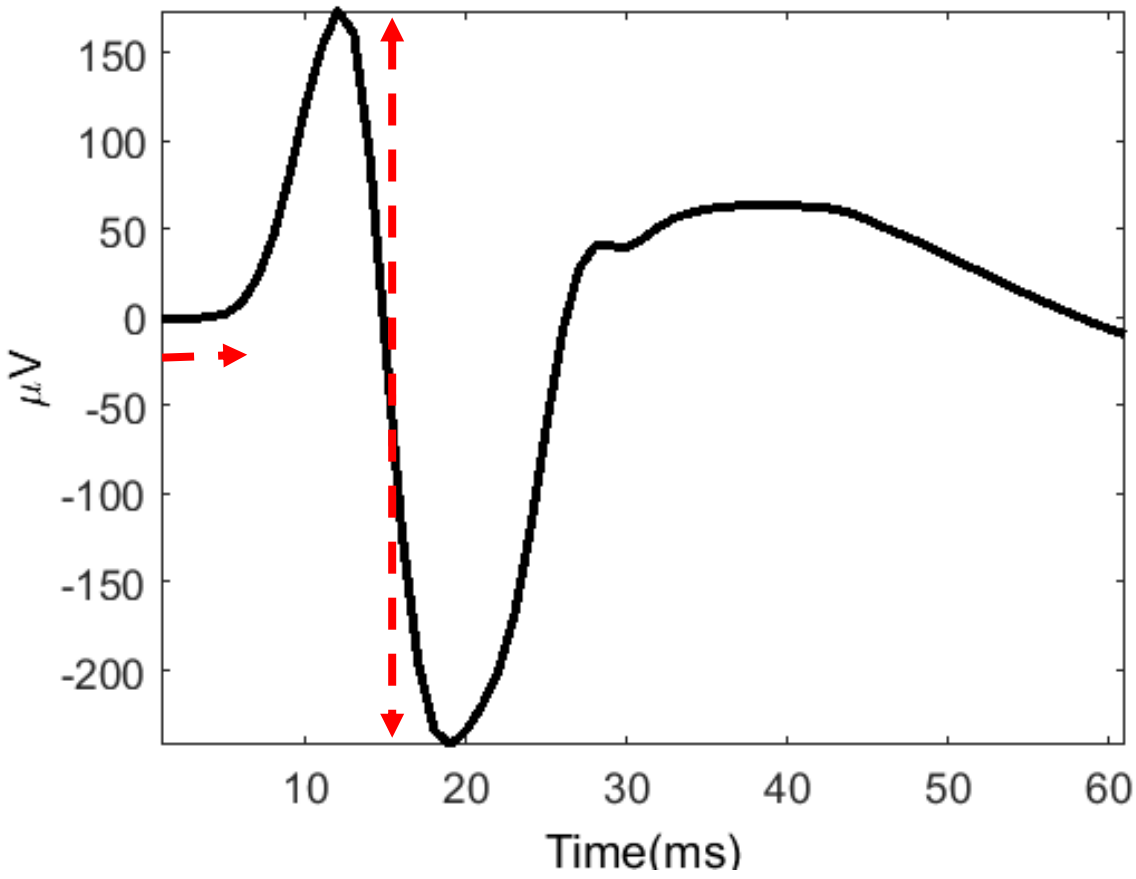

Figure 1.10. Exemplar MEP. The black line shows an example of an MEP averaged over 14 trials recorded from the left first dorsal interosseous (FDI) muscle. The red vertical dashed line shows the approximate P2PA, this measure has widely been used to test for changes in CSE due to sensory stimulation as well as after opposite hemisphere TMS stimulation. The short horizontal red line shows the approximate latency of the MEP, this relates more to the time taken for the first signal to reach the muscle (conduction time) (Bestmann and Krakauer 2015).

1.7.4 Diffusion Weighted Imaging

Diffusion is the term describing the movement of particles from a region with high, to a region with lower, concentration. Media in which diffusion can occur equally in any direction are known as isotropic and can be described by a single number (diffusion coefficient: D). In biological tissue various structures present prevent diffusion occurring equally in all directions e.g. axonal white matter fibres, such media are anisotropic and cannot be described by a single number but by a 3D matrix (diffusion tensor). Diffusion tensor imaging (DTI) is the most

commonly used DWI, which provides a measure of the direction of diffusivity of water within each voxel of the brain. In the brain, white matter fibres would result in direction specific diffusion and grey matter more isotropic diffusion. A pulsed gradient spin echo is the common basis of a DTI sequence (shown in Figure 1.11). This uses a 90^{o} RF pulse with slice selection followed by a pair of identical strong diffusion sensitising gradients, in between which is a 180^{o} RF pulse with slice selection (Huettel, Song et al. 2014). Only moving spins are affected by the gradient changes and as such movement in a single direction can be distinguished. A large number of different gradient directions (between 64-256) are required to accurately measure the diffusion tensor, an array of numbers expressing the diffusion rate in the three principle directions (x,y,z). An EPI readout is also acquired without the sensitising gradients (b0, where the b is the strength of the gradient), this is used as a baseline measure during analysis.

For most analyses, the diffusion tensor for each voxel is represented as a 3D ellipsoid representing the main direction of diffusion within that voxel (see Figure 1.12) (Jellison, Field et al. 2004). The strength of a voxel's anisotropy is commonly designated as a single number between 0 (isotropic: a circular ellipsoid representing no principle diffusion direction) and 1 (anisotropic; cigar shaped ellipsoid representing strong diffusion direction), calculated using the eigenvalues and known as fractional anisotropy (FA) (Basser and Pierpaoli 2011). Methods have also been developed to estimate structural connectivity between regions: deterministic and probabilistic tractography. Deterministic tractography uses the ellipsoids in each voxel to track the path of least resistance between two specified regions providing a number of 'streamlines' (connections) between them. Following tracts in this manner can lead to dead ends (e.g. via isotropic voxels), identifying non-existent tracts (Descoteaux, Deriche et al. 2009), or not detecting known tracts which is thought to relate to voxels possibly containing more than one tract each with a different direction (Behrens, Berg et al. 2007). Probabilistic tractography was developed to overcome the rigidity of deterministic tractography, by more realistically assuming that there is a distribution of directions within each voxel rather than a

single fixed direction. With a probability distribution for each voxel in the brain, multiple attempts can be made to connect two regions of interest together resulting in multiple streamlines and ultimately a probability of connectivity via tracts (Behrens, Johansen-Berg et al. 2003). Neither of these tractography methods provides a direct measure of underlying white matter fibre tracts, but instead an approximation of them. Problems still exist for DTI such as partial volume effects, and voxels containing crossing fibres which become difficult to interrogate (Jones, Knosche et al. 2013).

.

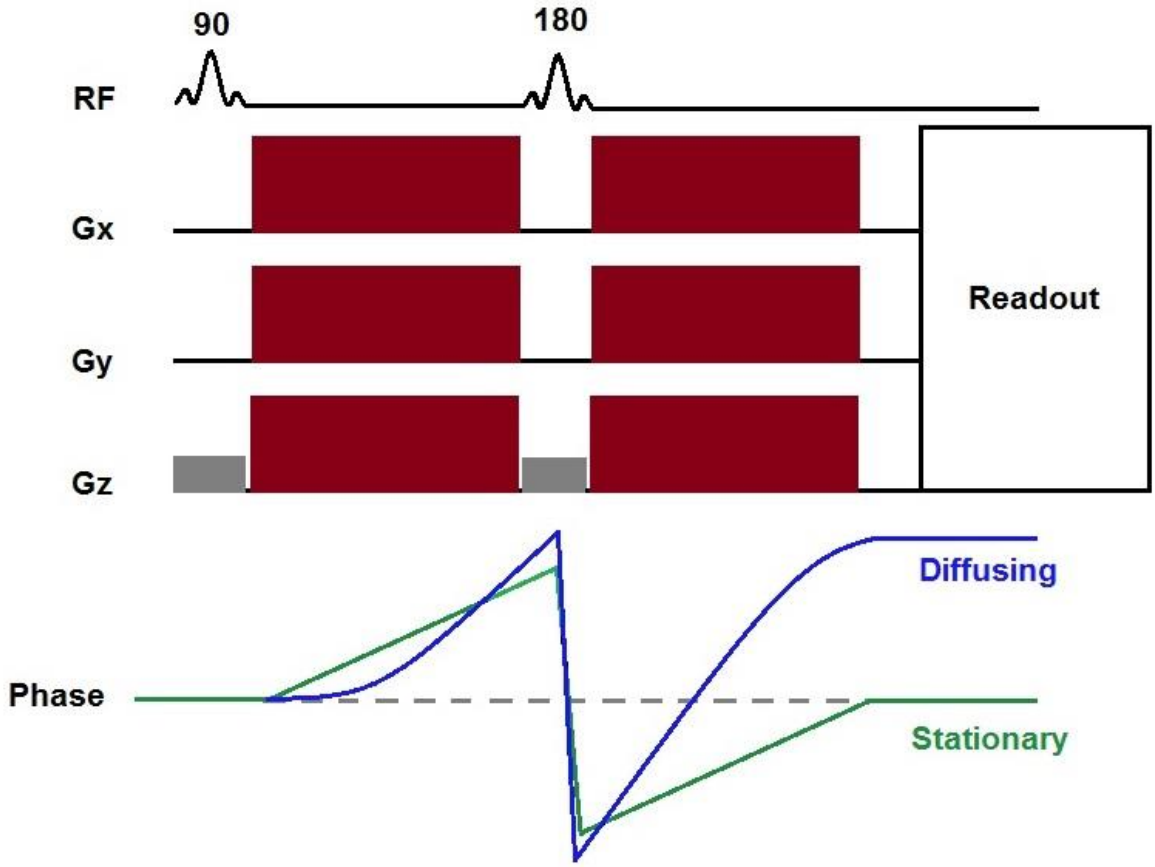

Figure 1.11. Basic DTI sequence. A 90º RF pulse leads to spin phase coherence, the first diffusion sensitising gradient (red block) then de-phases the spins. A 180 inversion pulse flips the spins allowing the second sensitising gradient to 're-phase' the signal. As depicted in green, it is only stationary spins which are unaffected by these gradient changes, while moving spins become de-phased and so distinguishable. A subsequent EPI readout is carried out in order to measure the MR signal. Grey block = slice selection gradient change. Gx, Gy and Gz relate to the gradients in the x, y and z direction respectively.Adapted from (Huettel, Song et al. 2014) and Allen D. Elster [MRIquestions.com])

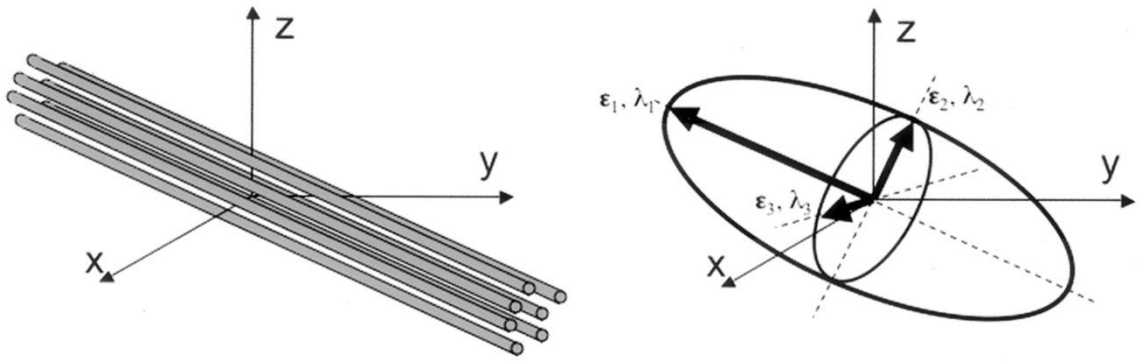

Figure 1.12. Diffusion ellipsoid. This is a cartoon image of diffusivity within a single voxel. The initial scanner reference Z, Y and X directions are shown. *Left*, highlights a structure, white matter 'fibres', which preferentially allow diffusion along their length. *Right*, shows the diffusion data represented as an ellipsoid whose frame of reference is changed to match that of the primary direction of diffusion (ε1), along the length of the 'fibres'. The ellipsoid is represented as three orthogonal vectors (ε1, ε2 , ε3: eigenvectors), with three lengths (λ1, λ2, λ3: eigenvalues, where λ1>λ2>λ3) associated with them. Figure adapted from (Jellison, Field et al. 2004)

1.8 Thesis motivation and aims

NBRs, despite being found in many regions during sensory stimulation, are poorly understood. The aim of this thesis is to investigate the origin and functional relevance of IM and CM NBRs that are evoked by simple sensory stimuli and motor tasks. The complex nature of the BOLD response requires that we use multiple neuroimaging measures to characterise its various key aspects: vascular changes, metabolic changes and neuronal changes. As such, combined BOLD-ASL-EEG measures will be taken during sensory stimulation, connectivity measures will also be acquired in order to investigate the relationship between the PBRs and NBRs. The focus of the thesis then moves to the functional nature of the IM and CM NBRs, with TMS and MRS measures used to further develop our understanding of these signals.

1.8.1 Main aims:

- Further understand the relationship between neuronal activity and IM/CM NBRs during stimuli.
- Decipher the metabolic and vascular components of the IM/CM NBRs.
- Ascertain similarities/differences in neuronal, metabolic and vascular origin between the IM and CM NBRs.
- Investigate whether the functional and structural connectivity between the PBR and IM/CM NBR regions relates to the responses themselves.
- Explore the relationship between functional measures of cortical excitability and IM/CM NBRs.

Chapter 2 uses simultaneously measured BOLD-ASL-EEG during basic motor tasks and visual stimuli to predominantly assess the relationship between neuronal excitability and the IM/CM NBRs via the BOLD-EEG data.

Chapter 3 utilises the same dataset but explores the metabolic and vascular components of the stimulus evoked NBRs using the BOLD-ASL data, in particular comparing whether IM and CM arise from similar or different neuro-metabolic coupling.

Chapter 4 investigates the functional and structural connectivity between the PBR and IM/CM NBR regions from the same dataset. Here, the effect of the connectivity is examined to find how subject's sensory cortex connectivity relates to the size of their task evoked NBRs and the PBR:NBR relationship.

Chapter 5 focusses on whether stimulus derived NBRs relate to measureable behavioural changes. TMS-EEG data and separately acquired BOLD and MRS data during sensory stimuli are first analysed separately here prior to combining the data in the following chapter.

Chapter 6 explores how the MRS data relates to or explains the NBRs, to find whether the NBR is driven in part by the underlying neurotransmitters. Changes in CSE are also related to the NBR to explore any functional role of the NBRs.

Chapter 7 brings together the results from throughout the experimental chapters and draws overarching conclusions relating specifically to NBRs. This chapter also covers future work which stems from the

CHAPTER 2

EEG CORRELATES OF INTRA- AND CROSS MODAL NEGATIVE BOLD RESPONSES IN VISUAL AND SENSORIMOTOR CORTEX

2.1 Abstract

Previous work has investigated the electrophysiological origins of intra-modal NBR but little attention has been paid to the origin of cross-modal NBRs. In the current study we use simultaneous EEG-fMRI recordings to assess the neural correlates of both intra- and cross modal responses to left-hemifield visual stimuli and right hand motor tasks and also evaluate the balance of activation and deactivation between the visual and motor systems. We study within and between-subject covariation of EEG and fMRI responses to both task types aiming to uncover how patterns of event-related desynchronization/synchronisation (ERD/ERS) of alpha/beta oscillatory response relate to NBR in the two sensory cortices.

We show that both visual and motor tasks induced intra and cross-modal NBR respectively, such that visual stimuli evoked NBR in the motor cortex and vice versa. In the EEG data, bilateral intra-modal alpha/beta ERD responses were consistently observed to both tasks, but the cross-modal response varied across subjects between an ERD and an ERS. We found

that both the mean cross-modal EEG and fMRI response amplitudes showed a small increase in magnitude with increasing task intensity.

In response to the visual stimuli, subjects displaying cross-modal ERS of motor beta power displayed significantly larger magnitude cross-modal NBR in motor cortex. The opposite pattern was however observed during motor tasks, where larger cross-modal ERD of visual alpha power was associated with larger cross-modal visual NBR. Single-trial correlation analysis provided further evidence of relationship between EEG and NBR, as motor cortex beta responses to motor tasks were significantly negatively correlated with cross-modal visual cortex NBR amplitude, in addition to positively correlating with intra-modal motor cortex PBR.

Taken together we provide a new body of evidence that the coupling between BOLD and low-frequency (alpha/beta) sensory cortex EEG responses extends to cross-modal NBRs, whose amplitude is linked to both between and within subject variability in ERD and ERS responses.

2.2 Introduction

As discussed in Chapter 1, unilateral stimulation of a single sensory modality induces both an IM and CM NBR in the brain's sensory cortices. Previous work has investigated the electrophysiological origins of IM NBR but little attention has been paid to the origin of CM NBRs. In the current study we use simultaneous EEG-fMRI recordings to assess the neural correlates of both IM and CM responses to left-hemifield visual stimuli and right hand motor tasks and also evaluate the balance of activation and deactivation between the visual and motor systems.

2.2.1 EEG-fMRI

The high spatial resolution of fMRI and the high temporal resolution of EEG suggest that measuring the two simultaneously would provide an optimal measure of brain activity. It is

possible using simultaneous EEG-fMRI to study how the fluctuations in one measure relate to those occurring concurrently in the other. As described in Chapter 1, the fMRI BOLD signal is only an indirect measure of neuronal activity (Logothetis, Pauls et al. 2001, Attwell, Buchan et al. 2010), whereas the EEG signal directly measures changes in scalp electric field that result from cortical neuronal activity (Lopes da Silva 1991). EEG can therefore be used to inform as to how large scale neuronal activity, across a range of frequencies, relates to BOLD responses. Although it is easier to measure EEG and BOLD responses separately, it is only the average responses that can then be compared. Any cognitive or physiological variation between the two sessions would likely result in different neuronal responses and so reduce the ability to compare directly between the data sets. Although on the surface combining these techniques appears to open up the holy grail of neuroimaging, the technique suffers from inherent issues of noise and artefacts that accompany the recording of very small EEG signals using metallic electrodes and cables within a massive magnet. Specialist MRI compatible EEG systems are required to enable the combined measurement. Even so, the signals gained from simultaneous EEG-fMRI recordings have lower signal to noise ratio (SNR) than when recorded separately as each suffers from artefacts related to the other measure, as described below.

There are three main artefacts that occur in EEG data when recorded in the MRI environment, the pulse artefact, the gradient artefact and motion artefact (Mulert and Lemieux 2010). The pulse and motion artefacts arise due to the nature of electromagnetic induction whereby movement of conductive EEG leads and electrodes within the MRI static magnetic field results in creation of electric forces (voltage) within those conductors. As such, even tiny (<1mm) head movements, caused by the cardiac pulse, can lead to an artefactual (non-neuronal) signal passing through the EEG leads to the amplifiers (Debener, Kranczioch et al. 2010). These pulse artefacts increase with increasing magnetic field strength of the scanner and differ in both amplitude and timecourse when compared between EEG channels (as movements due to the pulse differ across the head) (Debener, Mullinger et al. 2008). In order

to remove/reduce the artefact, an electrocardiogram (ECG) channel is used to measure the cardiac cycle from an electrode attached to the subject's chest (below the clavicle), using the same amplifier as the EEG data. More sophisticated measures of the ECG can be gained from using a four lead MR compatible vectorcardiogram (VCG) which is less susceptible to the static magnetic field (Chia, Fischer et al. 1999, Mullinger, Morgan et al. 2008). The gradient artefact is only present during slice acquisition, due to the magnetic field gradient changes required to measure the MRI signal (Ritter, Becker et al. 2010). These artefacts are more regular than the pulse artefacts, as they relate to the consistent change of the MRI gradients, but do differ channel by channel due to each channel experiencing a different magnetic field in its location (Eichele, Moosmann et al. 2010). It is important to record the full extent of the gradient artefacts and as such it is recommended that the EEG sampling is synchronized to the scanner gradient changes as well as the TR being an integer multiple of the EEG sample time (Mullinger, Morgan et al. 2008). The main technique used to remove the gradient and pulse artefacts is average artefact subtraction. This corrects each channel and each artefact in turn, by taking a local average of a number of artefacts surrounding the one to be corrected and subtracting the average of them from it (Allen, Polizzi et al. 1998). This subtraction technique is reliable so long as no movements occur alongside the artefacts, which would cause variations from one to another leading to residuals.

Reducing the movement of equipment due to scanner vibration during scanning can also provide a way of minimising the artefacts prior to correction, for example MRI scanners have helium pumps which can cause vibrations and hence artefactual signal, so it is recommended that this is switched off during scanning (Ritter, Becker et al. 2010).

The B_0 magnetic field can also be susceptible to the presence of the EEG cap, whereby electrodes can produce inhomogeneity and so, signal loss (Mullinger and Bowtell 2010). These artefacts are seen mainly on the surface of the scalp, penetrating up to approximately

10mm, but not to the depth of brain tissue (Krakow, Allen et al. 2000). Such loss can be countered with adequate employment of shimming (Mullinger and Bowtell 2010).

2.2.2 Study measurements

Although previous studies have found that NBRs in some contexts are dependent to a large degree upon CBF changes (as discussed in Chapter 1: (Harel, Lee et al. 2002, Kannurpatti and Biswal 2004, Puckett, Mathis et al. 2014)), we focus here primarily upon the supposed neuronal aspect of the IM and CM NBR which is the reason for measuring combined EEG and fMRI. We aim to extend previous combined EEG-fMRI studies in humans, discussed in detail in Chapter 1, which have indicated links between decreases in neuronal activity and IM NBRs (Mullinger, Mayhew et al. 2014, Maggioni, Molteni et al. 2015). In particular, we aim to study how changes in α/β frequency EEG power are related to IM and CM NBR during visual stimuli and motor tasks. CM NBR in visual cortex have been widely reported during auditory stimulation, and vice versa (Laurienti, Burdette et al. 2002, Hairston, Hodges et al. 2008, Mozolic, Joyner et al. 2008, Ciaramitaro, Chow et al. 2017). Due to the difficulty of reliably measuring EEG responses from auditory cortex and the requirement of quiet fMRI sequences for reliable BOLD measurement, we focus instead on investigating reciprocal responses between visual and sensorimotor cortex which have previously shown evidence of CM inhibitory effects on each other in rats (Iurilli, Ghezzi et al. 2012).

We also assess how stimulus intensity of motor task and visual stimuli relates to the magnitude of IM and CM NBRs in the respective cortices, which has not been investigated for CM NBRs, as well as visual and also somatosensory IM surround NBRs (Shmuel, Yacoub et al. 2002, Klingner, Hasler et al. 2010). However, the interplay between motor and visual cortices in this way has not been studied.

In the current study we used multimodal neuroimaging to record EEG, BOLD and CBF responses induced by separate visual and motor tasks to investigate whether:

1) CM NBR is elicited by motor tasks and visual stimuli and whether CM and IM NBRs are modulated by task/stimulus intensity
2) There are intrinsic links between:
    a. IM and CM NBRs
    b. IM and CM EEG responses
3) IM NBR and IM EEG responses are related therefore providing evidence for a neuronal origin of the IM NBR
4) CM NBR and CM EEG responses are related therefore providing evidence for a neuronal origin of the CM NBR

We hypothesise that:

1) CM NBR would be elicited by motor tasks and visual stimuli with both modulated by stimulus intensity
2) a) IM and CM NBRs would be positively correlated
    b) IM and CM EEG responses would be negatively correlated
3) IM NBR and IM EEG responses would show a negative correlation
4) CM NBR and CM EEG would show a negative correlation

2.3 Methods

17 healthy subjects (7 female; mean age 30.6 ±5; all right handed - tested using the Edinburgh handedness inventory) all gave informed consent to take part in the experiment. The University of Birmingham ethics committee approved the experimental procedures.

2.3.1 Paradigm

Four separate experimental runs of simultaneous BOLD-cerebral blood flow (CBF)-EEG data were recorded as subjects performed, in each run, one of two motor tasks and separately passively viewed two intensities of visual stimuli.

The visual stimuli were left-hemifield checkerboards of either 100% (High) or 10% (Low) contrast with pattern reversal at 3Hz (frequency chosen to maintain robust responses whilst avoiding contamination of the EEG α oscillation with stimulus-evoked responses). Subjects were instructed to fixate their eyes throughout on a central cross-hair to induce NBRs in ipsilateral visual cortex.

Subjects also performed either a “complex” Tap or a “simple” Grip Motor task using their right hand only. The Tap task (Tap) involved a paired finger-thumb opposition, tapping each finger to the thumb in a sequence from index finger to little finger, reversing and repeating. For the Grip task (Grip), a small, easily deformable rubber ball was repeatedly squeezed between the fingers and thumb in a rhythmic manner. Motor tasks were visually cued by central display of the word “Grip” or “Tap” throughout the stimulation period, and movements performed at a comfortable speed of approximately 2Hz. Instructions were given prior to testing for both tasks and all subjects underwent a ten-minute period of familiarisation with the Tap task and the Visual High stimuli outside of the scanner.

Each of the four runs started with a 30 second period of resting-fixation to enable measurement of the fMRI signal baseline. This was followed by 24 pseudo-randomly ordered trials of High, Low and either Tap or Grip. All trials consisted of 14s of stimulation followed by 20s of resting fixation. Of the 24 trials per run, 12 were one of the motor tasks, 6 were High and 6 Low. Thus, visual and motor trials were performed sequentially in separate trials. While in any single run either Tap or Grip was performed, never both, with the order of runs counterbalanced between subjects.

The intensities of motor task complexity and visual stimulus contrast were used to modulate BOLD response magnitude and to investigate question 1 posed above - whether CM NBR was elicited by motor task and visual stimuli and whether the IM and CM NBRs were modulated by stimulus intensity.

2.3.2 Data Collection

EEG

The EEG signal was recorded at 5 kHz using a 63-channel MR-compatible EasyCap following the extended international 10-20 system layout. An electrocardiogram (ECG) channel was also attached just below the subject's clavicle. Electrode AFz was used as the ground and FCz used as the reference electrode. All electrode impedances were maintained below 20 kΩ. Data were acquired using BrainAmp MR-plus amplifiers (Brain Products, Munich) and Brain Vision Recorder (Version 1.10).

Gradient artefacts were minimised by positioning the subject such that FP1 and FP2 were at the iso-centre of the scanner's static field whilst equipment related artefacts were minimized by isolating the EEG amplifiers from the scanner bed and ensuring cryopumps were off during acquisition (Mullinger and Bowtell 2011). For consistent waveform sampling EEG and MR scanner clocks were synchronised and the TR made a multiple of the EEG sampling period (Mandelkow, Halder et al. 2006, Mullinger, Morgan et al. 2008). A Polhemus fastrak 3D system (Polhemus, Vermont, USA) was used to digitize electrode positions for co-registration to the subjects T1 scan.

fMRI

FMRI data were acquired with a Philips Achieva 3T MR scanner (Philips Medical Systems, Best, Netherlands) using a whole body transmit plus 32 channel head receive coil.

Prior to the experimental runs subjects underwent High and Tap trials during a 5-minute BOLD localiser scan. IViewBOLD (Philips real-time processing of fMRI data) was used to statistically map responses and locate the position of the primary motor (M1), and visual (V1) cortex, and the required oblique orientation of the axial slices to cover both sensory regions. The double acquisition background suppressed (DABS) FAIR sequence (Mullinger, Cherukara et al. 2017) was then used to acquire both BOLD and arterial spin labelling (ASL) data simultaneously (TR=2.6, TE=16ms (ASL), TE=26ms (BOLD), voxel size 2.65x2.65x5mm, 12 slices, 212mm FOV, SENSE factor 2.3, label delay 1400ms, T_{BGS1}/T_{BGS2} = 339ms/560ms, 174 volumes [tag-control pairs] per run). Between runs two and three a 5-minute resting-state DABS scan was also acquired where subjects were asked to keep their eyes open and centrally fixate. A local anatomical image and a whole-head T1 anatomical image (1mm isotropic resolution) were also acquired to aid co-registration.

Throughout all scans, the Philips scanner vector cardiogram (VCG) and respiratory monitors were used to record cardiac and respiratory cycles respectively.

2.3.4 Pre-processing and Analysis

EEG pre-processing

EEG data were pre-processed in Brain Vision Analyser 2 (Version 2.1) for pre-processing. Heart beat events were detected from peaks in the VCG data and used to mark cardiac cycles in the EEG data. MR gradient and pulse artefact correction was performed using sliding template average-artefact subtraction (21 events per template for both artefacts) (Allen, Josephs et al. 2000, Mullinger, Cherukara et al. 2017). The data were initially filtered between 1-70Hz and downsampled to 600 Hz. Noisy trials/channels were found via visual inspection and excluded from further analysis and data were re-referenced to an average of all non-noisy channels. Data were exported to the Fieldtrip open source Matlab toolbox

(http://www.ru.nl/fcdonders/fieldtrip (Oostenveld, Fries et al. 2011)) and then band-pass filtered into separate α (7-13Hz) and β (13-30Hz) frequency datasets for source analysis.

EEG beamforming analysis

Sources of α and β responses to visual and motor tasks were reconstructed using a linearly constrained minimum variance (LCMV) beamformer (Van Veen 1997) implemented in FieldTrip. Digitized EEG electrode positions were co-registered with the subjects' T1 image. A 4-shell, anatomically realistic volume conduction boundary element model (BEM), was created by segmenting each subject's T1 anatomical into separate scalp, skull, cerebro-spinal fluid and brain compartments (conductivities: 0.33, 0.0042, 1, and 0.33 respectively). A template grid (5mm spacing) was created from the MNI brain and transformed to each subject's anatomical space. The leadfield matrix at each location on the template grid in individual subject space was then calculated using their BEM.

The LCMV beamformer analyses were carried out for each subject using: i) all of their visual data combined and, separately, ii) all of their motor data combined. The combination of data over stimulus intensities was carried out because preliminary analysis had shown comparable spatial response locations between conditions of the same stimulus modality and the accuracy of beamforming is increased with increasing amounts of data (Brookes, Vrba et al. 2008). Separately for each task and for both α and β frequency bands, the LCMV beamformer, with a regularization parameter of 0.01%, was used to calculate a spatial filter (weights of each EEG channel at each leadfield grid position) using the full timecourse of all relevant trials (0-34seconds). These weights were then used to calculate the source power for each position in the template grid during the stimulus period (0.5-13.5s) and also, separately, during the baseline period (20.5-33.5s). A contrast was then calculated between the source power of the stimulus period and baseline: (stimulus-baseline)/baseline. This generated a power ratio map to localize both ERD (stimulus power lower than baseline) and ERS (stimulus power higher

than baseline) in oscillatory power in response to the stimuli. From these maps two virtual electrode (VE) positions of peak ERD power change were separately located. The maximum α ERD was located in visual cortex to all visual trials combined (vVE), and the maximum β ERD in the motor cortex to all motor trials combined (mVE).

Timecourses of α and β frequency activity were extracted from the vVE and mVE for each run and the absolute value of the Hilbert transform used to obtain oscillatory power timecourse. VEs were then epoched into single-trials separately for each stimulus condition: Grip, Tap, High and Low. For each VE each subject's data was normalized to a zero amplitude baseline by subtraction of their passive period (20.5-33.5s) mean amplitude. Separately for both α and β frequency bands, the IM and CM single-trial response amplitudes were then calculated from the respective VEs as the mean VE amplitude during the stimulus window (0.5-13.5s). For each subject we classified the IM and CM responses into either ERD or ERS depending on whether their mean stimulus power showed lower or higher power than the passive period respectively. Group IM and CM responses were each tested for significant changes from baseline (student's t-test vs zero amplitude). To answer question 2b posed above, we then calculated within- and between-subject correlations of response amplitudes. For brevity, and due to the high degree of similarity found between EEG α and β response amplitudes (see results section for further clarification), β data were used as summary measures of the motor cortex response to tasks (IM motor and CM visual) while α data were used as summary measures of the visual cortex response to tasks (IM visual and CM motor).

Finally, the trial-by-trial amplitude during stimulation of the IM and CM responses were separately mean-subtracted and then used to form regressors for subsequent general linear modelling (GLM) to localise fMRI responses that correlated with this neuronal activity. These analyses were used to test the question 3 posed above – whether IM/CM EEG responses were related to the IM /CM NBRs.

fMRI processing

BOLD and ASL data were separated and RETROICOR (Glover, Li et al. 2000) used to correct for physiological noise in the BOLD data. This correction is unnecessary for the ASL data due to the background suppression and short TE: nulling the tissue magnetisation signal to zero leads to a reduction in physiological noise (Garcia, Duhamel et al. 2005). Data were motion corrected using MCFLIRT (Jenkinson and Smith 2001, Jenkinson, Bannister et al. 2002) (FSL, http://www.fmrib.ox.ac.uk/fsl/) and interpolated to an effective TR of 2.6. Perfusion-weighted CBF images were formed by subtracting tag and control ASL image pairs while BOLD image pairs were averaged creating mean BOLD-weighted data. Data were normalised to the standard MNI template using FLIRT.

fMRI analysis

Two subject's data were removed from further analysis due to a large number of head movement artefacts >4mm, as identified from realignment parameters.

Separate GLM analyses of BOLD and ASL data were carried out using FEAT V6.0 in FSL. The main effect of each of the motor and visual conditions was modelled using a constant amplitude boxcar regressor along with the stimulus period EEG variability regressor described above. Separate GLMs were performed using the IM and the CM EEG measures. This resulted in six regressors per GLM per run (main effect: motor task relating to that run, High, Low, EEG power for motor, EEG power for High, EEG power for Low). Two separate GLMs were performed for each run at the first level incorporating either the IM or the CM EEG measures: IM (motor = mVE β, visual= vVE α) and CM (motor = vVE α, visual = mVE β).

All regressors were convolved with a double-gamma haemodynamic response function (HRF). Positive and negative (to identify NBRs) Z-contrasts ($z>2.0$) were computed for each regressor and cluster corrected ($p<0.05$). Subject average responses across all runs were calculated at

the second-level using fixed effects and then group average maps were calculated across subjects using mixed effects FLAME 1+2 (Woolrich, Behrens et al. 2004) cluster corrected ($p<0.05$).

Pearson's correlations were carried out between the IM PBR and IM NBR, IM PBR and CM NBR, and the IM NBR and CM NBR in order to answer question 2a posed above - assessing the links between the BOLD responses.

Masks

A motor cortex mask and a visual cortex mask were created using the Harvard-Oxford Cortical Structural Atlas. These masks were used to restrict the analysed group data to those voxels in the sensory modalities of interest.

Regions of interest (ROIs), 1.5 voxel radius (total 27 voxel) spheres, were centred upon voxels with greatest main effect BOLD statistical significance at the subjects second level GLM results within the relevant sensory mask region. The ROIs defined were in: 1) contralateral M1 region for: i) IM motor PBRs, ii) CM visual NBRs. 2) ipsilateral M1 region for: i) IM motor NBRs; 3) contralateral V1 region for: i) IM visual PBRs; 4) ipsilateral V1 for, i) IM visual NBRs; 5) Left superior LOC for: i) CM motor NBRs. The average ROI BOLD responses to each stimulus were then extracted from each ROI. The mean percentage signal change of the BOLD response was calculated relative to baseline, which was taken as the first 60 seconds of the entire run and the last second of each trial to provide the most representative baseline. The mean BOLD responses were then correlated with the mean EEG responses.

2.4 Results

2.4.1 FMRI group main effect responses: *Question 1*

The main effect GLMs (Figure 2.1 and 2.2) showed that NBR and PBR, with respective spatially overlapping negative CBF (NCBF) and positive CBF (PCBF), were induced in IM and CM cortices to motor (Figure 2.1) and visual (Figure 2.2) stimuli. Here we compared the spatial extent and statistical significance of NBRs and PBRs between tasks and the spatial conjunction between BOLD and CBF responses; see Table 2.1 for IM and Table 2.2 CM fMRI response measures respectively. As only IM ipsilateral NBRs, and not IM surround NBRs, were observed over all tasks we simply refer to IM ipsilateral NBRs as IM NBRs unless otherwise stated.

					Peak voxel coordinate		
Task	Response	Spatial extent	% BOLD overlap	Peak BOLD Z-stat	X	Y	Z
High	PBR	8361	68	6.1	38	20	27
High	PCBF	6227					
High	NBR	3563	21	5.0	67	22	50
High	NCBF	1919					
Low	PBR	8668	70	5.9	38	18	30
Low	PCBF	6627					
Low	NBR	1623	46	3.6	47	18	42
Low	NCBF	1124					
Tap	PBR	6018	72	5.2	68	46	64
Tap	PCBF	5997					
Tap	NBR	884	21	4.6	43	38	64
Tap	NCBF	426					
Grip	PBR	6956	65	6.0	63	45	68
Grip	PCBF	5585					
Grip	NBR	564	8	4.3	35	44	68
Grip	NCBF	294					

Table 2.1. Summary of group level IM responses: All BOLD and CBF peak responses were taken from the BOLD peak voxel.
The spatial extent was calculated as number of voxels Z>2.0 within the bilateral IM mask. The percentage overlap is the conjunction of significant BOLD and CBF voxels (Z>2.0). Peak voxels and percentage overlap are taken from the contralateral (positive responses) and ipsilateral (negative responses) regions of the IM masks respectively.

					Peak voxel coordinate		
Task	Response	Spatial extent	% BOLD Overlap	Peak BOLD Z-stat	X	Y	Z
High	PBR	1836	1	4. 1	41	70	72
High	PCBF	63					
High	NBR	1634	52	4.1	48	52	61
High	NCBF	4168					
Low	PBR	4051	2	4.4	66	61	66
Low	PCBF	245					
Low	NBR	-	-	-	-	-	-
Low	NCBF	-					
Tap	PBR	3176	42	5.4	63	21	26
Tap	PCBF	1726					
Tap	NBR	5452	45	4.8	31	23	51
Tap	NCBF	7058					
Grip	PBR	11075	29	5.7	61	20	27
Grip	PCBF	3637					
Grip	NBR	859	24	3.9	66	20	46
Grip	NCBF	2115					

Table 2.2. Summary of group-level CM peak responses: All BOLD and CBF peak responses were taken from the BOLD peak voxel.
The spatial extent was calculated as the number of voxels Z>2.0 within the bilateral CM mask. The percentage overlap is the conjunction of significant BOLD and CBF voxels.

Motor Stimuli

IM responses

The IM NBR and NCBF evoked by both motor tasks were located in ipsilateral (left) M1, the cingulate cortex and bilateral frontal regions (Figure 2.1D&E). The contrast Tap > Grip showed that Tap IM NBR was significantly larger than Grip IM NBR (Figure 2.1F). Tap data also showed a higher NBR peak voxel Z-stat (Tap: Z=4.6, Grip: Z=4.3; locations specified in Table 2.1) and larger spatial extent of statistically significant NBR voxels (Tap: 884, Grip: 564; see Table 2.1) than Grip. Both Tap and Grip showed good spatial correspondence of IM NBR and IM NCBF responses as shown by the size of their conjunction (Tap: 21%, Grip: 8%; see Table 2.1).

The IM PBR and PCBF were observed in contralateral (right) M1 (Figure 2.1D&E) with considerable spatial overlap with PCBF responses (Tap: 72%, Grip: 65%, see Table 2.1). No statistically significant voxel-wise differences were evident between Grip and Tap IM PBRs, as shown by the Tap>Grip contrast (Figure 2.1F).

CM responses

The CM NBR and NCBF evoked by the motor tasks were observed in widespread areas of visual cortex including V1, cuneal cortex, and a mixture of the lateral occipital cortex (LOC) and intraparietal lobe, in bilateral regions for Tap but mostly contralateral regions for Grip (Figure 2.1A&B). Both CM NBR and NCBF were significantly larger in magnitude during Tap than Grip (Figure 2.1C). Furthermore, Tap evoked CM NBR with much greater spatial extent (Tap: 5452, Grip: 859, see Table 2.2), BOLD peak voxel Z-stat (Tap: Z=4.8, Grip: Z=3.9, locations specified in Table 2.2), and CM NBR/NCBF overlap (Tap: 45%, Grip: 24%, see Table 2.2) than Grip. In addition, CM PBRs were also evoked by both Grip and Tap in bilateral inferior LOC located inferior to the CM NBRs (Figure 2.1A&B).

Visual Stimuli

IM responses

The NBR and NCBF evoked by High and Low contrast visual stimuli were located in posterior ipsilateral V1, with responses also extending bilaterally in anterior V1. High visual stimuli also evoked IM NBR bilaterally in LOC and IPL (Figure 2.2A&B). Both High and Low showed good spatial correspondence between IM NBR and IM NCBF responses as shown by the size of their conjunction (High: 741 voxels, Low: 742 voxels, see Table 2.1). Contrasting responses between conditions (High>Low) showed significantly larger magnitude NBR only in small areas of the bilateral LOC during High compared to Low (Figure 2 2C). Compared to Low, the High condition evoked a larger NBR peak voxel Z-stat, and spatial extent of NBR (High: Z=5.0, Low: Z=3.6; High: 21%, Low: 46%, see Table 2.1).

Peak IM PBR and PCBF to both High and Low were located in contralateral V1 (Figure 2.2A&B) with high levels of spatial overlap (High: 68%, Low: 70%, see Table 2.1). PBR and PCBF response amplitudes and extent were very similar between High and Low stimuli (Figure 2.2C and Table 2.1).

CM responses

CM NBR and NCBF to High visual stimuli were located in bilateral M1 (stronger contralateral to the stimulus), bilateral secondary sensorimotor cortex and SMA (Figure 2.2E) (peak Z=4.09, extent 1634, NBR/NCBF overlap 52%, see Table 2.2). There was a notable spatial overlap between the location of the High CM NBR and the motor IM PBR in left M1 and SMA (overlap between High CM NBR and: 1) IM Tap PBR 1265 voxels; 2) IM Grip PBR 1391 voxels). No significant CM NBR was observed to Low visual stimuli (Figure 2.2D, Table 2.2) but this difference in NBR between High and Low did not pass cluster-correction (Figure 2.2F). In

addition some CM PBR was observed in regions bordering the motor cortices (Figure 2.2D&E) with no significant difference between High and Low stimuli.

2.4.2 Spatial relationship between IM and CM NBRs: Question 2a

Here we compared the locations of IM and CM NBRs and whether they represent deactivation of reciprocal regions. The Tap CM NBR was found to overlap with High IM NBR (453 voxels) in left LOC and left V1 as well as overlapping with Low IM NBR (171 voxels) in left V1. The Tap CM NBR also overlapped with High IM PBR (2125 voxels) and Low IM PBR (2302 voxels) bilaterally in the LOC. Grip CM NBR was found to overlap with High IM NBR (261 voxels) in left LOC and left V1 as well as overlapping with Low IM NBR (21 voxels) in left V1. The Grip CM NBR also overlapped with the High IM PBR (58 voxels) and with Low IM PBR (82 voxels) in the left LOC. The High CM NBR did not overlap with Tap or Grip IM NBR.

Finally we investigated relationships between sensory cortex BOLD responses to the same task by correlating subjects' CM NBR amplitude with either their IM PBR or IM NBR amplitude for each task condition. As shown in Figure 2.3, there were no significant relationships between the IM PBR and IM/CM NBRs, except a positive trend ($r=0.51$, $p=0.049$) in the Tap CM NBR data. However, we did find evidence of a significant positive correlation between subject's IM NBR and CM NBR to both of the motor tasks (Tap: $r=0.73$; Grip $r=0.68$ both $p<0.01$, Figure 2.4). No correlations were observed for the visual data between subjects' IM and CM NBRs.

Taken together these results show that our tasks induced both IM and CM NBRs reciprocally in primary sensory cortex and suggest that increased complexity/intensity in the motor/visual stimulation (Tap > Grip; High > Low) was accompanied by a small increase in the magnitude of both IM and CM NBR but no significant change in the magnitude of the IM PBR. In addition, the mean amplitude of IM NBR was positively related to the CM NBR amplitudes in the motor but not the visual data.

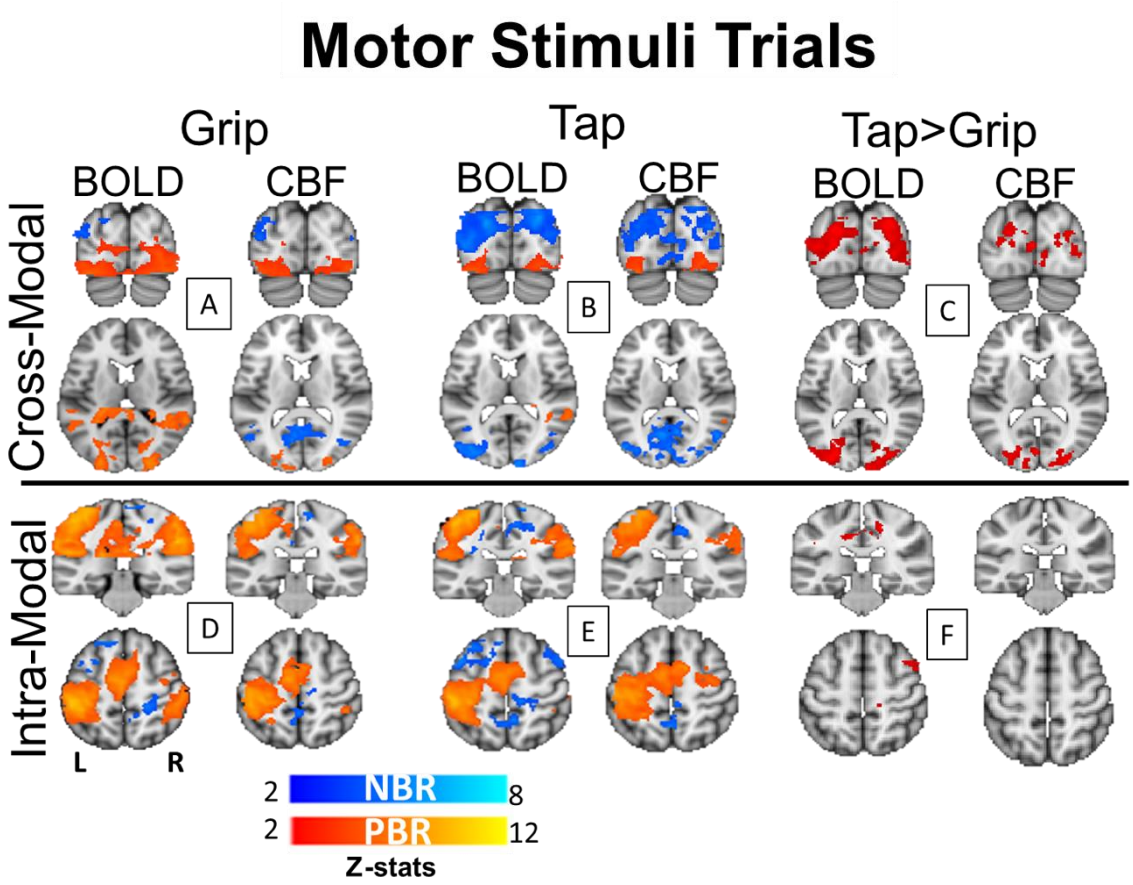

Figure 2.1. BOLD and CBF response to motor trials.
A and **D** show the main effect BOLD and CBF responses to Grip in the CM (top panel) and IM (bottom panel) cortices respectively. **B** and **E** show the main effect BOLD and CBF responses to Tap in the CM and IM cortices respectively. **C** and **F** show the contrast between Tap and Grip highlighting the CM (**F**) and IM (**C**) regions which are more significant in Tap than Grip respectively. Blue=NBR, red=PBR. Motor cortex (IM) y=48, z=63. Visual cortex (CM) y=22, z=42.

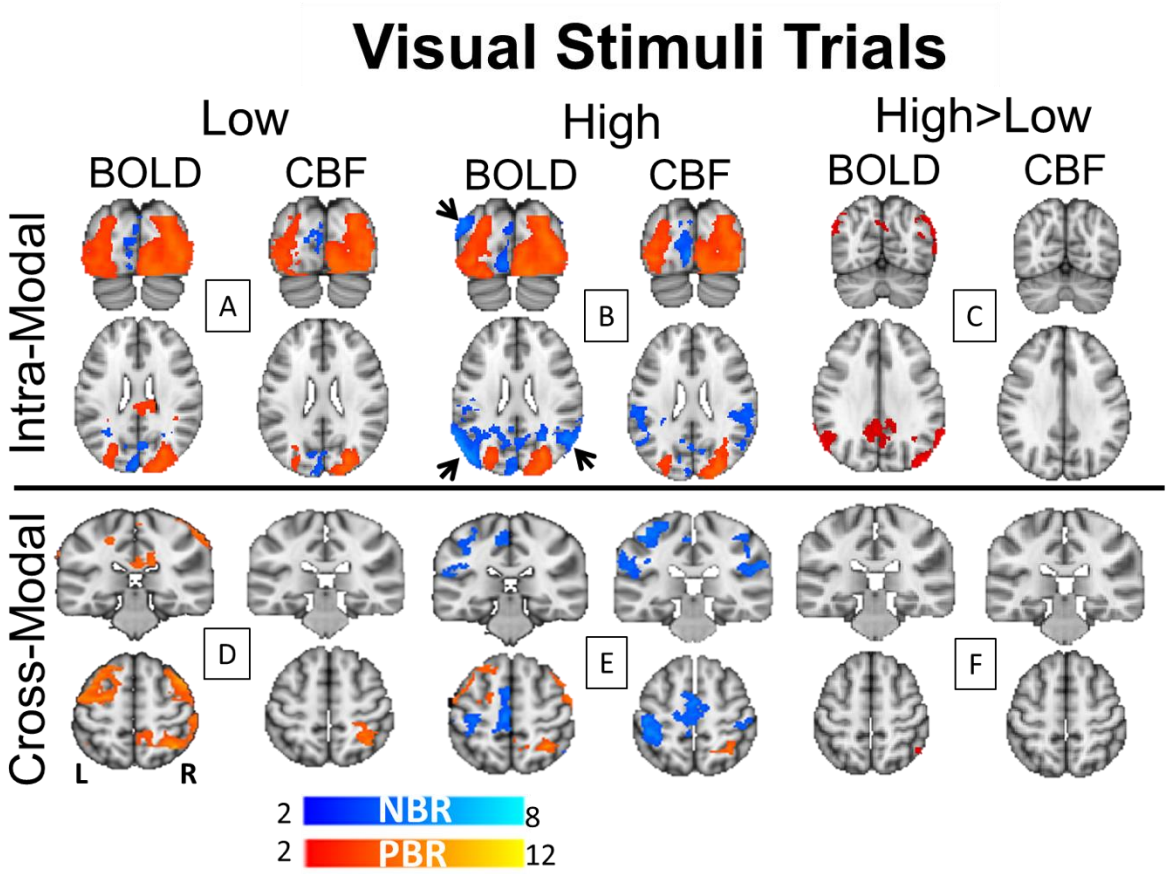

Figure 2.2. BOLD and CBF response to visual trials.
A and **D** show the main effect BOLD and CBF responses to Low in the CM (bottom panel) and IM (top panel) cortices respectively. **B** and **E** show the main effect BOLD and CBF responses to High in the CM and IM cortices respectively. Arrows highlight High NBRs located in the LOC/iPL. **C** and **F** show the contrast between High and Low highlighting the CM (**F**) and IM (**C**) regions which are more significant in Tap than Grip respectively. Blue=NBR, red=PBR; black arrows show position of lateral occipital cortex NBR. For **A,B,D** and **E**: Visual cortex (IM) y=22, z=48, Motor cortex (CM) y=48, z=63. For **C** and **F**: Visual cortex (IM) y=30, z=52, Motor cortex (CM) y=48, z=63.

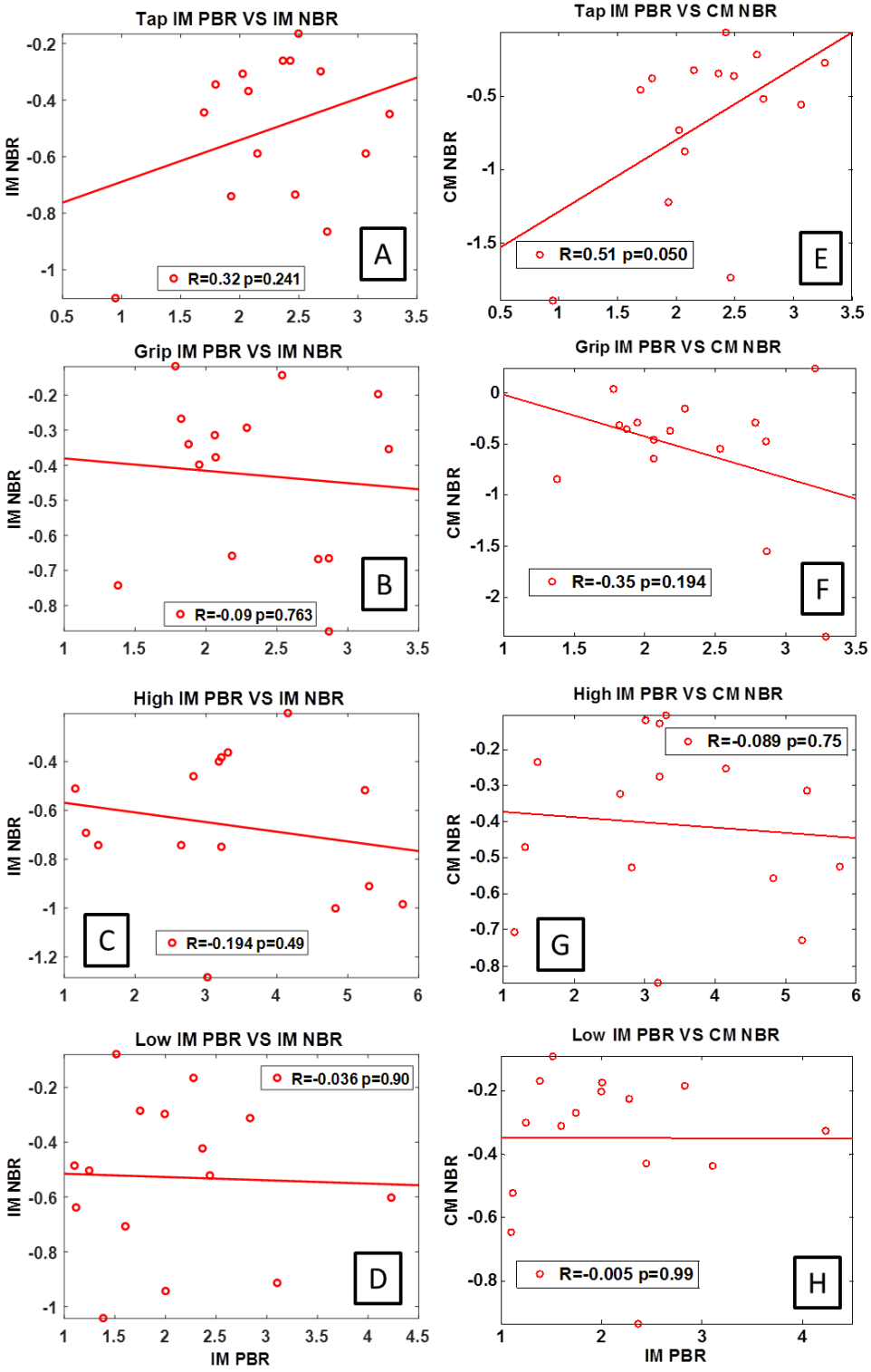

Figure 2.3. Across subject Pearson's correlations between IM PBR and IM/CM NBR. Across subject Pearson's correlations between IM PBR and IM/CM NBR. **A** and **B** show IM PBR:IM NBR correlations for Tap and Grip respectively, with no significant correlations found. **C** and **D** show IM PBR:IM NBR correlations for High and Low respectively with no significant correlations found. **E** and **F** show IM PBR:CM NBR correlations for Tap and Grip respectively. While no significant correlations were found, Tap exhibits a positive correlation trend. **G** and **H** show IM PBR:CM NBR correlations for High and Low respectively with no significant correlations found.

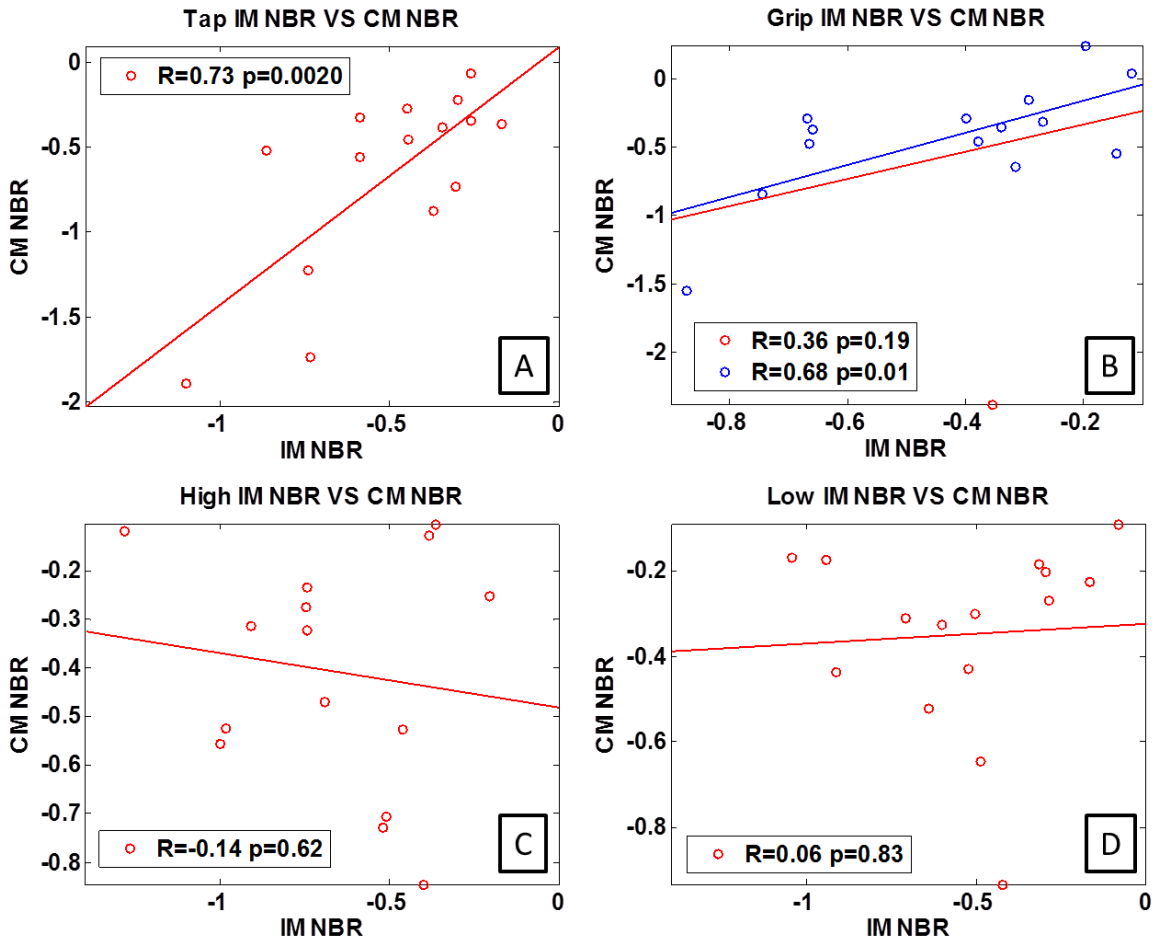

Figure 2.4. Across subject Pearson's correlations between IM NBR and CM NBR. **A** and **B** show IM NBR:CM NBR correlations for Tap and Grip correlations respectively. With a significant positive correlation noted for Tap. For Grip, a significant positive correlation was found after removal of an outlier (red line – all data, blue=without outlier). **C** and **D** show IM NBR:CM NBR correlations for High and Low respectively with no significant correlations found.

2.4.3 EEG Responses

Separately for motor and visual data, a beamformer was used to generate source power ratio maps of the difference in EEG oscillatory power between the active and passive periods for both α and β frequency bands. For each subject the peak location of the IM ERD was defined: the mVE from Grip and Tap data combined; and the vVE from High and Low data combined. IM and CM EEG responses were then extracted from these locations. For display purposes

group mean source maps were calculated on the MNI template grid and shown in Figure 2.5A-D.

Motor Trials: Intra-Modal responses

Figure 2.6 shows the timecourses taken from the mVE location showing a clear group level α and β power ERD throughout the stimulus period of both grip and Tap motor trials. We found that in all individual subjects, the peak IM motor ERD, defining the mVE location, was located in contralateral M1, with all subjects showing bilateral IM ERD (see Figure 2.5A).

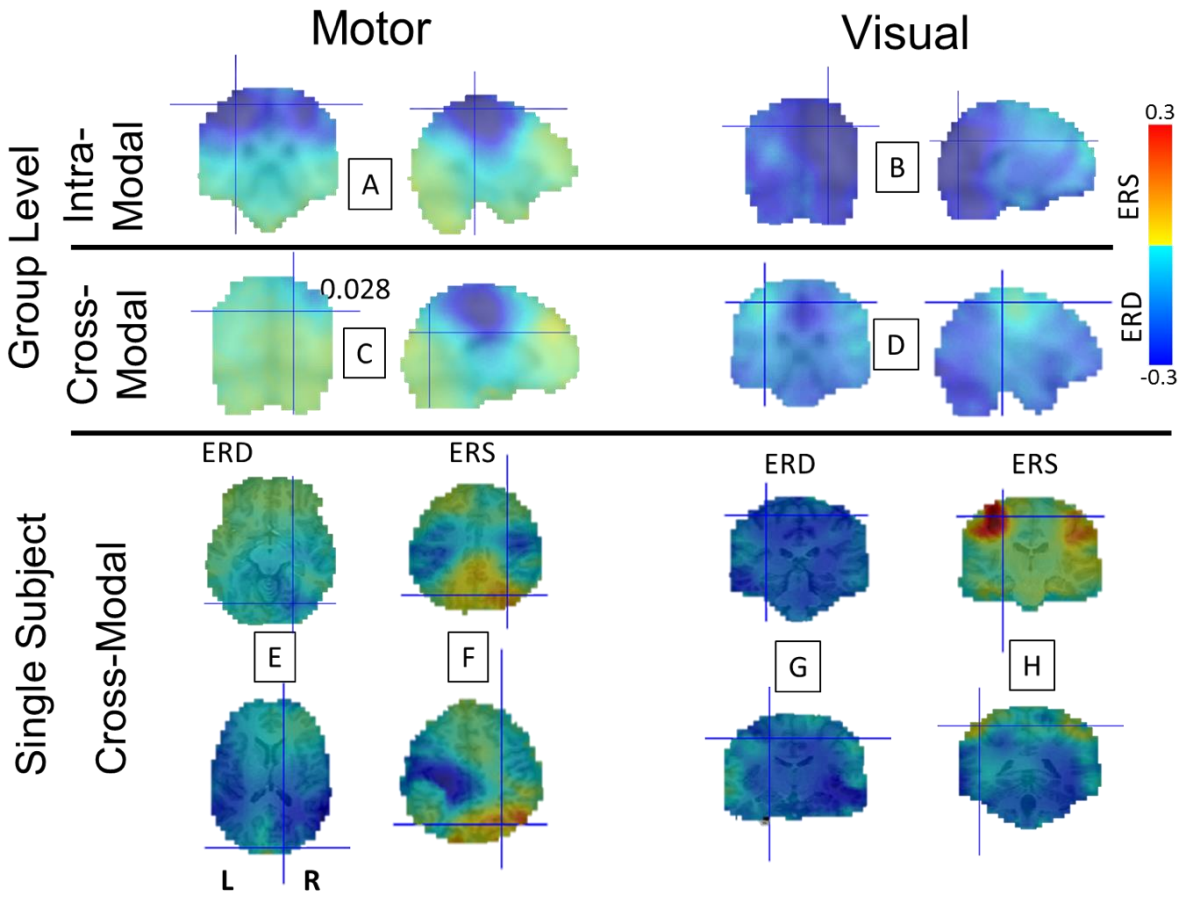

Figure 2.5. EEG beamformer maps.
A and **B** show group level beamformer maps of beta response to motor trials and α response to visual trials respectively; with the maximum IM ERD related to each modality highlighted by the crosshair. **C** and **D** show group level beamformer maps of α response to motor trials (**C**), and beta response to visual trials (**D**), the crosshair centred on the other modalities' peak ERD response. **E** shows two subjects which present with CM ERD in the vVE *to motor trials*. **F** shows two subjects which present with CM ERS in the vVE to the same *motor trials*. **G** shows two subjects which present with CM ERD in the mVE *to visual trials*. **H** shows two subjects which present with CM ERS in the mVE *to the same visual trials*. Heat maps: red = greater ERS, Blue=greater ERD.

Across subjects, the amplitude of the ERD was found to be significantly lower than the baseline level for both α (Tap = -29.3 ± 20.3nAm, $p<0.001$; Grip = -20.3 ± 19.1nAm, $p<0.01$; p values via one-sample t-test) and β (Tap = -22.5 ± 11.7nAm, $p<0.001$; Grip = -18.3 ± 10.4nAm, $p<0.001$) frequency oscillations (Figure 2.6A-D). Significantly larger magnitude ERD were observed in response to Tap than to Grip for both α (Figure 2.6E) and β (Figure 2.6F) power (paired t-test α: $p<0.05$; β: $p= 0.04$). There was no significant difference between α ERD and β ERD magnitude for either Tap ($p=0.05$, paired t-test), or Grip ($p=0.62$) (Figure 2.6G&H respectively). All responses showed a rebound of oscillatory power (a form of ERS) occurring between approximately 0-10s after stimulus cessation, the amplitude of which was larger in the β than the α band, but very similar between Tap and Grip tasks.

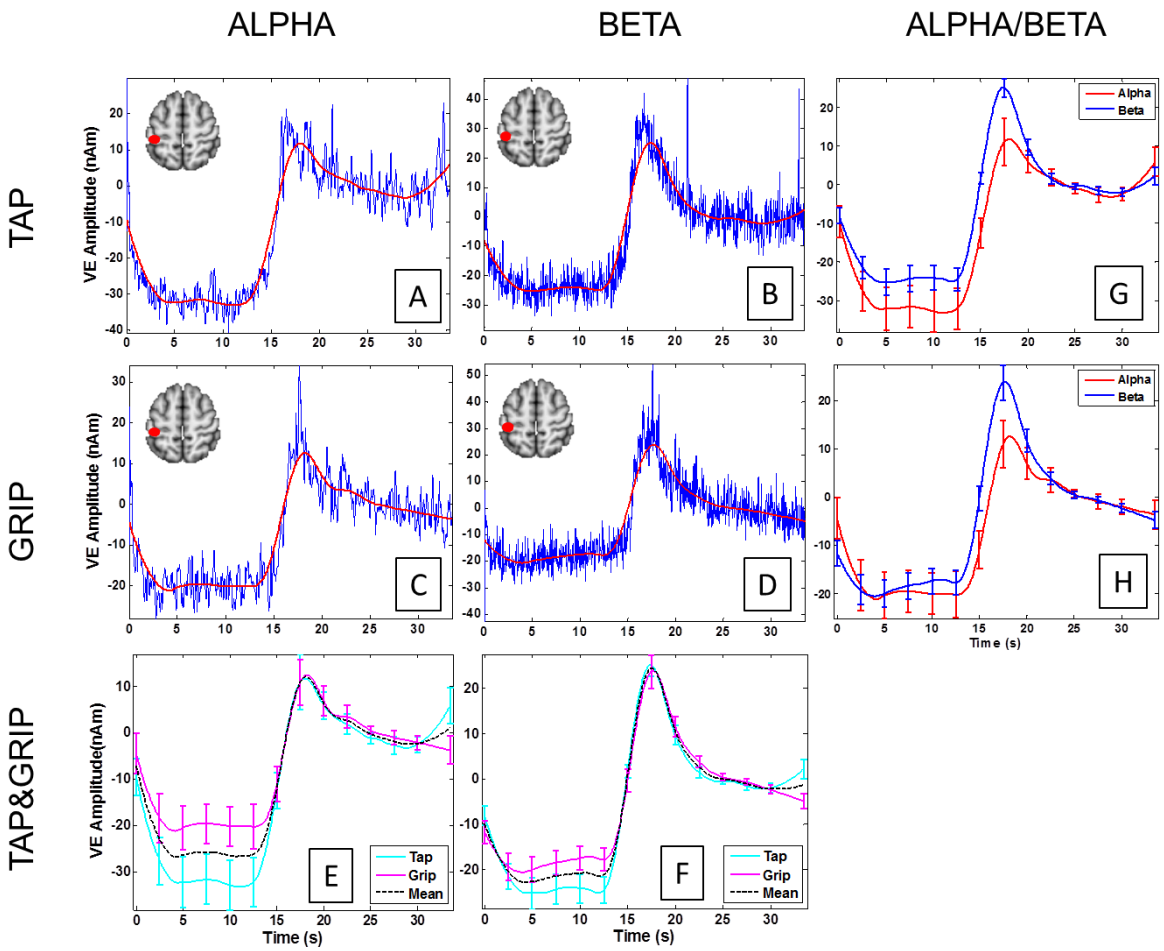

Figure 2.6. Group average IM motor EEG alpha and beta power timecourses, taken from the mVE.

A and **B** show Tap α and β timecourses respectively (blue= group average raw power timecourse, red=smoothed timecourse). **C** and **D** show Grip α and β timecourses respectively. **E** shows the comparison of Tap and Grip α responses (cyan/magenta = Tap/Grip smoothed timecourse, respectively); whilst **F** displays the same for β responses. Error bars denote the standard deviation across subjects. **G** displays the smoothed timecourses of Tap α (red) and β (blue) responses; whilst **H** shows the same for Grip. Stimulus onset at 0 s, 14 s duration. Baseline period 20.5-33.5 seconds. Insert of axial brain slices show general region timecourses were extracted from (mVE).

Motor Trials: Cross modal responses

The α and β responses to motor tasks extracted from the vVE showed no-significant change in oscillatory power between the stimulus period and baseline as shown in Fig 5 (α power Tap = -1.5 ± 9.7nAm, p= 0.57; Grip = -4.0 ± 13.8nAm, p=0.28 [p value via one-sample t-test]; β power Tap = 0.5 ± 5.2nAm, p=0.68; Grip = -0.1 ± 5.1nAm, p=0.92). Despite minimal mean stimulus response, both α and β CM motor responses showed a rebound in power between 0-10s post-stimulus.

No significant difference was found between Grip and Tap responses for either α (p=0.26; Figure 2.7E) or β (p=0.64; Figure 2.7F) frequencies; or between α and β power during either Tap (p=0.33, paired t-test) or Grip (p=0.19), Figure 2.7G&H. The group motor CM timecourses exhibited a short transient (~500ms) decrease in α and β power at the stimulus onset, and for β also at the offset, of the stimulus (Figure 2.7A-D). As this VE is located within the visual cortex, these transient decreases in power therefore likely represent onset and offset responses related to the presentation of the word ‘Grip’ or ‘Tap’ at the start of the trial and its removal at the end of the trial.

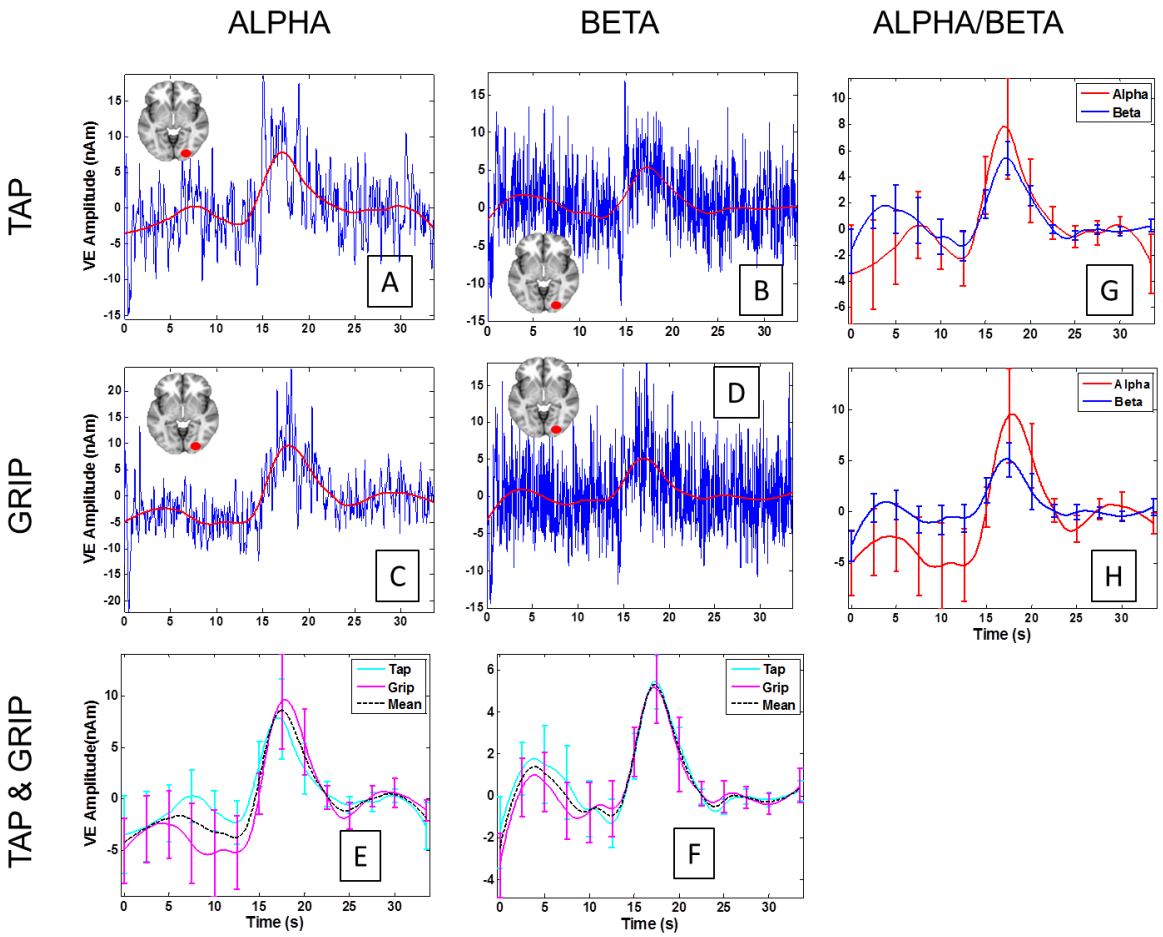

Figure 2.7. Group average CM motor EEG alpha and beta power timecourses, taken from the vVE.
A and **B** show Tap α and β group average timecourses respectively (blue= group average raw power timecourse, red=smoothed timecourse). **C** and **D** show Grip α and β timecourses respectively. **E** shows the comparison of Tap and Grip α responses (cyan/magenta = Tap/Grip smoothed timecourse, respectively); whilst **F** displays the same for β responses. Error bars denote the standard deviation across subjects. **G** displays the smoothed timecourses of Tap α (red) and β (blue) responses; whilst **H** shows the same for Grip. Stimulus onset at 0 s, 14 s duration. Baseline period 20.5-33.5 seconds. Insert of axial brain slices show general region timecourses were extracted from (vVE).

Visual Trials: Intra modal responses

Similarly to IM motor responses, Figure 2.8 shows the group level ERD throughout the stimulus period in both α and β power from the vVE with both High and Low visual trials, Figure 2.8A-D. The peak IM visual ERD, defining the vVE location, was located in contralateral V1 in 10 subjects, and in central V1 in 4 subjects. The amplitude of the ERD was significantly lower than the baseline level for both α (High = -15.7 ± 11.6nAm, $p<0.001$; Low = -15.9 ± 14.6nAm, $p<0.001$) and β (High = -5.4 ± 4.8nAm, $p<0.001$; Low = -7.4 ± 4.1nAm, $p<0.001$) frequency oscillations (Figure 2.8A-D). High and Low showed highly similar α ERD (paired t-test: $p=0.93$, Figure 2.8E), while Low showed significantly larger magnitude β ERD than High trials ($p<0.05$, Figure 2.8F). We observed significantly larger magnitude α ERD than β ERD during both High (paired t-test: $p<0.01$) and Low ($p<0.05$) trials, Figure 2.8G&H. All responses showed a rebound of oscillatory power between 0-10s after stimulus cessation, which had larger amplitude for α than β frequencies.

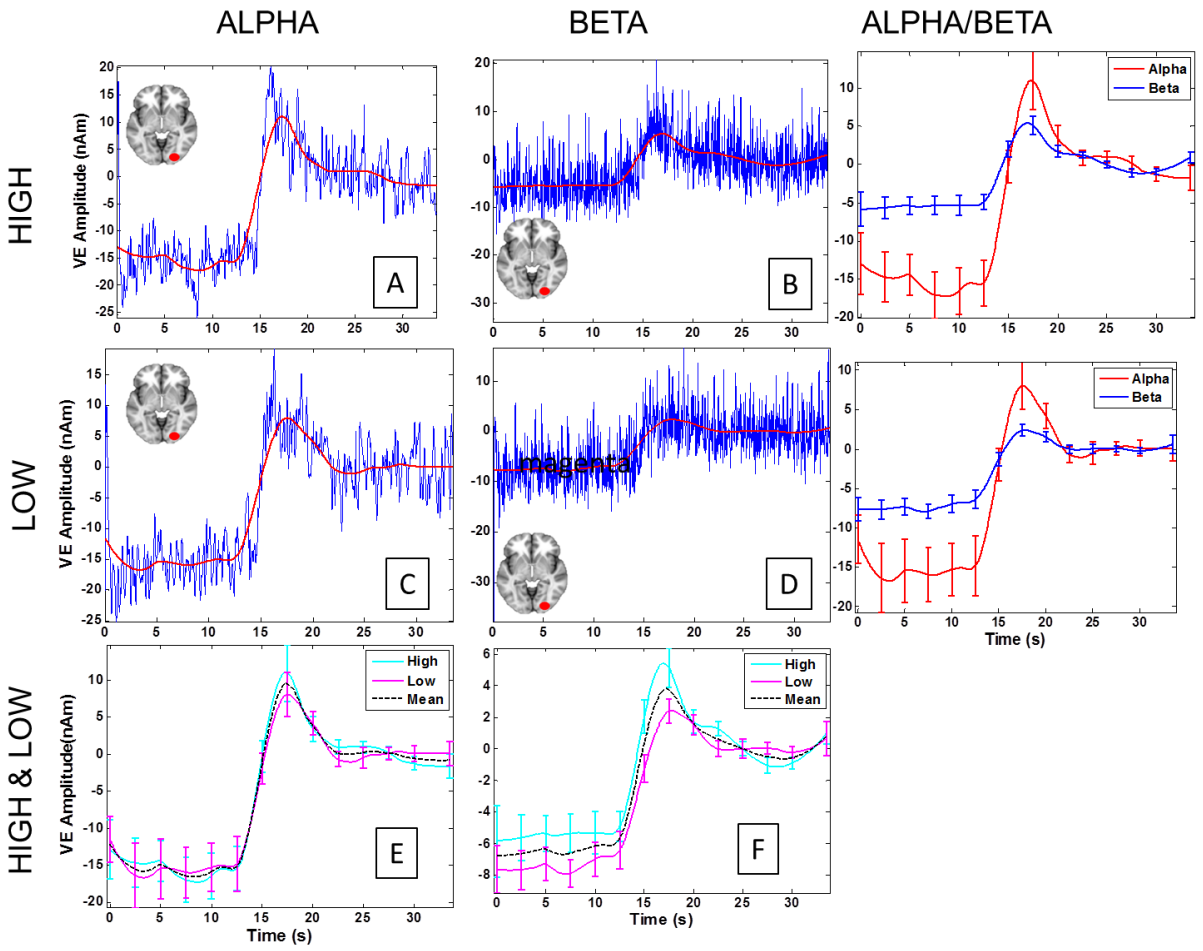

Figure 2.8. Group average IM visual EEG alpha and beta power timecourses, taken from the vVE.

A and **B** show High α and β timecourses respectively (blue= group average raw power timecourse, red=smoothed timecourse). **C** and **D** show Low α and β timecourses respectively. **E** shows the comparison of High and Low α responses (cyan/magenta = High/Low smoothed timecourse, respectively); whilst **F** displays the same for β responses. Error bars denote the standard deviation across subjects. **G** displays the smoothed timecourses of High α (red) and β (blue) responses; whilst **H** shows the same for Low. Stimulus onset at 0 s, 14 s duration. Baseline period 20.5-33.5 seconds. Insert of axial brain slices show general region timecourses were extracted from (vVE).

Visual Trials: Cross modal responses

The group level responses to the visual stimuli from the mVE showed that Low visual stimuli induced a small but significant CM ERD in motor cortex α power (Figure 2.9C) (ERD = -3.6±6.3nAm, $p<0.05$) but no significant change in α power was seen during High trials (Figure 2.9A; ERD= -1.4±6.5nAm, $p=0.41$), despite similar profiles being shown (Figure 2.9E; paired t-test: $p=0.21$). No significant CM β response was observed for either stimulus intensity (Figure 2.9B&D; High: ERD= -1.1±4.7nAm, $p=0.38$; Low: ERD= -2.7±5.7nAm, $p=0.088$), with no significant difference between intensities either (Figure 2.9F, $p=0.32$). Similarly no significant difference between α and β frequencies for either High (Figure 2.9G; paired t-test: $p=0.74$) or Low (Figure 2.9F; $p=0.35$) was found. The High α timecourse showed similar transient decreases in power at the onset and the offset of the stimulation to those observed for CM Grip and Tap timecourses (Figure 2.9A). All CM visual responses showed a rebound of oscillatory power between 0-10s after stimulus cessation, with larger amplitude for High than Low.

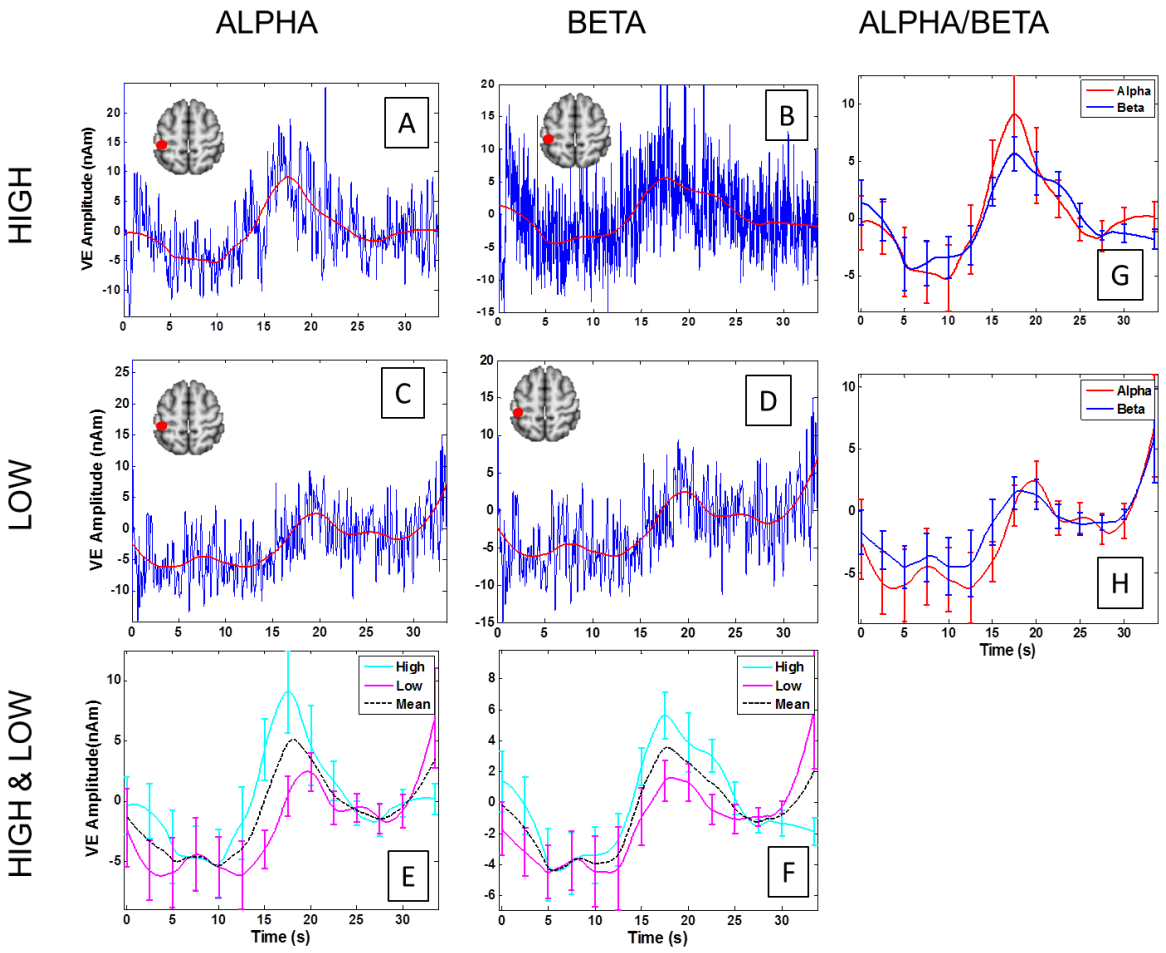

Figure 2.9. Group average CM visual EEG alpha and beta power timecourses, taken from the mVE.

A and **B** show High α and β group average timecourses respectively (blue= group average raw power timecourse, red=smoothed timecourse). **C** and **D** show Low α and β timecourses respectively. **E** shows the comparison of High and Low α responses (cyan/magenta = High/Low smoothed timecourse, respectively); whilst **F** displays the same for β responses. Error bars denote the standard deviation across subjects. **G** displays the smoothed timecourses of High α (red) and β (blue) responses; whilst **H** shows the same for Low. Stimulus onset at 0 s, 14 s duration. Baseline period 20.5-33.5 seconds. Insert of axial brain slices show general region timecourses were extracted from (mVE).

EEG response relationships between frequencies, modalities and stimulus conditions: Question 2b

We examined within- and between-subject correlations in EEG response amplitudes to obtain a greater understanding of the relationship of oscillatory responses when compared between: a) frequencies, e.g. IM α and IM β; b) modalities, e.g. IM vs CM responses; and c) stimulus conditions (i.e. Tap Vs Grip and High Vs Low).

a) *Between frequency bands:* Both Grip and Tap data showed significant positive correlations between IM β and IM α (mVE) responses as well as between CM α and CM β (vVE) responses both within-subject (Table 2.3B) and across-subjects (Table 2.3A). Similarly, both High and Low data showed significant positive correlations between IM α and IM β (vVE) responses as well as between CM α and CM β (mVE) responses both within- (Table 2.4B) and across-subjects (excluding inter-subject High IM α vs IM β which only showed a trend toward significance), Table 2.4A. These results indicate that single-trial and subject mean responses were highly similar between frequency bands, e.g. that the largest magnitude IM α ERD was associated with the largest magnitude IM β ERD and therefore to simplify subsequent analyses, without compromising functional information, we now focus on the primary oscillation of each modality: visual cortex α and motor cortex β.

b) *Between brain regions:* We investigated whether IM and CM response amplitudes were related to each other. Across subjects, for both Grip and Tap tasks, significant positive correlations were found between the IM (mVE β) and CM (vVE α) responses (Table 2.3A). Within subjects, only one subject showed significant positive trial-by-trial IM-CM correlation, no negative correlations were observed (Table 2.3B). Across subjects in the visual data significant positive IM-CM correlations were only found for High (IM vVE α vs CM mVE β, Table 2.4A). Within subjects, only one subject in the Low data showed

significant positive trial-by-trial IM-CM correlations, no negative correlations were observed (Table 2.4B), These results indicate that for average responses, subjects with the strongest IM ERD showed CM ERD to the same stimulus, and also that CM ERS was observed in subjects that showed the weakest IM ERD (see Figure 2.10 for correlation plots that visualise this). However, no clear within-subject relationship between IM and CM responses was seen when studying their trial-by-trial variability. To clarify whether those correlations found across subjects were influenced by potential signal leakage between the IM and CM EEG signals, CM EEG power responses were orthogonalised with respect to the IM EEG power (Brookes, Woolrich et al. 2012). For motor trials, CM α power was orthogonalised for each subject across trials with respect to the IM β power, and vice versa for visual trials. Using this data, across subjects, positive correlations between the IM and orthogonalised CM EEG power for motor trials were strengthened (Tap: $r=0.61$, $p<0.05$; Grip: $r=0.55$, $p<0.05$) while for visual they were unchanged. The data therefore seems unaffected by signal leakage.

	A		B	
	Grip (r, p)	**Tap (r, p)**	**Grip # Subjects**	**Tap # Subjects**
mVE α vs mVE β	.626* .012	.827** 0.00014	12/0	14/0
vVE β vs vVE α	.701** .004	.610* .016	9/0	8/0
mVE β vs vVE α	.553* .033	.613* .015	1/0	2/0

Table 2.3. Motor trial EEG correlations: α and β power was extracted from the Motor IM VE (mVE) and Motor CM VE (vVE) during the stimulus period (0.5-13.5s) of Grip and Tap tasks and then correlated across subjects (**A**) or within subjects between single-trials (**B**). Rows 1&2 show correlations between frequency bands for IM and CM responses respectively, whilst the 3rd row shows the correlation between IM and CM responses. **A**) Across-subject IM and CM correlations between α and β power response. **B**) Number of subjects showing significant positive/negative within-subject correlations ($p<0.05$) between single-trial responses.

	A		B	
	Low (r, p)	**High (r, p)**	**Low # Subjects**	**High # Subjects**
vVE α vs vVE β	.575* .025	.359 .19	12/0	12/0
mVE α vs mVE β	.810** 0.00025	.846** 0.000069	12/0	13/0
vVE α vs mVE β	.496 .078	.631* .012	1/0	0/0

Table 2.4. **Visual trial EEG correlations**: α and β power were extracted from the Visual IM VE (vVE) and Visual CM VE (mVE) during the stimulus period (0.5-13.5s) of Low and High stimuli and then correlated across subjects (**A**) or within subjects between single-trials (**B**). Rows 1&2 show correlations between frequency bands for IM and CM responses respectively, whilst the 3rd row shows the correlation between IM and CM responses, **A**) Across-subject IM and CM correlations between α and β power response. The mean power during the stimulus period was baseline corrected and then correlated across subjects. **B**) Number of subjects showing significant positive/negative within-subject correlations ($p<0.05$) between single-trial responses.

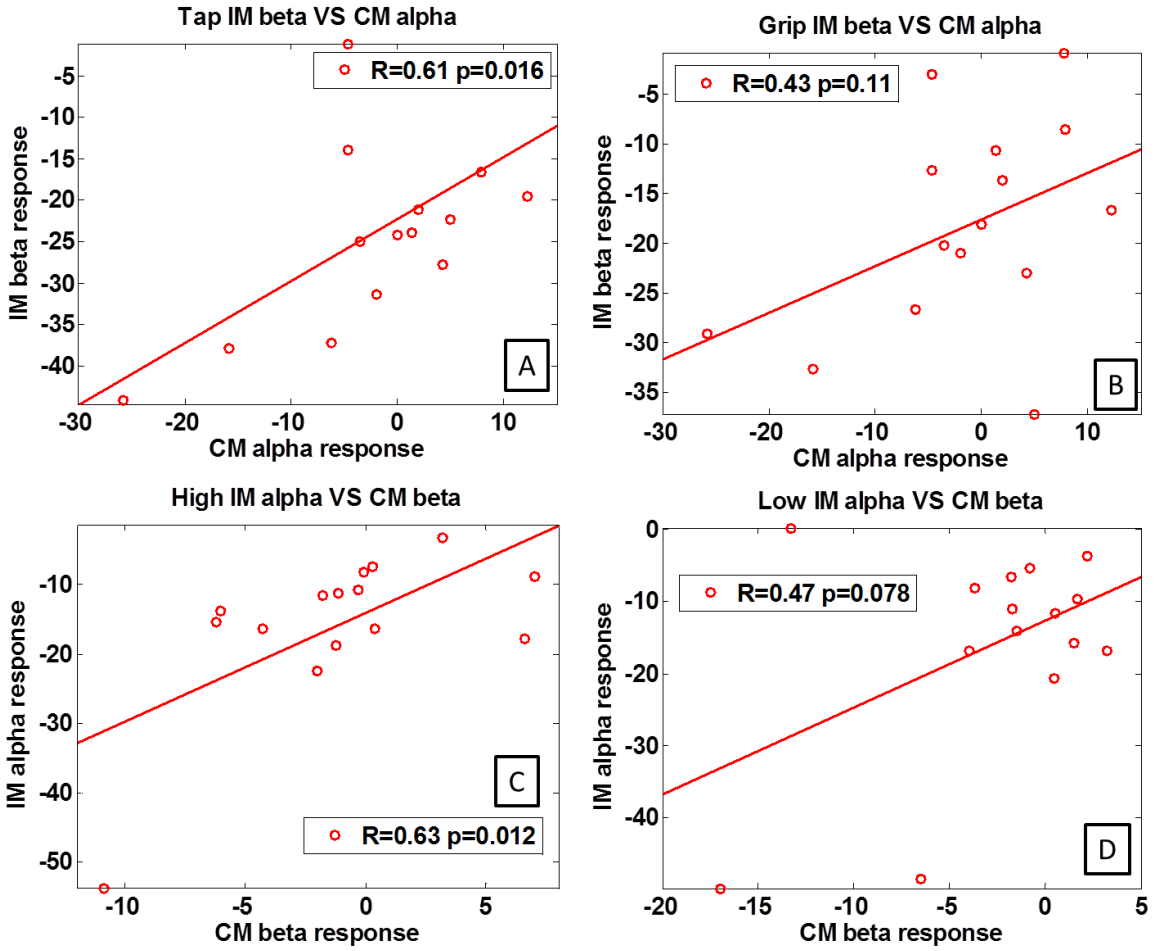

Figure 2.10. Across subject Pearson's correlations between IM and CM EEG responses.
A and **B** show correlations between IM EEG beta responses and CM EEG α responses for Tap and Grip respectively. Tap shows a significant positive correlation while grip exhibits a positive trend. **C** and **D** show correlations between IM EEG α responses and CM EEG β responses for High and Low respectively. Similar to the motor tasks, the more intense stimulus (High) exhibits a significant positive correlation while the less intense stimulus (Low) shows a non-significant positive trend. These positive correlations show that stronger IM ERD is related to CM ERD, while weaker IM ERD is associated with CM ERS.

c) *Between stimulus conditions:* Here the only correlations that could be assessed were across subjects. In the motor data, we found significant positive correlations between subject's mean Grip and Tap IM responses (mVE β) (Table 2.5). Subject's mean CM responses (vVE α) were also significantly positively correlated between Grip and Tap tasks. In the visual data, only the subject's mean High and Low IM responses (vVE α) were significantly positively correlated (Table 2.6). No correlation was seen between CM responses (mVE β). These results indicate that similar mean response amplitudes were seen across tasks, such that subjects that showed the largest magnitude response to one condition (e.g. Tap/High IM ERD) also showed the largest response to the other (e.g. Grip/Low IM ERD), relative to other subjects.

	(r, p)
Grip mVE β vs Tap mVE β	.587* .021
Grip vVE α vs Tap vVE α	.794** 0.00041

Table 2.5. Motor task across-subject EEG correlations: across-subject correlations between the Tap and Grip response for the Motor IM VE (mVE) β and also the Motor CM VE (vVE) α.

	(r, p)
Low vVE α vs High vVE α	.829** 0.00013
Low mVE β vs High mVE β	.334 .223

Table 2.6. Visual task across-subject EEG correlations: across-subject correlations between the High and Low response for the Visual IM VE (vVE) α and Visual CM VE (mVE) β.

2.4.4 Between-subject variability in CM ERD/ERS and corresponding BOLD responses: Question 3

We largely found no clear CM α or β ERD/ERS in the group average responses and in addition observed a positive correlation between subjects' CM and IM EEG response amplitudes. Therefore, we investigated between-subject variability in CM EEG responses to further understand the relationship between concurrent responses in the visual and motor cortex. For both visual and motor data we created subgroups of those subjects showing CM ERD and those showing CM ERS and examined the mean CM VE response timecourses of those subgroups. Beamformer maps from representative subjects displaying CM ERD and ERS for motor and visual data can be seen in Figure 2.5E-H.

The α power extracted from the vVE during motor tasks showed that the motor CM response varied between ERD and ERS across subjects (Figure 2.11A&B). Approximately half the subjects showed increased vVE α power that was sustained throughout motor task performance compared to baseline levels, denoting a CM ERS (Tap, subjects: 2,6,8,9,10,12,14, mean ERS = 5.8 ± 3.8nAm, Figure 2.11A; Grip subjects: 2,6,8,9,10 mean ERS= 7.7 ± 6.4nAm, Figure 2.11B). The remaining subjects showed sustained CM α ERD during the motor task (Tap Figure 2.11A: mean ERD = -7.8 ± 8.7nAm; Grip Figure 2.11B: mean ERD= -9.9 ± 12.8nAm). We observed that a greater number of subjects showed CM α ERS during the more complex Tap task than during Grip. A clear separation in amplitude between CM ERS and CM ERD subgroups was observed throughout the duration of the stimulus period. An interesting variation in the shape of the EEG response can be observed, where peak ERS amplitude was reached in the first half of the stimulation period, particular for the β responses. It is interesting to note that the "rebound" was still preserved following the ERS, suggesting the occurrence of this response was not necessitated by a preceding ERD

and making the description of it as a rebound of oscillatory power seem less appropriate in such circumstances.

Similarly, in the visual data we observed a sustained CM β ERS in motor cortex of a subset of subjects (High, Figure 2.12A, subjects: 1,5,6,14,15 mean ERS = 3.5± 3.2nAm; Low, Figure 2.12B, subjects: 1,2,4,6,13,14 mean ERS = 1.6 ± 1.0nAm), while the remainder showed CM β ERD (High: Figure 2.12A; mean ERD = -3.4 ± 3.4nAm, Low: Figure 2.12B; mean ERD = -5.6 ± 5.8nAm). Note the subjects who exhibited CM ERS to motor stimuli were not the same as those who exhibited it for visual stimuli. Similar to the motor data, the post-stimulus rebound appeared for ERS and ERD subjects, despite the clear differences in response amplitude during stimulation.

Given that we observed substantial variability in the CM response across subjects, it was important to investigate if equivalent effects in the fMRI data were present, specifically whether the presence of a CM ERS or ERD has any corresponding signature in the NBR of those subjects. However, whilst in general the mean IM EEG response did not vary in polarity across subjects (IM ERD was observed in all subjects), its amplitude was correlated with that of the mean CM EEG response (which varied between ERD and ERS, see Tables 2.3&2.4 and Figure 2.10) and therefore definitively attributing differences in fMRI response to CM response polarity, rather than IM responses, was not possible. Nevertheless, in order to explore this question we performed two further analyses. Firstly we examined the correlation between subject's CM ERS and CM BOLD amplitudes for both tasks. We found no correlation between subject's motor CM EEG (vVE α) and BOLD responses in visual cortex (Figure 2.11C&D), but we did observe a significant negative correlation between subject's visual CM EEG (mVE β) and BOLD responses in motor cortex (Figure 2.12C&D). To follow up on this we performed an additional fixed-effects group level GLM analysis ($Z>2.3$, $p<0.05$ cluster corrected) and compared the mean NBR between those subjects showing CM ERS and those showing ERD.

The number of subjects in each group was balanced by reducing the largest group size by removing the subjects with the weakest responses (closest to zero).

For the motor data, the mean CM NBR of the subjects who showed either CM ERS or CM ERD α power from the vVE are plotted in Figure 2.11E&F, Tap and Grip respectively. Results of a GLM contrast between the ERD and ERS groups are overlaid showing those regions with greater CM NBR (in red) for that specific group. This showed that the motor tasks evoked larger mean NBR in visual cortex in the subjects that showed CM ERD than in those subjects that showed CM ERS. The visual trials showed the opposite effect and supported the between-subject visual CM EEG-BOLD correlations (Figure 2.12C&D). The mean CM NBR for the subjects who showed mVE β CM ERD and separately ERS to visual trials are plotted in Figure 2.12E&F (High and Low respectively). These plots show that visual stimuli evoked larger mean NBR in motor cortex in the subjects that showed CM ERS than in those who showed CM ERD. These results demonstrate that both the polarity and amplitude of a subject's average CM EEG response is associated with differences in the amplitude of their CM NBR to the same stimulus.

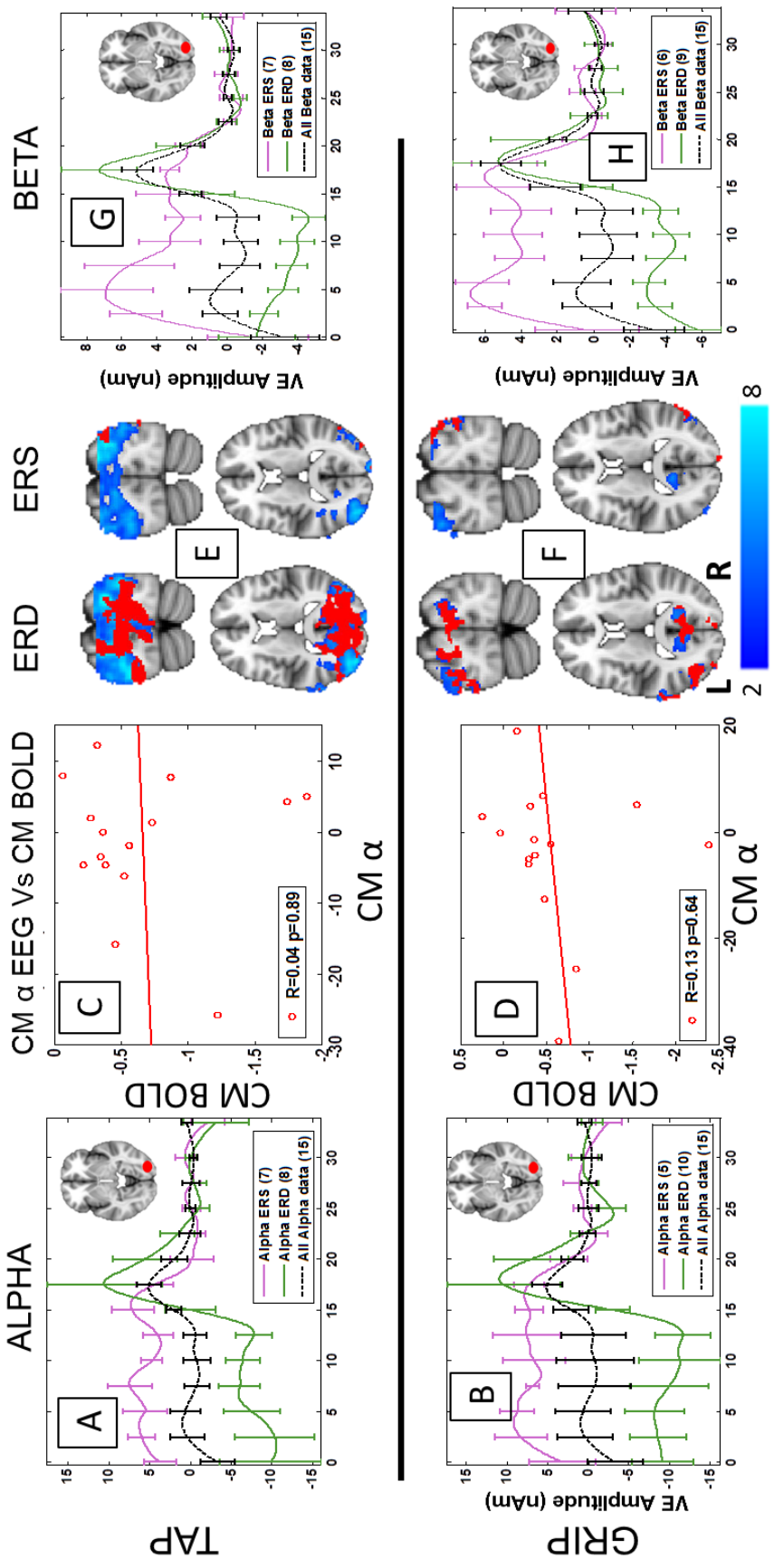

Figure 2.11. Exploration of CM EEG responses to motor trials.
A and B: subjects were divided into those showing α CM ERS (red) and those showing α CM ERD (blue) with mean subject response (as in Figure 7) in black. Legends show in brackets the number of subjects contributing to each plot. A and B show CM α responses to Tap and Grip respectively. C and D show Pearson's correlations between CM BOLD response and CM alpha power for Tap and Grip respectively, the legend shows the R and p value for the Pearson's correlation. E (Tap) and F (Grip) show the CM NBR (blue) from the group main effect GLM analysis Z>2.3, p<0.05 cluster corrected) for those subjects showing ERD and those showing ERS separately, with significant differences when contrasting one group against the other shown in red (e.g. red in the ERD data shows that the NBR in that region is significantly greater than for the ERS subjects). G and H shows those subjects with β CM ERS (red) and those with β CM ERD (blue) with mean subject response (as in Figure 7)

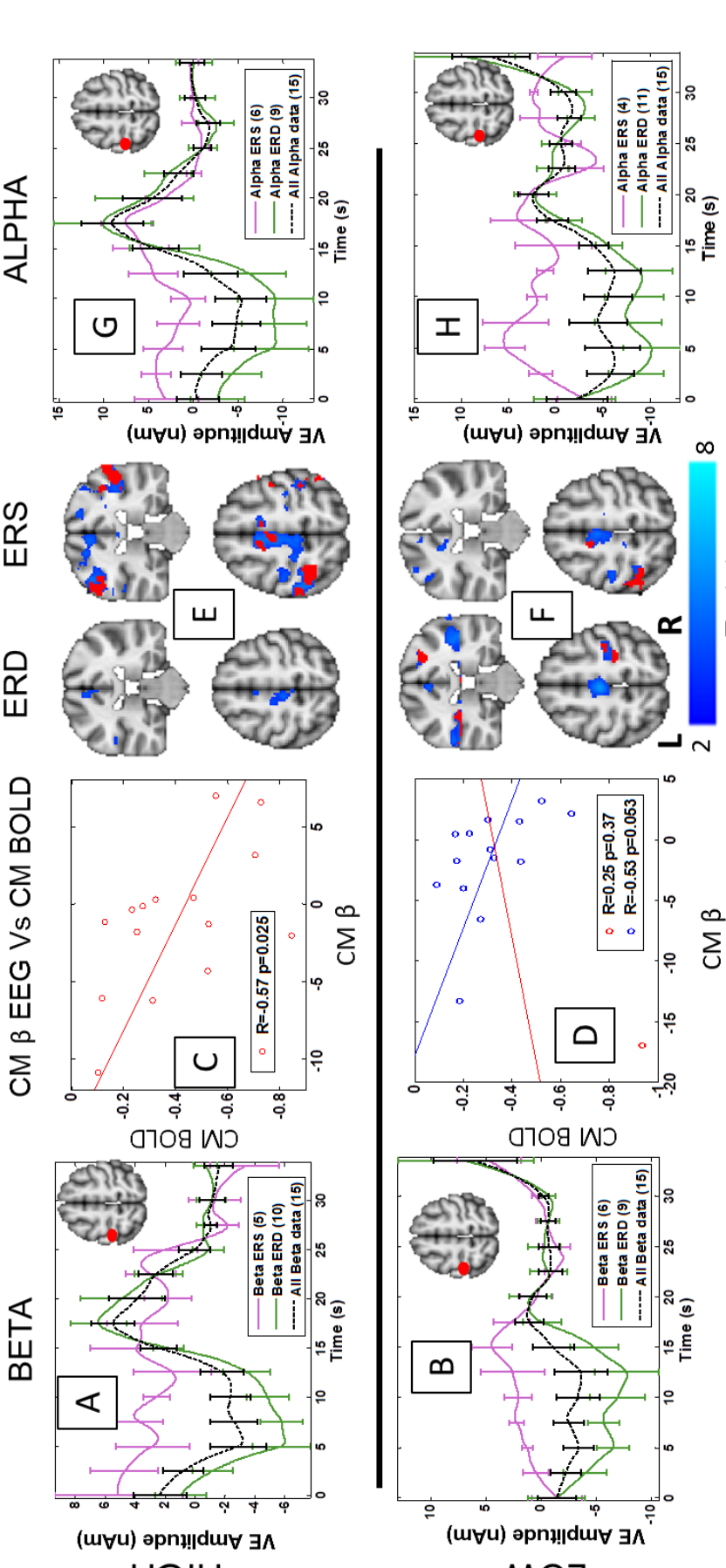

Figure 2.12. Exploration of CM β EEG responses to visual trials.
For A and B, subjects were divided into those showing β CM ERS (pink) and those showing β CM ERD (green) with mean subject response (as shown in Figure 2.9) plotted in black, legends show in brackets the number of subjects contributing. A and B show β CM responses to High and Low respectively. C and D show Pearson's correlations between CM BOLD response and CM β power for High and Low respectively, the legend shows the R and p value for the Pearson's correlation. E (High) and F (Low) show the CM NBR (blue) from the group main effect GLM analysis Z>2.3, p<0.05 cluster corrected) for those subjects showing ERD and those showing ERS separately, with significant differences when contrasting one group against the other shown in red (e.g. red in the ERD data shows that the NBR in that region is significantly greater than for the ERS subjects). Additionally, G and H show those subjects with α CM ERS (red) and those with α CM ERD (blue) with mean subject response (as shown in Figure 2.9)

2.4.5 Single-trial EEG-fMRI Correlations: *Questions 3 & 4*

The positive correlation in EEG response amplitude observed between frequency bands (Figures 6-9; Tables 3&4) and task conditions (Tables 5&6) suggested that α and β oscillations and the Tap-Grip or High-Low tasks shared a highly comparable response to the stimuli. This enabled, for the sake of brevity, concurrent EEG-fMRI single-trial correlation analysis to be conducted for all motor trials together and separately for all visual trials together, using regressors formed from only β responses in the motor cortex (IM/CM responses to motor/visual tasks respectively) and only α responses in the visual cortex (IM/CM responses to visual/motor tasks respectively).

Motor trials

IM β mVE-BOLD correlations:

Significant, group level, negative single-trial correlations were found between the mean IM β stimulus power and the BOLD response overlapping regions of IM PBR (Figure 2.13A&B); the direction of the correlations showing that the magnitude of the IM PBR increased as the magnitude of the IM ERD increased.

Positive correlations between the mean IM β stimulus power and the BOLD response were also found in areas of the bilateral LOC and IPL which overlapped with the CM NBR (Figure 2.13A), suggesting that with larger magnitude β mVE ERD during motor trials there was larger magnitude CM NBR in the LOC and IPL. This is consistent with our earlier finding when comparing responses between motor conditions (Tap>Grip) that larger mean IM mVE ERD (Figure 2.6F) was linked with larger CM LOC NBR (Figure 2.1), suggesting this cross-modal effect is a general principle of the responses to the motor task. Therefore for stimulus responses to motor tasks we observed correlations between IM EEG and IM PBR as well as IM EEG and CM NBR, with no correlation noted between IM EEG and IM NBR.

CM α vVE-BOLD correlations:

Significant, group level, negative single-trial correlations were found between the mean CM α stimulus power and the BOLD response overlapping regions of IM PBR, and small regions of CM PBR (Figure 2.13C&D); the location and direction of the correlations showing that as IM PBR increased CM ERD increased. No correlations were found between mean CM α stimulus period during motor trials and motor trial BOLD response.

Visual trials

IM α vVE-BOLD correlations:

Negative correlations were found between the mean IM α stimulus power and the IM BOLD response, overlapping regions of main effect PBR (Figure 2.13 E&F), showing that with greater IM α ERD during visual trials there was larger IM PBR.

The mean IM α vVE stimulus period power was also found to be significantly positively correlated with the BOLD response amplitude in the left, ipsilateral LOC and IPL during visual trials (Figure 2.13E), a region of IM NBR during High visual stimuli (Figure 2.2). This suggests that with greater α ERD at the vVE during visual trials there was a larger NBR in the left LOC.

Therefore for stimulus responses to visual tasks we observed correlations between IM EEG and IM PBR as well as IM EEG and IM NBR, with no correlation noted between IM EEG and CM NBR.

CM β mVE-BOLD correlations

Negative correlations were found between the mean CM β stimulus power and the IM BOLD response, overlapping regions of main effect PBR, suggesting that as IM PBR increased CM ERD increased. Positive β mVE-BOLD correlations were found in bilateral motor cortex during visual stimuli (Figure 2.13H; in regions that showed CM NBR in the main effect results). This

suggests that visual stimuli that induced higher β power responses in the motor cortex, also showed smaller magnitude NBR and vice versa.

Therefore for stimulus responses to visual tasks we observed a correlation between IM EEG and IM BOLD responses, and between CM EEG and CM BOLD responses, but not between IM EEG and CM BOLD responses.

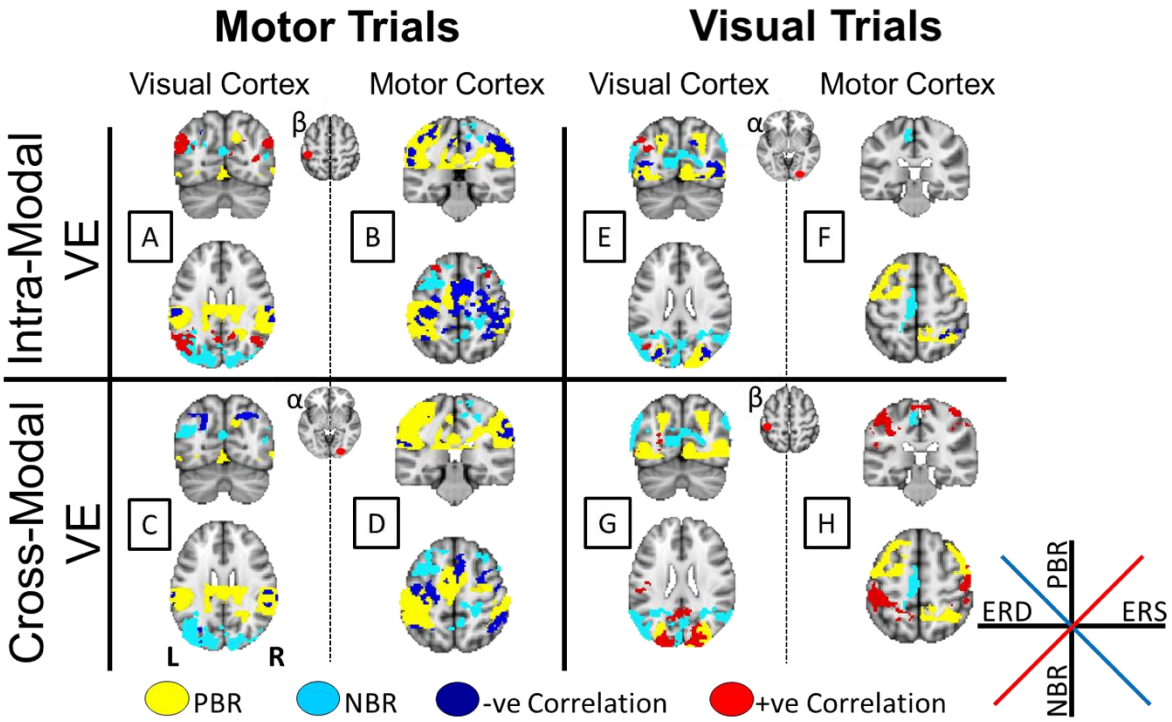

Figure 2.13. Overlaid main effect (all motor data combined or all visual data combined) and single-trial EEG-BOLD correlations (all significant regions shown).
Yellow denotes main effect PBR for all motor trials (**A-D**) and all visual trials (**E-H**). Cyan denotes main effect NBR for all motor trials (**A-D**) and all visual trials (**E-H**). Red shows regions of significant positive EEG-BOLD correlation and blue shows regions of significant negative EEG-BOLD correlation. **A**, **B**, **E** and **F** show correlation maps overlaid onto main effect maps for IM EEG correlations with BOLD responses (β for **A** and **B**; α for **E** and **F**). **C**, **D**, **G** and **H** show correlation maps overlaid onto main effect maps for CM EEG correlations with BOLD responses (α for **C** and **D**; β for **G** and **H**). Visual cortex: y=29, z=48; Motor cortex: y=48, z=63.

2.5 Discussion

In the current study we used simultaneous EEG-BOLD-CBF recordings to study two manifestations of NBR, occurring in either the ipsilateral sensory cortex to that which was directly stimulated (IM) or a separate unstimulated sensory cortex (CM). Our aim was to further understand the relationship of these two different NBRs with underlying CBF and EEG signal changes. To our knowledge this is the first study of reciprocal visual and motor NBRs using two separate tasks.

2.5.1 Question 1: CM NBR was elicited by motor tasks and visual stimuli and both IM and CM NBRs were modulated by task/stimulus intensity

The activity of the brain's networks is well reported to display both collaborative and antagonistic relationships (Fox, Snyder et al. 2005). Performance of many everyday tasks require a collaboration and balance between mutual co-operation and management of resources to maximise efficient processing and minimise unhelpful competition, as well as enabling suppression of distraction to optimise performance. Here we see that unilateral single modality stimuli induce NBRs in unstimulated areas of both motor and visual cortex with overlapping NCBF to both volitional motor tasks and passive visual stimuli. NBR of auditory cortex would also be expected (Laurienti, Burdette et al. 2002, Mozolic, Joyner et al. 2008), however our obliquely angled slices, with limited coverage due to the DABS sequence, did not enable measurement of fMRI data from that location. Similarly, default mode network (DMN) NBR may also have been expected, and although NBRs in the IPL were noted, the slice selection along with the simplicity of the stimuli used reduced our ability to detect any BOLD signal from the DMN in its entirety. Despite this we found that the amplitude of both IM and CM NBR to visual and motor conditions increased with increasing stimulus intensity or task difficulty.

In the current data we observed only a weak effect of stimulus intensity on the IM PBR in the visual or motor data, observing only a ~1% increase in PBR amplitude between 10% and 100% visual contrast and no change for different motor tasks (Figure 2.14). Whilst in contrast to some previous findings (Shmuel, Yacoub et al. 2002), we believe this is explained by our Tap and Grip motor tasks involving little difference in force output or pacing (Dai, Liu et al. 2001) and evidence suggesting the visual flicker rate is a stronger determinant of stimulus response amplitude than contrast (Kwong, Belliveau et al. 1992, Liang, Ances et al. 2013). We did however, observe that both IM and CM NBR magnitudes increased with stimulus intensity in both visual and motor conditions (see Figure 2.14) replicating and extending the finding that the intensity of passive visual and somatosensory stimuli increased the magnitude of IM NBRs (Shmuel, Yacoub et al. 2002, Klingner, Hasler et al. 2010). Previous reports have indicated that increasing the difficulty of an auditory target detection task increased the magnitude of visual cortex NBR (Hairston, Hodges et al. 2008), our work supports this finding of the CM NBR reflecting the level of suppression in the non-stimulated modality to prioritise processing of the stimulated modality. In addition, we observed parallels of this effect in the EEG data as, compared to Grip, the Tap motor task induced larger IM ERD, as well as a greater number of subjects with CM ERS of visual cortex α power. However, no differences were observed in the IM EEG responses between High and Low visual stimuli, matching the PBR result.

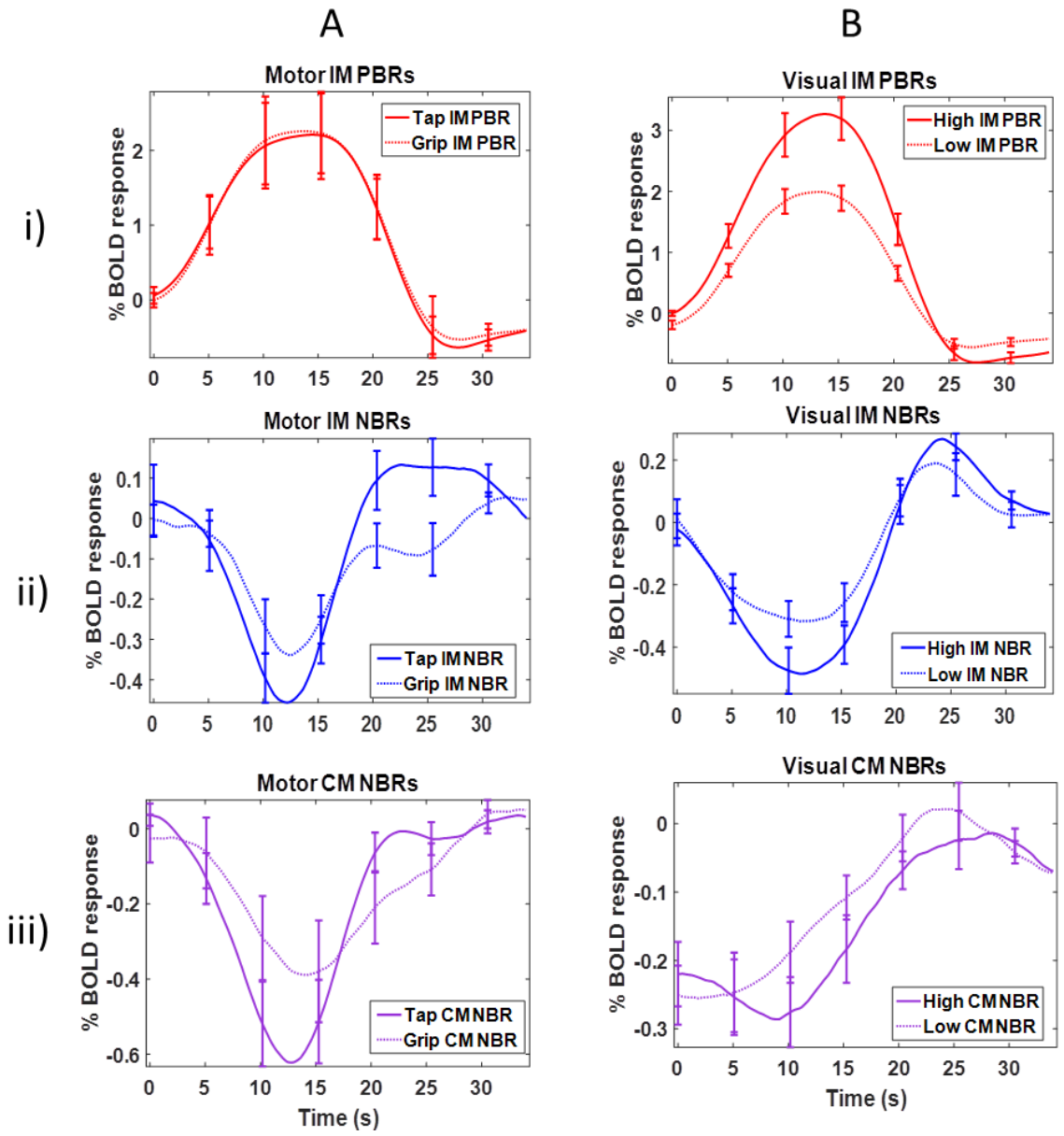

Figure 2.14. Comparison plots of BOLD response taken from ROIs centred over peak responses in IM/CM masks to each individual task.
A shows motor Tap (solid line) and Grip (dotted line) BOLD responses. **Ai** shows IM PBRs which show little difference in percentage change in BOLD response. Larger IM (**Aii**) and CM (**Aiii**) NBRs were found to Tap task than Grip task.
B shows High (solid line) and Low (dotted line) BOLD responses. **Bi** shows IM PBRs which show that High trials evoked a larger percentage change in BOLD response. Larger IM (**Bii**) and CM (**Biii**) NBRs were found to High than Low.

2.5.3 Question 2a: There are intrinsic links between IM NBRs and CM NBRs

From studying the correlation between mean BOLD amplitudes it has been shown that a subject's CM NBR was not related to the amplitude of PBR in their stimulated IM cortex (Figure 2.3), suggesting the level of CM suppression is not simply proportional to the degree of IM sensory activation. However, for the motor tasks CM NBR was positively related to the IM NBR (Figure 2.4). This finding suggests a relationship between the two instances of NBR, such that the largest magnitude IM NBR occurred concurrently with largest magnitude CM NBR. This indicates a mutual suppression of the two cortical areas not directly required for the task. The lack of coupling between the NBR and PBR across subjects suggests the intriguing possibility that the NBR amplitude was not solely determined by the level of bottom-up processing and contains contributions from systems outside of the primary sensory cortex.

2.5.3 Question 2b: IM EEG and CM EEG

Fluctuations in the power of α oscillations are widely reported to represent temporal variations in cortical excitability (Romei, Brodbeck et al. 2008). Alpha is often cited as an electrophysiological marker of inhibition, a mechanism that can both regulate higher frequency activity (Osipova, Hermes et al. 2008), influence the level of feedback from higher cortical areas (van Kerkoerle, Self et al. 2014) and act to block unwanted inputs and filter out potentially distracting sensory information (Mazaheri and Jensen 2010, Mathewson, Lleras et al. 2011). Consequently whilst α power is commonly decreased (ERD) in sensory cortex during the processing of information, reflecting increased excitation; increases in α power have been linked to increased cortical inhibition, such as occurs in the occipital hemisphere ipsilateral to the direction of spatial attention (Worden, Foxe et al. 2000, Rihs, Michel et al. 2007), or in the visual cortex during performance of memory retention (Jensen, Gelfand et al. 2002). Fluctuations in α power have been closely linked to both PBR and NBR amplitudes during passive visual stimulation (Mayhew, Ostwald et al. 2013). Additionally, the balance of α

power within the visual cortex due to attentional manipulation has also been previously linked to visual NBRs/PBRs during visual object recognition (Zumer, Scheeringa et al. 2014), in the current work we investigated whether such findings extend between sensory cortices using tasks involving minimal attentional demands.

Consistently across both modalities and conditions we observed a positive correlation of between-subject variability in IM and CM EEG response amplitudes (Figure 2.10). This can be interpreted as evidence that the subjects who showed a CM ERD also showed the strongest magnitude IM ERD (i.e. most negative EEG amplitude) to the same stimulus; and the subjects that showed a CM ERS also showed the weakest magnitude IM ERD. This occurred independently from task condition, as for all tasks we observed a similar pattern of positive coupling between visual and motor cortex EEG responses, a consistency which implies this is a fundamental property of the brain's response. The functional interpretation of this positive IM-CM EEG coupling may appear counter-intuitive, with a negative correlation expected such that greater activation (ERD) of the stimulated/IM cortex was associated with greater suppression (ERS) of the CM sensory modality, as previously reported in fMRI within a single modality (Shmuel, Yacoub et al. 2002, Klingner, Hasler et al. 2010). However, in line with our observation of a lack of relationship between IM PBR and CM NBR, both our EEG and fMRI data suggest that for average responses this was not the case for either task.

2.5.4 Question 3&4: IM and CM NBR are related to IM and CM EEG responses therefore providing evidence for a neuronal origin

ERS responses have previously been measured in the motor cortex to visual modality stimulation (Koshino and Niedermeyer 1975, Pfurtscheller 1992) and vice versa (Neuper and Pfurtscheller 2001). However this is not thought to occur in every individual, for example Koshino et al. (Koshino and Niedermeyer 1975) found that CM ERS (in motor cortex to visual stimulus) was elicited in only 54% of subjects tested. Here we found mean α and β CM ERS in

only a proportion of subjects (between 27% and 46%) depending upon the task and frequency band (Figures 11A&B and 12A&B). A hypothesis of the current work was that ERS would be observed over the unstimulated sensory cortex, reflecting a measure of the suppression of processing in the unstimulated system. ERS of low-frequency oscillations during a task have been less widely studied than the ERD, and most reports focus on α frequency ERS, often in the context of solely attentional modulations (Worden, Foxe et al. 2000, Jensen and Tesche 2002, Thut, Nietzel et al. 2006, Rihs, Michel et al. 2007, Rihs, Michel et al. 2009), rather than β. The exact relationship between α and β, and differentiation of their functional roles in sensory processing, remains unclear. Here we consistently measured IM ERD of both α and β, but as we find a high degree of similarity in their response amplitudes we focus analysis on visual cortex α and motor cortex β, which are arguably considered to be the dominant frequency responses in the corresponding cortices, to simplify reporting of results. The use of one spatial location per sensory cortex enabled us to assess CM EEG responses using an independently selected region of interest, assuming no spatial difference between IM and CM responses. Given the limited spatial resolution of EEG, this assumption is reasonable and visual inspection of single-subject beamformer maps confirmed that no CM responses occurred consistently in other regions of sensory cortex.

IM NBRs were consistently accompanied by a significant IM ERD in the power of α/β oscillations. In contrast, subjects were divided between those showing CM ERS and ERD despite showing CM NBR on average. We found that this between subject variability in CM ERS/ERD was related to individual subjects CM NBR amplitude. EEG-fMRI correlations were found between trial-by-trial variability of α/β power and both IM and CM NBR magnitude, providing further evidence for a relationship, albeit complex, between NBRs and neuronal activity. Together these results highlight that IM and CM NBRs are related to local changes in neuronal activity.

Our trial-by-trial EEG-fMRI analysis showed that a coupling of larger IM activation with larger CM deactivation occurred at the single-trial level in the motor data, where the mVE β ERD was negatively correlated with IM PBR and positively correlated with CM NBR in visual cortex (Figure 2.13). It has been shown in previous work that single-trial response correlations can occur with opposite polarity to that shown in the average responses (Mayhew, Mullinger et al. 2016). This suggests that the dynamic temporal evolution of behaviour contains the anticipated functional relationship of collaborating IM activation and CM suppression. No equivalent relationship between CM NBR and IM α ERD was observed in the visual dataset, although IM PBRs were found to correlate with IM and CM EEG responses (Figure 2.13E&G respectively). This represents the second instance (in addition to IM-CM NBR, Figure 2.4) where cross-modal coupling is observed only in the motor task, which we believe arises due to a difference in the brain's processing of the two tasks related to their differing demands. The passive nature of the visual stimuli induced more automatic, bottom-up sensory responses compared to the volitional, active performance, of the motor task good performance of which requires greater task engagement and top-down attentional control. We suggest that this top-down control exerts influence over the lower level sensory systems to optimise task performance and drives greater collaboration between the two sensory systems during Tap and Grip than during visual stimulation (Corbetta and Shulman 2002, Ciaramitaro, Buračas et al. 2007).

Investigating trial-by-trial EEG-fMRI correlations has provided further evidence that IM and CM NBRs are related to changes in neuronal activity. Two types of CM NBR (in visual cortex during motor tasks and in motor cortex during visual stimuli) showed a significant positive correlation with mVE β power. The CM NBR amplitude during motor tasks at the LOC was seen to increase as motor cortex β power increases (Figure 2.13A). For visual trials, both IM and CM NBRs showed positive correlations with IM and CM stimulus period power respectively (Figure 2.13 E&H). Similar to the LOC BOLD response modulation during motor

tasks, the region was also found to have increased BOLD response with increasing IM neuronal activity during visual trials (Figure 2.13 E). Surprisingly, CM ERS responses during the stimulus period were seen inconsistently both within- and between-subjects for a single modality (e.g. subject 4 showed CM β ERS during Low but CM β ERD during High), while other subjects showed consistent α and β CM ERS in a single modality (e.g. subject 2 shows α and β CM ERS during Grip and Tap).

Bilateral IM ERD of both α and β power, strongest contralaterally, were consistently measured across subjects during both motor tasks and visual stimuli, whilst, in contrast, a clear lateralisation of contralateral positive and ipsilateral negative IM BOLD and CBF responses was observed as previously reported (Allison, Meador et al. 2000, Mullinger, Mayhew et al. 2014). The source of this discrepancy between EEG and fMRI response polarities remains unresolved, however it is likely that the stronger contralateral α and β ERD are associated with the widely reported contralateral gamma ERS (Muthukumaraswamy 2010) and tentative reports suggest a gamma ERD occurring ipsilateral to finger movements (Huo, Xiang et al. 2010) would appear a plausible correlate of ipsilateral NBR in line with rodent work (Boorman, Kennerley et al. 2010, Boorman, Harris et al. 2015). A few previous studies have been able to measure gamma EEG responses by using sparse fMRI sequences (Mulert, Leicht et al. 2010, Scheeringa, Fries et al. 2011), however the implementation of the DABS sequence employed here was not designed to be used in that manner.

Visual stimulation induced CM NBR and negative CBF with a high degree of spatial agreement to the IM motor contralateral PBR (Figure 2.2) and the IM ERD (mVE). In comparison, motor stimulation induced a slightly more complex pattern of CM BOLD responses, with CM NBR in anterior and bilateral LOC and a CM PBR in small bilateral regions of posterior visual cortex. We suggest this pattern could arise from either visual imagery of the motor movement (as the subject's hand was at their sides and out of sight in the scanner) or focussing on the visual

word cue instructing the task performance. The relatively long duration of the stimulus period (14s) means that we would expect the visual cue to contribute little BOLD response, with it primarily generated at cue onset and offset rather than during the whole stimulation period. The presence of both CM NBR and PBR within the visual cortex complicates the understanding of the origin of the CM α response; although, as shown by the group mean beamformer maps, the location of the vVE lies in dorsal visual areas approximating the LOC (Figure 2.5), closer to the CM NBR observed in superior occipital cortex.

2.5.5 Between subject variability in CM ERS and NBR

It is important to note that we observe between-subject variability in the polarity, not just the amplitude of the CM EEG response, as we report that some subjects show CM ERD in addition to those showing ERS. This is despite the observation of CM NBR on average in the group fMRI data, indicating there wasn't a clear, direct correspondence between CM EEG and fMRI response polarities. Even when observed, our data suggests that the ERS had an inherently smaller response amplitude than the ERD (compare Figures 2.6&.8 with 2.11&.12). Therefore, this lack of a clear consistent CM ERS either reflects: a lack of measurement sensitivity, a limitation of EEG source analysis (as discussed below: Potential limitations) or an overt replacement by the ERD response. It also suggests that the CM ERS was a much less automatic process than the consistently observed IM bilateral ERD. Overall we found a relationship between the CM ERS and the CM NBR, but the direction of this relationship was dependent upon the exact task conditions. A negative relationship was seen in the visual data, where subject's with stronger mean CM ERS showed greater magnitude CM NBR in motor cortex, providing persuasive evidence of a link between the two responses. This negative coupling was not replicated in the motor data however, where instead a greater CM NBR was seen amongst subjects with CM ERD, a result that could partially arise from subject's fixation on the visually displayed motor cue, thus creating a visual ERD which counteracts any CM

ERS effect elicited by the motor task performance. However, our observation of subjects with CM ERD in response to both visual and motor tasks suggests that the presence of the visual cue in the motor paradigm cannot explain this effect alone. Instead we suggest that the CM ERD reflects differences in arousal and cortical excitability whereby in some subjects desynchronization of low frequency oscillations is more widespread across multiple cortical networks than in others, perhaps indicating an inefficiency of network segregation in some subjects and a reduced ability to suppress activity in task-irrelevant sensory systems.

It is interesting to note that the motor CM ERS responses display a relatively large increase in power in the first half of the stimulus period followed by a lower but still elevated level of power (Figure 2.11G&H). This perhaps arises due to the long duration of the stimuli (14s) and subjects not maintaining a consistent level of engagement after task initialisation. This observation may suggest that the ERS is a naturally more transient, less sustained response than the ERD. Although the allocation of attention has been widely related to changes in α power (Pfurtscheller and Klimesch 1991), we did not measure attention levels with this data. However, the lack of a similar pattern in the visual CM ERS responses (Figure 2.12A&B) suggests a difference between the two modalities which could relate to the volitional aspect of the motor conditions against the passive of the visual.

2.5.6 Potential limitations of methodology and comparison between EEG recorded inside and outside the MRI scanner

We cannot rule out an alternate explanation that the observed positive coupling of IM and CM EEG responses arises from limitations of the LCMV beamformer and EEG volume conduction that may impair our ability to distinctly separate activity from sources in the visual and motor cortices. For instance due to possible inaccuracies in the headmodels or imperfections in the solution of the inverse problem it is possible that signal leakage from the stronger IM source confounds measurement of the CM response, a situation that would be exacerbated in a

subject with naturally high levels of occipital oscillatory power who showed a widespread ERD that extended over parietal cortex and into anterior sensorimotor regions. However, correcting for signal leakage we have shown that there is little/no change in the correlations between IM and CM EEG power across subjects, therefore highlighting our ability to distinguish the signals using the VEs defined.

Due to MRI gradient and ballistocardiogram artefacts inherent in recording EEG-simultaneously with fMRI the reliability of our ability to measure CM ERS signals in the lower signal-to-noise MR environment could be questioned. To provide a comparative assessment of the reliability of the EEG recordings inside the scanner and to familiarise the subjects with the stimuli, EEG recordings of responses to Tap and High conditions only were collected outside of the scanner whilst subject's sat upright in front of a computer monitor that displayed the same visual stimulation and motor cues as during scanning. Twenty-two trials were recorded for each of the conditions, 14/14s stimulus/baseline (active period: 0.5-10.5s; passive period: 17.5-27.5s). EEG data were analysed as described for data recorded inside the scanner, and motor and visual cortex CM responses extracted from the IM VE locations as defined from the scanner data. We observed patterns of α and β CM ERS during stimulation that were highly similar to those seen in the inside scanner data. On average, Tap induced no CM response whereas High induced a weak CM ERD. On further inspection we found that subjects were again divided between those showing ERS and those showing ERD (Motor Tap: α, ERS subjects: 1,3,4,5,7,10,12,14; mean = 5.1± 5.5nAm; Visual High: β, ERS subjects: 1,3,4,9 mean = 3.4 ± 3.4nAm). This suggests that our observations inside the scanner are not confounded by the MR environment artefacts, or movements occurring inside the magnetic field, but reflect neuronal activity related to the stimuli.

2.5.7 Summary

Previous work has shown that IM NBRs are at least partially neuronal in origin (Shmuel, Augath et al. 2006, Mullinger, Mayhew et al. 2014), here we replicate this finding and go on to show that this is also the case for CM NBRs. We also show that the IM as well as CM NBRs are modulated by stimulus intensity. Taken together the results show that for fMRI GLM analyses, when IM and CM NBRs are located they can both be interpreted as resulting in part from neuronal changes.

CHAPTER 3

NEUROVASCULAR COUPLING OF INTRA- AND CROSS MODAL NEGATIVE BOLD RESPONSES IN VISUAL AND SENSORIMOTOR CORTEX

3.1 Abstract

In this Chapter, using the previously acquired BOLD-CBF data we calculate $CMRO_2$ for PBRs, IM and CM NBRs. In order to better understand the similarities/differences in metobolic/vascular origin between these BOLD responses we directly compare the ratio of $CMRO_2$:CBF (*n* value) between each of the regions. We also assess the timecourse of each of these BOLD (and CBF) responses to better understand the how these temporal dynamics may differ from one another. We find decreases in $CMRO_2$ for all IM and CM NBRs, suggesting they both originate in part from changes in neuronal activity. The *n* values were found to be similar for CM NBRs and PBRs when derived from group data while IM NBRs differ from both. However deriving *n* from single subject data shows both NBRs differ from PBRs. Assessing timecourse dynamics, NBRs were seen to have a slower offset in general than the PBRs.

3.2 Introduction

As discussed in Chapter 1 the BOLD signal is determined by the relationship between changes in cerebral rate of oxygen consumption ($CMRO_2$), cerebral blood flow (CBF) and cerebral blood volume (CBV) (Buxton, Griffeth et al. 2014). CBF and $CMRO_2$ are coupled at rest but become uncoupled during neuronal activity, with large increases in CBF and proportionately smaller increases in $CMRO_2$ and CBV leading to a PBR (Buxton, Wong et al. 1998) at the spatial location of increased neuronal activity. However, as described in Chapter 1, the physiological origin of NBRs remains the subject of much debate, as there are a number of potential generating mechanisms such as: a) decreased neuronal activity leading to reduced CBF and a smaller reduction in $CMRO_2$ (Shmuel, Yacoub et al. 2002, Pasley, Inglis et al. 2007, Mullinger, Mayhew et al. 2014); b) increased neuronal activity and $CMRO_2$ with no change in CBF (Schridde, Khubchandani et al. 2008); or c) potentially 'haemodynamic steal' causing a CBF reduction with no change in $CMRO_2$ due to a CBF increase in a nearby activated region (Harel, Lee et al. 2002).

If a BOLD response requires a change in $CMRO_2$ this implies there is a neuronal component involved in its generation. As each of the mechanisms above requires an understanding of the change in $CMRO_2$, to gain a deeper understanding of the metabolic and vascular origins of the IM and CM NBRs, simultaneous measures of CBF and BOLD can be acquired. Using these measures the ratio of the change in $CMRO_2$ to that in CBF ($\Delta CMRO_2/\Delta CBF$, n) during stimulation compared to baseline then allows examination of neuro-metabolic-vascular coupling separately for both PBRs and NBRs (Buxton, Wong et al. 1998). This enables the mechanism by which the BOLD responses are generated to be examined allowing the IM and CM NBRs to be compared to one another and both to be compared to the PBRs, something which has not previously been done.

Our results from Chapter 2 showed that both IM and CM NBRs were spatially congruent with decreases in CBF for both motor and visual tasks. We now perform a more detailed investigation into whether CBF changes alone account for the IM and CM NBRs, or if $CMRO_2$ changes are also required to explain the data. Such additional $CMRO_2$ changes would imply that changes in neuronal activity as well as CBF underlie the origin of the NBR. We calculated *n* separately for regions of IM and CM NBR using the Davis model (see Equation 3.1; (Davis, Kwong et al. 1998)). We also calculated *n* for IM PBRs in order to compare the underlying mechanisms to those of the NBRs.

Furthermore, our comparison of NBR and PBR is extended to also consider their temporal characteristics. Previously it has been shown that IM NBRs have a slower onset, a slower time to peak and a faster offset time than PBRs (Shmuel, Augath et al. 2006, Liu, Shen et al. 2011). Here we attempt to replicate this finding, examining the positive and negative IM BOLD timecourse dynamics (onset, peak and offset times). We also extended this to examine any differences between CM NBRs and IM BOLD response as well as examining differences between IM and CM CBF responses.

3.3 Methods

BOLD and CBF data during visual (Low, High) and motor (Tap, Grip) stimulation were collected as described in Chapter 2. IM and CM ROIs defined in Chapter 2 were used to extract the average BOLD and CBF response timecourses to each stimulus and percentage signal change of the BOLD and CBF responses (as per Chapter 2).

3.3.1 $CMRO_2$ calculations

The percentage signal change of the extracted BOLD and CBF in Chapter 2 were used to calculate the change in $CMRO_2$ relative to baseline via the Davis model (Davis, Kwong et al. 1998), see Equation 3.1.

Equation 3.1.

$$\frac{CMRO_2}{(CMRO_2)_0} = \left(1 - \frac{\left(\frac{\Delta BOLD}{BOLD_0}\right)}{M}\right)^{\frac{1}{\beta}} \left(\frac{CBF}{CBF_0}\right)^{1-\alpha/\beta}$$

Parameters for the Davis model were taken from recent literature: the Grubb coefficient, α=0.2 (Chen and Pike 2009) relating to the relationship between CBF and CBV (CBF^{α} = CBV); deoxyhaemoglobin concentration, β=1.3 (Mark, Fisher et al. 2011). A range of values for *M*, the maximum possible BOLD signal, were taken from literature reports for motor and visual cortices and adjusted for our field strength and TE (Chiarelli, Bulte et al. 2007). Motor cortex *M* values used were between 6% (Gauthier, Madjar et al. 2011) and 14.9% (Kastrup, Kruger et al. 2002), while visual cortex *M* values between 6% (Gauthier and Hoge 2013) and 40.2% (Uludağ, Dubowitz et al. 2004) were used. The change in CBF was plotted against the change in $CMRO_2$ and the "group-calculated" $CMRO_2$/CBF coupling ratio (*n*) taken from the gradient of the linear fit to these data across subjects, the error was the standard error in the fit.

To test for significance between IM NBR, IM PBR and CM NBR *n* values as calculated across subjects, we also defined "subject-calculated" *n* values (Griffeth, Perthen et al. 2011). Separately for each condition (High, Low, Tap and Grip) the average BOLD and CBF signal changes across 3 trials (from 24 trials in total across the 4 runs) within each subject were calculated. This provided 8 BOLD and CBF points for each condition per subject from which $CMRO_2$ values and subject specific *n* values were calculated. In order to reduce any possible bias in the calculations, we used 100 random permutations of the possible 24 trials, calculating the average BOLD and CBF changes across 3 trials for each condition in each permutation and subsequently an *n* value for each of the permutations. A mean *n* value was then taken for each subject across permutations. M was taken as 10.5 in the motor cortex and two values of 15 and 20 in the visual cortex. One-way ANOVAS with post-hoc Bonferroni correction

(independent variable of location [IM NBR, IM PBR and CM NBR], dependent variable of *n* value; $p<0.05$) were then used across all subject responses and conditions in a single cortex (motor or visual) to calculate significant differences in *n* between responses.

3.3.2 Timecourse calculations

The extracted BOLD and CBF data were used to test for differences in the temporal dynamics of the IM PBR, IM NBR and CM NBRs. The onset time (time to reach 5% of peak response), time-to-peak, and offset time (time to reach 50% of the peak response) were calculated for each subject's mean BOLD responses (IM PBR, IM NBR and CM NBR) as well as their CBF responses (IM PCBF, IM NCBF and CM NCBF). One-way ANOVAs, with post-hoc Bonferroni correction ($p<0.05$), were then used to compare each of the three temporal measures between all responses for BOLD and then CBF data.

3.4 Results

3.4.1 $CMRO_2$-CBF coupling ratio

As shown in Figure 3.1, with increasing M value, the PBR $CMRO_2$ increased and, conversely, for NBRs the $CMRO_2$ value decreased with increasing M values. We calculated $CMRO_2$ in IM PBR regions, which indicated that an increase in oxygen metabolism compared to baseline occurred alongside the observed increase in CBF in all conditions (see Figure 3.1). In contrast, we found decreases in $CMRO_2$ compared to baseline in both IM and CM NBR regions, accompanied by decreased CBF. This was the case across all stimulus conditions and the majority of *M* values tested (Figure 3.1).

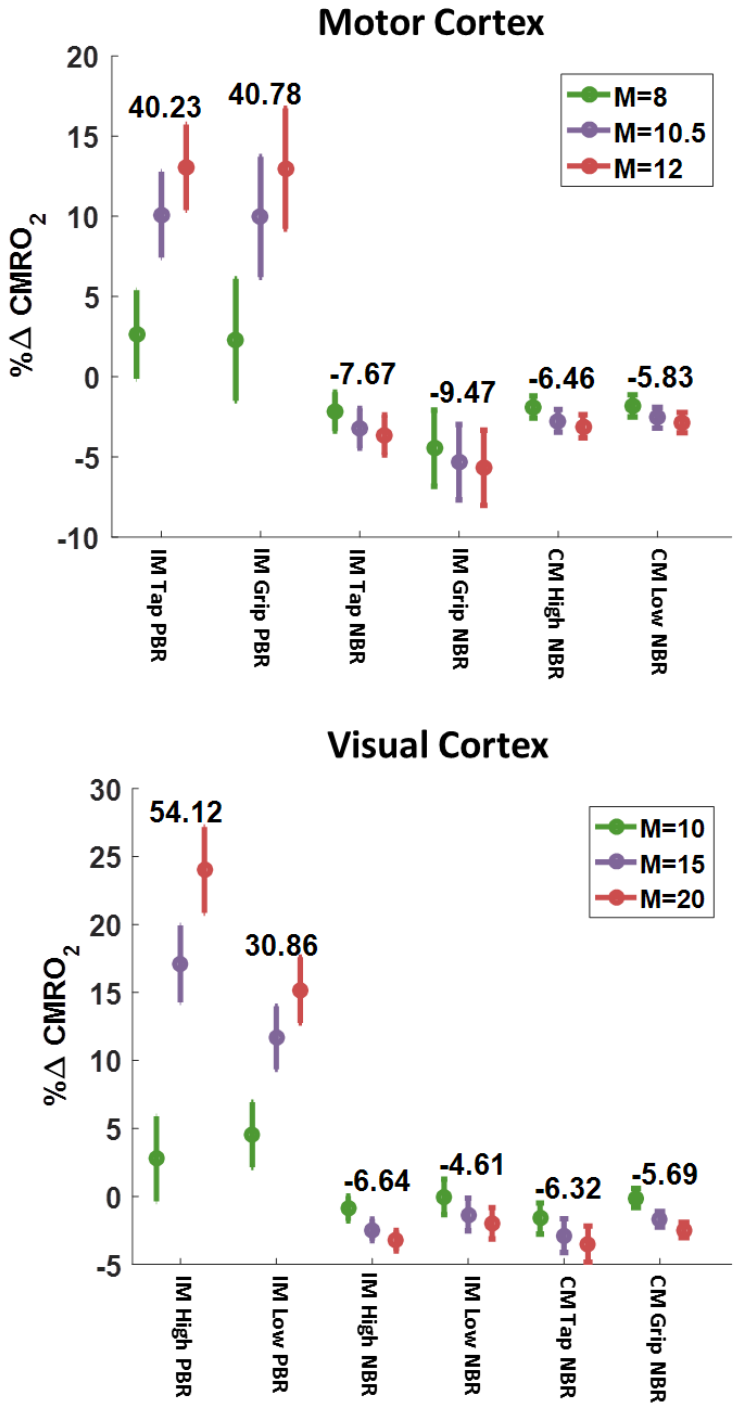

Figure 3.1. Calculated group mean $CMRO_2$ percentage change (mean and standard deviation across subjects) for each BOLD response region: IM PBR, IM NBR and CM NBR for different M values. For each condition (Tap, Grip, High and Low) here 3 M values are shown: 8,10.5 and 12 for responses within the motor cortex; and 10,15, and 20 within the visual cortex. The floating number is the mean percentage change in CBF across subjects for that condition.1

Group calculated *n* values remained consistent with increasing *M* in IM NBR regions but increased with increasing *M* in IM PBR and CM NBR regions (Figure 3.2). However, the relative pattern of *n* values between IM PBR, IM NBR and CM NBR regions was consistent across all values of *M* used.

As shown in Figure 3.2A&B, higher *n* values were calculated in IM NBR regions than in IM PBR regions, this is seen (as indicated by non-overlapping error bars) in all cases except for Tap. For the IM PBR and NBR regions we observed a pattern for the value of *n* to be lower for the more intense/complex task conditions (Tap/High) than for the less intense conditions (Grip/Low), which provides validation of our data quality as this agrees with previous reports in visual cortex PBRs (Liang, Ances et al. 2013). This effect was particularly evident between Tap and Grip IM NBRs (Figure 3.2A) as well as between High and Low IM PBRs (Figure 3.2B).

CM NBR region *n* values showed greater similarity with the *n* values of the IM PBR regions than with those of the IM NBR regions. In general, the *n* values of CM NBR regions were lower than the *n* values of IM NBR regions (Figure 3.2C&D). In the motor cortex, the High CM NBR *n* values were found to be lower than Grip IM NBR with a similar trend shown in relation to Tap IM NBR (Figure 3.2C). In the visual cortex, Grip and Tap CM NBRs *n* were both lower than High and Low IM NBR *n* values (Figure 3.2D). While the *n* values for the Tap CM NBR was significantly lower than the Grip CM NBR.

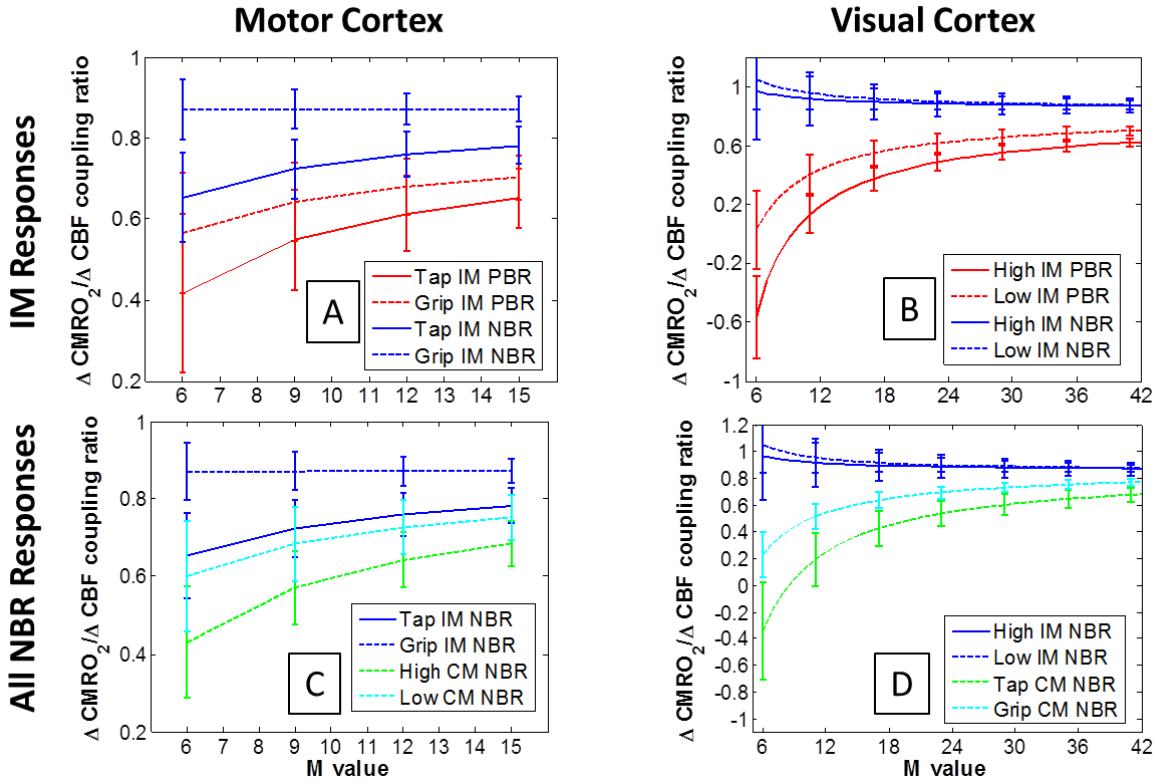

Figure 3.2. $\Delta CMRO_2/\Delta CBF$ coupling ratios (*n* values) for IM and CM ROIs. A) Motor trial IM BOLD response *n* values for varying M values (6-15), PBR (red) and NBR (blue). B) Visual trial IM BOLD response *n* values for varying M values (6 to 41). C) NBRs located in the motor cortex, IM NBRs (blue), CM NBRs (green and cyan). D) NBRs located in the visual cortex, IM NBRs (blue), CM NBRs (green and cyan). A trend is seen for higher *n* values for IM NBRs than IM PBRs or CM NBRs, with CM NBR *n* values showing greater similarity overall to IM PBRs.

To test the statistical significance of differences in *n* between regions, inter subject *n* values were calculated (Griffeth, Perthen et al. 2011) then one-way ANOVA used with ROI as the independent variable and *n* value as the dependent variable.

For the motor data, the single subject calculated *n* values were found to be similar to those of the group calculated values for 3 of the 6 ROIs (both IM PBRs and the Grip IM NBR), see Figure 3.3A. However, the Tap IM NBR, CM High and CM Low had larger *n* for the averaged single subject data than was calculated at the group level (see Figure 3.3A). In the visual data, there was a notable difference between the group level calculated *n* values for CM NBRs and

those calculated from single subject data, while all other values showed reasonable similarity (Figure 3.3B&C; M=15 and 20 respectively). As shown in Figure 3.3D&E, the gradients of the linear fit (*n* values) for single subject CM NBR data were consistent within each condition. However, the group level gradient was smaller than the average of all the single subject gradients. Subject's average responses are plotted in Figure 3.3D&E as crosses and show that the group result is not completely representative of the inter-subject ratio.

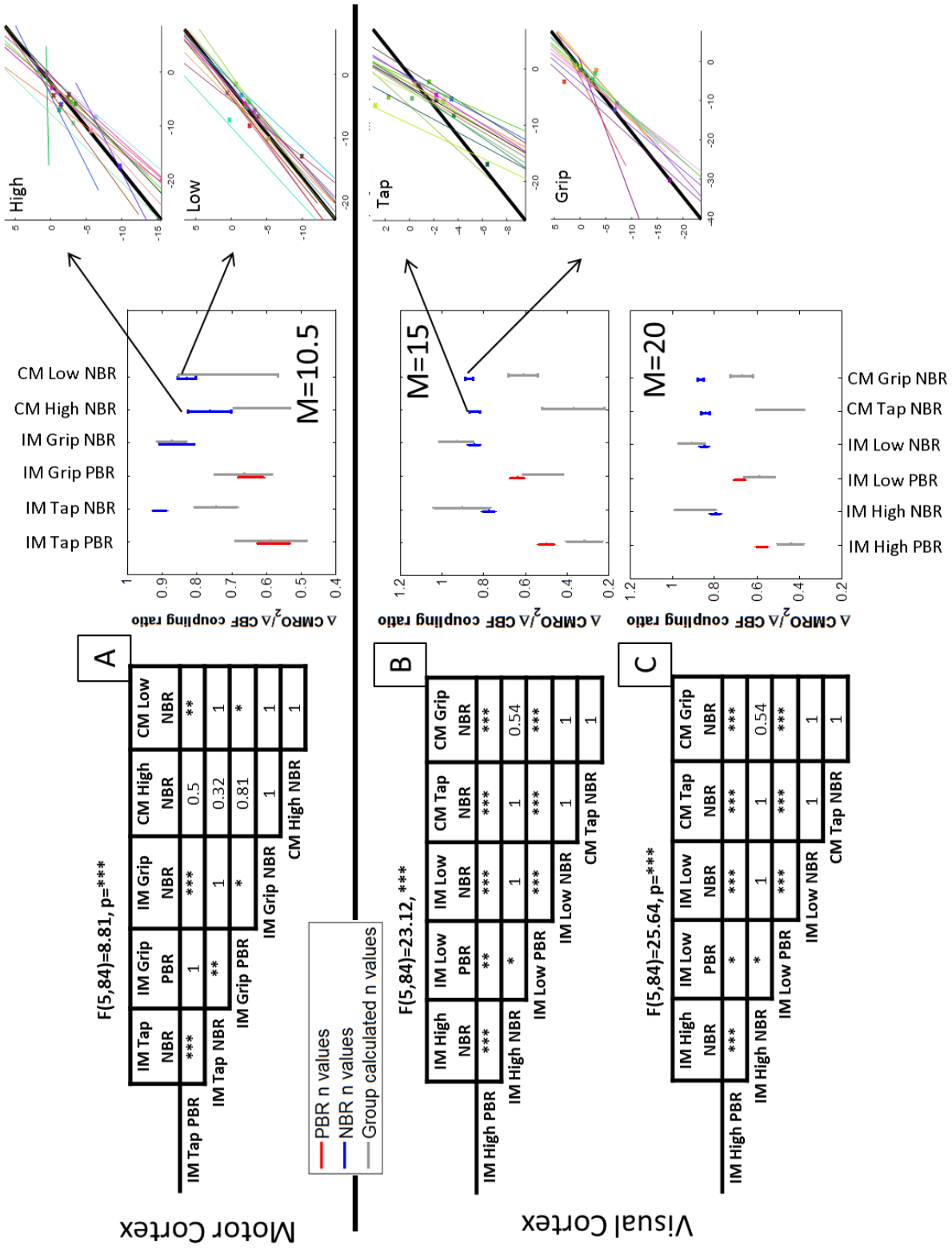
Motor Cortex
Visual Cortex
A
B
C
F(5,84)=8.81, p=***
F(5,84)=23.12, ***
F(5,84)=25.64, p=***
PBR n values
NBR n values
Group calculated n values
M=10.5
M=15
M=20
CM Low NBR
CM High NBR
IM Grip NBR
IM Grip PBR
IM Tap NBR
IM Tap PBR
CM Grip NBR
CM Tap NBR
IM Low NBR
IM Low PBR
IM High NBR
IM High PBR
High
Low
Tap
Grip

Figure 3.3. Inter-subject $\Delta CMRO_2/\Delta CBF$ coupling ratios (*n* values) for IM and CM ROIs. Tables show the results of ANVOA assessing differences between the ROIs *n* values (*=p<0.05, **=p<0.01, ***=p<0.001). With ANOVA F test results shown above each table. A shows the Motor cortex *n* value results calculated for M=10.5, the central figure displays the inter-subject *n* values in colour (mean ± SD) and the group calculated n values in grey (as per Figure 3.2) for each ROI. The two arrows point to two plots which show each individual subject *n* values calculated (line of best fit between $CMRO_2$ and CBF) in colour and the group n value in black for the CM results. B and C shows the Visual cortex *n* value results calculated for M=15 and 20 respectively, the central figure displays the inter-subject *n* values in colour (mean ± SD) and the group calculated n values in grey (as per Figure 3.2) for each ROI. These two plots highlight the difference between the inter-subject *n* values and the group calculated *n* values. The two arrows point to two plots which show each individual subject *n* values calculated (line of best fit between $CMRO_2$ and CBF) in colour and the group n value in black for the CM NBR ROIs when M=15. The Tap results here show the disparity between each subects *n* value and the averaged inter-subject *n* value.

Using one-way ANOVA, for the single subject motor data (M=10) no difference was found between the two IM PBR *n* values, while both were found to be significantly different from both IM NBR *n* values and the CM Low NBR *n*. However, the CM High *n* was not found to differ significantly from any other location. For the single subject visual data (M=15 and 20), a significantly larger *n* value was found for High IM PBR than for Low IM PBR *n* values (see Figure 3.3B&C). Both IM PBR *n* values were also found to be significantly lower than those of IM and CM NBRs for both M values (see Figure 3.3B&C). The IM and CM NBRs were not found to differ from one another (see Figure 3.3B&C).

For all the $CMRO_2$ analyses described above a fixed α value of 0.2 was used for all responses (Chen and Pike 2009), making the assumption that similar CBF-CBV coupling exists for all BOLD responses tested, where CBF^{α}=CBV (Davis, Kwong et al. 1998). However, as the CBF-CBV coupling of NBR regions has not been specifically investigated it remains theoretically possible that α could differ between PBR and NBR regions, especially if NBR features different neurovascular coupling. Therefore, to explore the implications of variations of α in NBR regions, using the group level data we maintained the IM PBR α value at 0.2 and methodically adjusted the NBR α values to find those which resulted in NBR *n* = PBR *n*. The resultant IM

NBR α values were 2-4 times larger than the PBR value (see Table 3.1) with the more intense trials (High/Tap) requiring larger α values than the less intense (Low/Grip) to reproduce the PBR *n* values. CM NBR regions required considerably lower α values than the IM NBR, with the more intense trials (High/Tap) requiring close to or lower than 0.2 whilst for the less intense trials (Low/Grip) α values ranged from 0.25 to 0.57 (Table 3.1).

		Condition	IM PBR	IM NBR	High CM NBR	Low CM NBR
A) Motor Cortex	**M=10.5**	**Grip**	0.2	0.4903	0.1309	0.2588
		Tap	0.2	0.4113	0.2339	0.3619
		Average		0.4508	0.1824	0.3104
		Condition	**IM PBR**	**IM NBR**	**Tap CM NBR**	**Grip CM NBR**
B) Visual Cortex	**M=20**	**High**	0.2	0.7798	0.2642	0.502
		Low	0.2	0.606	0.0706	0.311
		Average		0.6929	0.1674	0.4065
	M=15	**High**	0.2	0.9368	0.2651	0.5654
		Low	0.2	0.7215	0.0141	0.3218
		Average		0.8296	0.1396	0.4436

Table 3.1. Grubb constants. For Motor (A) and Visual (B) cortex, the α values of NBR regions required to provide NBR *n* equal to PBR *n* using the Davis model. Where PBR α values were set at 0.2.

3.4.2 BOLD response timecourse differences

A key factor in understanding the NBR lies in studying its similarities/differences to the better-known PBR. Therefore we additionally compared the dynamics of their timecourses (see Chapter 2; Figure 3.14). Results for onset, time-to-peak and offset times are plotted for motor

and visual cortex BOLD data in Figure 3.4 and 3.5 respectively, and for CBF data in Figure 3.6 and 3.7.

No differences in onset timings were found between BOLD responses in the motor cortex (Figure 3.4A). However, in the visual cortex only the onset of CM Grip NBR was found to be significantly later than the IM High PBR and IM Low NBR (Figure 3.5A). In the motor cortex, we observed that CM NBRs showed significantly earlier time-to-peak than all IM responses (Figure 3.4B). In the visual cortex we observed that IM NBRs showed significantly earlier time-to-peak than CM Grip NBR but not CM Tap NBR, with IM Low NBR showing an earlier peak time than the IM High PBR, Figure 3.5B. Motor cortex offset times were significantly earlier for all NBRs than for IM PBRs Figure 3.4C. Similarly, in the visual cortex both IM NBRs had significantly earlier offset times than the IM High PBR, but the IM Low PBR offset was only significantly later than the IM Low NBR Figure 3.5C.

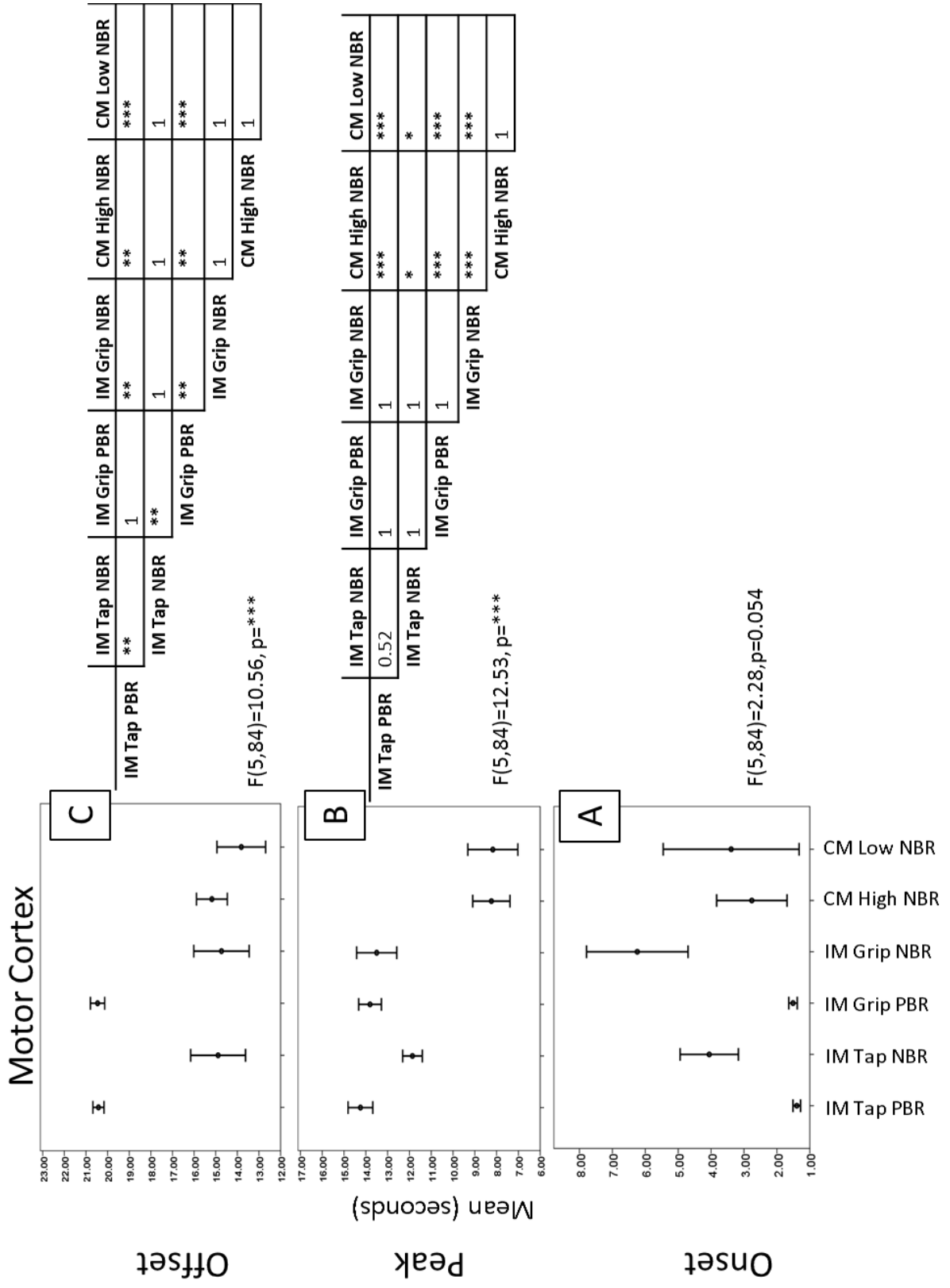
Motor Cortex
Onset
Peak
Offset
Mean (seconds)
A
B
C
F(5,84)=2.28,p=0.054
F(5,84)=12.53, p=***
F(5,84)=10.56, p=***
IM Tap PBR
IM Tap NBR
IM Grip PBR
IM Grip NBR
CM High NBR
CM Low NBR
IM Tap PBR 0.52 ** ** ** ***
IM Tap NBR 1 ** ** ***
IM Grip PBR 1 * ***
IM Grip NBR 1 ***
CM High NBR 1
IM Tap PBR ** ** ** ***
IM Tap NBR 1 1 1
IM Grip PBR ** ** ***
IM Grip NBR 1 1
CM High NBR 1

Figure 3.4. Motor cortex ROI BOLD response onset, peak and offset timing analysis. The three figures display the time in seconds for the onset (A), peak (B) and offset (C) of the BOLD data for each of the motor cortex ROIs. The F-test is shown for each ANOVA relating to onset, peak and offset with the table in peak (B) and offset (C) showing the p-values from the ANOVA (A: onset, results are not shown as the F test was not satisfied) assessing the difference between BOLD response timings (*=p<0.05, **=p<0.01, ***=p<0.001).

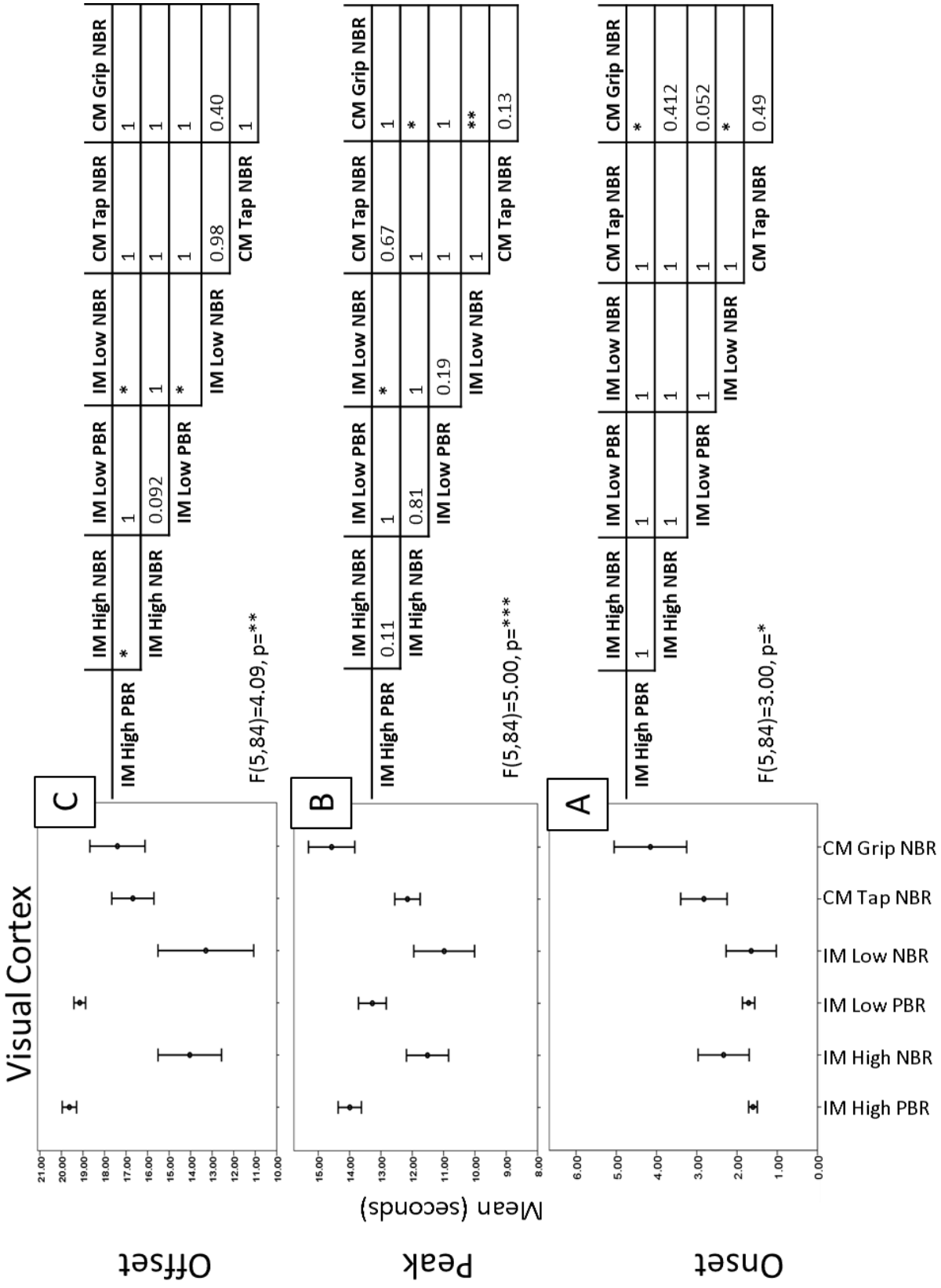
Visual Cortex
Onset
Peak
Offset
Mean (seconds)
A
B
C
F(5,84)=3.00, p=*
F(5,84)=5.00, p=***
F(5,84)=4.09, p=**
IM High PBR
IM High NBR
IM Low PBR
IM Low NBR
CM Tap NBR
CM Grip NBR
IM High PBR 1 1 1 1 1
IM High NBR 1 1 1 1 *
IM Low PBR 1 1 1 1 0.412
IM Low NBR 1 1 1 1 0.052
CM Tap NBR 1 1 1 1 *
CM Grip NBR * 0.412 0.052 * 0.49
IM High PBR 1 0.11 1 0.81 1 0.19 1 1 1 0.67 1 * 1 1 1 ** 0.13
IM High NBR 0.11 1 0.81 1 0.19 1 0.67 1 * 1 1 1 1 ** 0.13
IM Low PBR 1 0.81 1 0.19 1 1 * 1 1 1 1 ** 0.13
IM Low NBR 0.81 1 0.19 1 1 * 1 1 1 1 ** 0.13
CM Tap NBR 0.19 1 1 * 1 1 1 1 ** 0.13
CM Grip NBR 1 * 1 1 1 1 1 ** 0.13
IM High PBR * 1 0.092 1 * 1 0.98 0.40 1
IM High NBR 1 0.092 1 * 1 0.98 0.40 1
IM Low PBR 0.092 1 * 1 0.98 0.40 1
IM Low NBR * 1 0.98 0.40 1
CM Tap NBR 1 0.40 1
CM Grip NBR 1

Figure 3.5. Visual cortex ROI BOLD response onset, peak and offset timing analysis. The three figures display the time in seconds for the onset (A), peak (B) and offset (C) of the BOLD data for each of the visual cortex ROIs. The F-test is shown for each ANOVA relating to onset, peak and offset with the table in onset (A), peak (B) and offset (C) showing the p-values from the ANOVA assessing the difference between BOLD response timings (*=p<0.05, **=p<0.01, ***=p<0.001).

3.4.3 CBF response timecourse differences

As seen with the BOLD data, no differences in onset timings were found between any CBF responses in the motor cortex (see Figure 3.6A). In the visual cortex, the CM Grip NCBF onset time was significantly later than the IM High PCBF (in agreement with the BOLD data) and the IM Low PCBF (which showed a trend in the BOLD data) (see Figure 3.7A). The time-to-peak of the CM Low NCBF was significantly earlier than for both IM PCBF responses in the motor cortex (Figure 3.6B). While in the visual cortex no significant differences in time-to-peak were found between responses (Figure 3.7B). Motor cortex offset times were only found to differ significantly between the IM Grip PCBF and the CM Low NCBF (earlier time-to-peak) responses (Figure 3.6C), with no significant difference between offset times seen for CBF responses in the visual cortex (Figure 3.7C).

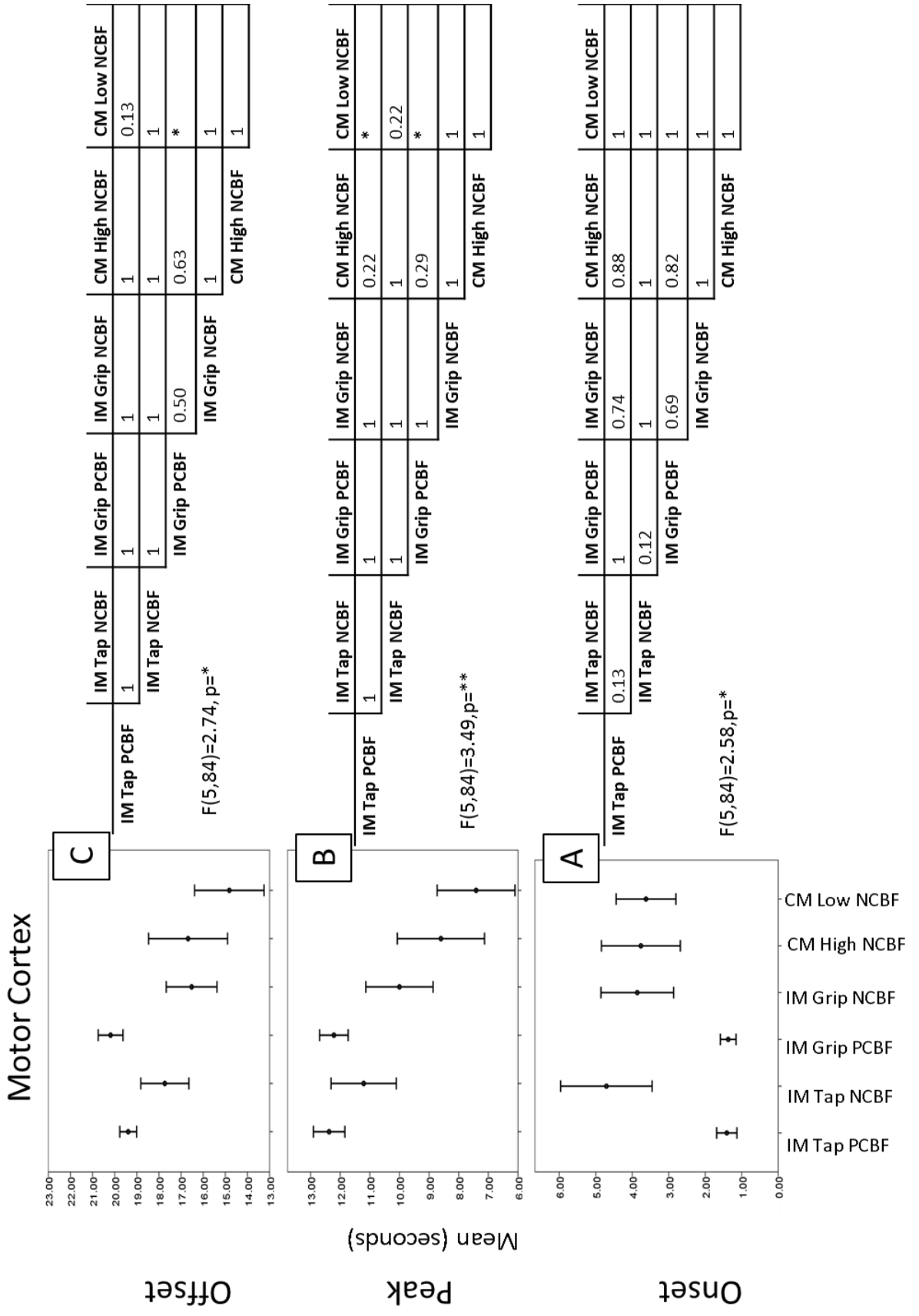
Motor Cortex
Onset
Peak
Offset
Mean (seconds)
A
B
C
F(5,84)=2.58,p=*
F(5,84)=3.49,p=**
F(5,84)=2.74, p=*
IM Tap PCBF
IM Tap NCBF
IM Grip PCBF
IM Grip NCBF
CM High NCBF
CM Low NCBF
IM Tap PCBF 1 0.13 1 0.74 0.88 1
IM Tap NCBF 0.13 1 0.12 1 1 1
IM Grip PCBF 1 0.12 1 0.69 0.82 1
IM Grip NCBF 0.74 1 0.69 1 1 1
CM High NCBF 0.88 1 0.82 1 1 1
CM Low NCBF 1 1 1 1 1 1
IM Tap PCBF 1 1 1 0.22 0.22 *
IM Tap NCBF 1 1 1 1 1 1
IM Grip PCBF 1 1 1 0.29 0.29 *
IM Grip NCBF 0.22 1 0.29 1 1 1
CM High NCBF 0.22 1 0.29 1 1 1
CM Low NCBF * 1 * 1 1 1
IM Tap PCBF 1 1 1 0.50 0.63 * 1 1
IM Tap NCBF 1 1 1 1 1 1
IM Grip PCBF 1 1 1 0.50 0.63 * 1 1
IM Grip NCBF 0.50 1 0.63 1 1 1
CM High NCBF 1 1 1 1 1 1
CM Low NCBF 1 0.13 1 1 * 1
CM Low NCBF
CM High NCBF
IM Grip NCBF
IM Grip PCBF
IM Tap NCBF
IM Tap PCBF

Figure 3.6. Motor cortex ROI CBF response onset, peak and offset timing analysis. The three figures display the time in seconds for the onset (A), peak (B) and offset (C) of the CBF data for each of the motor cortex ROIs. The F-test is shown for each ANOVA relating to onset, peak and offset with the table in onset (A), peak (B) and offset (C) showing the p-values from the ANOVA assessing the difference between CBF response timings (*=p<0.05, **=p<0.01, ***=p<0.001).

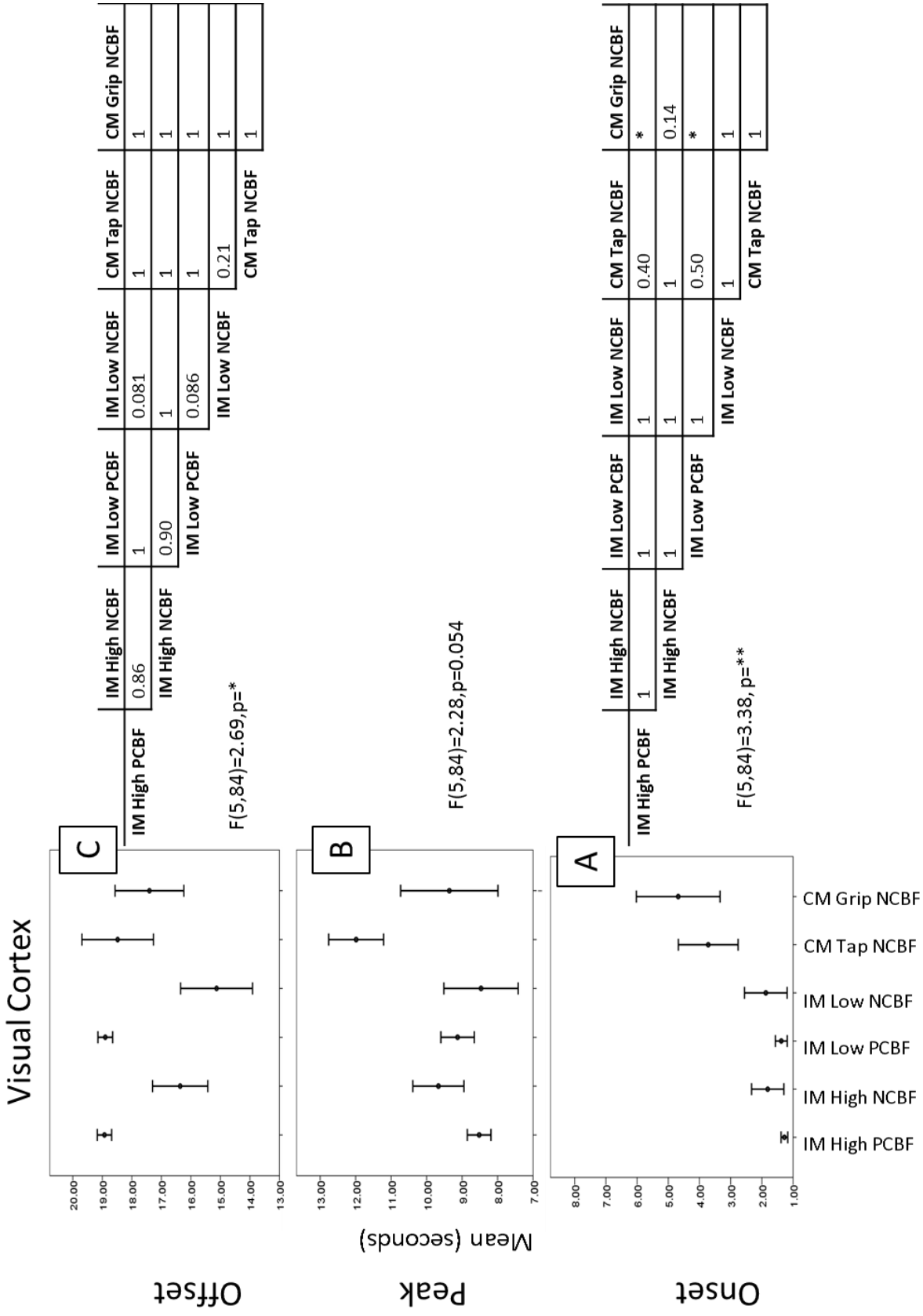
Visual Cortex
C
IM High PCBF
IM High NCBF
IM Low PCBF
IM Low NCBF
CM Tap NCBF
CM Grip NCBF
0.86
1
0.081
1
1
1
0.90
1
0.086
1
1
1
0.21
1
F(5,84)=2.69,p=*
B
F(5,84)=2.28,p=0.054
A
1
1
1
1
0.40
*
1
1
1
0.14
1
0.50
1
*
1
1
1
F(5,84)=3.38, p=**
CM Grip NCBF
CM Tap NCBF
IM Low NCBF
IM Low PCBF
IM High NCBF
IM High PCBF
Mean (seconds)
Offset
Peak
Onset

Figure 3.7. Visual cortex ROI CBF response onset, peak and offset timing analysis. The three figures display the time in seconds for the onset (A), peak (B) and offset (C) of the CBF data for each of the visual cortex ROIs. The F-test is shown for each ANOVA relating to onset, peak and offset with the table in onset (A) and offset (C) showing the p-values from the ANOVA (B: peak, results are not shown as the F test was not satisfied) assessing the difference between CBF response timings (*=p<0.05, **=p<0.01, ***=p<0.001).

3.5 Discussion

Similar to previous literature, concurrent decreases in CBF and $CMRO_2$ from baseline were measured in regions of IM NBR (Schafer, Blankenburg et al. 2012, Mullinger, Mayhew et al. 2014), extending this we have also shown that concurrent decreases in CBF and $CMRO_2$ occur in CM NBR regions, suggesting that both types of NBR involve a neural component and do not arise from purely vascular mechanisms. In addition, we observe differences between the timecourses of PBR, IM NBR and CM NBR, with earlier offset latencies in NBRs than PBRs (Figure 3.5&3.6), mirrored also in the CBF data.

Given that the CBF and $CMRO_2$ changes both contribute to the regional concentration of deoxyhaemoglobin and so, ultimately, the BOLD response, it is important to take into account the coupling ratio ($\Delta\%CMRO_2/\Delta\%CBF$), *n*, for a more nuanced understanding of the BOLD response (Buxton and Frank 1997). The *n* value has been suggested to reflect the ratio of excitatory and inhibitory neuronal activity in a region (Buxton, Griffeth et al. 2014, Mullinger, Cherukara et al. 2017). Here, using the Davis model of steady-state responses we calculated that $CMRO_2$ increased from baseline in PBR regions and decreased in both IM and CM NBR regions (Figure 3.1) in both motor and visual cortices. This is the first observation of decreased $CMRO_2$ for CM NBR but is similar to that previously shown in the visual cortex IM NBR (Shmuel, Yacoub et al. 2002) and motor cortex IM NBRs (Mullinger, Mayhew et al. 2014). Although the *n* values calculated cannot be compared between cortices (because the M

values were not individually estimated but a range for each cortex based on previous literature) for both the group level data (Figure 3.2) and inter-subject data (Figure 3.3) they were found to differ in general between IM PBRs and IM NBRs.

We were also able to replicate previous findings showing that in IM PBR regions the *n* value decreased with increasing visual stimulus intensity (Figure 3.2B) (Liang, Ances et al. 2013) with a similar trend also found for motor task intensity (Figure 3.2A). This suggests our data quality is sensitive to small alterations in the balance of excitation and inhibition, which gives us confidence to extend investigations into the NBR regions where SNR is inherently lower. In the NBR regions we find a similar inverse relationship between *n* and stimulus intensity, most notable in motor trials (Figure 3.2C&D).

A key component of the current study is the comparison of *n* between PBR and both IM and CM NBR regions. Previous work has helped evidence the neuronal origin of NBR by demonstrating that local decreases in BOLD cannot be explained solely by decreases in CBF, but also require decreases in $CMRO_2$ to fully explain the data implying a neuronal origin for NBR (Shmuel, Yacoub et al. 2002, Pasley, Inglis et al. 2007, Mullinger, Mayhew et al. 2014). Two previous studies have shown that NBR regions of the default mode network and the sensorimotor cortex ipsilateral to a median nerve stimulus showed *n* values higher than those of the PBR (Mayhew, Mullinger et al. 2014, Mullinger, Mayhew et al. 2014). However, this is the first study to directly investigate whether the neuro-metabolic origins of different types of NBR are comparable.

For both our visual and motor data we found that group-calculated CM NBR *n* values were lower than IM NBRs, and more similar to those of the IM PBRs (Figure 3.2). However, a test of significance using subject-calculated *n* showed no difference between the IM and CM NBR (Figure 3.3) therefore we are unable to unambiguously conclude that there was a difference in *n* between CM and IM NBR.

The *n* values of the IM NBRs imply marginally larger percentage decreases from baseline in CBF than $CMRO_2$ in line with previous literature (Shmuel, Yacoub et al. 2002, Stefanovic, Warnking et al. 2004, Pasley, Inglis et al. 2007, Mullinger, Mayhew et al. 2014). We posit that the differences found between the IM NBR and PBR *n* values are related to different underlying neurophysiological mechanisms of the two responses, with IM NBRs originating primarily from inhibitory processes compared to dominant excitation in the PBR.

The functional nature of motor cortex inter-hemispheric interaction provides support for IM NBRs as a measure of inhibition. During unilateral motor tasks the motor cortex ipsilateral to the movement displays cortico-spinal inhibition as measured using TMS (Chen and Hallett 1999). These inhibitory effects have been closely tied to IM NBR by Schafer et al. (Schafer, Blankenburg et al. 2012) who have shown that unilateral sensorimotor stimulation resulted in motor cortex IM NBR, whose amplitude was correlated with decreases in perceptual threshold of the unstimulated hand. Based on these findings, it seems likely that the IM NBRs measured in the current study, in motor cortex and potentially also the visual cortex, would appear therefore to be a result of inhibitory mechanisms.

The interplay of excitatory and inhibitory neurons of a region and the surrounding astrocytes are highly influential in the generation of the BOLD response (Lauritzen, Mathiesen et al. 2012). During excitatory (glutamatergic) neuronal activity CBF is increased by the release of vasodilatory molecules from neurons and astrocytes (Harris and Scott 2012), with a smaller increase in $CMRO_2$ (Buxton, Wong et al. 1998). Whereas, neuronal inhibition can cause either increases (Cauli, Tong et al. 2004, Enager, Piilgaard et al. 2009) or decreases in CBF (Stefanovic, Warnking et al. 2004, Devor, Tian et al. 2007, Kastrup, Baudewig et al. 2008). The $CMRO_2$ demands during these inhibitory processes are similarly unclear (Buzsáki, Kaila et al. 2007) but some literature does show there can be a relatively smaller decrease in $CMRO_2$ from baseline than that of CBF (Stefanovic, Warnking et al. 2004).

Buxton et al. (Buxton, Griffeth et al. 2014) hypothesise that as activity at inhibitory neuronal synapses increases *n* decreases. The CM NBRs measured in this study across subjects show similar group calculated *n* values to those of the PBRs, suggesting a relatively larger decrease in CBF than $CMRO_2$ for CM NBRs than is found within IM NBR regions. Such differences were not however found when assessing the data at the single subject level. IM and CM NBRs show decreased CBF and $CMRO_2$ implying that they may both originate from a similar mechanism, with differences in *n* values revealing differences in strength of the response.

It was the *n* values for CM NBRs which differed between inter- (similar to IM NBR values) and intra-subject (similar to CM NBR values) calculations. Although the *n* values calculated within subjects were similar for all subjects (gradients between $\Delta CMRO_2$ and ΔCBF as shown in Figure 3.3D&E), the average $CMRO_2$ and CBF values differed between subjects (particularly noticeable for the Tap CM NBR data: Figure 3.3E). This resulted in a difference between group level *n* value from that of the single-subject *n* calculated.

3.5.1 The Grubb constant in NBR regions

The Davis model, used here to calculate $CMRO_2$, requires the use of constants to model the underlying physiological complexity that is inherent in the BOLD response. The value of the Grubb constant (α) of 0.2 was derived from measurements of CBF and CBV during visual and somatosensory stimulation in PBR regions (Chen and Pike 2009). This constant was therefore applicable for the calculation of $CMRO_2$ in PBR regions but it is unknown if it is similarly applicable to NBRs. If there is a difference between the CBV-CBF coupling during PBRs and NBRs then it is possible that the $CMRO_2$ required to explain the NBR is different as well. The few studies of CBF and CBV changes in NBR regions have revealed contradictory results. Goense et al. (Goense, Merkle et al. 2012) found that CBV increased and CBF decreased in NBR regions, in central and superficial cortical layers respectively, while Huber et al. (Huber, Goense et al. 2014) found that with CBF decreases, CBV also decreased. Although these

studies were carried out in monkeys and humans respectively, the vasculature in both species is known to show a great deal of similarity and therefore would not be expected to account for the differences in the measurements. Here, we investigated what variations in α from the group calculation would be required to produce similar *n* values for NBRs to those of the PBRs. This tests the possibility that the $CMRO_2$/CBF coupling is the same but the CBF-CBV coupling is different between NBRs as PBRs, the opposite of what we assume. Doing so shows that the α value required for IM NBRs to attain the same *n* value would be 2-4.5 times higher than the 0.2 currently used. This value differs as well in relation to the cortex and the M value used (see Table 3.1). The CM responses show α values more similar to the 0.2 used which is to be expected given that the *n* values for IM PBRs and CM NBRs are already close when calculated at the group level (Table 3.1). The larger α values would translate as larger CBV changes in relation to CBF for IM NBRs than for IM PBRs. Although it is unlikely that the NBR and PBRs would show the same α values, this highlights that caution should be used in interpretation of the NBR *n* values calculated using the standard Grubb constant of 0.2. To clarify this issue more work examining the contribution of CBV and CBF to the NBR in humans is required.

3.5.2 The NBR timecourses and underlying origin

The main difference found between the PBR and NBR timecourses was an earlier NBR offset (for IM and CM NBRs). These are similar differences in timecourse dynamics as found by others (Shmuel, Yacoub et al. 2002, Maggioni, Molteni et al. 2015) although Liu et al. (Liu, Shen et al. 2011) also found that NBRs showed later onset and offset times than PBRs (in motor, occipital and frontal regions). Although the NBR is thought in part to be a measure of decreased neuronal activity it is not believed to be the direct inverse of the PBR (Mullinger, Mayhew et al. 2014). The shorter offset time of the NBR is hypothesised by Shmuel et al. (Shmuel, Yacoub et al. 2002) to relate to the NBR having a component of the CBF response

change unrelated to the $CMRO_2$ change. The slower PBR offset to baseline is thought to relate to a combination of a faster $CMRO_2$ decrease to baseline (causing an increase in the BOLD signal) occurring relative to a slower rate of CBF decrease (causing a decrease in the BOLD signal) in NBRs. It is this NBR CBF component that Shmuel et al. (Shmuel, Yacoub et al. 2002) believe to be the main driving force of the NBR, whereby the BOLD response follows more closely the CBF timecourse and is less affected by the $CMRO_2$ changes.

The differences commonly found between the PBR and NBR timecourses will translate into differences in the fit of the HRF used in GLM analysis. The HRF is based on the PBR and so will fit more accurately PBRs width and duration than NBRs. The seemingly inherent (and replicated) difference in NBR duration would lead to decreased fit of the HRF during GLM analysis. Creating a NBR specific HRF could therefore increase the ability of modelling, and so ability to locate, NBRs.

3.5.3 Summary

Here we have been able to replicate findings of the IM NBRs (in motor and visual cortices) being driven by both decreases in CBF and decreases in $CMRO_2$. We have also extended this to show that CM NBRs have similar CBF and $CMRO_2$ decreases to the IM NBRs. Using the Davis model we have shown there to be a significant difference between the NBRs (both IM and CM) and the PBRs which we argue relates to different underlying neurophysiological mechanisms, i.e. increases in inhibitory neuronal synaptic activity for NBRs. Although we suggest caution when using Grubbs constant to calculate $CMRO_2$ for NBRs until the CBF-CBV coupling relationship is better understood.

CHAPTER 4

THE EFFECT OF FUNCTIONAL AND STRUCTURAL CONNECTIVITY ON INTRA- AND CROSS-MODAL NEGATIVE BOLD RESPONSES

4.1Abstract

Having assessed the neuronal, metabolic and vascular origin of the IM and CM NBRs in Chapters 2 and 3, we now look at whether the level of connectivity between PBR and NBR regions affect the NBRs. Previous work has shown that regions with high levels of structural connectivity are often also highly functionally connected (Johansen-Berg, Behrens et al. 2004), while the level of functional connectivity between regions has been shown to be predictive of task evoked PBR (Cole, Ito et al. 2016). However, no previous work has examined whether the level of structural and/or functional connectivity between regions of stimulus evoked PBR and NBR affects the NBR. To study this, the motor and visual task evoked PBR, IM and CM NBRs, as described in the last two Chapters, were used here alongside structural and functional connectivity data measured between these regions (PBR to NBR) for the same subjects.

We found that greater interhemispheric structural connectivity across the CC between motor task evoked PBR and IM NBR regions was related to more variable IM NBRs. With total structural connectivity between those regions related to larger relative IM NBR. Conversely, no relationships were found between visual stimulus BOLD responses and their functional/structural connectivity. We propose that the IM NBRs to volitional motor tasks require interhemispheric connectivity, while the passive visual stimuli do not. Neither motor nor visual stimuli CM NBRs were found to be related to measures of their connectivity to PBR regions.

4.2 Introduction

In Chapter 2 and 3 we were able to assess the neuronal and metabolic components of IM and CM NBRs respectively. Although those chapters examined the underlying components, the signalling pathways associated with the NBRs are still obscure. Here, using the same task data combined with additional resting state (RS) BOLD and DTI data, acquired in the same subjects, we examine whether the structural and functional connections between regions of NBR and PBR (defined during tasks) are informative as to the comparative strength and variability of the NBR, as a means of assessing whether connectivity determines NBR characteristics.

As was discussed in Chapter 1, there is strong evidence of interhemispheric interaction between the left and right motor cortices (Chen and Hallett 1999) and also the visual cortices (Tettoni, Gheorghita-Baechler et al. 1998). Whether this cortical interaction is associated with the relationship between motor/visual task PBR and IM NBR is poorly understood, whereby the IM NBR (and possibly the CM NBR) may be a direct result of the PBR region's activity rather than being a consequence directly of the stimulus itself. One way of assessing this is by measuring the connectivity between stimulus evoked PBR and IM/CM NBR regions and

examining whether the level of connectivity (functional and structural) is related to the NBRs measured, which is the aim of this chapter.

Functional connectivity (FC) between the motor cortices (Biswal, Yetkin et al. 1995) are thought to be mainly mediated by direct structural connection through the CC (Meyer, Roricht et al. 1995). In comparison, the left and right visual cortices are also known to be structurally connected via the posterior aspect of the CC, splenium (Myers 1962), while separately also having been found to be functionally connected at rest (Andrews-Hanna, Snyder et al. 2007).

CM structural connectivity (SC) has also been shown to exist, using invasive methods, in marmosets between the primary somatosensory area (S1) and V1; V1 to auditory cortex; and S1 to auditory cortex (Cappe and Barone 2005) suggesting a white matter pathway linking the regions of IM PBR and CM NBR found during sensory stimulation in Chapter 2 may exist. Similarly, from rat studies, evidence of direct SC between the visual cortex and S1 has been shown to contribute directly to cross-modal inhibition (Iurilli, Ghezzi et al. 2012). Studies in humans have shown SC to exist between auditory and visual cortices (Beer, Plank et al. 2011), however to our knowledge no human studies have shown direct structural connections between motor and visual cortices. Whether this connectivity is found in humans and how this relates to task based BOLD responses are open questions.

There is some consensus that regions which share high structurally connectivity also show a high level of functionally connectivity, for example pre-SMA and SMA (Johansen-Berg, Behrens et al. 2004) and regions of the DMN (Greicius, Supekar et al. 2009, Khalsa, Mayhew et al. 2013). However, the opposite doesn't necessarily hold, i.e. that functionally connected regions are also structurally connected, where instead they could be indirectly connected (Greicius, Supekar et al. 2009, Honey, Sporns et al. 2009). Of particular relevance here to PBR-NBR relationships, is whether PBR and NBR regions exhibit resting state FC (RSFC) and also direct SC, which is currently unknown. Gaining an insight into this question would greatly

inform our understanding of whether network connectivity is implicated in the formation of these stimulus evoked NBRs.

RSFC as well as being linked to SC, has previously been shown to be similar to that of task FC during rapid instructed learning tasks in 264 regions across the brain, whereby the polarity of the connectivity is maintained, i.e. positive/negative RSFC remains positive/negative during tasks (Cole, Bassett et al. 2014). The voxel wise task specific BOLD response has also been shown to be predictable by the RSFC for a number of tasks: emotional, gambling, language, reasoning, social and N-back tasks (Cole, Ito et al. 2016), as well as a Flanker task (Mennes, Kelly et al. 2010) and response to pain (Mayhew, Hylands-White et al. 2013). However, whether these relationships between RSFC and task FC are maintained between regions showing PBR and NBR to tasks has not previously been studied.

Overall, motor and visual cortical hemispheres show strong within-network structural and functional connectivity. Whether this relates to motor and visual stimulus evoked PBR and IM/CM NBR is poorly understood. Increased SC between these regions may be linked to increased FC which together may lead to an increased tie between the two responses (i.e. with increased connectivity the NBR would be closer in magnitude to that of the PBR). If the level of connectivity between the PBR and NBR accounts in part to the NBR amplitude then it may be that the trial-by-trial variability of the NBR is affected by the level to which they are connected, something which to our knowledge has not previously been studied.

4.2.1 Aim

By utilising measures of SC and FC we aimed here to find whether the level of NBR:PBR relates to the functional and/or structural connectivity between the areas in which they arise. We also assess whether the large variability found in the amplitude of a subject's NBR across trials, found to be greater than that of the PBR, is related to these connectivity measures. We hypothesised that:

1. FC and SC between PBR and NBR (IM and CM) regions would be positively correlated.

2. For IM connectivity, the most direct physical connection via the CC (CC) would facilitate this structure-function relationship.

3. These measures of connectivity would be predictive of the ratio between the NBR and PBR as well as the consistency of the NBR, where greater connectivity would relate to larger BOLD ratio and more consistent NBRs.

4.3 Methods

4.3.1 Data acquisition and analysis

Task and RS BOLD data

Task and RS data were acquired and pre-processed as described in Chapter 2. Data from two of the 17 subjects scanned were removed from further analysis due to movement>4mm leaving n=15 for further analysis. Although the DABS sequence used provides both CBF and BOLD data, for brevity only the higher SNR BOLD data were used for the analyses below where the PBR-NBR interaction and the NBR variability alone are of primary interest, not the BOLD-CBF relationship. After pre-processing, group level main effect GLM analysis was carried out across subjects on the task based BOLD data for all motor data combined and all visual data combined (described in detail in Chapter 2). Task and RS data used for FC analysis were further low-pass filtered (>0.1Hz) after pre-processing (Fox, Snyder et al. 2005). Two WM voxels and two CSF voxels were identified from each scan and linear regression used to remove these signals, along with motion parameters, from each voxel of the BOLD data (Fox, Snyder et al. 2005).

Task specific ROIs were the same as those defined in Chapter 2 from the group GLM results. There were 12 ROIs in total, one for each response region (IM NBR, IM PBR and CM NBR) within each of the four task types (High, Low, Grip, Tap). These ROIs were registered to each individual or each subject, and used to extract the peak percentage BOLD signal change for each single-trial response as described in Chapter 2. For each task, the mean and standard deviation was calculated for all data obtained, across all trials of all runs. BOLD response amplitude ratios (mean NBR/mean PBR) were calculated to provide a single value per subject of IM ratio (IM NBR/IM PBR) and CM ratio (CM NBR/IM PBR). For each task, a single measure of NBR amplitude variability per subject was taken as the coefficient of variation (CoV): the standard deviation of the single-trial NBR amplitudes for that task divided by the mean of the NBR amplitude for that task, where larger values denote less consistent responses.

For task FC analysis, using the same ROIs as above, the mean timecourse of each ROI was extracted from the further filtered data. The time period containing trials within the run (from 60s to the end, excluding initial resting baseline), was then used to calculate task FC. Pearson's correlation was used to calculate Pearson's R (taken as FC strength) for IM ROI task FC (between IM PBR ROI and IM NBR ROI) and CM ROI task FC (between IM PBR ROI and CM NBR ROI) for each of the task ROIs in each run and an average taken across runs, resulting in one value per subject.

The same ROIs were also used to extract data from the RS scan and Pearson's correlation carried out between the ROIs in the same manner as above, providing a measure of IM (between the IM PBR ROI and the IM NBR ROI) and CM (between the IM PBR ROI and the CM NBR ROI) RSFC strength for each set of task ROIs.

DTI data

A DWI scan was acquired for 14 of the remaining 15 subjects who took part in the original study. The DWI scan was a 13 minute echo planar sequence, 48 slices were acquired, using b=0/1500mm^2/s in 61 directions: TR=5191ms, TE=77ms, FOV=224x150x224mm, angulation=0º, voxel size 1x1mm in plane and 2mm slice thickness. These images were brain extracted then correction for both eddy currents and motion was carried out using the FSL Diffusion Toolkit (Smith, Jenkinson et al. 2004). Using BEDPOSTX 10,000 streamline sample iterations were modelled at each voxel with a curvature threshold of 0.2 and step length of 0.5 (Behrens, Berg et al. 2007). ProbtrackX was used to estimate the connection distribution between the seed regions and the target regions.

The same twelve ROIs as used in the FC analysis above were also used here as the basis of seed and target definition for SC analysis. Being defined from functional BOLD response regions, these ROIs are embedded in grey matter which decreases the probability of white-matter streamlines connecting from one ROI to another. Three sizes of ROIs were therefore investigated, 1.5, 3 and 6 voxel radius spheres, which were centred on the same peak coordinate (as described in detail below) allowing the sensitivity of probabilistic tractography to be studied with varying ROI size (Exemplar 6 voxel sphere ROI positions can be seen in Figure 1 A&B). The seed was the IM PBR ROI while the target (IM NBR ROI for IM connectivity or the CM NBR ROI for CM connectivity) was set as both a waypoint and a terminal mask. Using the waypoint and terminal masks allows only those streamlines which pass from the seed to the target to be kept to minimise streamlines progressing further than the target. The value given to each voxel in the data when using this method is the probability that a path going from the seed ROI to the target ROI would travel through that voxel. A simple measure of tract strength (TS) was taken as the number of voxels whose value was over a threshold of 15% of the maximum voxels value, this can be considered to be the total TS

(tTS), a threshold shown previously to find a positive structure-function correlation (Bennett, Madden et al. 2011).

However, the probabilistic tractography maps provide all possible streamlines that are traced between a seed ROI and a target ROI. In the case of IM TS, some of these will include tracts which are not of primary interest for this study (e.g. not passing through the CC and therefore not reflecting the most relevant inter-hemispheric sensory connectivity). In order to optimally test our hypothesis that the connection between the IM ROIs across the CC is related to the other measurements taken (FC and NBR CoV) we further calculated a measure of the most direct within-network connectivity. Each subject's probabilistic tractography output was first thresholded at 5% to remove noise and then the shortest contiguous path between the seed and target ROIs was isolated (using the function bwdistgeodesic) in Matlab. This process was carried out iteratively, and each time the central portion of the discovered connection was severed so that the next iteration found a different path. This identified paths of possible connectivity between the ROIs which could then be expanded 6mm in each direction, using imdilate in Matlab, to create masks surrounding those paths. These masks were visually inspected and those which represented direct cortico-cortical connectivity for a single subject (i.e. linking ROIs with tracts through the CC without deviating to the thalamus, putamen or brain stem) were combined (if more than one was found) and used as the mask of primary connectivity (pTS mask) for calculation of the primary measure of TS (pTS) for that subject. The pTS measure was calculated by applying the threshold of 15% to all data as described above and then counting the number of voxels remaining in the pTS mask therefore providing a pTS measure per subject (exemplar masks generated are shown in Figure 4.1C and D).

The same process was carried out for the IM visual ROIs, whereby those tracts crossing at the splenium of the CC were taken as the pTS (after 15% threshold) with those crossing at the

thalamus or genu of the CC disregarded. As with the motor data, tTS was taken as the number of voxels within the whole-brain data over the 15% threshold.

No prior hypothesis was derived as to the specific path of physical connectivity between the CM ROIs therefore tTS was used as the only measure for both motor and visual CM data.

Henceforth, when reporting FC and TS measures we adopt a consistent convention. For example, IM motor FC refers to within network connectivity of the motor cortices between IM contralateral PBR and IM ipsilateral NBR ROIs. CM motor FC refers to network connectivity between the motor IM contralateral PBR ROI and the CM NBR ROI, located in the visual cortex.

4.3.2 SC and FC correlations

Correlations were carried out across subjects using the mean measures for each subject. The RSFC was correlated against task FC as well as both tTS and pTS. Both tTS and pTS were also correlated against task FC. To correct for multiple comparisons, Bonferroni correction was used taking the critical p-value as 0.05 and the number of comparisons as 3 (the number of comparisons made within a modality and a cortical region). Therefore, a correlation was deemed significant with a p-value<0.016 (0.05/3).

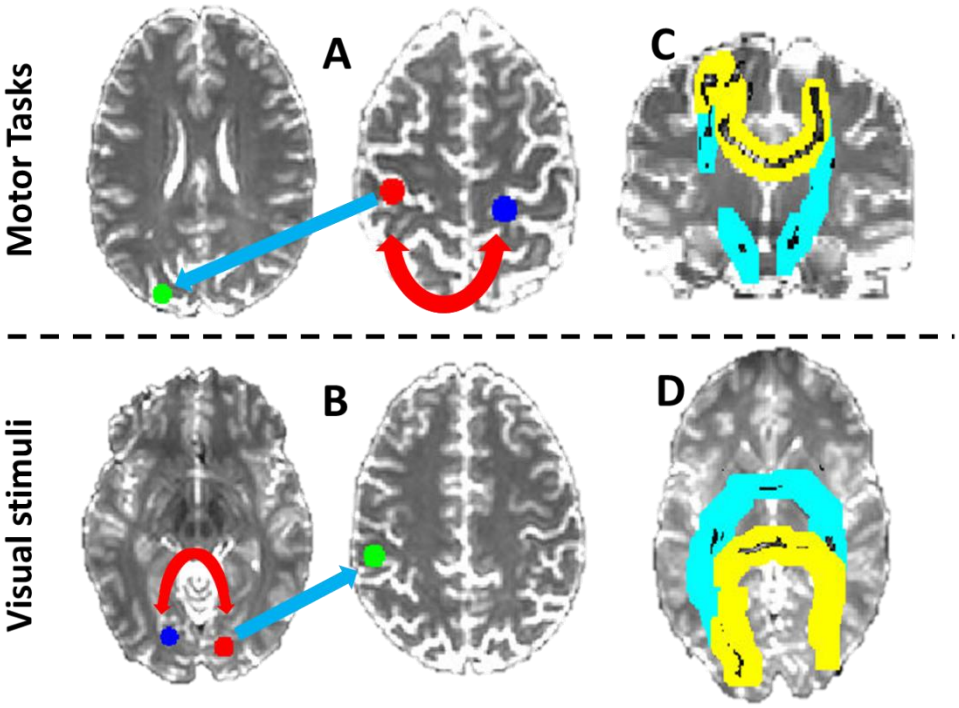

Figure 4.1. Exemplar data. Single subject ROI positions for DTI analysis. A) Motor task ROIs, and **B**) Visual task ROIs. IM PBR ROI (red), IM NBR ROIs (blue), CM NBR ROI (green). IM connectivity is measured between the IM ROIs (red arrow), CM connectivity between IM PBR ROI and CM NBR ROI (blue arrow). **C** & **D**: show masks created to isolate streamlines passing through CC between IM motor ROIs (**C**) and IM visual ROIs (**D**). Yellow masks assigned as pTS, cyan masks relating to streamlines passing through other regions.

4.3.3 Regression of NBR mean/CoV

Linear regression was carried out using SPSS to assess the ability of RSFC, task FC, pTS and tTS in predicting the BOLD ratio and separately the NBR variability. However, only the RSFC, task FC and tTS could be used for regression relating to the CM BOLD ratio or NBR variability, as no CM ROI pTS was calculated as described above. All regression analyses underwent 1000 bootstrap samples and Bonferroni correction.

4.4 Results

4.4.1 NBR variability

Both the IM and CM NBRs were found to be more variable, relative to their mean amplitude, than the PBR during sensory stimuli, as calculated via the mean CoV across subjects for each task (Table 4.1). Using the CoV captures the ratio of standard deviation (SD) to the mean for these responses, providing a measure of how consistent the NBR was, a measure potentially related to the level of connectivity between the PBR and NBR regions. Here, larger CoV values would denote larger NBR variability across trials for that subject. In searching for relationships with intrinsic network connectivity, using the CoV has an advantage over simply using the mean amplitude as some subjects may have similar mean NBR but substantially different standard deviations.

	Tap	**Grip**	**High**	**Low**
IM PBR	0.19±0.14	0.18±0.062	0.24±0.16	0.32±0.18
IM NBR	1.21±1.00	2.23±1.99	1.19±0.88	1.97±1.32
CM NBR	1.34±1.19	2.88±4.79	1.60±0.88	1.70±0.85

Table 4.1. Group mean and standard deviation of coefficient of variation for each BOLD response of each task. The NBRs show larger coefficient of variation than the PBRs in all conditions, showing that the NBRs are much more variable. These CoV values can be deciphered as how much larger the standard deviation (SD) is than the mean, with IM PBRs having SD less than the mean and NBRs having SD between 1.2 to 2.8 times the size of the mean.

To assess the driving force of the CoV, the mean amplitude NBRs were correlated with the CoV. For the motor data, NBR CoV was not found to correlate across subject with mean NBR in either the IM ROIs (Tap: r=-0.36, p=0.19; Grip: r=0.33, p=0.22; combined: r=0.12, p=0.52) or the CM motor ROIs (Tap: r=0.29, p=0.29; Grip: r=0.32, p=0.25; combined: r=0.29, p=0.12).

For the visual data, NBR CoV did positively correlate with mean NBR for IM ROIs combined (High: r=0.4, p=0.14; Low: r=0.5, p=0.057; **combined: r=0.5, p<0.01**) and also for CM visual ROIs combined (High: r-0.45, p=0.089; Low: r=0.46, p=0.085; **combined: r=0.46, p<0.05**).

4.4.2 Task FC

All results reported below are across subjects unless stated otherwise.

For Tap ROIs, negative IM task FC was found in 73% of the total runs containing Tap task, while negative CM task FC was shown in 87% of those runs (see Table 4.2). For Grip ROIs, negative IM task FC was found in 53% of runs containing Grip task and negative CM task FC was found in 60% of those runs (see Table 4.2).

For High ROIs, negative IM task FC was seen in 37% of runs (see Table 4.3), with negative CM task FC shown in 55% of runs (see Table 4.4). For Low ROIs, negative IM task FC was found in 42% of runs (see Table 4.3) while negative CM task FC was found in 57% of runs (see Table 4.4).

The task FC measures for IM and CM ROIs (Table 4.2 and 4.3) were tested for a significant difference from zero using a student's t-test. For IM motor ROIs, IM task FC was not found to significantly differ from zero (IM Tap ROIs, p=0.19; IM Grip ROIs, p=0.41; combined, p=0.11) while CM Tap ROI task FC and combined CM Tap and CM Grip ROI task FC measures were found to be significantly lower than zero (**CM Tap ROIs, p<0.01**; CM Grip ROIs, p=0.16; **Combined, p<0.001**).

For visual stimuli, only Combined High and IM Low ROI task FC was found to differ significantly from zero, being larger than, (IM High ROIs, p=0.19; IM Low ROIs, p=0.10; combined, p=0.046) while no CM visual ROI task FC measure was found to significantly differ from zero (CM High ROIs, p=0.89; CM Low ROIs, 0.76; combined, p=0.73).

Removal of subject 14 (an outlier: see Table 4.2) from the motor data resulted in the IM Tap FC and combined IM Grip and Tap FC being significantly lower than zero (**IM Tap ROIs: p<0.01**; IM Grip ROIs, p=-0.26; **combined, p<0.01**). While CM Tap ROI task FC and combined CM Tap and CM Grip ROI task FC showed greater significance levels and CM Grip ROI task FC also found to be significantly lower than zero (**CM Tap ROIs, p<0.001**; CM Grip ROIs, p=0.042; **Combined, p<0.001**).

4.4.3 Resting state FC

Only 1/15 subjects was found to have negative IM motor ROI RSFC (for both Tap and Grip ROIs), while 4/15 subjects were found to have negative CM Tap ROI RSFC with 3/15 showing negative CM Grip ROI RSFC (see Table 4.5).

Negative IM visual ROI RSFC was found in 1/15 subjects (both High and Low ROIs). Similarly to motor CM ROI RSFC, 3/15 showed negative CM High ROI RSFC and 4/15 showed negative CM Low ROI RSFC (see Table 4.5).

Using student's t-test, all IM motor ROI RSFC measures were found to be significantly higher than zero (**IM Tap ROIs, p<0.001; IM Grip ROIs, p<0.001; combined, p<0.001**), as were all CM motor ROI RSFC measures **(CM Tap ROIs, p<0.01; CM Grip ROIs, p<0.01; combined, p<0.001**).

All IM visual ROI RSFC measures were found to significantly differ from zero (**IM High ROIs, p<0.001; IM Low ROIs, p<0.001; combined, p<0.001**), as were all CM visual ROI RSFC measures, except Low (**CM High ROIs, p<0.05**; CM Low ROIs, p=0.018; **combined, p<0.01**).

Subject	IM				CM			
	Tap ROIs		Grip ROIs		Tap ROIs		Grip ROIs	
	run 1	run2	run 1	run2	run 1	run2	run 1	run2
1	-0.15	-0.20	-0.41	-0.16	-0.12	-0.31	-0.35	-0.20
2	-0.03	-0.49	0.25	0.11	-0.10	-0.31	0.10	0.20
3	-0.32	-0.12	-0.23	-0.20	-0.41	-0.31	-0.28	-0.09
4	0.11	-0.28	0.19	0.11	-0.18	-0.01	-0.28	-0.28
5	-0.25	-0.04	-0.16	0.18	-0.23	-0.37	-0.28	-0.05
6	-0.28	-0.16	-0.28	-0.21	-0.38	-0.31	-0.38	-0.19
7	-0.01	-0.03	-0.04	-0.08	-0.18	-0.19	-0.24	-0.03
8	-0.03	-0.18	-0.15	0.07	-0.22	-0.25	-0.38	0.20
9	0.10	0.02	-0.16	0.20	0.31	-0.03	-0.05	0.18
10	0.02	-0.01	0.08	0.01	-0.03	-0.22	0.03	0.08
11	-0.33	-0.03	-0.01	-0.22	-0.22	-0.24	-0.09	0.11
12	-0.11	0.06	0.26	-0.10	-0.20	0.01	0.04	0.06
13	-0.11	0.17	0.12	0.04	-0.30	-0.03	0.02	-0.03
14	0.78	0.40	0.13	0.23	0.59	0.05	0.36	0.16
15	-0.58	-0.39	-0.63	-0.07	-0.19	-0.40	-0.21	-0.03
Mean	-0.08	-0.09	-0.07	-0.01	-0.12	-0.19	-0.13	0.01
SD	0.29	0.21	0.25	0.15	0.25	0.15	0.21	0.15

Table 4.2. Motor IM and CM task FC (R value). IM R values show the direction and strength of the connectivity between the IM PBR ROIs and IM NBR ROIs during tasks. CM R values show the direction and strength of the task FC between IM PBR ROIs and CM NBR ROIs. Green = positive FC; red = negative FC.

Subject	Low ROIs				High ROIs			
	run1	run2	run3	run4	run1	run2	run3	run4
1	-0.03	0.09	-0.13	-0.05	-0.27	-0.05	-0.13	-0.31
2	0.52	0.48	-0.24	0.09	0.17	0.37	-0.29	0.01
3	-0.02	0.10	-0.26	0.12	-0.19	0.07	0.09	0.16
4	0.00	-0.09	-0.06	-0.21	0.12	0.09	0.13	0.10
5	0.09	-0.07	0.12	0.05	0.12	0.15	0.13	0.15
6	-0.24	-0.17	-0.02	-0.26	-0.24	-0.17	-0.02	-0.26
7	0.19	0.00	0.32	0.02	0.23	0.05	0.34	0.05
8	-0.17	0.23	-0.15	-0.17	-0.08	0.16	-0.05	-0.12
9	0.35	0.31	0.35	0.20	0.35	0.31	0.35	0.20
10	0.10	0.31	0.45	0.23	0.05	-0.19	-0.09	-0.01
11	0.21	0.28	-0.01	-0.17	0.11	0.24	-0.09	0.06
12	-0.09	-0.29	0.12	0.23	-0.05	-0.25	0.20	0.34
13	0.14	0.34	0.20	0.13	0.08	0.02	-0.14	0.03
14	0.41	0.77	0.20	0.19	0.38	0.72	0.13	0.10
15	-0.30	-0.36	0.06	0.16	-0.17	-0.24	0.09	0.13
Mean	0.08	0.13	0.06	0.04	0.04	0.08	0.04	0.04
SD	0.23	0.29	0.21	0.16	0.20	0.25	0.17	0.16

Table 4.3. Visual IM Task FC (R value). IM R values show the direction and strength of the connectivity between the IM PBR ROIs and IM NBR ROIs during tasks. Green = positive FC; red = negative FC.

Subject	Low ROIs				High ROIs			
	run1	run2	run3	run4	run1	run2	run3	run4
1	0.22	0.15	0.36	0.23	-0.23	0.06	-0.06	0.03
2	-0.02	0.17	-0.06	0.01	-0.08	0.10	-0.09	0.04
3	-0.20	-0.15	-0.08	0.06	-0.26	-0.06	0.01	0.04
4	-0.16	-0.28	-0.11	-0.11	-0.08	-0.21	-0.10	-0.05
5	-0.15	-0.09	-0.01	-0.20	-0.29	-0.21	-0.11	-0.31
6	0.24	0.12	0.19	0.27	0.23	0.15	0.18	0.29
7	-0.04	-0.34	-0.01	-0.10	0.00	-0.37	-0.01	-0.10
8	0.09	0.30	0.25	0.27	0.04	0.22	0.21	0.20
9	0.07	0.02	0.11	0.16	0.12	0.12	0.12	0.10
10	-0.08	0.02	0.07	-0.13	-0.03	-0.19	-0.04	-0.23
11	-0.19	-0.12	-0.09	-0.28	0.13	0.22	0.20	0.11
12	-0.01	0.09	-0.10	-0.19	0.02	0.05	-0.11	-0.15
13	-0.02	0.10	0.00	-0.05	-0.02	0.10	0.00	-0.05
14	0.24	0.75	0.00	0.07	0.12	0.48	-0.05	-0.06
15	-0.15	-0.16	-0.06	-0.12	-0.13	-0.15	-0.02	-0.11
Mean	-0.01	0.04	0.03	-0.01	-0.03	0.02	0.01	-0.02
SD	0.15	0.25	0.14	0.17	0.15	0.21	0.11	0.15

Table 4.4. Visual CM Task FC (R value). CM R values show the direction and strength of the connectivity between the IM PBR ROIs and CM NBR ROIs during tasks. Green = positive FC; red = negative FC.

Subject	IM		CM		IM		CM	
	GRIP ROIs	TAP ROIs	GRIP ROIs	TAP ROIs	Low ROIs	High ROIs	Low ROIs	High ROIs
1	0.32	0.41	0.09	0.32	0.53	0.86	-0.01	0.41
2	0.52	0.44	0.20	0.30	0.72	0.59	-0.03	0.07
3	0.24	0.67	-0.06	0.50	0.83	0.83	0.33	0.53
4	0.34	0.39	0.03	0.00	-0.01	0.76	0.12	0.02
5	0.68	0.55	0.41	0.19	0.34	0.55	-0.07	-0.01
6	0.61	0.25	0.24	0.16	0.05	0.05	0.02	0.10
7	0.43	0.43	-0.15	0.54	0.45	0.72	0.20	0.20
8	0.18	0.22	-0.18	-0.12	0.66	0.55	0.19	0.13
9	0.45	0.63	0.27	0.24	0.67	0.67	0.00	-0.02
10	0.73	0.74	0.59	0.62	0.85	0.79	0.54	0.30
11	0.71	0.62	0.51	0.33	0.45	-0.09	-0.11	-0.31
12	0.29	0.16	0.08	-0.05	0.54	0.43	0.27	0.44
13	0.53	0.72	0.45	0.35	0.81	0.12	0.08	0.08
14	0.60	0.75	0.36	0.40	0.51	0.27	0.03	0.06
15	-0.45	-0.11	0.06	-0.15	0.37	0.82	0.44	0.47
Mean	0.41	0.46	0.19	0.24	0.52	0.53	0.13	0.16
SD	0.28	0.24	0.23	0.23	0.25	0.30	0.19	0.22

Table 4.5. Motor and Visual RSFC. IM FC values show the direction and strength of the RSFC between IM contralateral ROIs and the IM ipsilateral ROIs. CM RSFC values show the direction and strength of the RSFC between IM contralateral ROIs and CM ROIs. Green = positive FC; red = negative FC.

4.4.4 Relationship between resting state and task FC

Only the combined IM motor RSFC and task FC (mean across runs) were found to significantly positively correlate (Tap ROIs: n=15, r=0.59, p=0.021; Grip ROIs: n=15, r=0.49, p=0.061; **combined: n=30, r=0.51, p<0.01)**.

No significant correlations were found for CM motor RSFC and task FC (Tap ROIs: n=15, r=0.13, p=0.65; Grip ROIs: n=15, r=0.43, p=0.11; combined: n=30, r=0.23, p=0.22)

IM visual RSFC was found to significantly positively correlate with IM visual task FC for Low IM ROIs but not High IM ROIs (High ROIs: n=15, r=-0.047, p=0.87; Low ROIs: n=15, r=0.56, p=0.028; combined: n=30, r=0.25, p=0.19).

No significant correlations between CM visual RSFC and CM task FC were noted (High ROIs: n=15, r=-0.43, p=0.11; Low ROIs: n=15, r=-0.25, p=0.37; combined: n=30, r=-0.34, p=0.068).

Summary

Unlike task FC, RSFC was found to be significantly different from zero. IM motor ROIs were found to be the only locations in which the RSFC and task FC were correlated.

4.4.5 Structural Connectivity

Of the three ROI sizes used to calculate TS (1.5, 3 and 6 voxel radius) only the 6 sphere radius ROI measure was used for correlation with other measures due to the inconsistency in the ability to measure tTS using the 1.5 and 3 radius sphere ROIs across all conditions and for all subjects (see Table 4.6 and 7). Therefore, from this point onward only data relating to the 6 voxel ROI is discussed.

With the exception of 2 subjects for IM Tap ROIs, and 3 subjects for IM Grip ROIs all subjects showed a direct structural connection via the CC between IM ROIs for Tap, Grip, High and Low. Table 4.8 shows the difference, in voxels and percentage, between the 6 sphere ROI radius tTS and pTS measures. This highlights the much larger number of voxels found over the 15% threshold in the tTS than the pTS measure for motor data, with pTS accounting for only ~48% of the tTS measure. Within the IM visual ROIs, little difference was found between the tTS and pTS measures, with pTS accounting for ~94.5% of the tTS measure.

The region of the CC through which the pTS mask most often passed, when taken across subjects, was found to be highly similar for IM Tap ROIs and IM Grip ROIs (Figure 4.2A&B) and also for IM High ROIs and IM Low ROIs (Figure 4.2C&D). A difference was found between

the motor and visual modalities, whereby masks of the motor ROI data were found to be anterior to those of the visual data (Figure 4.2E). With the motor modality data showing similar location to that of previous motor hemispheric SC work in which the transcallosal connection passed through the isthmus (Wahl, Lauterbach-Soon et al. 2007).

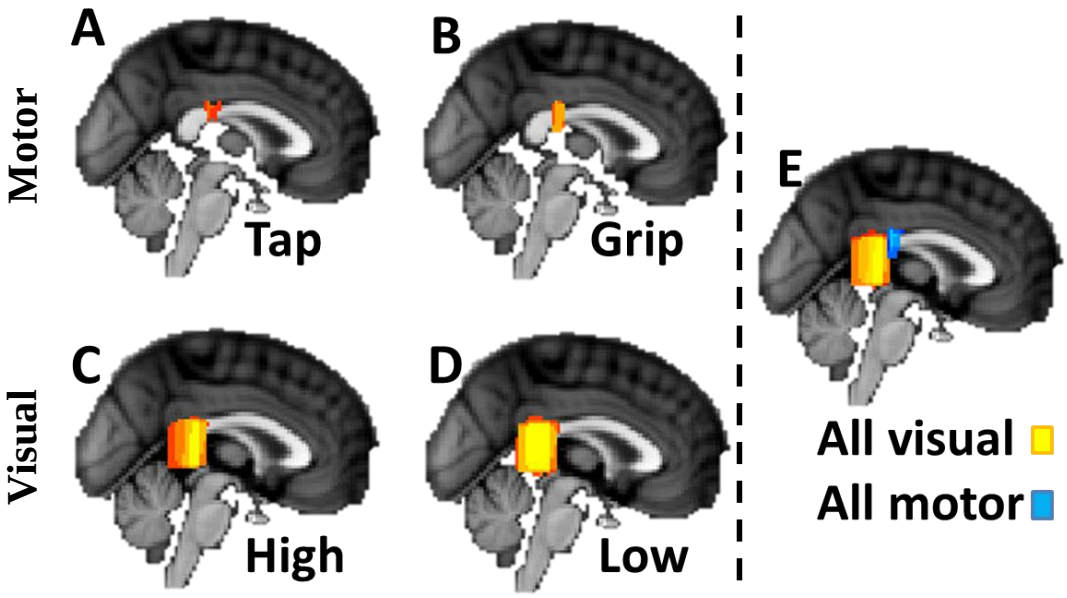

Figure 4.2. Corpus callosum location of pTS mask. pTS masks were binarised and summed across all subjects**. A** and **B** show the location of the Tap and Grip group level pTS masks, respectively, thresholded to show the region at which at least 7 out of 12 subjects masks overlapped. **C** and **D** show the location of the High and Low group level pTS masks, respectively, thresholded to show the region at which at least 10 out of 14 subjects masks overlapped. **E** shows all motor pTS masks (blue) thresholded at 16/19 subjects, and all visual pTS masks (yellow) thresholded at 24/28 subjects. This shows that the visual pTS masks across the group sit in the posterior section of the CC, the splenium, whereas the motor pTS masks are slightly anterior, in a region similar to the isthmus.

	IM TAP			CM TAP			IM GRIP			CM GRIP		
ROI radius	**1.5**	**3**	**6**	**1.5**	**3**	**6**	**1.5**	**3**	**6**	**1.5**	**3**	**6**
Subjects												
1	0	447	1010	632	500	1552	280	440	699	479	410	667
2	0	0	1809	578	871	1243	0	307	1589	146	830	931
3	0	1150	994	0	342	356	1152	225	1152	0	883	2049
4	0	727	1614	1339	602	1323	0	302	951	581	1065	517
5	0	194	925	0	559	679	0	192	1349	0	857	998
6	337	637	513	0	1052	2170	843	855	843	0	685	1085
7	0	778	965	0	1693	391	1226	280	1226	780	711	783
8	0	0	0	0	1046	758	0	0	199	0	394	539
9	249	1160	1596	572	1161	1794	1313	1134	1313	0	995	1349
13	0	241	672	0	298	307	582	1618	582	0	0	234
14	0	550	961	865	234	432	872	784	872	428	611	887
15	181	659	791	1152	563	834	741	522	741	480	636	683
16	265	343	478	0	585	669	808	940	967	0	228	998
17	0	0	404	0	359	1928	0	0	509	245	301	444
MEAN	74	492	909	367	705	1031	558	543	928	224	615	869
STD	120	375	485	466	396	610	484	449	361	263	299	431

Table 4.6. Subject specific Tap and Grip ROI total tract strength (tTS) measured as the number of voxels with probabilistic values greater than 15% of the maximum voxel value for three sizes of ROI. IM values represent tract strength between the IM ROIs. CM values show tract strength between IM contralateral ROIs and CM ROIs. Data realised from each set of spherical ROIs of radius 1.5, 3 and 6 voxels is shown. The 1.5 radius and 3 radius ROIs were unable in some instances to produce results: 31/56 instances and 6/56 instances respectively.

	IM HIGH			CM HIGH			IM LOW			CM LOW		
ROI radius	**1.5**	**3**	**6**	**1.5**	**3**	**6**	**1.5**	**3**	**6**	**1.5**	**3**	**6**
Subjects												
1	213	2216	1543	0	1354	1720	0	856	2853	0	3090	1720
2	0	502	542	0	246	3266	0	774	650	0	247	3266
3	0	663	559	0	0	2501	0	1260	223	0	0	243
4	0	924	1172	0	0	2157	0	564	1199	0	0	2157
5	0	1055	928	0	0	776	0	556	983	0	227	1009
6	0	1645	1469	0	0	1124	854	1645	1469	0	0	1124
7	0	1282	2353	0	0	339	0	1059	1077	0	0	343
8	0	526	977	0	1037	2017	0	542	849	240	251	2017
9	0	1571	737	0	0	2838	0	1571	737	241	268	2074
13	0	1186	1114	0	0	1296	0	2413	1350	0	0	0
14	0	992	1093	0	0	2247	0	690	1036	0	0	129
15	0	943	764	0	1777	688	0	901	1112	0	1777	688
16	0	469	763	0	0	1867	0	540	881	2011	0	263
17	0	663	1070	291	0	2755	0	851	937	0	0	2933
MEAN	15	1046	1077	21	315	1828	61	1016	1097	178	419	1283
STD	55	485	456	75	582	851	220	522	570	515	866	1042

Table 4.7. Subject specific High and Low ROI total tract strength (tTS) measured as the number of voxels with probabilistic values greater than 15% of the maximum voxel value for three sizes of ROI. IM values represent tract strength between the IM ROIs. CM values show tract strength between IM contralateral ROIs and CM ROIs. Data realised from each set of spherical ROIs of radius 1.5, 3 and 6 voxels is shown. The 1.5 radius and 3 radius ROIs were unable in some instances to produce results: 50/56 instances and 38/56 instances respectively.

Subjects	*IM Tap*	*IM Grip*	*IM High*	*IM Low*
1	736 (27)	146 (21)	365 (76)	594 (79)
2	1478 (18)	604 (62)	2 (100)	39 (94)
3	378 (62)	594 (48)	9 (98)	72 (68)
4	1614 (NM)	951 (NM)	4 (100)	2 (100)
5	639 (31)	1092 (19)	0 (100)	9 (99)
6	104 (80)	595 (29)	41 (97)	41 (97)
7	513 (47)	674 (45)	312 (87)	8 (99)
8	0 (NM)	199 (NM)	1 (100)	14 (98)
9	621 (61)	1313 (NM)	6 (99)	6 (99)
11	241 (64)	104 (82)	15 (99)	35 (97)
12	217 (77)	68 (92)	170 (84)	139 (87)
13	125 (84)	11 (99)	39 (95)	74 (93)
14	55 (88)	104 (89)	0 (100)	0 (100)
15	404 (NM)	436 (14)	6 (99)	8 (99)
Mean	509 (49)	492 (47)	69 (95)	74 (94)
SD	496 (31)	414 (37)	123 (7)	154 (9)

Table 4.8. Difference in number of voxels between tTS and pTS, tTS-pTS, with percentage of pTS relative to tTS (pTS/tTS*100) in parentheses, NM highlights no pTS measure. There is a larger discrepancy between the motor TS measures than the visual, with visual pTS and tTS showing very similar values.

4.4.6 Relationship between tract strength and resting state FC

The IM motor tTS and RSFC did not correlate (Tap ROIs: n=14, r=0.28, p=0.33; Grip ROIs: n=14, r=0.41, p=0.14; Combined: n=28, r=0.33, p=0.087), nor did IM motor pTS and RSFC (Tap ROIs: n=14, r=0.51, p=0.062; Grip ROIs: n=14 r=0.35, p=0.23; Combined: n=28, r=0.41, p=0.032). CM motor pTS and RSFC were not correlated (Tap ROIs: n=14, r=-0.37, p=0.19; Grip ROIs: n=14, r=-0.13, p=0.65; Combined: n=28, r=-0.25, p=0.2).

No correlations were found between IM visual tTS and RSFC (High ROIs: n=14, r=0.094, p=0.75; Low ROIs: -0.32, p=0.26; Combined: n=28, r=-0.11, p=0.57) nor were any found between IM visual pTS and RSFC (High ROIs: n=14, r=0.021, p=0.94; Low ROIs: n=14, r=-0.44, p=0.11; Combined: n=28; r=-0.21, p=0.29). Similarly, no correlations were found

between CM visual pTS and visual RSFC (High ROIs: n=14, r=0.29, p=0.32; Low ROIs: n=14, r=0.063, p=0.83; Combined: n=28, r=0.21, p=0.29).

4.4.7 Relationship between tract strength and task FC

IM motor task FC was not found to correlate with tTS (Tap ROIs: n=14, r=-0.052, p=0.86; Grip ROIs: n=14, r=0.42, p=0.13; Combined: n=28, r=0.12, p=0.56) or pTS (Tap ROIs: n=14, r=0.35, p=0.22; Grip ROIs: n=14, r=0.35, p=0.22; Combined: n=28, r=0.35, p=0.072) . Similarly, CM motor task FC did not correlate with tTS (Tap ROIs: n=14, r=-0.036, p=0.9; Grip ROIs: n=14, r=0.011, p=0.97; combined: n26, r=-0.055, p=0.78).

There was no correlation between IM visual task FC and tTS (High ROIs: n=14, r=-0.23, p=0.43; Low ROIs: n=14, r= -0.27, p=0.34; combined: n=28, r=-0.25, p=0.19) or task FC and pTS (High ROIs: n=14, r=-0.18, p=0.53; Low ROIs: n=14, r= -0.28, p=0.33; combined: n=28, r=-0.24, p=0.22). CM visual task FC was not found to correlate with tTS (High: n=14, r=0.079, p=0.79; Low: n=14, r=0.11, p=0.7; combined: n=28, r=0.083, p=0.68).

Summary

No significant correlations were found between pTS/tTS and task FC or RSFC for motor or visual ROIs. However, a trend was found between the combined IM motor ROI RSFC and pTS, uncorrected.

4.4.8 NBR regression

Linear regression was used to test whether the measures of RSFC, pTS/tTS, and task FC were able to predict either the NBR CoV, for IM and CM ROI data.

IM Motor ROIs

CoV

No variable was found to be a significant predictor of IM Tap NBR CoV, (Overall, a linear relation was found between NBR CoV and the variables: **F(4,9)=10.57, p<0.01,** R^2_{adj}=0.75; although after bootstrapping there was no significant predictor : Tap ROI: pTS, β=0.015, p=0.95; RSFC, β=-0.012, p=0.97; task FC, β=0.91, p=0.055; tTS, β=-0.024, p=0.91).

IM Grip task FC was found to be significant predictor of IM Grip NBR CoV (**F(4,9)=8.45, p<0.01**, R^2_{adj}=0.70; **Grip ROI:** pTS, β=0.55, p=0.05; RSFC, β=-0.22, p=0.32; **task FC, β=0.64, p<0.05;** tTS, β=0.013, p=0.94).

Combined IM motor pTS and task FC were found to be significant predictors of combined motor IM ROI NBR CoV (**F(4,23)=10.41, p<0.001**, R^2_{adj}=0.58; motor ROI: **pTS, β=0.40, p<0.05;** RSFC, β=-0.23, p=0.16; **task FC, β=0.68, p<0.01;** tTS, β=0.041, p=0.74).

BOLD ratio

No variable was found to be a significant predictor of IM Tap BOLD ratio (F(4,8)=1.24, p=0.37, R^2_{adj}=0.075).

No variable was found to be a significant predictor of IM Grip BOLD ratio (F(4,9)=2.3, p=0.13, R^2_{adj}=0.39).

Combined IM motor tTS was found to be a significant predictor of motor IM BOLD ratio (**F(4,23)=3.25, p<0.05,** R^2_{adj} =0.26; motor ROI: pTS, β=-0.099, p=0.53; RSFC, β=-0.18, p=0.52; task FC, β=0.26, p=0.16; **tTS, β=0.58, p<0.05**).

CM Motor ROIs

CoV

No CM Tap measure was found to predict Tap CM NBR CoV (**F(3,9)=11.27, p<0.01,** R^2_{adj} =0.72; Tap ROI: RSFC, β=0.16, p=0.39**;** task FC, β=0.84, p=0.081; tTS, β=0.25, p=0.23).

No CM Grip measure was found to be a predictor of CM Grip NBR CoV (F(3,10)=2.5, p=0.12, R^2_{adj} =0.72).

No CM motor measure was found to predict combined CM motor NBR CoV (**F(3,23)=7.4, p<0.01**, R^2_{adj} =0.43; motor ROI: RSFC, β=0.11, p=0.51; task FC, β=0.67, p=0.37; tTS, β=0.14, p=0.28).

BOLD ratio

No CM Tap measure was found to be a predictor of CM Tap BOLD ratio (F(3,9)=1.50, p=0.28, R^2_{adj}=0.11).

No CM Grip measure was found to be a predictor of CM Grip ratio (F(3,10)=0.68, p=0.58, R^2_{adj}=-0.079).

No combined CM motor ROI measure was found to predict pooled CM motor BOLD ratio (F(3,23)=1.75, p=0.19, R^2_{adj} =0.26).

IM Visual ROIs

CoV

No IM High measure was found to be a significant predictor of IM High NBR CoV (F(4,9)=1.80, p=0.21, R^2_{adj}=0.20).

No IM Low measure was found to be a significant predictor of IM Low NBR CoV ($F(4,9)=1.8$, $p=0.21$, $R^2_{adj}=-0.079$).

Combined IM visual task FC was found to be a significant predictor of IM visual NBR CoV (**$F(4,23)=3.18$, $p<0.05$,** $R^2_{adj}=0.20$; visual ROIs: pTS, β=-1.40, p=0.11; RSFC, β=-0.064, p=0.74; **task FC, β=0.59, $p<0.05$;** tTS, β=1.55 p=0.069).

BOLD ratio

No IM High measure was found to be a significant predictor of IM High BOLD ratio ($F(4,9)=0.52$, $p=0.72$, $R^2_{adj}=-0.17$).

Only IM Low RSFC was found to be a significant predictor of IM Low BOLD ratio (**$F(4,9)=6.88$, $p<0.01$**, $R^2_{adj}=-0.64$; Low ROI: pTS, β=3.46, p=0.13; **RSFC, β=1.51, $p<0.05$**, task FC, β=-0.56, p=0.27; tTS, β=-3.10, p=0.14).

No combined IM visual ROI measure was found to be a significant predictor of IM visual BOLD ratio ($F(4,23)=2.24$, $p=0.096$, , $R^2_{adj}=0.16$).

CM Visual ROIs

CoV

No CM High ROI measure was found to predict CM High NBR CoV ($F(3,10)=0.21$, $p=0.89$, $R^2_{adj}=-0.22$).

No CM Low ROI measure was found to predict CM Low NBR CoV ($F(3,10)=1.27$, $p=0.84$, $R^2_{adj}=0.076$).

No combined CM visual ROI measure was found to predict CM visual NBR CoV ($F(3,24)=0.43$, $p=0.73$, $R^2_{adj}=-0.067$).

BOLD ratio

No CM High ROI measure was found to predict CM High BOLD ratio ($F(3,10)=0.77$, $p=0.53$, $R^2_{adj}=-0.055$).

No CM Low ROI measure was found to predict CM Low BOLD ratio ($F(3,10)=1.08$, $p=0.40$, $R^2_{adj}=0.019$).

No combined CM visual ROI measure was found to predict CM visual BOLD ratio ($F(3,24)=2.10$, $p=0.13$, $R^2_{adj}=0.11$).

Summary

In summary, the IM task FC was found to be a significant predictor of the IM NBR CoV measure but not BOLD ratio for motor and visual data. For TS, pTS was found to be a significant predictor of IM motor NBR CoV, while tTS was found to be a significant predictor of IM motor BOLD ratio with no such relationship found in the visual data. No CM relationships were found for motor or visual data.

4.5 Discussion

In this Chapter we assessed the strength of the functional and structural connections between primary sensory cortex regions that displayed PBR and NBR during visual and motor tasks. We were able to show that features of these BOLD responses could be predicted by these connectivity measures. However, our hypothesis of a positive correlation between pTS and RSFC was shown only to occur for motor IM ROIs (uncorrected).

The main findings related specifically to the motor cortex data (IM motor ROIs) which showed that NBR variability increased with increasing task FC and with increasing pTS (though not with tTS). While IM motor RSFC, although not directly related to IM NBR CoV, did positively correlate with both IM motor task FC and pTS (uncorrected). Taken together these results

suggest that those ROIs which were highly intrinsically connected at rest remained so during tasks, resulting in greater NBR variability as discussed further below. In addition to this, the IM motor NBR:PBR ratio was found to increase with increasing tTS showing a more complex picture of the DTI-BOLD relationship. With variability linked to direct CC connectivity and the size of the IM NBR in relation to IM PBR linked to the overall connectivity.

Although IM visual NBR variability was found to increase with increasing IM visual task FC in a similar manner to the IM motor data, no other relationships were noted for the visual data. The lack of findings in the visual modality in comparison with those in the motor could be representative of differences in the type of task (passive vs. active) or structural and functional differences between the two modalities, discussed further below.

4.5.1 The utility of the NBR CoV

In general, across both motor and visual modalities the NBR amplitude was found to be more variable than that of the PBR (see Table 4.1). PBR CoV values were highly similar across conditions (range=0.17-0.32) showing that the response amplitudes mean value was approximately 3-5 times greater than the standard deviation. In contrast, the NBR CoV ranged between 1.21 - 2.88, indicating that the response amplitudes mean value was approximately 2-3 times smaller than its standard deviation. IM and CM NBR CoV and mean amplitude were found to be positively related in the visual data, in direct contrast to the motor data, showing that those subjects with smaller visual mean NBR displayed larger CoV. A similar relationship was also seen between visual mean PBR and CoV (all visual data combined, $R=-0.61$, $p<0.001$) but not for motor (all motor data combined, $R=-0.38$, $p<0.05$). Therefore, for visual data those subjects whose mean NBR or PBR was closer to zero had less consistent BOLD responses, which may be expected, whereas the motor data did not follow that pattern. An obvious difference between the task modalities was that the visual stimuli were passively viewed whereas the motor tasks were actively performed. The volitional aspect of the motor

data complicates the measure of response variability by introducing two main contributors, variability in pressure and pacing, which can influence evoked BOLD responses (Ismail, Mohamad et al. 2014). The BOLD responses to the consistent visual stimuli would therefore be expected to fluctuate less than those of the more variable motor tasks. Although EMG could have been recorded in the scanner to account for this, correction of gradient artefacts during muscle contraction would be problematic. This difference in fluctuation of the response was shown in part by the correlation across subjects, between the visual mean BOLD responses and the visual CoV measures, something not apparent in the motor data. This suggests that the visual CoV was driven mainly by the mean amplitude whereas the motor data was not. There does however appear to be a high level of similarity between the CoV of the IM visual PBR and the CoV of the IM motor PBR. Similarly, there was no discernible difference between the NBR CoV (IM or CM) for motor or visual trials. This suggests that although there are apparently greater complexities in the make-up of the BOLD responses to motor trials, the actual variation in the responses was very similar to those of the visual trials.

4.5.3 ROI influence on functional and structural connectivity measures

The exact position of the ROIs was found to have a substantial effect on the strength and often the magnitude of the task FC and RSFC measured. This was seen clearly in the visual ROI data, e.g. subject 11 exhibited negative CM Low task FC and positive CM High task FC, Table 4.5. It would have been possible to create only 3 visual ROIs and 3 motor ROIs e.g. in the visual modality: IM contralateral visual cortex ROI, IM ipsilateral visual cortex ROI, and a CM ipsilateral motor cortex ROI could have been used. However, this would have come at the cost of reducing the specificity of the connectivity measures obtained; as previous work has shown small movements in the placement of an ROI can lead to very different connectivity results (Cohen, Fair et al. 2008).

The size of the ROI also had a large impact on the ability to measure TS, with the 6 voxel radius sphere ROIs allowing calculation of streamlines for a greater proportion of subjects than the smaller ROIs (Tables 4.6&4.7). The smaller 1.5 and 3 voxel radius sphere ROIs were more fully imbedded in the GM than the 6 voxel radius sphere. Therefore, the smaller ROIs create a more problematic solution for tractography than the larger ROIs which are more likely to contain regions of WM and so have a greater chance of being connected by the algorithm. This creates a secondary problem: the directness with which the BOLD data and the TS data can be compared when using different ROI sizes for both. Previous studies have used an approach of dilating the GM ROIs (defined from BOLD data) in order to capture WM within the ROI (Mazerolle, Beyea et al. 2010, Preti, Makris et al. 2012). Here we attempted to compare different sizes of ROI to find how this changes the TS measured and the relationship to the NBR.

In the DTI analysis, the larger ROIs would seem to result in a more general measure of TS than using the 1.5 radius voxel, albeit one that is still more specific than using simply the whole left and right motor and visual cortices. It is difficult to compare GM and WM measures with certainty in this manner, for example the large size of the BOLD voxels, smoothing, and the registration of subjects' data to their anatomical scans during pre-processing all reduce the certainty of the spatial location gained from the BOLD task based analysis. Although previous work in mice has shown that the size of the ROIs used in the two hemispheres of the visual cortex resulted in the same number of connections found, these ROIs were centred within the WM tracts studied and not based on fMRI BOLD ROIs (Huang, Zhang et al. 2004). Here, we found that larger BOLD specified ROIs were most useful for this particular tractography analysis.

4.5.4 Factors driving functional connectivity

The mean motor and visual RSFC across subjects was significantly positive for each set of ROIs, this is in agreement with a large body of previous literature which has shown positive RSFC between motor regions (Biswal, Yetkin et al. 1995, Lowe, Mock et al. 1998, Cordes, Haughton et al. 2000, Cordes, Haughton et al. 2001) and visual regions (DeYoe, Bandettini et al. 1994, Lowe, Mock et al. 1998, Cordes, Haughton et al. 2000). While task FC was found to be negative for most subjects between motor ROIs (i.e. reflecting the opposite polarity of the BOLD responses in those ROIs) it did show considerable between-subject variability, while no overall negative or positive pattern in task FC was observed for visual ROIs. However, across all task FC data only IM and CM Tap task FC were found to differ significantly from zero, showing negative connectivity. Although previous task FC work has focussed upon the PBR and has used the residuals left after GLM analysis (i.e. after regression of the PBR from the data) (Fair, Schlaggar et al. 2007, Fox, Snyder et al. 2007, Mennes, Kelly et al. 2010, Cole, Bassett et al. 2014) we were primarily interested here in the interplay between the PBR and NBRs and how that related to the NBR measure. It has been shown that the removal of the PBR from task based data does not greatly affect the level of task FC found between PBR regions, including motor-to-motor and visual-to-visual cortices (Cole, Bassett et al. 2014). However, the data from that study only contained single stimuli per run, while our data was a combination of visual and motor trials which is likely to have influenced the task FC as discussed below.

The direction and magnitude of the task FC appear to be dependent on the BOLD responses to the ROI specific task. For example IM Tap task FC being driven by the PBR in the IM PBR ROI and NBR in the IM NBR ROI: with larger negative task FC resulting from greater opposition of the two BOLD responses as well as a larger proportion of trials of that task within the entire timecourse of the run. Stimuli were interleaved in each run so that a single run contained only a Grip or Tap task but both visual stimuli. Therefore, for a motor task the

combined duration of all trials in a single run would be 408s (task baseline and stimulus combined) out of a total 816s of the entire timecourse used for the task FC analysis. Whereas for visual trials, each would separately account for a lesser proportion of 204/816s of each runs timecourse. Of task FC, 68% of all motor task FC measurements across all subjects were negative while only 48% of visual task FC measurements across subjects were negative (see Table 4.2, 4.3 and 4.4). On average, stronger negative task FC, along with larger PBR and NBR, was found for Tap, which was the more complex motor task, than for Grip, the simpler task. Taken together these data suggest task FC is driven mainly by the BOLD responses of the task.

4.5.5 Predicting BOLD response features from intrinsic connectivity

Previous work linking RSFC with task BOLD responses have focussed primarily on PBRs (Mennes, Kelly et al. 2010, Mayhew, Hylands-White et al. 2013, Cole, Ito et al. 2016) with no previous work looking specifically at the link between NBR and RSFC. Here, the positive relationship of IM task FC with IM NBR CoV was the most significant finding in this study. If, as argued above, task FC was driven by the opposition of PBR and NBR amplitude polarities during tasks, then this suggests that the relationship between the NBR and the PBR was important for the NBR variability where those subjects showing larger negative task FC (greater opposition of PBR and NBR during tasks) also showed more consistent NBRs. This was also in line with the relationship noted between IM motor RSFC and task FC which showed that with larger RSFC there was larger task FC (with a similar trend also seen for CM visual ROIs and Low IM ROIs). Taken together these results suggest two possibilities: either that when the FC was highly positive between two regions it limited the degree to which those region's task responses could become opposed (a NBR with a PBR) during tasks; or that the level to which the regions are opposed during tasks limits the degree to which they will be functionally connected during rest. The later possibility gains a certain amount of credence

from studies showing that simple motor tasks do in fact change the RSFC between motor cortices (Tung, Uh et al. 2013). This challenges the oversimplification that there is a steady consistent resting state in the brain from which actions occur.

4.5.6 Evaluation of tract strength measures

The spatial location of the pTS masks within the CC showed a high level of similarity with known divisions of the CC. The splenium, known to connect right and left visual cortices (Myers 1962), was here shown to be the region captured by our visual pTS mask (See Figure 4.2C,D&E). The section of the CC more anterior to the splenium is the Isthmus, a region shown by Genç et al. (Genc, Ocklenburg et al. 2015) to most directly correlate with the ipsilateral BOLD response during motor tasks. Here we show that a region of the CC similar in position to that of the Isthmus is also captured by our motor pTS mask (see Figure 4.2A,B&E). Although we have not taken the approach of segmenting the CC, the similarities between the previous identified CC regions and the current results highlight the utility of our pTS measure.

4.4.7 Tract strength and Functional connectivity

We found only a trend towards a positive correlation between the IM motor pTS and IM motor RSFC, with no other correlation between RSFC and TS found. As discussed it is apparent that there is not a necessary one-to-one relation of SC to FC with indirect connections potentially being influential (Honey, Sporns et al. 2009). Klingner et al. (Klingner, Hasler et al. 2010) posited that somatosensory evoked PBRs and IM NBRs are connected via an intermediary in the ipsilateral motor cortex (described in Chapter 1). Future work could aim to find whether the strength of SC and FC between the contralateral PBR region and ipsilateral PBR found in secondary somatosensory cortices (see Figure 2.1D; top row), and onto the IM NBR region, are related and whether this can explain IM NBR changes. The current work implies that direct connectivity is not implicated in the RSFC between the motor and visual ROIs, even though

the BOLD responses themselves appear to be associated with specific functional or structural measures, particularly for motor data.

4.5.8 Tract Strength and NBR

In addition to previous research of interhemispheric interaction, as outlined in Chapter 1, we have been able to directly relate TS between regions of task induced IM contralateral PBR and ipsilateral NBR to both the CoV of the NBR and the NBR:PBR ratio. Although, due to the limitations of DTI as discussed in Chapter 1 we can only say that these regions are connected with a high degree of probability, and it is apparent that this level of probable connectivity is related to both the NBR CoV (pTS) and BOLD ratio (tTS). Both the relation of NBR CoV to pTS and also BOLD ratio to tTS is positive, in that as the TS increases so does the BOLD measure. This suggests that it is not the most direct CC connection between the motor IM ROIs that is influential in the NBR:PBR ratio but the overall connectivity, including possible subcortical commissures. The two TS measures, were found on average to differ in size by 52% for motor ROIs, pTS<tTS. This finding requires us to consider the importance of the different connections between motor cortices to their function. For instance it is known that the complete resection of the CC does not mean that all interhemispheric connectivity is lost (Sperry, Zaidel et al. 1979) with possible subcortical commissures, including the thalamus, capable of relaying information between hemispheres (Holtzman 1984, Gazzaniga, Holtzman et al. 1987).

The tTS does of course contain within it the pTS measure. Additional analysis of IM motor ROI difference in TS (tTS-pTS) correlated to IM motor NBR:PBR ratio found no significant relationship (Tap: r=-0.26, p=0.37; Grip: r=-0.24, p=0.41; Combined: r=0.22, p=0.26) suggesting that the whole structural wiring was important. Taken together these results, although requiring replication, are indicative of different sections of TS potentially being important for different aspects of motor interhemispheric connectivity during motor tasks.

This adds complexity to the studies discussed in Chapter 1 which speculate that the CC is the main pathway of connectivity between the cortices during unilateral motor stimulation for the generation of ipsilateral BOLD responses (Fabri, Polonara et al. 2005, Feige, Scheffler et al. 2005, Klingner, Hasler et al. 2010, Schafer, Blankenburg et al. 2012). Our data instead suggest that greater connectivity between the motor IM ROIs via the CC actually decreased the consistency of the IM NBR. To our knowledge no previous studies have assessed the link between the NBR CoV and TS, however, this apparently counter-intuitive finding is consistent with the NBR-FC relationships we have observed, such that when the RSFC was high it limited the degree to which their task FC could become opposed (larger NBR with larger PBR).

Within the visual modality we found that neither visual NBR CoV nor BOLD ratio was related to TS: tTS or pTS. The strength of the structural connection, as we have been able to measure it, between these regions therefore appeared to play no role in maintaining consistency or the magnitude of the visual NBR. Visual cortex pTS and tTS were found to differ by an average of 5.5% for visual ROIs, showing with high probability that the main interaction between hemispheres occurs though this posterior (splenium) pathway. This discrepancy was much lower than was seen from the motor TS measurements in which a large difference, an average of 52%, was found between tTS and pTS. The lack of relationship between the visual TS and BOLD responses could be related to the passive nature of the visual stimuli. Here the response to visual stimuli could be a result of the direct bottom-up afferent input from subcortical structures rather than from interhemispheric interactions. For the motor tasks however, the necessity of initiating and maintaining the actions requires an element of attention which may be fundamental in the FC-BOLD relationships noted in this modality, something we cannot test here.

Although measures were gained for the TS in all CM conditions (except CM Low ROIs), neither the CM NBR CoV nor the BOLD ratio were found to be predicted by tTS. The CM

motor NBR was located in the same hemisphere as the IM PBR to motor tasks, the close proximity of the two areas would be expected to enable TS to be better represented than the longer distance connection between CM visual ROIs due to probabilistic tractography decreasing in ability with increasing distance (Morris, Embleton et al. 2008). However, the lack of relationship between the CM NBR CoV or BOLD ratio to CM motor ROI TS suggests any direct connection between the regions was not implicated in generation of these CM BOLD responses. The large distance between the CM visual ROIs makes it more complicated to assess the CM TS, similarly making it difficult to relate this measure to the NBR CoV or BOLD ratio. The lack of findings for CM data implies that the connectivity between the CM NBR and IM PBR are not required for generation of the CM NBR.

4.5.9 Summary

Here we have found an apparent difference between the ability of TS to predict the IM NBR CoV and NBR:PBR ratio during motor trials in comparison to the lack of relationship during visual trials. Specifically, direct structural connectivity via the CC was found to be predictive of IM NBR CoV during motor trials whereas total structural connectivity (via any route) was found to predict motor task NBR:PBR ratio.

Differences were noted between the visual and motor cortex ROIs in the ability of RSFC and TS to predict IM NBR CoV. With only the most direct TS measure able to predict motor IM NBR CoV. These differences may in part relate to the passive and volitional aspects of the visual and motor trials respectively, rather than just the fundamental cortical physiology. The ability of the task FC to predict the IM NBR CoV measures of both motor and visual trials provides a link between the relation of PBR and NBR during the trials and the regulation of the NBR. Lastly, the CM NBR does not appear to be affected directly by its connection to the IM PBR.

CHAPTER 5

TMS, EEG AND MRS MEASURES OF NEURONAL ACTIVITY FOR THE ASSESSMENT OF INTRA- AND CROSS-MODAL NBRS

5.1 Abstract

NBRs have been shown to occur in the motor cortex to somatosensory stimulation (IM NBRs; (Allison, Meador et al. 2000)) as well as in the motor cortex via visual stimulation (Chapter 2). Although evidence mounts that these NBRs are a measure of neuronal suppression (Shmuel, Yacoub et al. 2002, Shmuel, Augath et al. 2006, Pasley, Inglis et al. 2007, Mullinger, Mayhew et al. 2014), whether such suppression is always behaviourally relevant is still unclear. Previous work has however found that the amplitude of IM NBRs in the somatosensory cortex increases with increased perceptual threshold of somatosensory stimulation of that region (Kastrup, Baudewig et al. 2008, Schafer, Blankenburg et al. 2012).

In this Chapter we use multiple measures (session 1: fMRI and MRS; session 2: TMS-EEG) to probe the functional relevance of the IM and CM NBRs located in the right motor cortex to separate stimuli: right MNS, basic right hand grip motor task, flashing full-field checkerboards

and bilateral auditory stimuli. We find that IM NBRs are evoked to the MNS and motor task and CM NBRs in the motor cortex to the visual and auditory stimuli. EEG artefacts from the TMS pulse were cleaned from the data allowing its use for further analysis, i.e. in comparison with other measures. Although CSE shows no change from stimulus baseline for visual and auditory stimuli it is seen to initially decrease for MNS and increase for motor data.

5.2 Introduction

The relationship between IM NBR and decreased perceptual threshold has been shown previously (Kastrup, Baudewig et al. 2008). In the following 2 Chapters we aim to test whether this functional relevance of IM NBRs in the motor cortex can be replicated using different tasks, motor and somatosensory stimuli, and also whether it is applicable to CM NBRs via auditory and visual stimuli. We also aim to test the relationship between IM/CM NBRs and GABA and Glx measures. To do so, in this Chapter we first look at the multiple measures (fMRI, MRS and EEG-TMS) separately to assess whether they can be utilised for further analyses.

5.2.1 Transcranial magnetic stimulation and electroencephalography

As described in Chapter 1, single pulse TMS can be used to gain a measure of CSE via MEP P2PA. In particular, it has previously been shown that unilateral sensorimotor stimulation leads to a decrease in CSE (i.e. smaller MEP P2PA) at the ipsilateral motor cortex (Chen, Corwell et al. 1999, Liepert, Dettmers et al. 2001). Unilateral sensorimotor tasks are known to lead to ipsilateral IM NBR (Allison, Meador et al. 2000, Mullinger, Mayhew et al. 2014), while we have also shown that CM NBRs are elicited in the motor cortex during visual stimulation (Chapter 2). Both MEP amplitudes and NBRs are thought to reflect a large scale balance of inhibitory and excitatory neuronal activity (Buxton, Griffeth et al. 2014, Bestmann and Krakauer 2015).

Therefore, tentative links can be drawn between these two measures, where IM NBRs occur during unilateral somatosensory stimuli (Mullinger, Mayhew et al. 2014) and decreases in CSE measured via TMS also occur in the same region during similar stimuli (Chen, Corwell et al. 1999). However, whether IM and CM NBRs relate in similar ways to such changes in CSE is unknown. Here we aim to test and compare how MEP P2PA is changed by four different sensory stimuli that are may induce NBR in the motor region. Further, we study relationships amongst the between-subject variability of different measures of neural inhibition, for instance whether larger subject NBRs relate to larger decreases in subject's MEP P2PA during various sensory stimuli and also test whether their EEG α and β power relate to the NBR or MEP P2PA.

Although a large number of studies have attempted to understand how MEPs relate to CSE, very few have sought to work out how this relates specifically to neuronal activity in the cortex. There have been combined TMS-EEG studies which have attempted this to assess whether EEG measures relate, if at all, to MEP P2PA. Early studies found that β oscillatory power measured in the motor cortex shows transient synchronisation as a result of single pulse TMS at rest (Paus, Sipila et al. 2001, Van Der Werf and Paus 2006) with similar effects noted in α power (Fuggetta, Fiaschi et al. 2005). These are thought to be a resetting of the oscillations on a large scale in that region (Van Der Werf and Paus 2006).

In addition, the ongoing motor cortex α and β power preceding the TMS pulse is believed to affect the P2PA of the MEP. With pre-TMS α power correlating negatively with the MEP P2PA at rest (Zarkowski, Shin et al. 2006, Sauseng, Klimesch et al. 2009). While some studies have been unable to find correlations between β power and MEP P2PA (Mitchell, Baker et al. 2007), others have noted a negative relationship between them during the execution of, but not during the observation of, motor tasks (Lepage, Saint-Amour et al. 2008), or during a gripping task (Schulz, Ubelacker et al. 2014). The possible link between lower pre-TMS α/β power and

larger MEP P2PA are in line with the gating hypothesis posited by Jensen and Mazaheri (Jensen and Mazaheri 2010) who suggest that resting fluctuations in α power are related to the level of excitation in the system, with lower power indicative of a more excitable, more responsive, system and higher power more inhibitory.

5.2.2 Combined TMS-EEG

There are inherent issues related to combining TMS and EEG. The TMS pulse creates a large amplitude, short duration artefact in the EEG data due to the rapidly changing magnetic field of the TMS pulse inducing a change in electrical current in the EEG electrodes and wires (Taylor, Walsh et al. 2008). Other potential EEG artefacts can be found: exponential decay (from muscle contraction), remaining muscle artefacts, capacitor recharge, and electrical artefacts, (for examples see Figure 5.1) (Rogasch, Sullivan et al. 2017). These artefacts, although relatively short in duration, heavily corrupt the underlying signal, however post-processing of the data can reduce such corruption. TMS artefacts can be reduced by: using a high sampling rate to provide a reliable measure of the EEG signal; using electrodes that have a small diameter to reduce the possibility of overheating and reduce movement due to the force of the TMS pulse; and minimising subject movement during the experiment (Ilmoniemi and Kicic 2010). There are a number of approaches for the removal of the TMS artefacts from EEG data during post-processing (Rogasch, Sullivan et al. 2017). A common approach is that of Herring et al. (Herring, Thut et al. 2015) which, after deletion and subsequent interpolation of the main TMS pulse artefact, uses independent component analysis (ICA) to remove the other artefacts. Although principle component analysis (PCA) can be used (Hernandez-Pavon, Metsomaa et al. 2012) ICA is more common and is capable of decomposing the entire signal into a set of components which are maximally temporally dissimilar from one another. It is commonly used to remove eye blinks and saccades from EEG and MEG data (Hoffmann and Falkenstein 2008) and, due to the independence of the TMS artefacts from any underlying

neuronal signal, can be used to remove the artefacts from the data (Vigario 1997, Onton, Westerfield et al. 2006, Agulhon, Petravicz et al. 2008). Where artefacts are easily identified due to them being time locked to the TMS pulse.

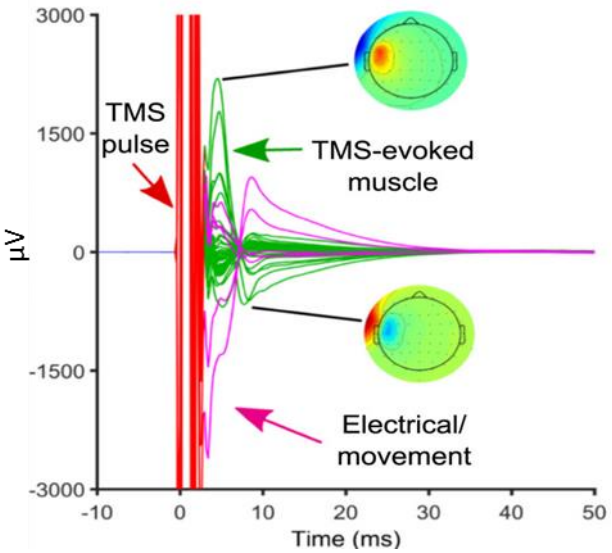

Figure 5.1. TMS artefact with two possible ICA components which would relate to specific elements of the artefact. Adapted from (Rogasch, Sullivan et al. 2017)

5.2.3 GABA and NBR

A further important, yet minimally studied, potential contributor to the NBR is the cortical availability of the primary neurotransmitter GABA. The resting level of GABA has been shown in a number of studies to increase across subjects as local mean NBR amplitude (measured from a region near the GABA measure) increases, particularly in the DMN (Northoff, Walter et al. 2007, Hu, Chen et al. 2013) (discussed in detail in Chapter 1). In contrast, higher resting glutamate levels were related to lower levels of NBR during a working memory task (Hu, Chen et al. 2013). However, the relationship between the resting GABA and glutamate levels and both the IM and CM NBRs in the motor cortex have not previously been studied.

5.2.4 Aim of this Chapter

Here we collected measures of CSE using TMS concurrent with α and β EEG power, and in a separate session measures of motor cortex NBR and resting levels of GABA and glutamate. In this chapter we aim to asses each of the measures independently. We will then go on to combine these measures in Chapter 6 to better understand how each relates to the IM and CM NBRs in the motor cortex, as well as how they relate to one another.

5.3 Methods

18 healthy subjects (7 female; mean age 24±5; all right handed) all gave informed consent to take part in the experiment. The University of Birmingham ethics committee approved the experimental procedures.

5.3.1 Paradigm

Two sessions were carried out featuring the same four sensory stimuli (described below) each stimulus was delivered in separate runs. While full details of the measurements taken are provided below while an overview is given here. The first session involved recording of BOLD fMRI responses to the stimuli, resting-state MRS situated over the left motor cortex and a T1-weighted anatomical. Subjects were subsequently brought back for a second resting-state MRS scan situated over the right motor cortex. For the second session EEG was recorded during the same sensory stimuli while single pulse TMS was applied.

5.3.2 Stimuli

The four stimuli comprised: a full-field 7Hz reversing checkerboard (visual), a 1kHz binaural tone repeating at 7Hz (auditory), right-wrist 40Hz median nerve stimulation (MNS) (Kastrup, Baudewig et al. 2008, Klingner, Hasler et al. 2010) just above the motor threshold and a sustained pinching of the right-hand index and middle finger to the thumb (Grip). The visual

and auditory stimuli were both bilateral in an attempt to facilitate the largest possible motor cortex NBR. The frequency of each of the stimuli was chosen to provide a robust measure of BOLD/EEG response while minimising the possibility of an evoked potential swamping the IM α ERD for that stimulus. One run of each stimulus type was acquired during separate MRI and EEG-TMS sessions.

For the MNS two electrodes were attached to the right wrist and square wave pulses of 0.5ms duration applied at 40Hz (Digitimer DS7A, Letchworth Garden City, UK). The stimulation current amplitude was set just above an individual's motor threshold at a level able to cause a small thumb distension with a single pulse. The subjects were instructed to fixate their eyes on a central cross throughout each run during both sessions. The Grip task was visually cued by central display of the word “Grip” throughout the stimulus period. Subjects were asked to passively observe visual, auditory and MNS and to maintain a consistent contraction during the Grip task. All stimuli were controlled using Psychtoolbox in Matlab.

For the fMRI session, 20 trials were carried out per run, 8s stimulus presentation with an equal number of alternating 14/15s baseline periods. The baseline duration was jittered in this way to maximise the temporal sampling of the BOLD responses and improve GLM fitting.

During the EEG session 30 trials were carried out per run: 9s stimuli with a 12s baseline. TMS pulses were delivered at four time points 1s (P1) ,7s (P2), 11/12s (RB11/12) and 18s (BL) relative to stimulus onset. These timings allowed both short and long term effects of the stimulus on CSE to be tested (P1 and P2) as well as possible differences in excitability during specific periods of the rebound (see Figure 5.2 for session 2 outline).

The difference in stimulus duration between fMRI and EEG sessions was to:

1) Allow the application of TMS pulses with at least 4s between each of the 4 pulses that were applied in each trial.

2) Measure NBR at the comparative time of the TMS pulse during stimulus presentation, therefore only requiring 8s.

The difference in baseline duration between the two sessions was designed for:

1) the TMS-EEG session, to maximise the baseline for beamformer analysis of the EEG data without overly lengthening the recording time. A period of 0.5s was left after a TMS pulse to reduce the impact of residual TMS artefact and/or TMS evoked potential confounding the beamformer analysis of oscillatory power. Therefore, leaving a 5.4s time window in the stimulus period (between 1.5 and 6.9s after stimulus onset), the baseline was extended to produce the same length of useable data (i.e. compromised as little as possible by the rebound).

2) the fMRI session, to leave the minimum but sufficient time for the BOLD signal to recover between trials.

Trial numbers were selected to allow a large enough sample to measure a robust NBR; and a reliable estimation of the MEP P2PA at each TMS pulse timing (Cuypers, Thijs et al. 2014). 26 MEPs were measured at each time point (104 MEPs per run in total) as for each TMS time point 4 pulses were pseudo-randomly omitted per run. For each trial (stimulus+baseline) we ensured a minimum of 3 TMS pulses of the 4 possible (P1, P2, RB and BL). Pulses were omitted in this way to minimise subjects becoming accustomed to a regular, predictable TMS delivery.

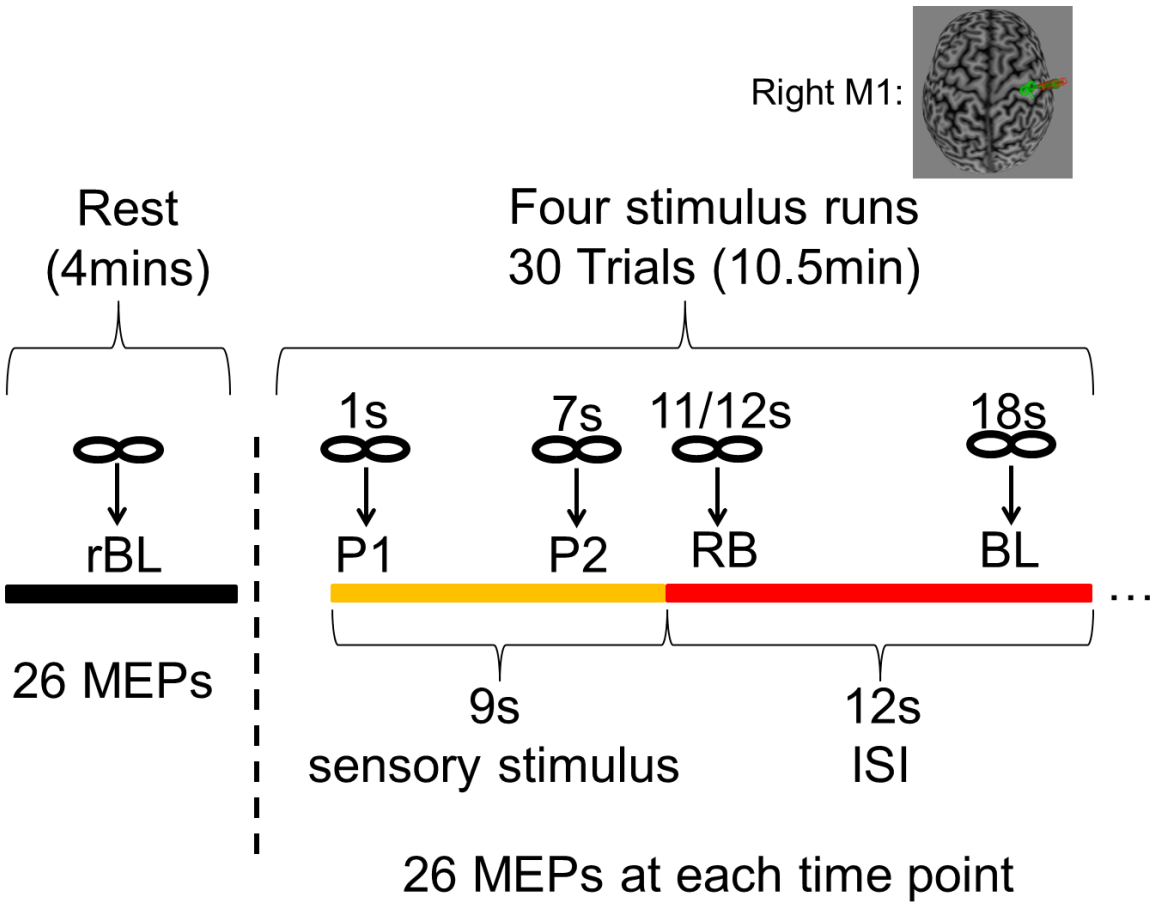

Figure 5.2. Session 2: TMS-EEG paradigm. All TMS pulses were applied to right M1. Each stimulus run was preceded by a pre-task baseline (rest), this consisted of 30 trials of 7s duration with a single TMS applied 6s into the trial, at random 4 of these trials contained no TMS pulse. Each of the 4 stimulus runs consisted of 30 trials of 9s stimulation (yellow bar) and 12s ISI (red bar). Pulses were randomly omitted (4 from each timing) across the run, with a minimum of 3 pulses per trial.

5.3.3 Session 1 – fMRI-MRS

fMRI data were acquired with a Philips Achieva 3T MR scanner (Philips Medical Systems, Best, Netherlands) using a 32 channel head coil.

For each subject, a whole-head T_1 anatomical image (1mm isotropic resolution) was acquired for co-registration of fMRI data, planning the MRS voxel location and neuronavigation during the EEG-TMS session. MRS was always acquired after the T_1 and prior to fMRI data acquisition to minimize signal drift that can be caused by the EPI sequence (Edden,

Oeltzschner et al. 2016). The MRS voxel (3x3x3cm) was centred manually over the subjects' left motor hand-knob region keeping the voxel in the brain, avoiding the skull, while minimizing the amount of CSF. At a later date a MRS voxel of the same dimensions was centred over the right motor hand-knob region in the same manner (ipsilateral to the Grip and MNS). This second voxel was used for acquisition of a GABA measurement in the region known to consistently show NBR to MNS and motor tasks (Mullinger, Mayhew et al. 2011, Mullinger, Mayhew et al. 2014) and which would be stimulated by TMS during the second session. A macro-molecule suppressed MEGA-PRESS sequence (TE=80ms) was used with 20ms editing pulse at 1.9ppm in ON scans and 1.5ppm in OFF scans (Edden, Puts et al. 2012, Edden, Oeltzschner et al. 2016). Whole-head fMRI data were recorded (gradient-echo EPI, 3x3x4mm voxels, TE = 35, TR = 2000ms, SENSE = 2.3, FOV = 80x80, slices = 29) during each of the four stimulus runs. The order of the stimulus runs was counterbalanced across subjects. Each run featured 30s of initial resting baseline fixation making a total of 8mins per run.

5.3.4 Session 2 – TMS-EEG

The same EEG system, set-up and acquisition was used as described in Chapter 2. Electrode positions were digitized using a Polhemus Isotrak to facilitate source analysis.

MEPs were measured from EMG (Delsys Inc) recorded from the left thumb first dorsal interosseous muscle (FDI) and recorded on a laptop running Signal V6.01 software (Cambridge Electronic Design). Matlab was used to interface with a power 1401 to automatically trigger the TMS pulses and simultaneously place markers as to the specific timing of the pulse in the EMG data.

After setting up the EEG cap on the subject, the motor-hotspot in the right M1 was located by finding the TMS coil position and stimulation intensity which evoked an MEP greater than 50μV peak to peak at the left thumb in 5 out of 10 pulses (Devanne, Cassim et al. 2006). A

Brainsight (Rogue Research) system, with coil and head trackers, was used with the subjects' T1 anatomical scan to guide localisation of their motor cortex and to ensure maintenance of both the position and angle of the TMS coil within close proximity of the motor hotspot (target) throughout the experiment. The stimulator sent a trigger to Brainsight on every TMS pulse which logged the time, TMS coil distance and angle which was used in post-processing to reject trials where subject's head movement resulted in distance > 3mm and coil orientation angle > 3^{O} from the hotspot.

Preceding every stimulation run a, "non-stimulus baseline" (Rest: rBL; see Figure 5.2) dataset was collected to assess initial resting-state cortical excitability and obtain a baseline MEP measure, independent of sensory stimulation conditions. This comprised of 30 TMS pulse "trials", of 7s duration, whilst subjects fixated on a centrally displayed fixation cross. In a randomly selected four of these trials TMS pulse were omitted, leaving 26 TMS pulses in total per rBL run.

For all EEG-TMS recordings, subjects were comfortably seated with their heads leant back against a head rest facing the stimulus display monitor, their hands rested on their lap relaxed.

5.3.5 Pre-processing and Analysis

fMRI

FSL 5.0.9 (FSL, http://www.fmrib.ox.ac.uk/fsl/) was used to implement the GLM, using a single boxcar regressor of stimulus timings, for analysis of all fMRI data. Prior to the GLM, the following pre-processing was carried out: automated brain extraction using BET (Smith 2002), motion correction using MCFLIRT (Jenkinson and Smith 2001, Jenkinson, Bannister et al. 2002), slice-timing correction, spatial smoothing using a Gaussian kernel (5 mm FWHM) and high-pass temporal filtering (> 0.01 Hz). FLIRT (Jenkinson and Smith 2001, Greve and Fischl 2009) was used to carry out registration of the subjects fMRI data to their T_1 image and the

MNI standard brain image. Clusters of statistically significant activation were threshold, using the bilateral motor mask as a pre-threshold mask, at z>2.3 and a significant cluster threshold of p<0.05 (corrected). At the group level whole brain analysis was carried out for each stimulus separately (z>2.3, cluster threshold of p<0.05, Fixed Effects) in order to assess the impact on the BOLD response in each sensory cortex (visual, auditory and motor) to each of the tasks.

MRS

MRS imaging data were imported into TARQUIN MRS quantification software (Wilson, Reynolds et al. 2011) from which GABA and Glx (glutamate + glutamine) water corrected levels were calculated. Subjects' anatomical T1 scans, those used to plan the MRS voxel, were segmented using FAST (Zhang, Brady et al. 2001) to provide fractional percentage of GM, WM and CSF. This was carried out in order to correct for differences in GABA levels of GM and WM across subjects (Jensen, Frederick Bde et al. 2005, Bhattacharyya, Phillips et al. 2011), whereby a GM/WM fraction was used as a regressor within linear regression analysis described in detail in Chapter 6.

TMS processing

MEP peak to peak amplitude (P2PA), (maximum value minus minimum value, measured between 0.02-0.05s post TMS pulse) and pre-MEP baseline P2PA (measured between 0.101-0.051s prior to the TMS pulse) were extracted from the EMG data for all pulses and all runs using scripts written in Signal software. These measures were imported into Matlab along with TMS coil location and orientation relative to the target motor-hotspot as extracted from BrainSight. MEPs were removed from further analysis if: the pre-MEP baseline P2PA was greater than 25μV, the orientation of the coil was greater than 3^{O} from that at the target and/or the distance of the coil from the target was greater than 3mm.

After removal of artefactual MEPs a high number of rBL MEPs still remained, across all subjects and runs (MNS: mean=25.82±0.53 MEPs; Motor: mean=25.65±0.79; Visual:

mean=25.65±1.00; Auditory: mean=25.53±1.70). We used a data driven approach to generate a cut-off of the number of MEPs required to provide a good estimate of the MEP P2PA for a single pulse timing condition in any run, known as the confidence interval (CI) approach (Cuypers, Thijs et al. 2014).

A 95% CI for each subject and each run was calculated based upon the mean of all rBL MEP P2PAs for that specific run. By also calculating a cumulative mean, each TMS pulse was assigned either a 1 or a 0 depending upon whether the MEP P2PA cumulative mean at each point was inside (1) or outside (0) of the 95% CI. Figure 5.3A&B show subject specific data related to one particular run, where the black dotted lines show the 95% CI boundary. A group level percentage could then be calculated showing the chance that each of the TMS pulses,1 to 26, sat within the 95% CI. As shown in Figure 5.3C, at 20 pulses, 100% of the data was within the 95% CI boundary, while at 16 pulses 95% of the data was within the 95% CI boundary, i.e. there was a 95% probability that the cumulative mean after 16 MEPs would be within the 95% CI of the mean of rBL MEPs for any run and any subject. Therefore, we took 16 MEPs as the number required to provide a reasonable measure of MEP P2PA for each pulse timing (P1, P2, RB11, RB12 and BL). Any run for which one of the pulse timings did not have 16 MEPs was removed from further ANOVA analysis, this led to subject 3 being removed from further P2PA analysis for the Motor condition, subject 6 for the MNS condition and subject 7 for the Visual condition. Also, subject 2 was completely removed from further analysis due to an error in acquisition of EMG data combined with a large number of noisy EEG channels, 10 in total.

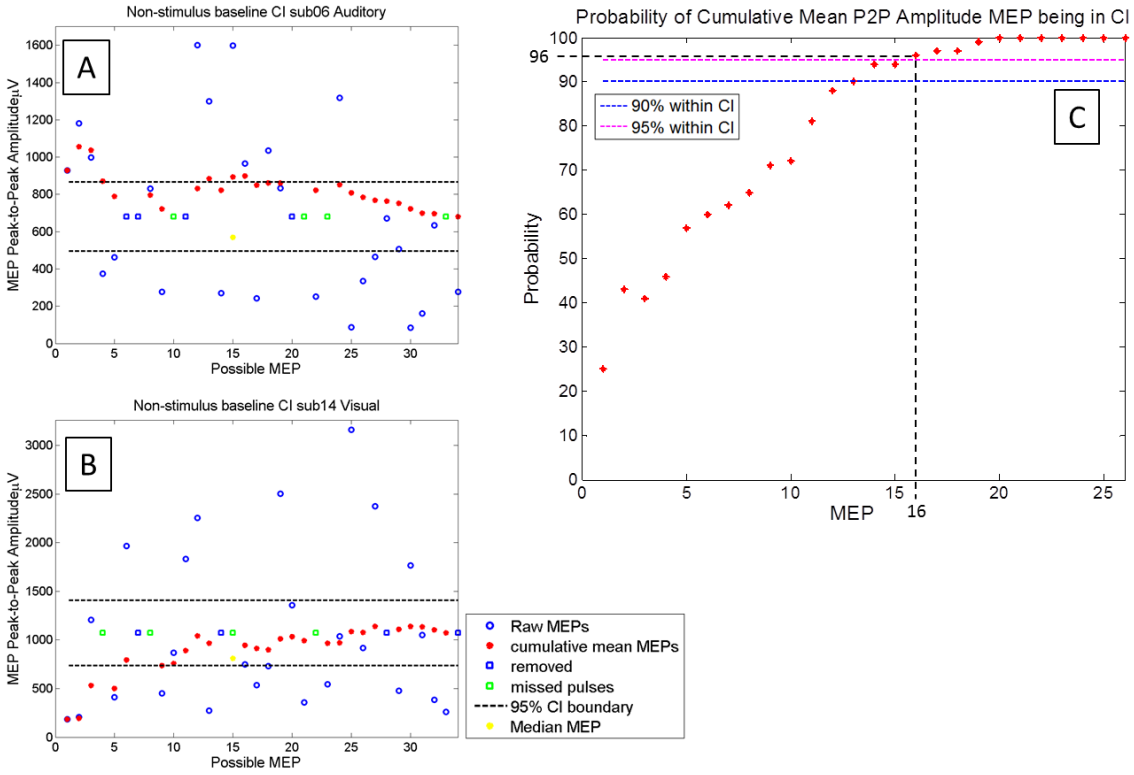

Figure 5.3. Confidence interval calculation. A and **B** show single subject confidence interval plots for subject 6 auditory run and subject 14 visual run respectively. The blue circles representing the raw resting baseline MEP P2PA data, the green squares are those TMS pulses pseudo randomly missed to reduce subjects becoming accustomed to the pulses. The blue squares are those TMS pulses removed due to TMS coil position being sub optimal or pre-MEP baseline being too high. The red circles show the cumulative mean, each of which is checked to see if it sits within the 95% confidence interval (black dotted lines). For completeness, the yellow circle shows the median MEP P2PA. **C** displays the probability of any of the TMS pulses sitting within the 95% confidence interval boundary across all subjects and runs. The 90 and 95% probability boundaries are shown (blue and pink line respectively). The dotted black line highlights the number of MEPs required in a resting baseline run to have over 95% probability that the mean MEP is within the 95% confidence interval of a mean of 26 MEPs.

Requiring 16 MEPs for a reliable estimate of MEP P2PA therefore prevents separate analysis of the two rebound periods where each have a maximum of 13 MEPs in each run. Therefore, we combined the two rebound measures (RB11 and RB12) into a single measure (RB) for subsequent repeated measure ANOVA analysis. Interestingly, taking a cut-off at 90% probability (13 MEPs) produced the same number of subjects for each condition, this being the maximum number of each RB (at 11 or 12 seconds). However, even at this more liberal cut-

off, taking RB11 and RB12 as separate time points would only leave 8 subjects in each condition for analysis therefore considerably reducing power.

MEP data were analysed in two ways, the first using a repeated measures ANOVA to test specifically for differences between median P2PA between the pulse timing conditions, and the second using a GLM based regression, using a template MEP, that is more sensitive for assessing differences between the timecourses of pulse timing conditions. Both methods are described in detail below.

P2PA differences: repeated measures ANOVA

The median absolute deviation (MAD) of P2PA was calculated for each rBL in turn, and used to normalise their respective stimulus MEPs P2PA (separately for P1, P2 RB and BL). Repeated measure ANOVAs were then used to assess any differences in the median P2PA between the pulse timings: P1, P2, RB and BL for each run separately (MNS, Motor, Visual and Auditory). This analysis produces an overall F-test of significance between pulse timing P2PA and individual tests of significance between each of the timing condition P2PAs.

MEP timecourse GLM analysis

Previously, it has been shown that contraction of the muscle, from which EMG is being measured, results in increased MEP P2PA (Thickbroom, Byrnes et al. 1999). TMS coil position is also known to lead to inevitable changes in P2PA measured, where deviation from the optimal position would produce a smaller MEP P2PA. Using a regression analysis offers the potential to fit and measure this timecourse variability and then contrasts between the pulse timing conditions can be calculated within and across subjects, and trial-by-trial variability in the MEP timecourse can be assessed to see how they covary with pre-MEP EMG BL, α/β EEG power/phase and coil position. Here we used a regression analysis approach analogous to GLM of fMRI data whereby a template MEP was created based upon the subject's average

rBL and used as a regressor against the rest of that subjects' single trial MEP timecourse data, explained in greater detail below.

To our knowledge, no previous research has attempted to use regression analysis in this way for MEP data, although such GLM analysis has been used previously to assess EEG event related potentials (ERPs) (Mayhew, Iannetti et al. 2006). For the regression analysis, the MEP timecourses (30ms from TMS pulse onset) were extracted from Signal (see Figure 5.4A&B for average stimulus and rBL example data). The stimulus-run MEP timecourses from all four pulse timing conditions were temporally concatenated into a single timecourse, whereby all P1 MEPs were followed by all P2, all RB and lastly all BL (see Figure 5.4Ci for example data). As the shape of the mean rBL MEP was consistent across rBL runs (see Figure 5.4B example data), the average rBL MEP was used as the template timecourse. For each subject, a design matrix was formed for each run from four regressors one for each of the four pulse timing conditions: P1, P2, RB and BL, to allow separate estimation of each condition's effects and contrasts to be made between them. The contrast between pulse timings provides a method of testing for significant differences between them, analogous to the test of significance between timings using the ANOVA approach. Each regressor was formed by concatenating as many template MEPs as there were single-trial MEPs in each condition of each run (see Figure 5.4Cii for example regressors). The main difference between the ANOVA approach and the regression approach is in the ability to assess trial-by-trial variability when using regression. The MEPs are known to have a large degree of variability (Kiers, Cros et al. 1993, Thickbroom, Byrnes et al. 1999), which is also evident in Figure 5.4C, and accounting for this is important in order to be able to best interpret results gained from TMS studies.

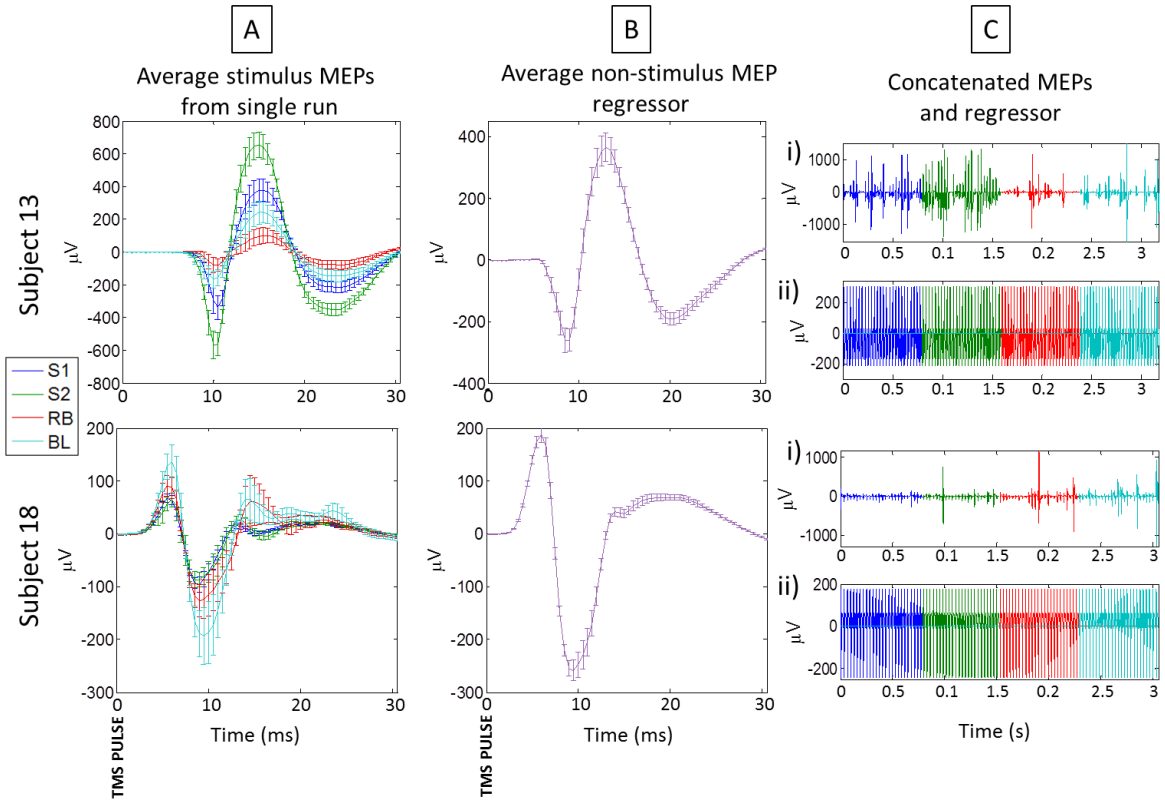

Figure 5.4. MEP regression pre-process. **A** shows are two subjects (subjects 13 and 18) mean stimulus run MEP data for each pulse timing condition : P1 (blue), P2 (green), RB (red) and BL (cyan), from a single run, where error bars are standard error. **B** shows each of the subjects mean resting baseline MEP, which shows a consistent pattern across all 4 resting baseline recordings (as denoted by the error bars, standard error. The resting baseline for each subject is also seen to have a similar timecourse to those of the stimulus run pulse timings. **Ci** for both subjects shows all MEP data concatenated together for the same run. **Cii** shows the mean resting baseline concatenated to create a timecourse regressor for each of the pulse timing conditions. **Ci&ii** were then ready to be used in the regression analysis.

FSL 5.0.9 was used to perform the regression analysis. To enable this, input data had to be set up to mimic 4D fMRI data. Therefore, a square matrix consisting of 6x6x6 “voxels” was set up with the same voxel (2, 2, 2) always containing the MEP timecourse and all others containing noise (created using the rand function in Matlab). Matlab and shell scripts were developed to use the FSL function fsl_glm in order to calculate, for each subject and each run, the fit of the rBL regressors to the MEPs from each pulse timing condition (P1, P2, RB and BL). For each run a corrected voxel threshold of $p<0.001$ was used with contrasts taken to

calculate comparisons between the fits of all possible pairs of conditions. FEAT was then used to calculate the group level Z-statistic of the main effect of each condition and the contrasts between conditions (Fixed effects: corrected voxel threshold $p<0.001$). Analogous to an fMRI GLM, this analysis reflects both the fit of the stimulus MEPs shape and the size of the stimulus MEPs in relation to the average rBL MEP regressor, therefore taking into account the whole MEP timecourse (consisting of a latency, peak and trough and return to baseline). Here, if one pulse timing (e.g. P1) had a significantly larger parameter estimate value than another (e.g. than BL) it would reflect that the P1 MEPs were a combination of being more similar in shape to the rBL regressor and larger in size than the BL MEPs (while taking into account the variability of the data as well). This is potentially more sensitive to detect differences in MEPs between conditions when compared to the repeated measures ANOVA approach which takes only one aspect of the MEP, the P2PA, into account.

In this chapter, the same data used for the ANOVA analysis were also used in the regression analysis (i.e. the same data exclusion criteria were employed as described above). In this manner the results from both techniques can be compared. The ultimate goal being to incorporate additional experimental measures into the analysis, e.g. the EEG data (α/β power and phase prior to the TMS pulse), TMS position measurement (orientation and distance from the target of the TMS coil) and pre-MEP EMG baseline as parametric modulators to see whether they could explain any of the MEP variability for each condition; an analysis explored in the following chapter.

EEG

All EEG data were imported into Brain Vision Analyser 2 and noisy channels removed by visual inspection. The data was then exported to EEGlab and a robust method of TMS artefact removal employed via Matlab scripts. The main ringing TMS artefacts were interpolated out of the data (-2ms to 18ms from the TMS pulse) (Herring, Thut et al. 2015), see example data in

Figure 5.5A. All data were epoched, 0 to 21s for stimulus run data and 0 to 7s for rBL data, and noisy trials removed. All four rBL runs were then temporally concatenated and runICA was performed in EEGlab. This method was employed to provide a large sample of data for capturing artefacts related to eye blinks and remaining TMS artefacts at the 5000Hz sampling rate, subsequently the ICA components deemed artefacts (see Figure 5.5B for examples) were removed from all non-stimulus baseline data separately and then these rBL ICA weights were used to remove these components from the stimulus run data as well. In this way, sufficient data were available for ICA from the rBL and the TMS artefacts could be estimated from the baseline data without any possible contamination of stimulus presentation. Any remaining cranial artefact was interpolated out (~8ms) (Herring, Thut et al. 2015) of each timecourse before the data was downsampled to 600Hz, band-pass filtered (0.5 -80Hz) and a notch filter at 50Hz applied (specifically to remove electrical noise). All data were then exported to the Fieldtrip open source toolbox (http://www.ru.nl/fcdonders/fieldtrip) and filtered into separate α (7-13Hz), β (13-35Hz), frequency datasets for beamformer analysis.

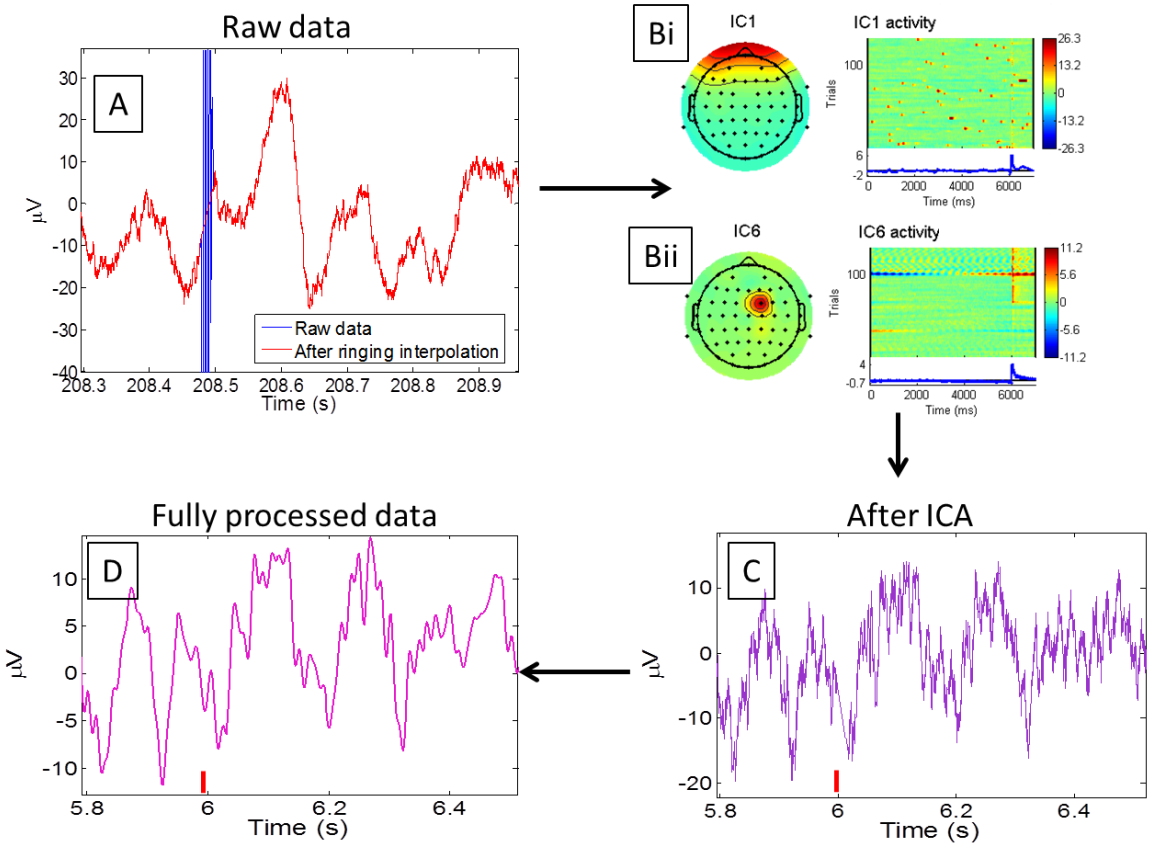

Figure 5.5. EEG artefact removal. A single example of the removal of TMS artefacts from EEG data. **A** shows 0.6s of raw unprocessed EEG data (blue line) from a single channel 0.2s prior to and 0.4s after a single TMS pulse. The red line shows the data after removal and interpolation of the main TMS ringing artefact. **B** shows two examples of ICA components which were removed from this particular subjects data. The timescale (x axis) of the plots is representative of the resting baseline data (from which the ICA components were calculated), 0 to 7000ms, in which the TMS pulse was applied after 6000ms, while the y axis represents the trials. **Bi** represents eye blinks which can be seen throughout the timecourse of the data, at varying times in most trials, while a distinctive eye blink can be seen immediately after the TMS pulse (6000ms). The topographical plot also shows the frontal element of the ICA component related to the eye blinks. **Bii** shows an ICA component relating to the exponential decay from muscle artefact, seen predominantly after the TMS pulse and located at an electrode close to the stimulation region. **C** shows the same section and duration of data after ICA component removal (the data at this point having been epoched). The red bar showing the time of TMS pulse. **D** shows the same section of data after pre-processing, showing that little of the artefact remains.

A linearly constrained minimum variance (LCMV) beamformer was implemented in Fieldtrip as described in Chapter 2. Weights were calculated using all data (concatenated rBL and stimulus data) least likely to still be contaminated with TMS artefacts, 0.5seconds after a TMS pulse and 0.1 second prior to a TMS pulse: rBL data: 0.5 to 5.9s; stimulus data, 0.5 to 0.9s, 1.5 to 6.9s, 7.5 to 10.9s, 11.5 to 11.9s, 12.5 to 17.9s. Doing so allowed for the calculated beamformed data to be used to extract virtual electrode measures of neural activity during any of these time points (i.e. to ascertain the α/β power immediately prior to any TMS pulse). An active window of 1.5-6.9s and a passive window (stimulus baseline) of 12.5-17.9s relative to stimulus onset were used to localise changes in EEG power for each stimulus and frequency band.

IM Virtual electrode (VE) timecourses were extracted from the peak ERD in each IM cortex to each stimulus: the visual cortex peak α power ERD to visual stimuli used to define the visual VE; the auditory cortex peak α power ERD to auditory stimuli used to define the auditory IM VE; the contralateral motor cortex peak β power ERD to MNS used to define the MNS VE; and the contralateral motor cortex peak β power ERD to the motor task used to define the motor task VE. Both α and β data were then extracted from these IM VEs. A TMS mask, definition described below, was used to mask the EEG data and extract a TMS VE. First, a mean power change was taken across the whole mask and if the mean was greater than 0 the data VE was defined as ERS and the peak ERS β power taken as the TMS VE, if the mean was less than 0 the data was defined as ERD and the peak ERD β power in the mask taken as the TMS VE. Data were extracted from the VEs and for each stimulus and Hilbert transformed to calculate the power envelope.

The rBL data between 0.5 and 5.9s post TMS pulse was also beamformed to obtain subject specific α and β power VE timecourses. This allowed for direct comparison between the average baseline of the stimulus runs, and what could be viewed as an alternative definition of

baseline neural activity in the rBL runs, to test how closely the activity during "rest" between sensory stimuli resembles activity during resting-state fixation. In order to calculate whether any significant difference was observed between the stimulus baseline and rBL, the average stimulus baseline power was subtracted from the average rBL power for each subject and each of the runs: e.g. the MNS average baseline subtracted from the rBL prior to MNS etc. For each subject and each run, a one sample t-test was then performed to assess whether the rBL differed significantly from zero across subjects for each of the stimuli. In addition, for each subject the average corrected α and also separately β rBL across stimuli was calculated, and a one sample t-test used to calculate any significant difference across subjects for α or β.

fMRI masks

For regional description of fMRI data, MNI space masks of right and left motor cortex (postcentral gyrus and precentral gyrus); bilateral visual cortex (Lateral Occipital Cortex, superior and inferior, Occipital Pole, Occipital Fusiform gyrus, Intracalcarine Cortex, Lingual gyrus and the Supracalcarine cortex) and bilateral auditory cortex (Heschl's gyrus, Planum Temporale, Planum Polare, anterior Superior Temporal Gyrus, posterior Superior Temporal Gyrus) were created using the Harvard-Oxford Cortical Structural Atlas (threshold at 25% probability), see Figure 5.6A.

Two further masks were formed to allow extraction of the right M1 NBR timecourse for future correlation with MEPs and also MRS measures of GABA concentration from that region. The MRS voxel was used as one subject-specific mask. A TMS mask was also created by converting the location of the TMS hotspot (from Brainsight) from T1 anatomical into MNI coordinates and using that as the centre of a spherical mask of 10 voxel radius (2x2x2mm). This TMS mask was constrained to only include voxels within the MNI brain. Both these right MRS and TMS masks were transformed to each of the runs fMRI data for BOLD timecourse extraction and future comparison with MEP data. For extraction of BOLD data from the masks,

a spherical ROI of 3 voxel diameter was used, centred upon the peak response of interest (PBR/NBR) within the mask of interest.

Within subject space the MRS mask contained an average 1233voxels±59, while the TMS mask contained an average of 776voexls±84. The TMS mask was also registered with subject's beamformed EEG data for extraction of α/β power for future comparison with the MEP data.

For the TMS mask, a radius of 10 voxels was used due to the probability of the TMS pulse attenuating ~1.9cm into the brain (Deng, Lisanby et al. 2013) and each voxel being (2x2x2). The electrical field is not focal but spreads outwards (Deng, Lisanby et al. 2013), this coupled with the potential of maximum 6mm measurement error in TMS coil position (i.e. a tolerance of 3mm during neuronavigation anatomical to subject registration and 3mm of TMS coil to target during stimulation) suggests that the size of the TMS mask is appropriate.

5.4 Results

5.4.1 fMRI

		Mask								
		Motor (17374 voxels)			**Visual (31091 voxels)**			**Auditory (713 voxels)**		
		Max	x, y, z	%	Max	x, y, z	%	Max	x, y, z	%
MNS	PBR	**30.6**	**71,51,64**	**33.1**	**7.3**	**35,35,29**	**0.06**	**17.3**	**71,54,42**	**23.3**
	NBR	**19.6**	**44,47,69**	**48.7**	**14.0**	**53,20,53**	**89.0**	**11.0**	**13,56,36**	**49.1**
Motor	PBR	**37.7**	**65,52,64**	**59.8**	**34.3**	**38,17,33**	**61.4**	**14.8**	**71,54,42**	**36.1**
	NBR	**10.5**	**21,52,67**	**12.8**	**5.1**	**65,23,54**	**5.6**	-	-	-
Visual	PBR	**17.0**	**22,66,51**	**22.7**	**47**	**49,23,35**	**81.9**	**5.1**	**17,45,45**	**1.3**
	NBR	**7.2**	**14,61,44**	**17.5**	**9.7**	**67,25,54**	**8.2**	**8.5**	**14,55,35**	**67.6**
Auditory	PBR	**23.4**	**12,57,42**	**3.8**	**5.8**	**57,14,33**	**4.9**	**37.7**	**70,52,40**	**90.3**
	NBR	**7.4**	**73,54,57**	**56.6**	**6.4**	**23,25,40**	**33.2**	-	-	-

Table 5.1. Main effect group GLM result summary. The PBR and NBR Max (maximum Z stat), % (percentage of voxels within each mask) and x,y,z (coordinate position) are shown for each of the stimuli in each of three masks: Auditory cortex, Visual cortex and Motor cortex. The number of MNI? voxels within each of the masks is shown in brackets next to the mask name. All stimuli elicited IM PBR as well as CM NBR in at least one other cortex.

Group fMRI responses

For all stimuli, both main effect PBRs as well as IM and CM NBRs were observed (Figure 5.6). IM PBRs were found in primary sensory cortex for all stimuli, bilaterally for visual and auditory and in contralateral S1/M1 for motor and MNS. The lateralisation of the motor stimulus and the MNS also induced IM NBRs ipsilaterally in S1/M1. NBRs were elicited in central and right motor cortex regions by all stimuli, although the spatial extent and location varied considerably

between stimuli. Furthermore, stimuli produced CM NBRs in at least one sensory cortex as outlined in detail below.

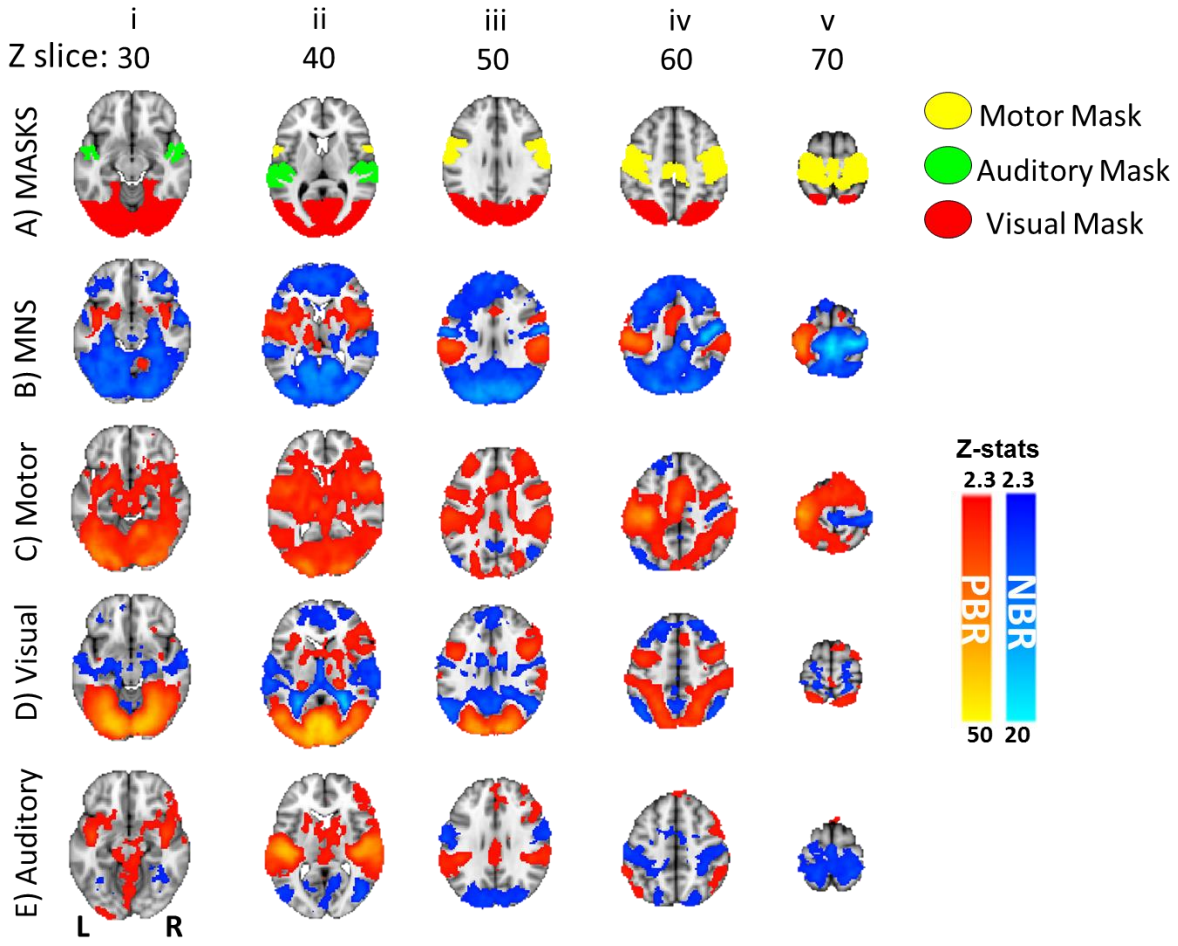

Figure 5.6. Sensory cortex masks and BOLD response to each stimulus. A shows the location of the masks used to compare statistics of BOLD response to the stimuli (yellow=motor cortex, green=auditory cortex, red=visual cortex masks). **B – E** show the group level fixed effects BOLD response to MNS, motor task, visual and auditory stimuli respectively. **i-vi** show the axial slice in MNI space of each of the stimuli, 30 – 70 respectively. Red=PBR, Blue=NBR

MNS

The MNS induced an IM PBR in bilateral SMA, and bilateral secondary sensorimotor cortex (SII) with the peak response in contralateral S1/M1 (Figure 5.6Biii-v). PBRs were also located

in bilateral insula (Figure 5.6Bi-ii), right cerebellum (Figure 5.6Bi), and subcortical regions: bilateral putamen and left thalamus (Figure 5.6Bii).

The NBR to the MNS was extensive throughout the brain with the peak IM NBR located in ipsilateral S1/M1 (see Table 5.1 and Figure 5.6Biv-v). CM NBRs were found in the visual and auditory cortices. NBRs were also located in the DMN: medial prefrontal cortex (mPFC), medial temporal lobes, intra parietal cortex (IPL) and precuneus/posterior cingulate cortex (PCC) (Figure 5.6Bii-v).

Motor

Similar to the MNS, IM PBRs to the Motor task were found in bilateral SMA, bilateral secondary motor cortex with the peak response in contralateral M1 (see Figure 5.6Ciii-v); with a greater magnitude and extent than for MNS (Table 5.1). The motor task also induced PBRs bilaterally in the visual cortex (see Figure 5.6Ci-ii & Table 5.1), as well as PBRs in parietal cortex (Figure 5.6Civ), saliency network (Figure 5.6Ci-iii), and also subcortical regions: bilateral Putamen and Thalamus (Figure 5.6Cii).

IM NBR was located in ipsilateral M1 (see Table 5.1 & Figure 5.6Civ) as well as a central premotor cortex region (Figure 5.6Cv). The IM NBR was lesser in extent and magnitude than for MNS despite the motor task eliciting greater IM PBR (Table 5.1). NBRs were also located in the PCC and bilateral IPL DMN regions (see Figure 5.6Aiii) while no auditory CM NBR was found.

Visual

IM PBR was found bilaterally in the visual cortex to the visual stimulus, with the peak response in central V1 (Figure 5.6Di-iii, Table 5.1), with PBRs also noted in the pre-motor cortex (Table 5.1 & Figure 5.6Di-v) and the superior parietal cortex (Figure 5.6Div). PBRs were also found in subcortical regions: bilateral caudate, putamen, insular and thalamus (See Figure 5.6Dii).

NBR was also evoked in the mPFC, the PCC and bilaterally in the IPL DMN regions (Table 5.1 & Figure 5.6Diii-iv). CM NBRs were located bilaterally in the auditory (Table 5.1 & Figure 5.6Dii) and motor cortices (Table 5.1 & Figure 5.6Dv). NBRs were also widely observed in the ventricles (Figure 5.6Dii). Such ventricular NBRs are thought to overlap with large veins found downstream of stimulus induced increases in neuronal activity and mainly be driven by increases in CBV (Bianciardi, Fukunaga et al. 2011).

Auditory

The auditory stimulus evoked IM PBR bilaterally in the whole auditory cortex (Table 5.1 & Figure 5.6E), with regions of PBR also found in the border between posterior motor cortex and parietal cortex (Table 5.1 & Figure 5.6Ei&iii). PBRs to the auditory stimuli were also found in subcortical regions, in particular in bilateral putamen and thalamus (Figure 5.6Eii).

Although no IM NBR was found to the auditory stimulus, CM NBRs were found bilaterally in the visual cortex (Table 5.1 & Figure 5.6Ei-iv), specifically in bilateral anterior V1 (Figure 5.6Eii) and bilateral LOC (Figure 5.6Eii&iv). CM NBRs were also seen bilaterally in the motor cortex (Table 5.1 & Figure 5.6Eiii-v), in particular bilateral S1 and the SMA (Figure 5.6Eiv) as well as bilateral superior M1 (Figure 5.6Ev). NBRs were also found bilaterally in superior parietal cortex regions that resembled the dorsal attention network (Figure 5.6Eiv), in direct contrast to the PBR found in that region to visual stimuli. Also in contrast to the other three tasks, no DMN NBR was observed to auditory stimuli.

BOLD mask comparison

The three masks (right motor cortex mask, TMS mask and MRS voxel mask) used to measure NBRs within the right motor cortex were compared here to ascertain their similarity and utility for further analysis.

MNS

Overall 17 subjects showed a peak IM NBR voxel in the right motor mask. Of the 15 subjects with a right hemisphere MRS mask, 15 showed a peak IM NBR voxel in the right motor mask, for 11 that peak was located in the MRS mask, for 10 it was located in the TMS mask and for 8 it lay in both (see Figure 5.7Ai). Only 1 subject had motor cortex peak IM NBR voxels outside both the TMS and MRS masks (see Figure5.7Ai). All masks showed a similar proportion of voxels with NBR (see Figure 5.7Aii), with mean mask coverage: right motor mask= 34.71±14.17; TMS/MRS overlap mask=39.73±18.84; MRS mask=31.22±12.28; TMS mask=33.96±16.49.

Motor

Overall 13 subjects showed a peak IM NBR voxel in the right motor mask. Of the 15 subjects with a right hemisphere MRS mask, 12 showed a peak IM NBR voxel in the right motor mask, for 9 that peak was located in the MRS mask, for 8 it was located in the TMS mask and for 7 it lay in both (see Figure 5.7Bi). Only 2 subjects had motor cortex peak IM NBR voxels outside both the TMS and MRS masks (see Figure 5.7Bi). All masks showed a similar proportion of voxels with NBR (see Figure 5.7Bii), although lower than for MNS, with mean mask coverage: right motor mask=13.16±15.59; TMS/MRS overlap mask=20.98±21.92; MRS mask=15.08±15.42; TMS mask=15.11±18.60.

Visual

Overall 17 subjects showed a peak IM NBR voxel in the right motor mask. Of the 15 subjects with a right hemisphere MRS mask, 14 showed a peak CM NBR voxel in the right motor mask, for 3 that peak was located in the MRS mask, for 2 it was located in the TMS mask and for 2 it lay in both (see Figure 5.7Ci) demonstrating that the spatial location of this CM NBR was inconsistent across subjects and explaining that the GLM main effect looked weak due to lack

of overlap across the group (Figure 5.7Dv). Eleven subjects had motor cortex peak CM NBR voxels outside both the TMS and MRS masks (see Figure 5.7Ci). All masks showed a similar proportion of voxels with NBR (see Figure 5.7Cii), although lower than was seen to the MNS or motor task, with mean mask coverage: right motor mask=6.71±6.77; TMS/MRS overlap mask=7.06±9.50; MRS mask=5.62±6.06; TMS mask=4.63±5.63.

Auditory

Overall 13 subjects showed a peak IM NBR voxel in the right motor mask. Of the 15 subjects with a right hemisphere MRS mask, 10 showed a peak CM NBR voxel in the right motor mask, for 4 that peak was located in the MRS mask, for 3 it was located in the TMS mask and for 4 it lay in both (see Figure 5.7Di). Five subjects had motor cortex peak CM NBR voxels outside both the TMS and MRS masks (see Figure 5.7Di). Across subjects the masks showed variable proportion of voxels with NBR (see Figure 5.7Dii): right motor mask=13.03±17.37; TMS/MRS overlap mask=17.36±23.84; MRS mask=12.53±16.57; TMS mask=16.28±22.51.

In summary, these data highlight that the IM NBRs for MNS and motor tasks were more often similarly captured by all three of the masks than the CM NBRs that were evoked by the visual and auditory tasks. Therefore, CM NBR showed greater spatial variability and were more sensitive to mask choice.

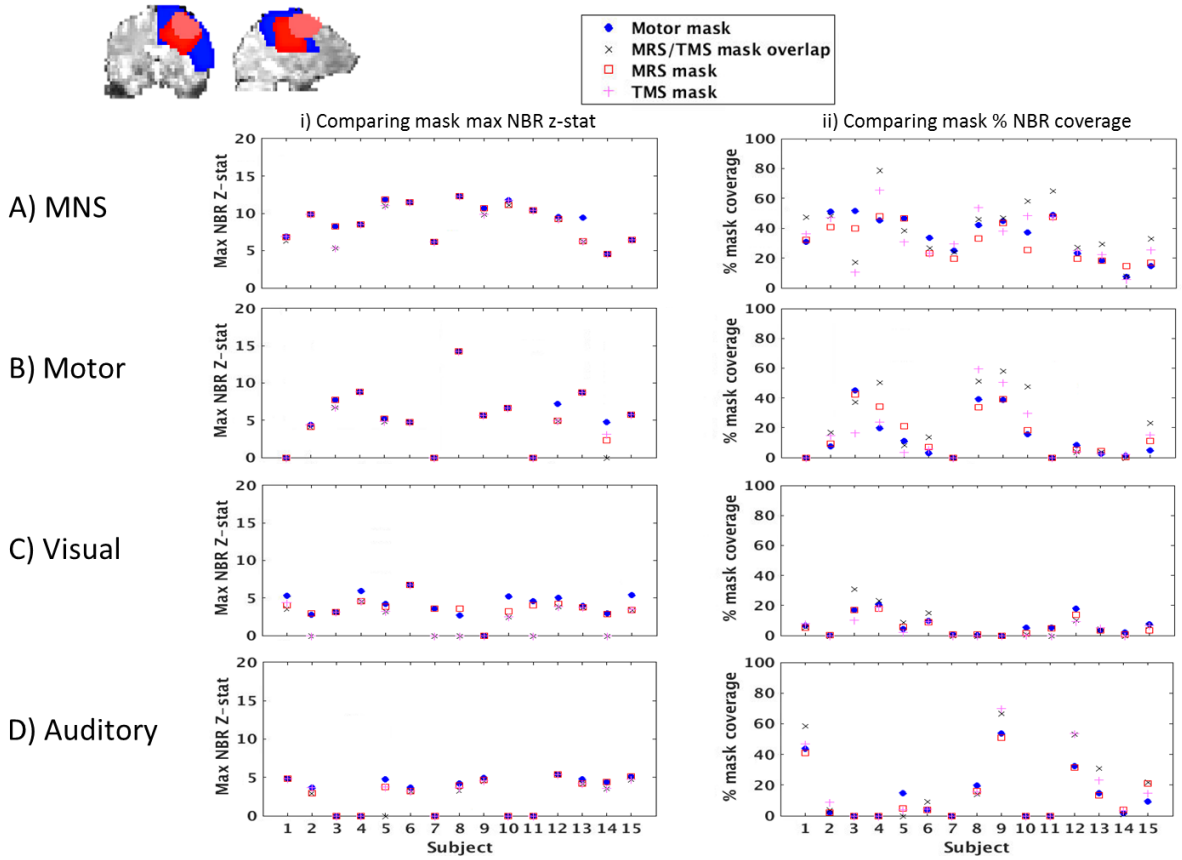

Figure 5.7. Comparison of 3 right hemisphere masks ability to capture subject NBR to stimuli. Ai-Di show the MNS, motor task, visual and auditory stimuli maximum peak z-statistic for each subject (those with a right hemisphere MRS mask) within the right hemisphere motor mask (blue circle), MRS mask (red square), TMS mask (pink plus sign) and the overlap between the MRS mask and the TMS mask (black cross). Examples of the right hemisphere motor cortex mask (blue), MRS mask (red) and TMS mask (pink) are shown within a single subjects data (subject 7) in the top left corner. **Aii-Dii** show the percentage of NBR coverage within each of the masks.

5.4.2 MRS

No correlation was found between GABA level and percentage of GM (right hemisphere: r=0.08, p=0.79; left hemisphere: r=0.09, p=0.75), WM (right: r=0.15, p=0.59; left: r=-0.05, p=0.86) or CSF (Right: r=0.04, p=0.89; left: r=-0.36, p=0.19) within the MRS voxel.

Significant positive correlations were found between the right and left hemisphere levels of GABA (**r=0.55, p<0.05**) and Glx (**r=0.59, p<0.05).** 14 of the 15 subjects showed greater levels

of GABA in the right hemisphere (right-left GABA: mean=0.54±0.33; which is the opposite to that previously found (Oeltzschner, Hoogenboom et al. 2014)) and 12/15 showed larger Glx levels in the right hemisphere than the left (right-left Glx: mean=0.55+0.56). No significant correlations were noted between the levels of GABA and Glx for either the right (r=0.44, p=0.10) or left (r=-0.41, p=0.13) hemispheres. Right hemisphere GABA was not found to correlate with left hemisphere Glx (r=-0.06, p=0.10), similarly right hemisphere Glx was not found to correlate with left hemisphere GABA (r=-0.03, p=0.91).

Motor Evoked Potentials

During the analysis we noticed a discrepancy when using the average rest MEP to form the regressor for GLM based analysis of MEP data. Figure 5.8 shows the regressors and residuals of the linear fit for six representative subjects, ranging in how similar their rest MEP and stimulus MEPs waveforms were. We found that the waveform of the rBL MEP was not consistently, for each subject, comparable to that of the average stimulus MEP (across P1, P2, RB and BL). Using the rBL as a regressor in this manner therefore led to large residuals, due in part to the inability to adequately model the shape of the MEPs. Although even those subjects whose rest MEPs were highly similar to their stimulus MEPs were found to have large residuals (see Figure 5.8iii). Therefore, the average stimulus MEP for each single subject was used as the regressor for that subjects stimulus run data, which was found to reduce the residuals (Figure 5.8iii). As an example, calculating the percentage difference between residual sum of the squares (RSS) for MNS, average stimulus/average rest, regressor shows an average reduction across subjects of 6.36%±10.16%. An attempt to explain the remaining MEP residuals using the covariates of: EEG power, EEG phase, TMS coil distance, TMS coil orientation and EMG pre-MEP BL is described in the following chapter. The following regression results are taken from the results when using the average stimulus MEP as the regressor, where Figure 5.9Ai-Ci show plots of normalised mean P2PA at P1, P2, RB and BL for MNS, motor task, visual and auditory stimuli respectively.

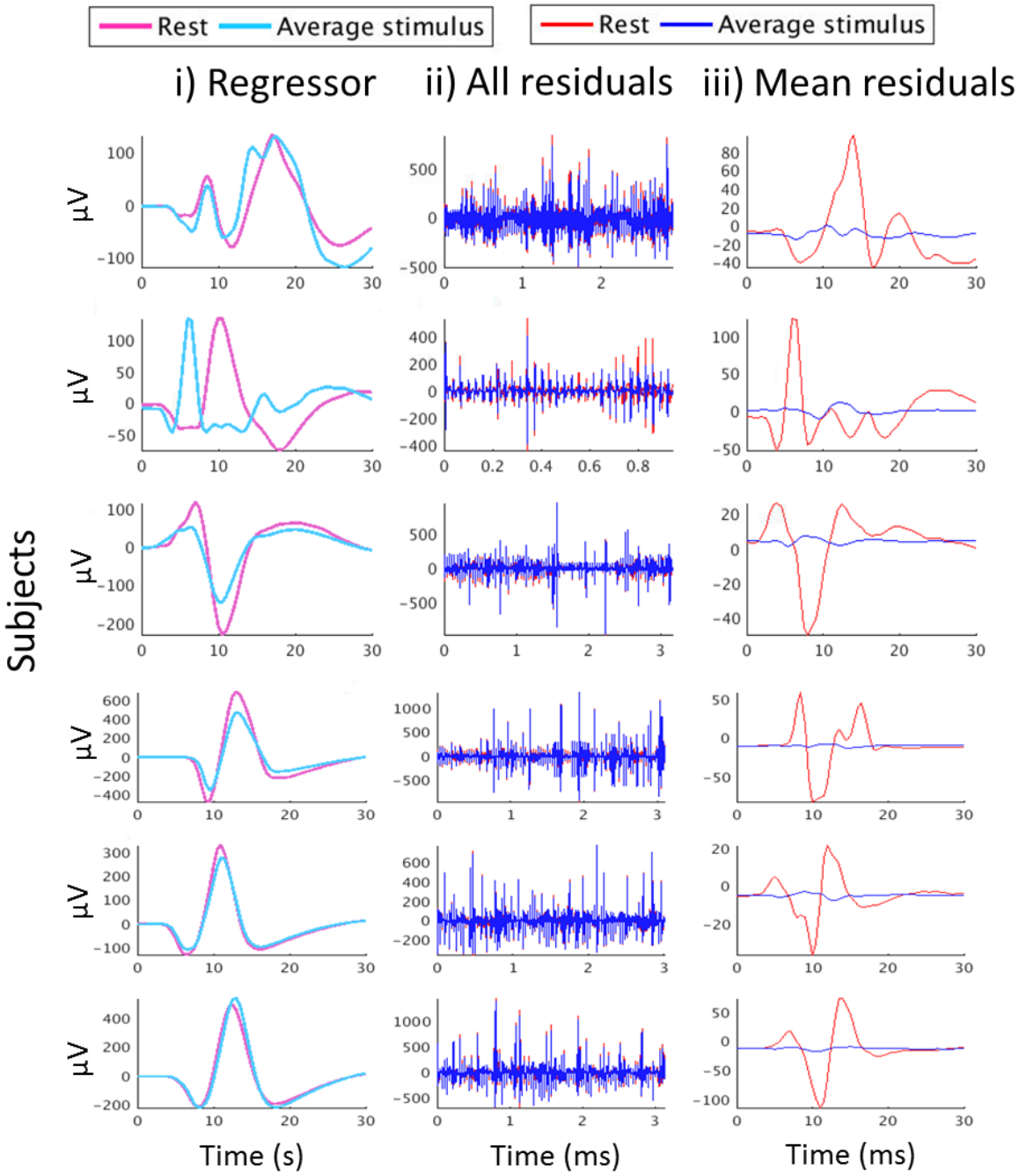

Figure 5.8. TMS GLM analysis: comparison between residuals when using the average rest MEP and average stimulus MEP as regressors. Data from 6 subjects are shown. i) shows the rest (magenta) and average stimulus (blue) regressors plotted together – note the large difference in the timing of the positive peak for subject 6 between the two regressors. ii) displays the residuals of the entire timecourse when using the average rest MEP (red) and the average stimulus MEP regressor (blue) overlaid. iii) shows the mean of the residuals when using the two regressors (red: rest, blue:stimulus). The average rest MEP regressor show consistently larger mean residuals than when using the average stimulus MEP as a regressor.

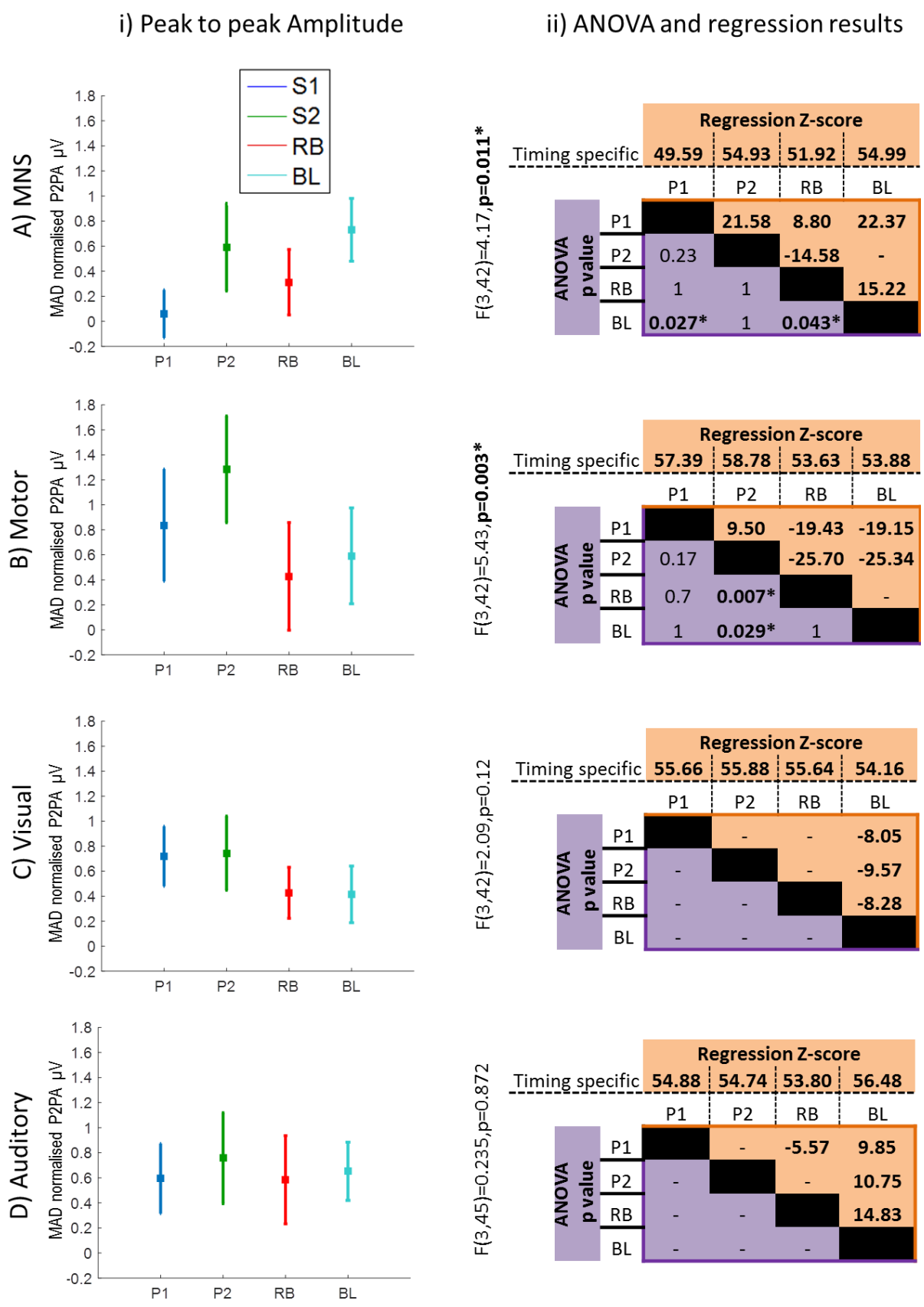
i) Peak to peak Amplitude
ii) ANOVA and regression results
A) MNS
B) Motor
C) Visual
D) Auditory
MAD normalised P2PA µV
S1
S2
RB
BL
P1
P2
RB
BL
F(3,42)=4.17,p=0.011*
F(3,42)=5.43,p=0.003*
F(3,42)=2.09,p=0.12
F(3,45)=0.235,p=0.872
Regression Z-score
Timing specific
49.59 54.93 51.92 54.99
ANOVA p value
P1 21.58 8.80 22.37
P2 0.23 -14.58 -
RB 1 1 15.22
BL 0.027* 1 0.043*
57.39 58.78 53.63 53.88
P1 9.50 -19.43 -19.15
P2 0.17 -25.70 -25.34
RB 0.7 0.007* -
BL 1 0.029* 1
55.66 55.88 55.64 54.16
P1 - - -8.05
P2 - - -9.57
RB - - -8.28
BL - - -
54.88 54.74 53.80 56.48
P1 - -5.57 9.85
P2 - - 10.75
RB - - 14.83
BL - - -

Figure 5.9. MEP analysis comparison. Ai-Di show the MNS, motor task, visual and auditory stimuli median peak to peak amplitude across subjects (MAD normalised to the resting baseline MEPs) for each pulse timing condition (P1:blue; P2:green; RB: red; and BL: cyan), error bars denote standard error. Here, the closer the value to zero, the more similar the median P2PA for that pulse timing condition is to the resting baseline MEPs. **Aii-Dii** show the results of the repeated measures ANOVAs (purple) and the regression analysis (orange). For the ANOVA results: the F-test for each of the modalities ANOVAs is shown along with the p-values (Bonferroni corrected) relating to the contrast between each contrast where the F-test is met (the direction of the significant contrast scan be seen by those differences shown in the peak-to-peak amplitude figures **Ai-Di**). For the regression analysis: the z-score from the analysis is shown, for each pulse timing condition separately (displayed as timing specific in the table). The z-score for each contrast (which was found to be significant at Fixed effects corrected voxel threshold <0.001). Contrasts are displayed here as the column pulse timing- row pulse timing therefore positive values show that the column timing is larger than the row timing. Although z-scores are by definition directionless, here a negative score is used to show that the row pulse timing is larger than that of the column pulse timing.

MNS

Using repeated measure ANOVA, significant differences in P2PA were found between time points, $F(3,42)=4.17$, $p<0.05$ showing that the presence of MNS modulated the MEP. With BL found to have significantly larger P2PA than either P1 ($p<0.05$) or RB ($p<0.05$), see Figure 5.9Aii (purple) for all p values. This suggests that the CSE, as measured by P2PA, decreased from that of the stimulus baseline during MNS but only at the start of the stimulus (1s) and not after sustained MNS (at 7s). It also suggests that the RB P2PA was significantly lower than the stimulus baseline.

Using the regression analysis, the average stimulus MEP was found to be a significant predictor of P1 ($Z=49.59$), P2 ($Z=54.93$), RB ($Z=51.92$) and BL ($Z=54.99$) MEPs (see Figure 5.9Aii, orange).

The GLM contrasts between timepoints at the group level (see Figure 5.9Aii, orange) showed that P2 was significantly larger than P1 ($Z=21.58$), something that was not found through the traditional ANOVA P2PA analysis. The fit of BL was also found to be significantly larger than

P1 and RB: BL>P1, Z=22.37; BL>RB, Z=15.22. This matches that found using the repeated measure ANOVA. The RB was also found to be larger than P1 and smaller than P2: RB>P1, Z=8.80; P2>RB, Z=14.58, which although not replicated in the ANOVA, does follow the same pattern as the P2PAs (Fig7Ai).

Motor

Using ANOVA, significant differences in P2PA were found between the timepoints, $F(3,42)=5.43$, $p<0.01$ showing that the presence of motor task modulated the MEP. P2 was found to be significantly larger than RB ($p<0.01$), and BL ($p<0.05$), see Figure 5.9Bii (purple) for all p values. This shows that the P2PA increased significantly from that of the stimulus baseline after 7s of sustained contraction but not 1s of contraction. The difference between P2 and RB shows that the CSE was much greater after 7s of contraction than during the RB period.

Using the regression analysis, the average-stimulus MEP was found to be a significant predictor of P1 (Z=57.39), P2 (Z=58.78), RB (Z=53.63) and BL (Z=53.88) MEPs (see Figure 5.9Bii, in orange). The contrasts between timepoints showed that the fit of P1 was significantly smaller than P2 (Z=9.50), and significantly larger than RB (Z=19.43) and BL (Z=19.15), see Figure 5.9Bii, orange. This is in stark contrast to the P2PA results which showed no difference between P1 and any other timepoint. The fit of P2 was also found to be significantly larger than RB (Z=25.70) and BL (Z=25.34).

Visual

Using ANOVA, no significant differences in P2PA were found between the timepoints, $F(3,42)=2.09$, $p=0.12$.

However, using the regression analysis, the average-stimulus MEP was found to be a significant predictor of P1 (Z=55.66), P2 (Z=58.78), RB (Z=53.63) and BL (Z=53.88) MEPs

(see Figure 5.9Cii, in orange). The contrasts between timepoints highlighted that the fit of the BL was significantly smaller than all other timepoints: P1>BL, Z=8.05; P2>BL, Z=9.57; RB>BL, Z=8.28, an effect not found with the ANOVA analysis.

Auditory

Using ANOVA, no significant differences in P2PA were found between the timepoints, $F(3,45)=0.235$, $p=0.87$

However, using the regression analysis, the average-stimulus MEP was found to be a significant predictor of P1 (Z=54.88), P2 (Z=54.74), RB (Z=53.80) and BL (Z=56.48) MEPs (see Figure 5.9Dii, in orange). The contrasts between timepoints highlighted that the fit of the BL was significantly larger than P1 (Z=9.85), P2 (Z=10.75) and RB (Z=14.83). This effect was not found with the ANOVA analysis but suggests that the auditory task did modulate the MEP and decrease CSE from that at the stimulus BL. P1 was also found to be smaller than the RB (Z=5.57).

5.4.3 EEG

Group level beamformer maps and IM VE timecourses are shown in Figure 5.10 for each stimulation type. The subjects specific IM VE positions were defined from the beamformer maps as the maximum ERD magnitude to the stimulus in the stimulus specific cortex (i.e. visual cortex ERD to visual stimuli): maximum β power ERD for motor and MNS, maximum α power ERD for visual and auditory stimuli. For each stimulus, α and β responses were extracted from the same VE. As has previously been shown (Fuggetta, Fiaschi et al. 2005), the TMS pulses produced an increase in β power immediately with TMS application lasting for ~0.5s. This has been removed from all plots for better visualisation of the data. It has been hypothesised that these increases in power are related to resetting of the ongoing oscillations due to the TMS pulse (Paus, Sipila et al. 2001, Van Der Werf and Paus 2006).

MNS

MNS α and β power beamformer maps both showed bilateral IM ERD to the stimulus, with group, as well as all single subject, peak ERD located in the motor cortex contralateral to MNS (Figure 5.10Ai & ii). The α and β responses show similar timecourses (Figure 5.10Aiii), with similar levels of ERD during the stimulus, however only the α data showed a rebound (Figure 5.10Aiii).

Motor

Motor α and β power beamformer maps both showed IM ERD specific to the contralateral motor cortex , with ipsilateral motor cortex showing slight α, but not β ERS (see Figure 5.10Bi & ii). The α and β responses show very similar timecourses, with near equal levels of ERD to the task and matching short duration rebounds (Figure 5.10iii).

Visual

Visual α and β beamformer maps showed different patterns of activity, with the β power group map highlighting a large ERS centrally in the visual cortex (Figure 5.10Cii), a result of the 7Hz visual stimulus eliciting a visual evoked potential (VEP) in that frequency band . The α power beamformer map also shows a slight group level VEP although an overall α power ERD is shown in the VE timecourse (Figure 5.10Ci). The group beamformer maps show little response in the motor cortex.

The α and β group level responses showed very different timecourses, the α power timecourse displaying a large ERD, while the β timecourse, apparently compromised more by the VEP, showed a timecourse that didn't deviate from the baseline (Figure 5.10Ciii). The large ERD of the α power timecourse was accompanied by a long rebound lasting for the duration of the period taken as the stimulus baseline (see Figure 5.10Ci & iii).

Auditory

Auditory α and β beamformer maps displayed very similar patterns of activity, with group peak IM ERD found within left/contralateral auditory cortex (Figure 5.10Di & ii) in both cases. The right motor cortex (ipsilateral to MNS/motor) was also found to display ERS in both α and β maps (Figure 5.10Di & ii) as did the visual cortex. The α and β power timecourses both displayed a level of ERD, strongest in the α timecourse (Figure 5.10Diii). The auditory stimulus did not produce a noticeable rebound in α or β power (Figure 5.10Di-iii).

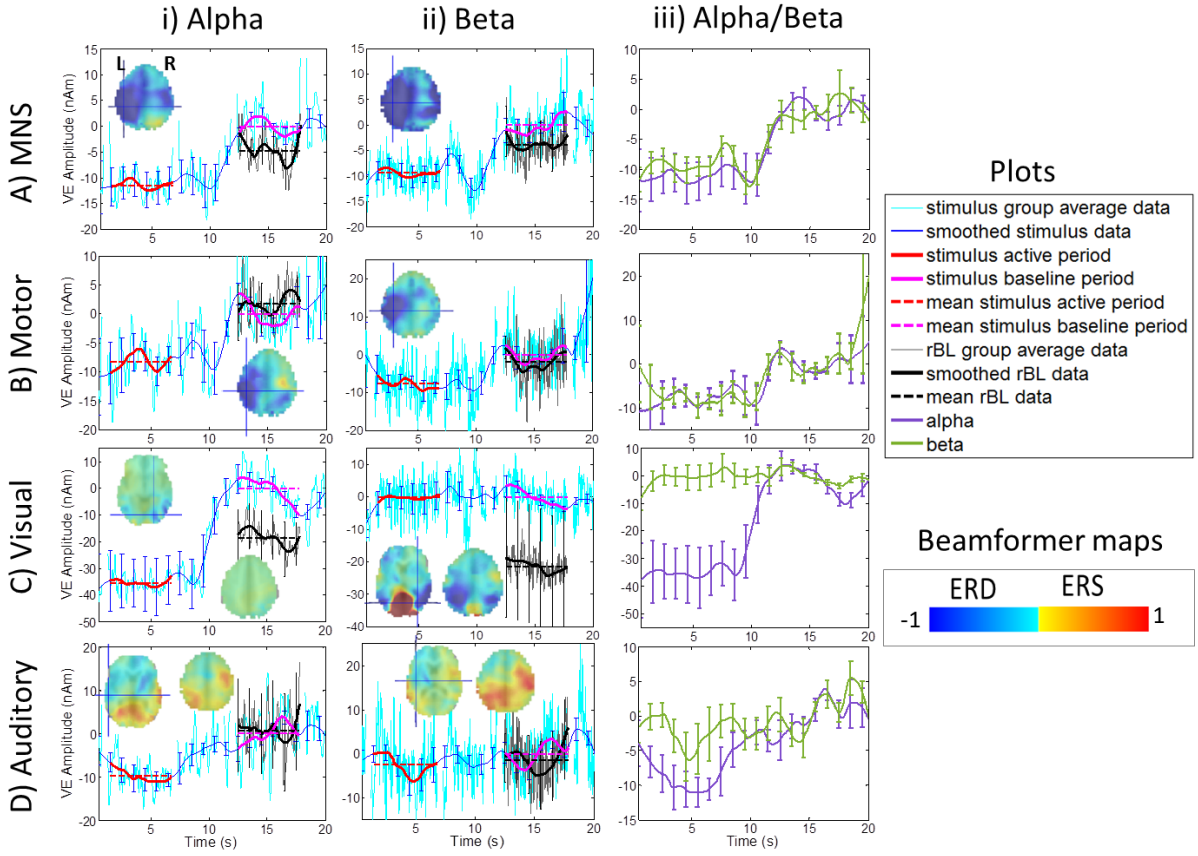

Figure 5.10. EEG α and β power taken from the IM VE during each condition. Ai-Di show the α power timecourse taken from the IM VE during the MNS, motor task, visual and auditory stimulus respectively. The brain map shows the group level beamformer map for each condition, the crosshair highlighting the group level VE location. The group mean raw timecourse (light blue) shown along with the smoothed group timecourse (dark blue), the stimulus period and stimulus and baseline are also displayed (red and magenta respectively). The resting baseline recorded prior to the stimulus is also displayed (black) for comparison with the stimulus baseline. All timecourse data has been corrected using the stimulus baseline (mean corrected). Aii-Dii show the β power timecourse for each condition. Aiii-Diii show the overlap of the smoothed α and β power timecourses for each condition.

IM VE baseline power comparison

We assessed whether the two baseline measures of EEG power (rBL and inter stimulus interval) were equivalent. We subtracted each of the mean stimulus run baselines from the mean baseline of their respective rBLs, and the difference was then assessed using a one sample t-test i.e. if the baseline power remaining after rBL-stimulus was significantly different from zero. The only significant difference found was a borderline result between the visual rBL and the visual stimulus baseline for α power ($p=0.045$). This difference in α power is most likely a result of the previously mentioned rebound elevating the power during the stimulus baseline period, whereas this effect does not occur in the rBL. No other differences were observed (α: MNS, $p=0.15$, Motor, $p=0.54$, Auditory, $p=0.95$; β: MNS, $p=0.37$, Motor, $p=0.42$, Visual, $p=0.25$, Auditory, $p=0.84$).

By taking a subject mean rBL (across all runs) each having been corrected to their corresponding stimulus baseline periods as before, no significant differences were found between rBL and stimulus baseline for α power (t-test, $p=0.95$) or β power ($p=0.84$).

TMS mask

For all stimuli, the TMS VE EEG data was found to show less ERS or ERD to the stimulus, see Figure 5.81 than was seen in the IM VEs. As with the IM VE data, the TMS pulses produced an increase in β power immediately after TMS application lasting for ~0.5s (removed from the plots for better visualisation of the data). In contrast to the IM VE data this increase in power was followed by a separate 'rebound' (lasting ~1.5-2s), most noticeable in the auditory β data (Figure 5.11D) which shows power increases after each TMS pulse.

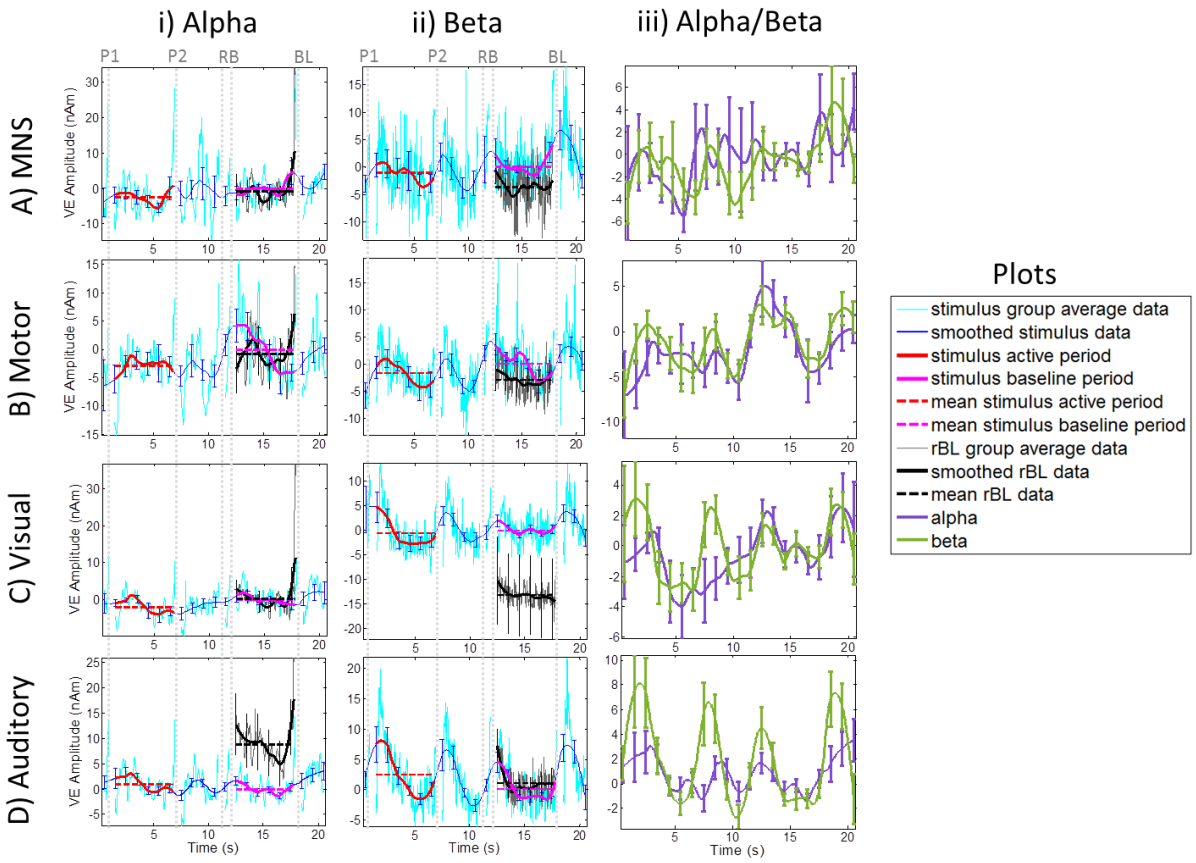

Figure 5.11. EEG α and β power taken from the TMS VE during each condition. Ai-Di show the α power timecourse taken from the TMS VE during the MNS, motor task, visual and auditory stimulus respectively. The group mean raw timecourse (light blue) shown along with the smoothed group timecourse (dark blue), the stimulus period and stimulus and baseline are also displayed (red and magenta respectively). The resting baseline recorded prior to the stimulus is also displayed (black) for comparison with the stimulus baseline. All timecourse data has been mean corrected using the stimulus baseline. Aii-Dii show the β power timecourse for each condition. Aiii-Diii show the overlap of the smoothed α and β power timecourses for each condition. The section overlapping the TMS pulse (500ms) has been interpolated out for plotting purposes as it contains the known TMS pulse related synchronisation in power.

As on average across subjects little EEG response was observed in this TMS VE we divided subjects into those with ERS responses and those with ERD responses. This highlighted that ERS subjects showed larger TMS induced power increases than the ERD subjects (Figure 5.12). In fact, the designation as a subject with ERS appeared to be driven by the effect of the TMS rather than any response to sensory stimulation, unlike the ERD subject data which appears to show more sensory related response. In order to check whether this data can be

used for subsequent analysis, the average group timecourse for ERS and ERD subjects was examined (Figure 5.13). The phase prior to the TMS pulse is contaminated by the power increase in the β band induced by the TMS pulse, due to the 'smoothing' of the power data during the Hilbert transform. As shown in Figure 5.13, it is possible to measure the phase 0.1s prior to the TMS pulse, as indicated by the red line on each of the plots, although this is not as informative as it would be measured closer to the pulse, it still may contain relevant information. The same plots show that the power prior to the pulses (0.5 to 0.1s prior) are contaminated very little by the increases in power or any remaining artefact from the pulses.

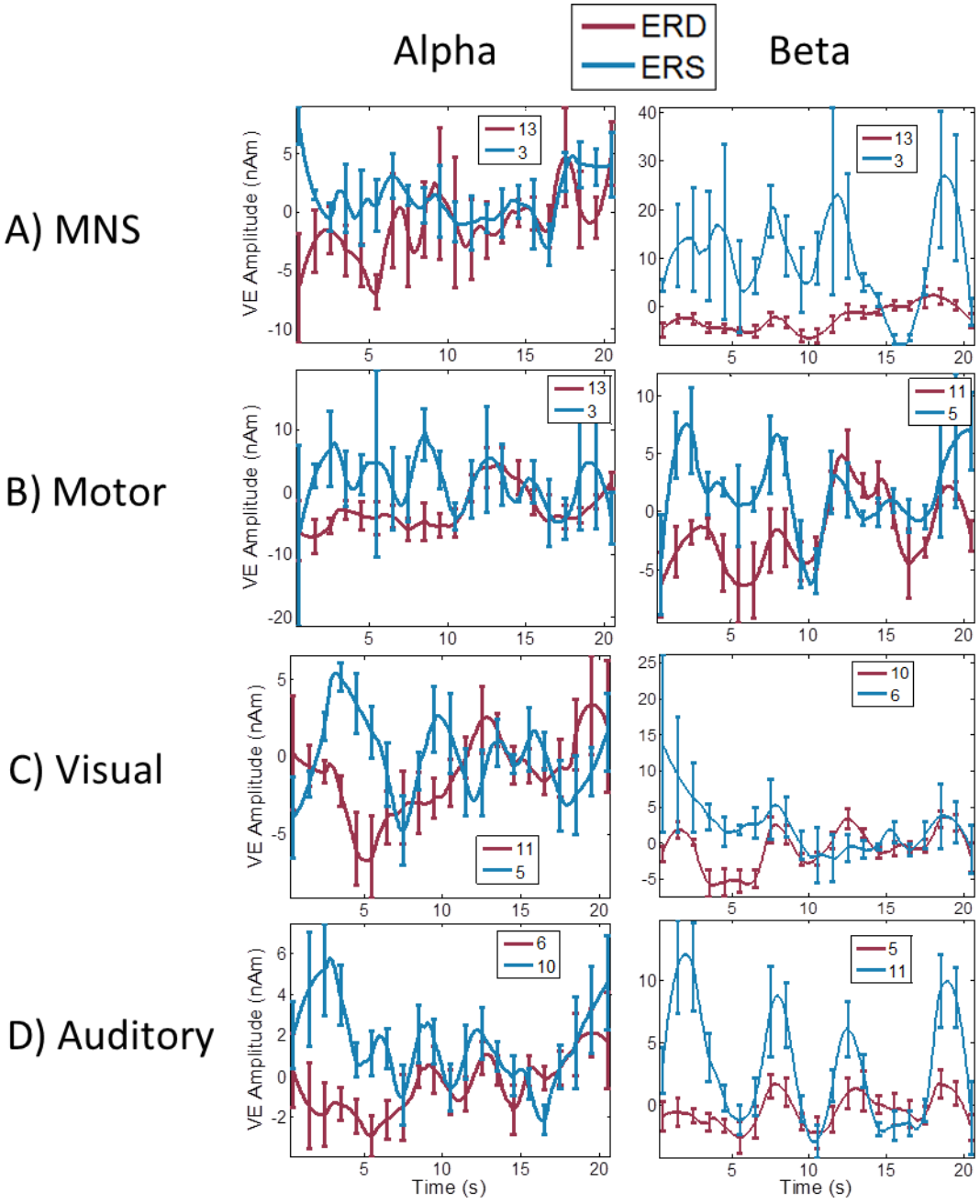

Figure 5.12. Average *smoothed* group level ERS and ERD subject timecourses for each condition and each frequency band. Ai-Di show the alpha and Aii-Dii show the beta responses respectively for subjects with ERD (red) and ERS (blue) at the TMS VE to the MNS (A), motor task (B), visual stimulus (C) and Auditory stimulus (D).

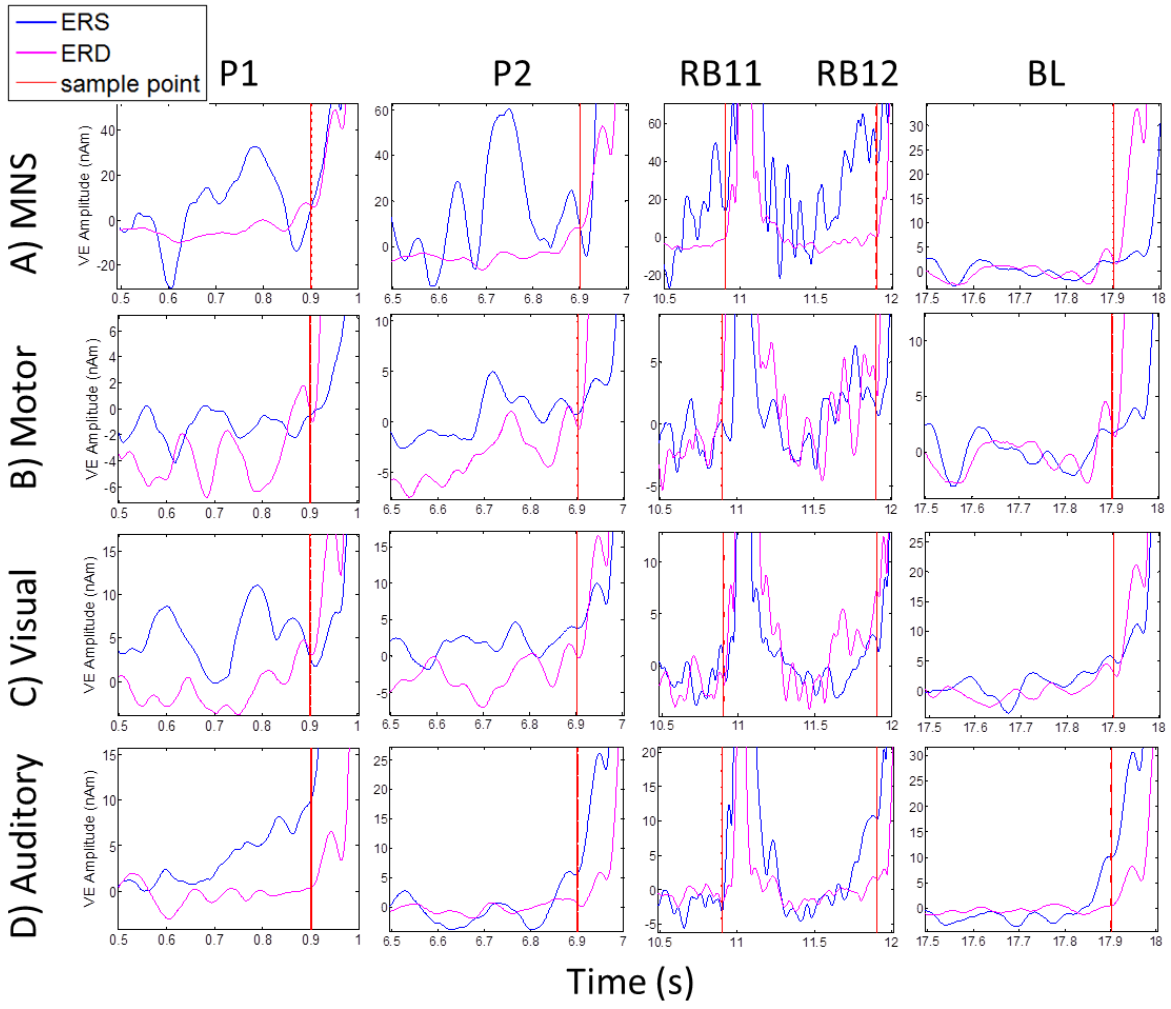

Figure 5.13. Averaged TMS VE β timecourses showing data 0.5 seconds prior to each of the TMS pulses (P1, P2, RB11 RB12 and BL). Subjects are spilt into those showing ERS (blue) and those showing ERD (magenta). The sample point for extracting the phase of the timecourse is shown (red vertical line). A-D shows the MNS, motor task, visual stimuli and auditory stimuli for each of the TMS pulses.

5.5 Discussion

The aim of this Chapter was to outline the basic results of the fMRI, TMS, EEG and MRS measures collected prior to Chapter 6 in which we relate these measures primarily to the NBR and also to one another. Here we were able to measure NBRs in the right motor cortex (the region stimulated using TMS) to all four sensory stimuli at the group level. The MEP, MRS and

EEG measures were also shown here to be reliable and valid for use in further analysis as discussed below.

5.5.1 NBRs across conditions

The NBR results which particularly stand out are those of the MNS which showed near domination in the visual, auditory and right motor cortex. These CM NBRs in visual and auditory cortices to MNS to our knowledge have not been shown before. The CM NBRs to the motor task are in stark contrast to the MNS data, showing no CM NBR in auditory cortex and very little in the visual cortex. The motor task NBR found here is similar to that found in Chapter 2 for the Grip task, although here the Grip was sustained and in Chapter 2 it was repetitive. The differences in slice coverage prevent full comparison between the two BOLD responses, but CM NBRs were found in both the LOC/iPL.CM NBRs have been shown to be evoked in the visual cortex to auditory stimuli and vice versa (Laurienti, Burdette et al. 2002, Mozolic, Joyner et al. 2008) which we have replicated here. In addition to this we have also shown that passive visual and auditory stimuli evoke CM NBRs in motor cortices.

NBR in the DMN was found during the MNS, motor task and visual stimuli, but not for the auditory stimuli where PBRs were found in the iPL regions and no significant response noted in the precuneous. Passive sensory tasks (auditory and visual) have previously been shown to evoke little or no NBR in the DMN (Greicius and Menon 2004), while NBRs have been shown in the DMN to emotional processing tasks (Northoff, Heinzel et al. 2004) and to increase with increasing difficulty of auditory detection tasks (McKiernan, Kaufman et al. 2003). Although only the motor task required top down attention in order to perform the task, the full field visual checkerboard could be said to create more stimulus driven bottom-up attention (as could the MNS) than the auditory beeps and may explain the difference in DMN NBR found here. Potentially these differences in the stimuli could also explain the NBR seen during the auditory task in a set of brain regions commonly referred to as the fronto-parietal network (FPN) (see

Figure 5.6Eiv) which is often associated with attentional control (Scolari, Seidl-Rathkopf et al. 2015). Increased activity in this network is believed to relate to increasing task difficulty (Leech, Kamourieh et al. 2011) and has previously been shown to activate to auditory identification and localisation tasks (Maeder, Meuli et al. 2001). The FPN showed particularly prominent PBR in the visual condition (see Figure 5.6Div; the PBRs in that slice showing the extent of the full network), and it is also seen to the motor task (Figure 5.6Civ). However, for MNS although PBR was found in the anterior aspects of this network, it evoked NBR in the posterior aspects (Figure 5.6Aiv). To our knowledge no studies have shown NBR in this network before. The main focus of the study is however NBRs evoked in the right motor cortex which is discussed further below.

5.5.2 Mask utility and NBR validity

The NBR has been widely shown to be evoked in IM (See Chapter 2, also: (Allison, Meador et al. 2000, Mullinger, Mayhew et al. 2014)) as well as CM (See Chapter 2, also: (Laurienti, Burdette et al. 2002, Hairston, Hodges et al. 2008, Mozolic, Joyner et al. 2008, Ciaramitaro, Chow et al. 2017)) sensory cortices during sensory stimuli. Previous work into CM NBRs has focussed primarily on visual-auditory cortices, while the motor-visual and motor-auditory NBRs are much less studied. In Chapter 2 we found that CM NBRs were evoked in the motor cortex to single hemifield visual stimuli, here we replicate and extend this showing that at the group level NBRs were evoked bilaterally in the motor cortex to both full-field visual stimuli and binaural auditory stimuli. Although more subjects displayed CM NBR during visual than auditory stimuli in the right motor cortex (17 and 13 respectively) the auditory stimulus CM NBR was considerably greater in spatial extent in the group level map. This could be explained by the visual CM NBR overlapping less across subjects while also possibly being more focal than the auditory CM NBR. Of particular interest was the magnitude of NBR within

the right motor cortex for further comparison with the subject specific TMS and MRS measures taken from that region.

The right motor cortex NBR was found to reside in both the MRS mask and TMS mask for a larger percentage of subjects during IM than CM stimuli: MNS 41%; Motor 41%; Visual 18%, Auditory 33%. We can interpret from this that in general there isn't a neat overlap between the NBR and either or both of the masks, and that we cannot simply use one of these masks to gather a measure of NBR for comparison with the TMS and MRS measures, but instead the mask used should be specific to each measure. As such, in the following chapter the TMS mask will be used to find both the NBR and the EEG response in that region for relation of those measures to the MEP data, whereas the GABA and Glx measures will be related to the NBR data from within the MRS mask. The TMS mask could be criticised as being too large, however it was developed so as to capture the whole area that was potentially affected by the pulse. As described in the methods section, a TMS pulse is not perfectly focal but instead spreads outwards (Deng, Lisanby et al. 2013). This coupled with potential imperfections in registration and coil positioning (maximum combined error of 6mm) mean that the exact position of the TMS pulse cannot be determined, although given MEPs were recorded from the FDI muscle it was situated close to the hand region of M1. The size of the mask therefore captures the non-focal aspect of the electric field generated while compensating for minor errors of coil position in relation to the brain.

5.5.3 Confidence intervals anyone?

The number of MEPs required to best represent a particular measure, for example, a measure at rest, is still a contentious issue. The CI system used here was adapted from that used by Cuypers et al. (Cuypers, Thijs et al. 2014). They used the CI method to find the number of MEPs required to best represent the overall mean MEP P2PA of 40 consecutive MEPs. MEPs P2PAs are known to be highly variable (Kiers, Cros et al. 1993, Roy Choudhury, Boyle et al.

2011), as such this CI system enables a data driven method of generating a specific cut off for the number of MEPs required to be confident that the average measure derived from them is informative. Here, our 24 MEPs per condition was markedly less than the 40 used by Cuypers et al. By their results there would be a 90% probability that the mean P2PA of 24 MEPs would be within the 95% CI of the mean amplitude of 40 MEPs. The actual cut off we used here was 16 MEPs which from their data would relate to 78% probability of being within the 95% CI of 40 MEPs. However, as we only measured 24 MEPs we are instead able to show that this cut-off related to a 95% probability of being within the CI of the maximum number of MEPs we collected. Collecting 40 MEPs per timing condition (P1, P2, RB11, RB12 and BL) would have more than doubled the time per run and also the rBL time making the experiment length unfeasible given that the TMS-EEG session recording already lasted for between 1.5 to 2 hours plus an hour to set-up. The comfort of the subject would likely have been compromised by adding the additional MEPs, decreasing both the level of participation as well as potentially reducing the data quality.

Using the cut-off of 16 MEPs prevented conducting a separate analysis of the rebound measures (RB11 and RB12), each of which had a maximum of 13 MEPs per run, when using the repeated measures ANOVA. By combining the two RB measures together interpretation of contrasts between RB and other timings becomes difficult as the two RBs potentially differ from one another. In the following chapter using the GLM approach all MEPs will be used along with covariates (including coil position and pre-MEP EMG BL) allowing the two RBs to be modelled separately to provide clarity on this issue.

5.5.4 Can GLM analysis tell us anything new about MEPs?

Using the repeated measures ANOVA approach, we found significant differences between pulse timing conditions in the MNS and motor task conditions (See Figure 5.9). These differences were also highlighted using the GLM approach, which was found to be the more

sensitive of the two methods showing a greater number of significant differences between pulse timings in all stimulus conditions.

The more traditional ANOVA method of analysing MEPs focusses upon the P2PA which is widely interpreted as a measure of CSE (Rothwell 1997, Di Lazzaro, Oliviero et al. 2004, Chen, Cros et al. 2008). Here, we found that the first second of an 8s period of MNS significantly reduced CSE from the stimulus baseline (Figure 5.9Aii, orange). The RB was also found to be significantly reduced from the stimulus baseline (Figure 5.9Aii, orange). It is important to remember that the MNS was not continuous, but rapidly pulsed and therefore that the timecourse of any resultant inhibition has to be considered. The timing of a contralateral TMS pulse in relation to MNS has been shown to affect the level of CSE, with a TMS pulse applied 200ms after MNS found to decrease CSE, but eliciting no change at other times (Chen, Corwell et al. 1999). Within this study, using 40Hz MNS meant delivering a pulse every 25ms, which elicits a sustained thumb muscle contraction rather than individual twitches. The constant barrage of MNS would therefore appear to elicit the same change in CSE (after 1s of stimulation) as a single pulse 200ms prior to TMS application. Conversely for the motor task, a 7s duration of static gripping and therefore constant motor activation was found to significantly increase the CSE from that of the stimulus baseline. Previous work has shown that a tonic grip results in larger MEP P2PA in the same hand (i.e. contralateral stimulation), in comparison to rest, when the force applied was greater than 20% of the maximal contraction (Muellbacher, Facchini et al. 2000, Liepert, Dettmers et al. 2001). Although decreases in P2PA from rest were found with minimal contraction (2% of max) this effect was only found between 1-100ms after grip initiation, with a subsequent near linear return to rest levels between 200-500ms (no data was recorded after 500ms) (Liepert, Dettmers et al. 2001). The increase in P2PA observed in the current study could therefore relate to subjects performing the grip task by exerting a force >20% of their maximal contraction, which is very likely. Although this level of contraction could result in bilateral M1 recruitment (Muellbacher, Facchini et al. 2000) our

results do not reflect this. It is also possible that a lower force was applied and that after 500ms the trend for increasing P2PA continues leading to P2PAs greater than that at rest. From the data gathered we cannot calculate the force used as a percentage of maximal contraction, although it is likely that the grip force was greater than 20% of the subjects maximum.

The findings from the ANOVA were replicated by the GLM analysis, with further significant differences also noted between pulse timing conditions using this method. This increased sensitivity is highlighted by the GLM analysis finding differences between TMS pulse timings within all stimulus conditions, even during visual and auditory stimuli for which no ANOVA based P2PA differences were found. Interestingly, the GLM analysis found that P2 was significantly larger in amplitude than P1 for both MNS and motor task. The difference found between the MNS P1 and P2 may relate to inter-trial adaptation previously shown to occur to MNS over 18s. Using MEG, Wright et al. (Wright, Brookes et al. 2008) showed that evoked responses to 2Hz MNS measured in the contralateral motor cortex decrease over time, reaching baseline levels by ~10s, while no similar adaptation was found to occur across trials. This adaptation would likely relate to a decrease in interhemispheric interaction between contralateral and ipsilateral motor cortices due to a decrease in neuronal activity to the stimulus. The decrease in CSE that we initially observed would then be less likely to be mirrored by that at P2. As discussed above for the motor task, it is possible that this increase in CSE is a result of increasing grip pressure through the trial or alternatively CSE continuing to increase with duration. Having only the two time points at 1s and 7s and having not explicitly measured the contraction force exerted removes our ability to understand how the MEPs change throughout the stimulus period and how they relate to force.

There are a number of differences between the two analysis methods employed here which may relate to the greater sensitivity of the GLM analysis. Primarily, the approaches differ in

that the GLM method utilises the whole timecourse and all trials for each subject unlike the ANOVA approach which uses the P2PA median of each subjects' data. The two approaches also differ in their relation to the rBL data, whereby for the ANOVA method the stimulus P2PA data is normalised using the rBL P2PA data, while the GLM approach does not relate to the rBL (with the average-stimulus MEP used as the regressor). Although for the ANOVA approach the data is normalised to the rBL the variability in the stimuli runs for each subject is still not taken into account. The known variability of trial-by-trial MEP data is therefore unused in the ANOVA data analysis. For the GLM analysis use of the whole MEP timecourse means that it is not only the P2PA change that accounts for the fit of the stimulus timing data, but instead, the overall shape of the timecourse is important. Changes in MEP latency, amplitude and duration are all modelled at once in the GLM analysis. Here, increases in MEP amplitude, relating to P2PA, would increase the statistical significance of the fit, while increases in other aspects of the MEP such as latency (stable within subject (Bestmann and Krakauer 2015)) and duration (thought to increase with increasing ipsilateral muscle contraction during TMS (van den Bos, Geevasinga et al. 2017)) would reduce the overall fit.

The methods of statistical correction differ between the two analyses, with the stringent Bonferroni correction used for the repeated measures ANOVA, and the less stringent fixed effects correction used for GLM analysis. However, using a less stringent SIDAK post-hoc correction for the ANOVA does not greatly change the p-values shown in Figure 5.9, nor does it reveal any other significant differences between pulse timings conditions due to the low number of subjects used.

5.5.5 The relativity of MEP baseline measures

Here we found that by effectively normalising all stimulus run MEPs (using the median absolute deviation of the rBL MEPs) the P2PA of all pulse timings, in all runs, were larger than those of the rBL. There appears therefore to be a general increase in subject's CSE during

stimulus run recordings. As a highly connected system, brain regions are not seen to act in isolation but as part of a dynamic fluctuating whole, this is apparent in the motor cortex in which there are a large number of regions known to interact with M1 (Bestmann, Ruff et al. 2008). Input into M1 from other regions, such as the premotor cortex and lateral prefrontal cortex (Duque, Labruna et al. 2012), frontal cortex (Civardi, Cantello et al. 2001), and dorsolateral prefrontal cortex (Hasan, Galea et al. 2013), have been shown to influence the amplitude of MEPs measured during motor tasks. The increase in P2PA during the stimulus periods compared to the rBL could relate to dynamic changes in the system as a whole. Such changes during a stimulus run could relate to the increase in stimulus BL CSE from that of the rBL, even though the MNS, visual and auditory stimuli are passive, and the motor task is active, there is little difference between any stimulus condition stimulus baseline P2PA. Such stimulus vs rest changes in underlying CSE may be expected to be related to the underlying neuronal activity. However, the rBL EEG α/β power as not found to be different to the stimulus baseline α/β power. This suggests that the overall increase in CSE could relate more to an increase in the excitability between spinal cord to muscle than an increase specifically in cortical neuronal excitability.

5.5.6 EEG artefacts and EEG utility

The TMS artefact correction method used in this study was found to successfully remove the artefacts from the condition specific IM VE data (see Figure 5.5). Similar to previous studies (Paus, Sipila et al. 2001, Fuggetta, Fiaschi et al. 2005, Van Der Werf and Paus 2006), we found increases in oscillatory power after a TMS pulse within the TMS VE, thought to relate to the resetting of oscillatory power in the region, with the addition here of 'rebounds' (see Figure 5.11). Even with this TMS interference upon the EEG, the data used for relation to other measures, i.e. the data prior to the TMS pulse from the TMS VE, was found to still contain information that is of use (see Figure 5.13).

5.5.7 Summary

Here we show that all stimuli evoke NBR in the right motor cortex at the group level. We also show that all other measurements taken from that region are useful for further analysis comparisons with NBR and with each other.

CSE was found to increase from that at rest for all stimulus runs and at all timing conditions (during stimulus, rebound and baseline). The GLM approach to MEP analysis was found here to show increased sensitivity to the differences between timing conditions from that of the ANOVA approach. Both approaches found MNS lead to an initial decrease in CSE from that of the stimulus baseline. While the motor task CSE was found to be larger than that at stimulus baseline after 7s.

CHAPTER 6

EXPLAINING INTER-SUBJECT VARIANCE IN INTRA- AND CROSS-MODAL NBRS USING TMS, EEG AND MRS MEASURES OF NEURONAL ACTIVITY

6.1 Abstract

As outlined in Chapter 5, the data explored there was combined here to test whether there are links between the multiple measures acquired. Specifically, testing whether these measures explain the between subject variability in NBR amplitude

We find a trend in the ability of GABA and Glx to predict the amplitude of NBR, whereby increases in GABA and decreases in Glx are predictive of IM NBR but not CM NBR. That there is a difference between the IM and CM NBRs and their relation to neurotransmitter levels implies a difference in the origin of these two BOLD responses. However, no other measures were found to relate to IM or CM NBRs.

6.2 Introduction

From the fMRI, MRS, EEG and TMS data collected as described in the previous chapter we hypothesised the following between subject relationships:

1) The level of GABA measured in the motor cortex will be positively correlated, and the level of Glx negatively correlated, with the amplitude of NBR found in that region, for IM and CM responses to the four stimuli.

2) The amplitude of NBR measured during each stimulus type in the motor cortex would be negatively correlated with the β power measured in that region.

3) The degree to which CSE decreased in the motor cortex during each stimulus type would be positively correlated with the amplitude of NBR in that region to the same stimulus.

4) Trial-by-trial CSE would be negatively related to the concurrent β power in the region.

6.3 Methods

The peak percentage change in BOLD response (NBR/PBR) was used for all comparisons unless stated otherwise.

6.3.1 fMRI-MRS regression

Linear regression analysis was used to test the ability of subject's GABA and Glx (corrected to water concentration) to predict their percentage change of:

1) NBR in the right hemisphere, that ipsilateral to MNS and motor task, for all tasks;

2) PBR in the left hemisphere for MNS and motor task;

3) CM NBR in the left hemisphere for auditory and visual stimuli.

An additional covariate of GM:WM ratio used to correct for partial tissue volume differences across subjects within the MRS voxel (Mullins, McGonigle et al. 2014). Each stimulus was separately analysed and only those subjects showing significant BOLD responses (z>2.3) were included (see Figure 5.7 for right hemisphere data).

Due to the various ways of scaling/correcting GABA levels, a number of other methods were also tested GAAB/Cr (Violante, Ribeiro et al. 2013), GABA/NAA (Stagg, Bachtiar et al. 2011), and GABAw/(GM+WM) (Harris, Puts et al. 2015).

6.3.2 fMRI-EEG correlations

Separately for each stimulus, subject's mean TMS VE EEG β and α power (calculated between 1.5 and 6.5s) were correlated with their percentage change of NBR, during that stimulus, in the right motor cortex (from the TMS mask).

This correlation analysis was repeated using the EEG β and α power from the left motor cortex: motor task IM VE for motor data; MNS IM VE for MNS data; and the IM MNS VE for visual and auditory data. Data was taken from the IM MNS VE for the visual and auditory conditions to locate a location within the left motor cortex, although the motor IM VE could have been used little difference in position was noted between the two VEs (Euclidian distance 1.53±0.87mm [mean±std]). This EEG data was correlated with the NBR taken from the right motor mask.

A corrected significance level of $p<0.006$ (0.05/8: the number of stimuli, 4, multiplied by the number of frequency bands tested, 2) was used.

6.3.3 MEP P2PA Linear Regression

Robust linear regression was carried out within subject and separately for each stimulus, a constant amplitude regressor of the mean P2PA was used, along with the addition of five parametric modulators to test whether they could account for any of the trial-by-trial variability in the raw MEP data: the TMS coil orientation and distance from the hotspot; the pre-MEP BL; the β power (mean between -0.4 to -0.1s prior to each MEP pulse) and the instantaneous β phase (0.1s prior to the TMS pulse), taken from the TMS VE. Each parametric modulation regressor was mean subtracted.

Data used were those meeting the cut off criteria described in the previous chapter. The beta values for each regressor and each subject were normalised using the standard error of that specific beta and a t-test across subjects was used to test the significance of the normalised betas against zero (Cohen and Cavanagh 2011). A corrected significance level of $p<0.008$ (0.05/6: the number of t-tests per condition) was used.

6.3.4 MEP GLM analysis

To facilitate comparison with the ANOVA, the same data were used for the GLM analysis. This analysis was carried out separately for each subject and each task. The design matrix construction was similar to that described for the MEP linear regression above, with a mean regressor and five parametric modulators, the difference between the two analyses being that here the full timecourse was being utilised, not just the P2PA.

6.3.5 fMRI-MEP correlation

For each stimulus, across-subject correlations were carried out between the peak percentage change in NBR, taken from the TMS mask, and MAD normalised P2PA at P1 and separately P2. In order to find whether the ratio of the P2PA changes between the stimulus baseline (BL) and the stimulus period (P1 or P2) were more closely related to the NBR, the uncorrected

P2PAs of the P1:BL ratio as well as, separately, the ratio of the uncorrected P2PAs of P2:BL was correlated with the NBR taken from the TMS mask region. A corrected significance level of $p<0.012$ (0.05/4: the number of t-tests per condition) was used.

6.4 Results

6.4.1 Relationships between fMRI and MRS

Right hemisphere

Neither right M1 GABAw nor Glxw (both corrected for water concentration) were significant predictors of IM NBR during MNS (n=15, R^2=0.18, F(3,11)=0.79, p=0.52). After removal of a NBR outlier (greater than 2.5 standard deviations from the mean), a positive trend emerged but still no significant relationship was found (n=14, R^2=0.51, F(3,10)=3.52, p=0.06). A similar significance level was found for motor data, where neither right M1 GABAw nor Glxw were significant predictors of IM NBR during the motor task (n=12, R^2=0.58, F(3,8)=3.74, p=0.06).

While neither right M1 GABAw nor Glxw were significant predictors of CM NBR during visual (n=14, R^2=0.32, F(3,10)=1.57, p=0.26) or auditory stimuli (n= 10, R^2=0.20, F(3,6)=0.51, p=0.69).

Left hemisphere

Neither left M1 GABAw nor Glxw was a significant predictor of percentage change of IM PBR during MNS (n=15, R^2=0.03, F(3,11)=0.13, p=0.94) or during the motor task (n=15, R^2=0.19, F(3,11)=0.88, p=0.48).

Neither left M1 GABAw nor Glxw was a significant predictor of percentage change of left M1 CM NBR during visual (n=12, R^2=0.05, F(3,5)=0.14, p=0.93) or auditory stimuli (n=10, R^2=0.10, F(3,6)=0.21, p=0.88).

GABA corrections

As there is large variability across the literature in the method of correcting GABA when relating it to BOLD responses, Table 6.1 shows correlation and regression analyses for varying GABA corrections.

			GABA/Cr	GABA/NAA	GABAw/(GM+WM)	GABAw
MNS (n=14)	Correlation	(r,p)	-0.43, 0.12	-0.37, 0.19	-0.32, 0.26	-0.32, 0.26
	Regression	F test	R^2=0.61, F(3,10)=5.11, p<0.05	R^2=0.45, F(3,10)=2.72, p=0.1	R^2=0.36, F(4,9)=3.05, p=0.09	R^2=0.51, F(3,10)=3.52, p=0.06
		(beta,p)				
		Mean	-2.65, 0.02	-	-	-
		GABA	-4.57, 0.01	-	-	-
		Glx	0.35, 0.01	-	-	-
		GM:WM	0.14, 0.13	-	N/A	-
Motor task (n=12)	Correlation	(r,p)	-0.50, 0.1	-0.62, 0.03	-0.35, 0.26	-0.50, 0.10
	Regression	F test	R^2=0.60, F(3,8)=4.08, p<0.05	R^2=0.58, F(3,8)=3.75, p=0.06	R^2=0.43, F(4,9)=3.38, p=0.08	R^2=0.58, F(3,8)=3.74, p=0.06
		(beta,p)				
		Mean	-5.34, 0.10	-	-	-
		GABA	-15.62, 0.01	-	-	-
		Glx	0.97, 0.03	-	-	-
		GM:WM	0.41, 0.18	-	N/A	-

Table 6.1. The effect of correction method on the relationship between GABA and IM NBR. Here, four different methods of GABA correction were compared: GABA/Cr (Violante, Ribeiro et al. 2013), GABA/NAA (Stagg, Bachtiar et al. 2011), GABAw/(GM+WM) (Harris, Puts et al. 2015) and GABA/water (Northoff, Walter et al. 2007). Correlations between the corrected GABA measurement and the NBR were then carried out for each (r and p values shown) with uncorrected negative correlation found between motor task IM NBR and GABA/NAA. Regression analysis were also carried out for each correction, using corrected GABA, Glx (water corrected) and GM/WM fraction (for all except GABAw/(GM+WM)). All regression results show a similar trend, suggesting a possible relationship, but that we may be underpowered to detect it significantly. The GABA/Cr regression analysis for MNS showed that with increasing GABA there was an increase in IM NBR, while with increasing Glx there was a decrease in IM NBR. This was in stark contrast to the CM NBRs as shown in the text: assessed only with GABAw, corrected with water.

6.4.2 fMRI Vs EEG

No significant correlations were found for any stimuli between IM NBR (taken from the TMS mask) and TMS VE β power (MNS: n=14, p=0.09, r=0.47; Motor: n=13, p=0.47, r=0.22; Visual, n=8, p=0.69, r=0.17; Auditory, n=9, p=0.90, r=-0.048), or TMS VE α power (MNS: n=14, p=0.16, r=0.40; Motor: n=13, p=0.92, r=0.03; Visual, n=8, p=0.63, r=0.20; Auditory, n=9, p=0.40, r=-0.32).

No significant correlations were found between IM NBR (taken from the right motor cortex) and stimulus IM β power (ERD; left motor cortex) for the MNS (n=15, p=0.55, r=0.17; outlier removed as above) or motor data (n=13, p=0.95, r=0.02). Similarly, no correlations were found between CM NBR (right motor cortex) and visual stimulus CM β power (from left motor cortex IM MNS VE: n=15, p=0.79, r=0.08) or auditory stimulus CM β power (IM MNS VE: n=11, p=0.34, r=0.32).

6.4.3 MEP Regression

P2PA Regression

Robust regression was carried out using 6 covariates: the TMS VE β power and phase, coil distance and orientation and pre-MEP BL. Across subjects no covariate was found to statistically predict P2PA for MNS, motor task, visual or auditory stimuli (see Table 6.2).

The same regression analysis was also carried out using the β power and phase taken from the left motor cortex instead of that from the TMS VE (right motor cortex). Across subjects no covariate was found to statistically predict P2PA for MNS, motor task, visual or auditory stimuli (see Table 6.2).

		i) TMS VE		ii) Left M1 VE	
	Regressor	Mean β (regression)	p-value (t test)	Mean β (regression)	p-value (t test)
A) MNS	Mean	12.41	<0.001	12.46	<0.001
	Power	0.23	0.24	0.4	0.13
	Phase	-0.04	0.84	-0.08	0.8
	Orientation	0.38	0.35	0.31	0.47
	Distance	0.14	0.77	0.07	0.88
	Pre-MEP BL	0.35	0.36	0.28	0.44
B) Motor	Mean	14.11	<0.001	13.99	<0.001
	Power	0.78	0.01	0.02	0.93
	Phase	0.11	0.56	-0.09	0.73
	Orientation	0.04	0.92	0.08	0.85
	Distance	0.12	0.75	0.13	0.7
	Pre-MEP BL	0.15	0.67	0.11	0.74
C) Visual	Mean	12.48	<0.001	12.49	<0.001
	Power	0.69	0.02	0.19	0.81
	Phase	0.06	0.79	0.34	0.22
	Orientation	0.48	0.11	0.57	0.07
	Distance	0	0.99	0.18	0.6
	Pre-MEP BL	0.51	0.03	0.69	0.01
D) Auditory	Mean	13.09	<0.001	13	<0.001
	Power	0.69	0.02	0.5	0.02
	Phase	0.33	0.79	0.36	0.15
	Orientation	0.8	0.11	0.97	0.01
	Distance	-0.15	0.74	-0.06	0.88
	Pre-MEP BL	0.61	0.06	0.54	0.1

Table 6.2. P2PA regression results across subjects. The covariates EEG power, EEG phase, coil orientation, coil distance and pre-MEP EMG BL were used in linear robust regression to test whether they covaried with the P2PA of trial-by trial MEP data. For each subject the regression coefficient (β value) was corrected using the β value SE and a t-test used to find whether the β values across subjects were significantly different from zero. The average corrected β value across subjects is shown as is the p-value from for each stimulus: A) MNS, B) motor task, C) visual stimuli and D) auditory stimuli. Two sets of regression analyses were calculated using EEG β power and phase extracted from the TMS VE (Ai-Di) and EEG β power extracted from left M1 (IM MNS VE for MNS, visual and auditory data; IM motor task VE for the motor data). A corrected significance level of $p<0.008$ was used.

6.4.4 Timecourse Regression: MEP GLMs

Exploring the models' residuals waveforms showed that although there were differences between residuals calculated with and without covariates (Figure 6.1i), the mean residuals remained the same between the two models (Figure 6.1ii), with only minor differences noted between the medians of the residuals (Figure 6.1iii). For MNS, the difference in residual sum of squares (RSS) showed an average reduction of 6.30%±5.09% (mean±sd across subjects) from the model without to the model with covariates. This is similar to the RSS reduction calculated in Chapter 5 from using the average rest MEP to using the average stimulus MEP as regressors.

As a way of checking the validity of the results gained when using covariates the same procedure as carried out for the stimulus data was also performed for the rest data. This data would be unaffected by any variation caused by stimuli and so be more homogenous. For each subject the average rest MEP was used as the regressor in a GLM analysis for all four rest data (that prior to each stimulus) concatenated. The average rest MEP was then used in conjunction with the covariates: β power, β phase, coil orientation, coil distance and the pre-MEP EMG BL. From this we found (using Fixed effects, voxelwise correction $p<0.001$) that the mean regressor without covariates was highly predictive of the rest data ($Z=64.20$). With

addition of the covariates into the model we found a reduction of the RSS of 2.76%±1.69% with significant positive correlations found for phase (Z=2.39), coil orientation (Z=4.81), coil distance (Z=8.40) and pre-MEP EMG BL (Z=8.2). This is similar to that found for MNS analysis across the group (Fixed effects, voxelwise correction $p<0.001$) in which we found a positive correlation with coil orientation (Z=11.15), coil distance (Z=10.43) and pre-MEP EMG BL (Z=7.06). As the rest data is uncomplicated by any factor of stimulation it arguably provides more reliable results, with the small effect of covariates on RSS and the large level of residuals suggesting caution in interpretation. However the same trends are found for coil orientation and distance, as well as pre-MEP EMG BL, with the direction of these correlations suggesting that as the amplitude of these measures increased so did the MEP amplitude .

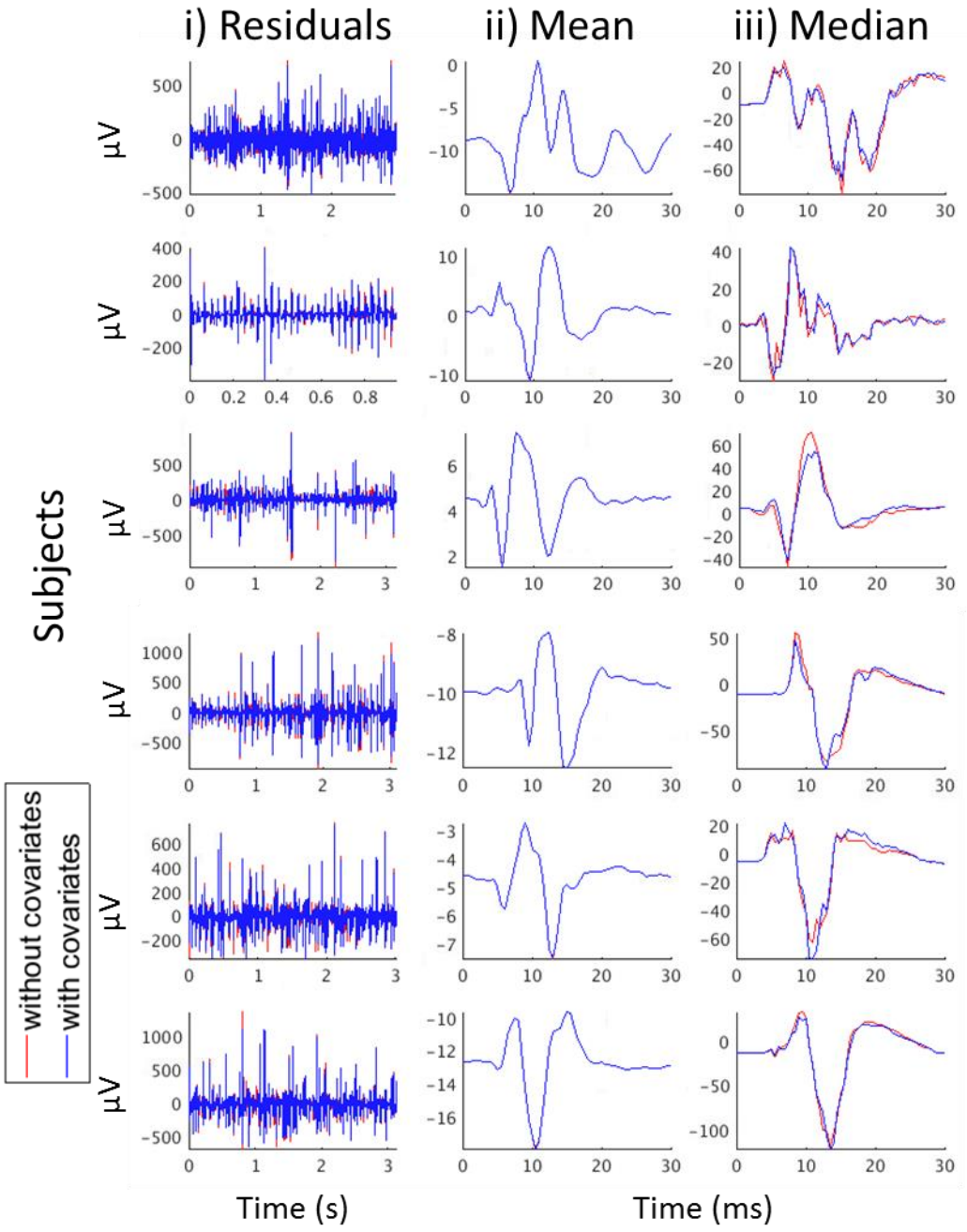

Figure 6.1. Residuals from MEP GLM analysis with and without covariates. Six subjects residuals are shown from GLM analysis performed with (blue) and without (red) covariates. i) shows the residuals over the entire timecourse ii) shows the mean residuals across all trials, note the similarity between the two residuals, and iii) shows the median of the residuals which highlights again the similarity between the residuals calculated when using covariates and when no covariates are used.

6.4.5 fMRI Vs MEP

P1 P2PA Vs NBR

No correlations across subjects were found for any condition between NBR and median normalised P1 P2PA (MNS: n=16, r=-0.17, p=0.53; Motor task: n=13, r=0.28, p=0.35; Visual: n=11, r=-0.17, p=0.62; Auditory: n=11, r=-0.15, p=0.66).

P2 P2PA Vs NBR

No correlations across subjects were found for any condition between NBR and median normalised P2 P2PA (MNS: n=16, r=-0.32, p=0.23; Motor: n=13, r=0.33, p=0.27; Visual: n=11, r=-0.11, p=0.75; Auditory: n=11, r=-.10, p=0.76).

P1:BL P2PA ratio Vs NBR

No correlations across subjects were found for any condition between NBR and the P1:BL P2PA (MNS: n=16, r=-0.12, p=0.65; Motor task: n=13, r=0.14, p=0.66; Visual: n=11, r=-0.03, p=0.93; Auditory: n=11, r=0.32, p=0.33).

P2:BL P2PA ratio Vs NBR

No correlations across subjects were found for any condition between NBR and P2:BL P2PA (MNS: n=16, r=-0.27, p=0.31; Motor task: n=13, r=-0.01, p=0.96; Visual: n=11, r=0.02, p=0.96; Auditory: n=11, r=0.24, p=0.47).

6.5 Discussion

Here, we used neuroimaging measures acquired from the motor cortex described in Chapter 5 (BOLD-fMRI, β/α EEG power, MEP P2PA and GABA/Glx) and assessed the relationships between them. Our main aim was to understand links between various neural markers of the balance of cortical inhibition/excitation to the NBRs found during the four stimuli, MNS, motor, visual, and auditory to gain further insight into the functional and neuronal aspects of IM and CM NBRs. We found only that there was a strong trend for IM NBR amplitude increases (MNS and motor task) to be coincidental with increases in GABA and decreases in Glx measured in the same region, with no similar relationship noted for CM NBRs. Implying a local balance of excitatory/inhibitory neuronal activity is important for IM but not CM NBRs.

6.5.1 MRS NBR trend methodological considerations

A trend was noted between GABA/Glx and IM NBRs (MNS and motor task) in the right motor cortex showing that as GABA increased and Glx decreased, IM NBR amplitude increased across subjects. Although previous work has shown that the resting levels of GABA are highly correlated with mean NBR in the DMN during emotional stimulation (Northoff, Walter et al. 2007) and working memory tasks (Hu, Chen et al. 2013), no studies to our knowledge have examined links between MRS measures and NBR in sensory cortices.

A potential confound here is that the right M1 MRS measurements were acquired at a different time to the BOLD responses. Changes in GABA have been shown to occur through specific interventions such as motor learning (Floyer-Lea, Wylezinska et al. 2006), working memory tasks (Michels, Martin et al. 2012), via transcranial direct current stimulation (Stagg, Best et al. 2009), and also at stages of the menstrual cycle (Harada, Kubo et al. 2011). Such fluctuations in GABA levels could therefore relate to our inability to show robust relationships between GABA and NBR in right M1 taken at different times. However, we also acquired MRS from left M1 immediately prior to the stimuli and found significant positive correlations in GABA and Glx

levels between hemispheres (Chapter 5) suggesting that the measures were characteristic to the individual and not especially sensitive to hemispheric or temporal differences. Further, we tested whether the amplitude of visual and auditory CM NBR in left M1 was related to these MRS measures. The left M1 MRS measures showed the same lack of relationship to the CM NBR in left M1 as observed in the right hemisphere data, strongly suggesting a lack of relationship between GABA or Glx and these CM NBRs.

That we also found no relationship between GABA or Glx and PBR (IM for MNS and motor task, CM for visual and auditory stimuli) is in line with previous work showing that in 5 different regions (including the motor and visual cortices) no correlations were found between GABA and PBR evoked by corresponding tasks (Harris, Puts et al. 2015). Other studies have found however that GABA was negatively correlated with PBR in the visual cortex (Muthukumaraswamy, Edden et al. 2009, Donahue, Near et al. 2010). The difference in findings between various studies which attempt to relate BOLD measures and GABA/Glx could be a result of a number of factors discussed below.

The choice of the internal reference for scaling GABA concentration is still debated, with three references commonly used: water, NAA or creatine (Mullins, McGonigle et al. 2014), where scaling is required to provide an estimate of the concentration of GABA. Some studies also correct for the known difference in concentration of GABA within the GM and WM using the fraction of these tissues found within the MRS voxel (Jensen, Frederick Bde et al. 2005). Although implementation of corrections for this can vary, for example, the addition of the fraction of GM in regression analysis (Hu, Chen et al. 2013) or dividing the GABA concentration by the fraction of GM+WM (Harris, Puts et al. 2015), while some studies use no correction (Stagg, Bachtiar et al. 2011).

Here we found that using common methods of scaling/correcting GABA (for MNS and motor data only: see Table 6.1) produced a consistent trend for a negative relationship between the

IM NBRs and the MRS measures. Suggesting that the main drivers of this are GABA and Glx, with correction having little effect on the relationship calculated and also that with more subjects a significant relationship would be evident. The disparity between the IM and CM results implies that the IM NBRs are more closely tied to the level of the primary inhibitory and excitatory neurotransmitters than the CM NBRs. The CM NBRs may instead be related more to decreases in neuronal input to that motor region which could result in decreased neuronal activity in the area (Figley and Stroman 2011), although this cannot be examined using the data acquired here.

The differences found between previous studies which link BOLD and GABA may not only be a result of the variability in GABA correction methods. The GABA and Glx measures are known to represent all pools of the molecules throughout the neurons, for example the GABA measure being a mix of the cytoplasmic and pre-synaptic concentrations (Stagg, Bachtiar et al. 2011). How these measures relate to the actual level of available neurotransmitter involved in stimulus responses is currently unknown. Added to this is the complexity of the BOLD response itself whereby, as discussed in Chapter 1, there is not a direct one-to-one relationship between the amplitude of the BOLD response and the underlying neuronal activity. The large MRS voxel size complicates matters further as the GABA or Glx levels cannot be measured from exactly the same region as the NBR, the voxel may in fact contain both NBR and PBR. It is important to note that Northoff et al. (Northoff, Walter et al. 2007) who found a correlation between anterior cingulate cortex GABA and NBR did not spatially restrict their measure of the NBR to the MRS voxel as we did here, which could again cause difficulty in comparing issues in interpretation of these results .

6.5.2 The EEG-NBR relationship conundrum

The trial-by-trial variability of the MNS IM NBR has previously been shown to correlate with IM EEG power (Mullinger, Mayhew et al. 2014). Here however we did not find any relationship

between mean NBR and mean TMS VE EEG power for MNS across the two experimental sessions. Nor did we find relationships between the EEG power and NBR for motor, visual or auditory stimuli. It is possible that the EEG data was contaminated by artefacts from the TMS pulses which could have reduced our ability to find correlations between EEG power and NBR. Further reduction of TMS artefacts could be attained by running ICA on the combined stimulus and rest data, but only using the period relating to the artefact itself (e.g. -15 to 100ms either side of the pulse). ICA components gathered would then relate specifically to the artefact as sampled across more data. Although by removing these components the post-TMS increase in power we found for all modalities may still remain. Recent work has shown that TMS artefacts can be reduced during the acquisition of the data by using a plastic spacer (which sits between the coil and the electrodes), preventing contact between the coil and electrodes and so artefacts from the movement of one against the other (Ruddy, Woolley et al. 2018).

As the TMS VE was the region most contaminated we also correlated the left motor cortex EEG power with the motor cortex NBR. This region was not as affected as the region directly underneath the TMS coil (as shown in Figure 5.10; see IM motor and MNS data) but still showed no correlation between power and NBR. Although minor aspects of the artefacts are still likely to remain in this region, measuring from the period least contaminated by these (i.e. immediately prior to P2) produces a good representation of the power change to the stimulus.

The lack of relationship between the NBR (IM & CM) and the EEG power for all stimuli may not be a result of using only mean responses taken in two separate sessions. It is still possible that trial-by-trial correlations may occur, although as shown in Figure 2.13, the grip motor task (repetitive, not held) trial-by-trial IM β power was not found to correlate with the IM NBR. Taken together these results for a simple grip motor task suggest that though the IM NBR does appear to have a neuronal component, it is not necessarily directly related to the IM β ERD. This is in opposition of that found for MNS (Mullinger, Mayhew et al. 2014), suggesting

these active and passive tasks may relate to different neuronal processes. The use of two sessions allowed us to gather a number of different measures that would have been more complicated to do in a single session but may in turn have reduced our ability to compare these measures together – using only average responses. Any differences between sessions (e.g. attentiveness of the subject due to less sleep prior to one session than another) could decrease the likelihood that the signals measured would be correlated. For example the volitional motor task required attention, while contraction strength and duration of the grip can both affect the BOLD response (Dai, Liu et al. 2001).

6.5.3 MEP GLM analysis difficulties

One of this Chapters' aims was to account for the large residuals still remaining after GLM analysis using the average stimulus MEP (Chapter 5). To do so we incorporated covariates of interest in the model's design matrix: pre-stimulus β power and phase, coil distance and orientation and the pre-MEP EMG BL. However, we still observed large residuals although a small difference was seen between running the GLM with and without the covariates when calculating the RSS, with no mean difference between the residuals noted (see Figure 6.1). As a sanity check, GLM analysis was also ran using the rest data, with and without covariates. Here a similar pattern was found, although a smaller decrease was found between the RSS with or without covariates (only ~2%). The large remaining residuals for both stimulus data and rest data when using the residuals and the small change in RSS suggest caution in interpretation of the resulting correlations.

The difficulty in modelling MEP waveforms in this way appears mainly to be a result of the high level of variability in amplitude of the MEPs as well as shape variability. The large variability in MEP amplitude (as can be seen in Figure 5.4Ci: ~50μV to 100μV) results in an overfitting of smaller MEPs and an under-fitting of the larger MEPs, i.e. not conforming to a mean response, resulting in large residuals. That the residuals' waveforms remain the same on average after

the addition of the covariates shows that the covariates explain little that cannot already be explained using the mean regressor. The resulting beta values for the covariates (as shown for MNS data in the results section) are most likely a result of large scaling of the regressor to the data rather than in their providing a good 'fit'. One possibility is that modelling all of the timing conditions (P1, P2 etc.) together could induce a confound via variability in the MEPs due to the stimuli. The covariates were modelled across all timing conditions in order to provide the greatest statistical power. However, it has been shown that although at rest pre-TMS α power is negatively correlated with MEP P2PA (Zarkowski, Shin et al. 2006, Sauseng, Klimesch et al. 2009), this may not be the case during a grip task (Schulz, Ubelacker et al. 2014).

That the relationship between oscillatory power and P2PA could differ between tasks and rest may relate in part to our inability to effectively model the data. Although it would be possible to model each timing condition separately, it would in turn increase the effect size required to find significant results. Instead of this we modelled the rest data as a check and found similar correlations to those for the stimulus data. This suggests that although the stimulus affects the MEPs, this is not the main reason for our inability to model the variability in these waveforms.

The positive correlations found imply that larger coil positional error (distance and orientation) and pre-MEP EMG BL are coincident with larger MEPs. There is a known relationship between MEP P2PA and the pre-EMG MEP BL whereby increasing the activity in the monitored muscle increases its CSE, therefore facilitating a larger MEP with TMS stimulation (Hallett 2007). The positive correlations found for coil position error however are the opposite of that expected and could relate to the true motor hot spot not having been located in some subjects. If during stimulation the coil position moved regularly towards this true hot spot then larger MEPs would be expected. It appears from the data that there were a minority of subjects driving these effects (2 for orientation, 4 for distance). That these correlations were

not noted when the more stringent Mixed Effects modelling was used, which accounts for inter-subject variance, suggests that these outliers may be the ones driving this effect.

Although the GLM approach does appear able to model a small amount of the data, the large level of residuals is concerning. It may be possible to reduce these by first reducing the high level of variability inherent in the data through exclusion of those MEPs that are apparent outliers (e.g. greater than 4 standard deviations from the mean). This is common practice for regression analysis and could enable a better fit of the model. Alternatively, it is possible that the covariates used actually have a non-linear relationship to the MEP timecourses. As such, a machine learning approach may be a more effective method of testing the ability of various combinations of the covariates and interactions between them to effectively model the MEPs.

6.5.4 MEP complexity and the NBR

We did not find any correlation between subjects NBR (IM or CM) amplitude and either the P1/P2 MEP P2PA or the change in P2PA between task and rest. Previous research into the relationship between the BOLD response and MEPs has focussed predominately upon the BOLD response elicited by TMS in studies using simultaneous fMRI-TMS. In particular how far reaching the effect of a TMS pulse is, and whether the different regions in which a PBR is evoked by a TMS pulse are directly or indirectly connected (Koch, Del Olmo et al. 2008, Ruff, Driver et al. 2009). Here, conversely, we attempted to find out whether MEPs, as a marker of cortical excitability, could in fact provide any insight into the neuronal origin of the BOLD response. Such a link was hypothesised due to both being noted in overlapping regions (in M1 ipsilateral to a unilateral MNS (Chen and Hallett 1999, Mullinger, Mayhew et al. 2014)). Significant differences were only noted between the stimulus BL MEP and the stimulus (P1/P2) MEPs for MNS and motor tasks, with the visual and auditory data showing no effect (see Figure 5.9). For the BOLD data however, group level NBRs were found in right M1 (the region in which TMS was applied) to all stimuli. The differences seen between the decrease in

cortico-spinal excitability during MNS and the increase during motor task show the complexity of the measure which appears highly related to the strength of contraction and timing of the pulse relative to other ongoing stimuli (Chen, Corwell et al. 1999, Muellbacher, Facchini et al. 2000). In contrast to this, the BOLD measure is a slower response, related to neuronal and vascular changes. Direct comparison between such complex measures of MEPs and NBRs taken during different sessions could be the reason no relationship was found, whereby the NBR could relate to a summation/average over the stimulus period and CSE be a more temporally direct measure.

6.5.5 Summary

We have shown here possible links between a subjects level of GABA/Glx and their IM NBR amplitude to both MNS and motor tasks. Which suggest that IM NBR amplitude is larger with larger levels of GABA and lower levels of Glx. Given no similar relationship was found for CM NBRs, this implies the two types of NBR may have different origins. Lastly, no relationships were found between NBRs and EEG power or NBRs and MEP P2PA.

CHAPTER 7

CONCLUSION

This thesis has used multimodal neuroimaging methods, in many combinations, to investigate the origin and behavioural relevance of the sensory evoked IM and CM NBRs. These BOLD responses are common, undoubtedly present in many datasets, and yet are under-represented in fMRI literature due to the limited understanding of their origin and therefore how they can be interpreted in terms of changes in brain function. In order to unravel the complex metabolic, vascular and neuronal origins of these BOLD responses multimodal imaging methods are required (Buxton, Griffeth et al. 2014). This chapter summarises the work in this thesis showing how it has extended our knowledge of NBRs and what future work may look to accomplish.

Although research has been carried out into the origin of the IM NBR, in general highlighting a substantial neuronal component to its origin (Shmuel, Yacoub et al. 2002, Shmuel, Augath et al. 2006, Mullinger, Mayhew et al. 2014), whether these findings are similar for CM NBRs and the extent to which IM and CM NBRs differ depending upon the sensory modality stimulated was previously unknown. Here we have shown that CM NBRs can be evoked in the motor cortex to visual and auditory stimuli, as well as in visual cortex to motor tasks and MNS. We found that these IM and CM sensory evoked NBRs show a number of similarities and potentially also modality dependent differences as discussed in detail below.

7.1 NBR origin

The use of BOLD-ASL-EEG measures during visual stimuli and motor tasks enabled us to show that both IM and CM NBRs are related to changes in neuronal oscillatory power and reduced $CMRO_2$. Taken together these provide strong evidence for a neuronal component for both responses.

Strengthening this, the IM NBRs amplitude appears to increase with increasing GABA levels and decrease with increasing levels of glutamate/glutamine implying that the IM NBR could be a result of increased inhibitory neuronal activity and decreased excitatory neuronal activity. Such relationships were not found for CM NBRs from visual or auditory stimuli, suggesting that although there is a correlation with neuronal activity, there may be a decrease in long range neuronal activity input to the region for CM responses, although further research would be needed to clarify this.

7.2 NBR connectivity

The structural and functional connections between PBR and NBR were of interest in this thesis in an attempt to ascertain whether IM/CM NBRs are initiated via the PBR or generated directly via the stimulus itself. The volitional motor tasks examined appear to require interhemispheric interaction for regulation of the IM NBR: with larger IM NBR variability related to greater CC interhemispheric SC and greater IM NBR:PBR ratio related to overall SC. The passive visual stimulus IM NBR appeared however to be driven more by subcortical areas (directly evoked from the stimulus, not from the PBR region) as no relationship was noted between connectivity and NBR. Similarly, CM NBRs were not found to relate to their connectivity to PBR regions. Such lack of relationship between the CM NBR and IM PBR was also noted when the two response amplitudes were correlated with one another across subjects where no significant relation was found. Moving on from this, the structural and functional connectivity between the IM and CM NBRs should be studied, with the aim to find whether such connectivity influences

those responses during the motor/visual trials. For example to elucidate whether direct or indirect pathways allow mediation of the CM response by the stimulated IM network.

7.3 NBR and behaviour/physiology

Although previous work has found links between behavioural measures and IM NBR (Kastrup, Baudewig et al. 2008) we were unable to find any associated link between either IM/CM NBR and a measure of cortico-spinal excitability. We demonstrate that although cortico-spinal excitability changed during motor tasks and MNS, such changes do not appear to be influential in the amplitude of the NBR.

7.4 Future work

7.4.1 NBR Origin

Building upon the work carried out in this thesis, future work could further elucidate the underlying origin of NBRs, IM/CM as well as within other regions (e.g. DMN). The use of multimodal imaging appears to be a prerequisite of understanding the BOLD response. The limited number of slices acquired by DABS could be overcome by implementing a multiband sequence. These sequences acquire 2 or more slices simultaneously via simultaneous slice selection and accelerated imaging readouts (Feinberg, Reese et al. 2002). Collecting 2 slices simultaneously would double the number of slices that can be acquired within the same TR (up to 24 slices), therefore providing full brain coverage. This would enable the measure of whole-brain BOLD-ASL, and the study of NBRs in auditory, visual and motor cortices via auditory, visual and motor stimuli. NBRs within the DMN would also be measureable and as such the neurovascular coupling within all regions could be examined in response to the various stimuli. It would also be possible to increase the SNR of simultaneous BOLD-ASL using a 7T scanner to enable more accurate measures of CBF (Ivanov, Gardumi et al. 2017).

Multiband factors can also be used to measure simultaneous BOLD-EEG, allowing for quiet periods in the fMRI sequence which provide the opportunity to measure gamma oscillatory power (>30Hz) (Uji, Wilson et al. 2018). Gamma power has previously been shown to be correlated with NBR (Boorman, Harris et al. 2015) although it occurs at frequencies similar to those of BOLD-EEG artefacts and is therefore contaminated by noise with traditional sequences. Using multiband fMRI sequences would overcome this problem and enable trial-by-trial correlations between NBRs (IM, CM and DMN) and gamma power. Although our data does not provide a way to probe the gamma/NBR trial-by-trial relationship, further analysis of the data reported in Chapters 5 and 6 could be used to evaluate any link between the average IM/CM/DMN NBR and gamma power.

7.4.2 NBR Connectivity

As stated above, further connectivity analysis could be carried out using the data already available from this thesis. However, the structural connectivity work carried out here used a DTI sequence which due to the fast pace of the DWI field is somewhat outdated (Tristan-Vega, Westin et al. 2009). Increasing the number of directions attained, e.g. from 64 to 128 would allow any connectivity between NBRs and PBRs to be more readily identified. While exploration of possible subcortical connectivity could be investigated with greater clarity such as the possible contribution of inter-thalamic connectivity driving motor task NBR:PBR ratio.

7.4.3 NBR and behaviour/physiology

The analysis of TMS data could be more easily relatable to the task/stimulus of the experiment if the data can be modelled in such a way as to remove the influence of changes in coil position and pre-EMG BL. Although GLM analysis does not appear to provide the solution, other non-linear forms of analysis could be attempted in order to gain a greater appreciation of the intricacies surrounding the trial-by-trial variations in shape and amplitude of MEPs. One

possibility is using a Bayes framework in which the average MEP is the prior, with various scaling of this parameter to the data related to the various parameters.

7.5 Summary

The main aims of this thesis were to better understand the neuronal, metabolic and vascular origin IM and CM NBRs evoked during sensory stimulation. We also sought to understand whether NBR variability or relative amplitude was related to connectivity between the NBRs and the PBR. Lastly we were interested in whether the balance between inhibitory and excitatory neuronal populations/activity was fundamental to these IM and CM NBRs. We were able to show that both IM and CM NBRs were concomitant with decreases in CBF and both resulted from decreases in neuronal activity. However, while both related to changes in neuronal activity due to stimuli, the IM NBRs appear to be dependent upon the local balance between GABA and glutamate unlike the CM NBRs. We also found that structural connectivity was only important for IM NBRs during motor tasks, whereby increased direct connectivity related to more variable NBRs and overall connectivity related to larger relative NBRs. We also found that the short direct measure of CSE was not related to the amplitude of IM or CM NBRs. Overall these IM and CM NBRs are useful for the interpretation of fMRI GLM experiments, showing that in those regions there is a reduction in neuronal activity.

REFERENCES

Agulhon, C., J. Petravicz, A. B. McMullen, E. J. Sweger, S. K. Minton, S. R. Taves, K. B. Casper, T. A. Fiacco and K. D. McCarthy (2008). "What is the role of astrocyte calcium in neurophysiology?" Neuron **59**(6): 932-946.

Akgören, N., M. Fabricius and M. Lauritzen (1994). "Importance of nitric oxide for local increases of blood flow in rat cerebellar cortex during electrical stimulation." Proceedings of the National Academy of Sciences **91**(13): 5903-5907.

Allen, P. J., O. Josephs and R. Turner (2000). "A method for removing imaging artifact from continuous EEG recorded during functional MRI." Neuroimage **12**(2): 230-239.

Allen, P. J., G. Polizzi, K. Krakow, D. R. Fish and L. Lemieux (1998). "Identification of EEG events in the MR scanner: the problem of pulse artifact and a method for its subtraction." Neuroimage **8**(3): 229-239.

Allison, J. D., K. J. Meador, D. W. Loring, R. E. Figueroa and J. C. Wright (2000). "Functional MRI cerebral activation and deactivation during finger movement." Neurology **54**(1): 135-142.

Amedi, A., R. Malach and A. Pascual-Leone (2005). "Negative BOLD differentiates visual imagery and perception." Neuron **48**(5): 859-872.

Andrews-Hanna, J. R., A. Z. Snyder, J. L. Vincent, C. Lustig, D. Head, M. E. Raichle and R. L. Buckner (2007). "Disruption of large-scale brain systems in advanced aging." Neuron **56**(5): 924-935.

Attwell, D., A. M. Buchan, S. Charpak, M. Lauritzen, B. A. Macvicar and E. A. Newman (2010). "Glial and neuronal control of brain blood flow." Nature **468**(7321): 232-243.

Attwell, D. and C. Iadecola (2002). "The neural basis of functional brain imaging signals." Trends Neurosci **25**(12): 621-625.

Azevedo, F. A. C., L. R. B. Carvalho, L. T. Grinberg, J. M. Farfel, R. E. L. Ferretti, R. E. P. Leite, W. J. Filho, R. Lent and S. Herculano-Houzel (2009). "Equal numbers of neuronal and nonneuronal cells make the human brain an isometrically scaled-up primate brain." The Journal of Comparative Neurology **513**(5): 532-541.

Barnes, G. R. and A. Hillebrand (2003). "Statistical flattening of MEG beamformer images." Hum Brain Mapp **18**(1): 1-12.

Basser, P. J. and C. Pierpaoli (2011). "Microstructural and physiological features of tissues elucidated by quantitative-diffusion-tensor MRI. 1996." J Magn Reson **213**(2): 560-570.

Beer, A. L., T. Plank and M. W. Greenlee (2011). "Diffusion tensor imaging shows white matter tracts between human auditory and visual cortex." Exp Brain Res **213**(2-3): 299-308.

Behrens, T. E., H. J. Berg, S. Jbabdi, M. F. Rushworth and M. W. Woolrich (2007). "Probabilistic diffusion tractography with multiple fibre orientations: What can we gain?" Neuroimage **34**(1): 144-155.

Behrens, T. E., H. Johansen-Berg, M. W. Woolrich, S. M. Smith, C. A. Wheeler-Kingshott, P. A. Boulby, G. J. Barker, E. L. Sillery, K. Sheehan, O. Ciccarelli, A. J. Thompson, J. M. Brady

and P. M. Matthews (2003). "Non-invasive mapping of connections between human thalamus and cortex using diffusion imaging." Nat Neurosci **6**(7): 750-757.

Bennett, I. J., D. J. Madden, C. J. Vaidya, J. H. Howard, Jr. and D. V. Howard (2011). "White matter integrity correlates of implicit sequence learning in healthy aging." Neurobiol Aging **32**(12): 2317.e2311-2312.

Bestmann, S. and J. W. Krakauer (2015). "The uses and interpretations of the motor-evoked potential for understanding behaviour." Exp Brain Res **233**(3): 679-689.

Bestmann, S., C. C. Ruff, F. Blankenburg, N. Weiskopf, J. Driver and J. C. Rothwell (2008). "Mapping causal interregional influences with concurrent TMS-fMRI." Exp Brain Res **191**(4): 383-402.

Bhattacharyya, P. K., M. D. Phillips, L. A. Stone and M. J. Lowe (2011). "In-vivo MRS measurement of gray-matter and white-matter GABA concentration in sensorimotor cortex using a motion-controlled MEGA-PRESS Sequence." Magnetic resonance imaging **29**(3): 374-379.

Bianciardi, M., M. Fukunaga, P. van Gelderen, J. A. de Zwart and J. H. Duyn (2011). "Negative BOLD-fMRI signals in large cerebral veins." J Cereb Blood Flow Metab **31**(2): 401-412.

Biswal, B., F. Z. Yetkin, V. M. Haughton and J. S. Hyde (1995). "Functional connectivity in the motor cortex of resting human brain using echo-planar MRI." Magn Reson Med **34**(4): 537-541.

Blankenburg, F., B. Taskin, J. Ruben, M. Moosmann, P. Ritter, G. Curio and A. Villringer (2003). "Imperceptible stimuli and sensory processing impediment." Science **299**(5614): 1864.

Bloom, J. S. and G. W. Hynd (2005). "The role of the corpus callosum in interhemispheric transfer of information: excitation or inhibition?" Neuropsychol Rev **15**(2): 59-71.

Blüml, S. (2013). Magnetic Resonance Spectroscopy: Basics. MR Spectroscopy of Pediatric Brain Disorders. S. Blüml and A. Panigrahy. New York, NY, Springer New York**:** 11-23.

Boorman, L., S. Harris, M. Bruyns-Haylett, A. Kennerley, Y. Zheng, C. Martin, M. Jones, P. Redgrave and J. Berwick (2015). "Long-latency reductions in gamma power predict hemodynamic changes that underlie the negative BOLD signal." J Neurosci **35**(11): 4641-4656.

Boorman, L., A. J. Kennerley, D. Johnston, M. Jones, Y. Zheng, P. Redgrave and J. Berwick (2010). "Negative blood oxygen level dependence in the rat: a model for investigating the role of suppression in neurovascular coupling." J Neurosci **30**(12): 4285-4294.

Bressler, D., N. Spotswood and D. Whitney (2007). "Negative BOLD fMRI response in the visual cortex carries precise stimulus-specific information." PLoS One **2**(5): e410.

Brookes, M. J., J. Vrba, S. E. Robinson, C. M. Stevenson, A. M. Peters, G. R. Barnes, A. Hillebrand and P. G. Morris (2008). "Optimising experimental design for MEG beamformer imaging." Neuroimage **39**(4): 1788-1802.

Brookes, M. J., M. W. Woolrich and G. R. Barnes (2012). "Measuring functional connectivity in MEG: A multivariate approach insensitive to linear source leakage." Neuroimage **63**(2): 910-920.

Buckner, R. L., J. R. Andrews-Hanna and D. L. Schacter (2008). "The brain's default network: anatomy, function, and relevance to disease." Ann N Y Acad Sci **1124**: 1-38.

Buxton, R. B. and L. R. Frank (1997). "A model for the coupling between cerebral blood flow and oxygen metabolism during neural stimulation." J Cereb Blood Flow Metab **17**(1): 64-72.

Buxton, R. B., V. E. Griffeth, A. B. Simon and F. Moradi (2014). "Variability of the coupling of blood flow and oxygen metabolism responses in the brain: a problem for interpreting BOLD studies but potentially a new window on the underlying neural activity." Front Neurosci **8**: 139.

Buxton, R. B., E. C. Wong and L. R. Frank (1998). "Dynamics of blood flow and oxygenation changes during brain activation: the balloon model." Magn Reson Med **39**(6): 855-864.

Buzsáki, G. and A. Draguhn (2004). "Neuronal Oscillations in Cortical Networks." Science **304**(5679): 1926-1929.

Buzsáki, G., K. Kaila and M. Raichle (2007). "Inhibition and brain work." Neuron **56**(5): 771-783.

Cappe, C. and P. Barone (2005). "Heteromodal connections supporting multisensory integration at low levels of cortical processing in the monkey." Eur J Neurosci **22**(11): 2886-2902.

Cauli, B., X. K. Tong, A. Rancillac, N. Serluca, B. Lambolez, J. Rossier and E. Hamel (2004). "Cortical GABA interneurons in neurovascular coupling: relays for subcortical vasoactive pathways." J Neurosci **24**(41): 8940-8949.

Chatton, J.-Y., L. Pellerin and P. J. Magistretti (2003). "GABA uptake into astrocytes is not associated with significant metabolic cost: implications for brain imaging of inhibitory transmission." Proc Natl Acad Sci U S A **100**(21): 12456-12461.

Chen, J. J. and G. B. Pike (2009). "BOLD-specific cerebral blood volume and blood flow changes during neuronal activation in humans." NMR Biomed **22**(10): 1054-1062.

Chen, J. J. and G. B. Pike (2009). "Origins of the BOLD post-stimulus undershoot." Neuroimage **46**(3): 559-568.

Chen, R., B. Corwell and M. Hallett (1999). "Modulation of motor cortex excitability by median nerve and digit stimulation." Exp Brain Res **129**(1): 77-86.

Chen, R., D. Cros, A. Curra, V. Di Lazzaro, J. P. Lefaucheur, M. R. Magistris, K. Mills, K. M. Rosler, W. J. Triggs, Y. Ugawa and U. Ziemann (2008). "The clinical diagnostic utility of transcranial magnetic stimulation: report of an IFCN committee." Clin Neurophysiol **119**(3): 504-532.

Chen, R. and M. Hallett (1999). "The time course of changes in motor cortex excitability associated with voluntary movement." Can J Neurol Sci **26**(3): 163-169.

Chia, J., S. Fischer, S. Wickline and C. Lorenz (1999). Clinical application of vectorcardiographic triggered MR imaging. Proc ISMRM.

Chiarelli, P. A., D. P. Bulte, S. Piechnik and P. Jezzard (2007). "Sources of systematic bias in hypercapnia-calibrated functional MRI estimation of oxygen metabolism." Neuroimage **34**(1): 35-43.

Ciaramitaro, V. M., G. T. Buračas and G. M. Boynton (2007). "Spatial and Cross-Modal Attention Alter Responses to Unattended Sensory Information in Early Visual and Auditory Human Cortex." Journal of Neurophysiology **98**(4): 2399-2413.

Ciaramitaro, V. M., H. M. Chow and L. G. Eglington (2017). "Cross-modal attention influences auditory contrast sensitivity: Decreasing visual load improves auditory thresholds for amplitude- and frequency-modulated sounds." J Vis **17**(3): 20.

Civardi, C., R. Cantello, P. Asselman and J. C. Rothwell (2001). "Transcranial magnetic stimulation can be used to test connections to primary motor areas from frontal and medial cortex in humans." Neuroimage **14**(6): 1444-1453.

Cohen, A. L., D. A. Fair, N. U. Dosenbach, F. M. Miezin, D. Dierker, D. C. Van Essen, B. L. Schlaggar and S. E. Petersen (2008). "Defining functional areas in individual human brains using resting functional connectivity MRI." Neuroimage **41**(1): 45-57.

Cohen, M. X. (2014). "Analyzing neural time series data : theory and practice."

Cohen, M. X. (2017). "Where Does EEG Come From and What Does It Mean?" Trends in Neurosciences **40**(4): 208-218.

Cohen, M. X. and J. F. Cavanagh (2011). "Single-trial regression elucidates the role of prefrontal theta oscillations in response conflict." Front Psychol **2**: 30.

Cole, M. W., D. S. Bassett, J. D. Power, T. S. Braver and S. E. Petersen (2014). "Intrinsic and task-evoked network architectures of the human brain." Neuron **83**(1): 238-251.

Cole, M. W., T. Ito, D. S. Bassett and D. H. Schultz (2016). "Activity flow over resting-state networks shapes cognitive task activations." Nature neuroscience **19**(12): 1718-1726.

Corbetta, M. and G. L. Shulman (2002). "Control of goal-directed and stimulus-driven attention in the brain." Nat Rev Neurosci **3**(3): 201-215.

Cordes, D., V. M. Haughton, K. Arfanakis, J. D. Carew, P. A. Turski, C. H. Moritz, M. A. Quigley and M. E. Meyerand (2001). "Frequencies contributing to functional connectivity in the cerebral cortex in "resting-state" data." AJNR Am J Neuroradiol **22**(7): 1326-1333.

Cordes, D., V. M. Haughton, K. Arfanakis, G. J. Wendt, P. A. Turski, C. H. Moritz, M. A. Quigley and M. E. Meyerand (2000). "Mapping Functionally Related Regions of Brain with Functional Connectivity MR Imaging." American Journal of Neuroradiology **21**(9): 1636-1644.

Cuypers, K., H. Thijs and R. L. J. Meesen (2014). "Optimization of the Transcranial Magnetic Stimulation Protocol by Defining a Reliable Estimate for Corticospinal Excitability." PLoS ONE **9**(1): e86380.

Dai, T. H., J. Z. Liu, V. Sahgal, R. W. Brown and G. H. Yue (2001). "Relationship between muscle output and functional MRI-measured brain activation." Exp Brain Res **140**(3): 290-300.

Davis, T. L., K. K. Kwong, R. M. Weisskoff and B. R. Rosen (1998). "Calibrated functional MRI: mapping the dynamics of oxidative metabolism." Proc Natl Acad Sci U S A **95**(4): 1834-1839.

Debener, S., C. Kranczioch and I. Gutberlet (2010). EEG Quality: Origin and Reduction of the EEG Cardiac-Related Artefact. EEG - fMRI: Physiological Basis, Technique, and Applications. C. Mulert and L. Lemieux. Berlin, Heidelberg, Springer Berlin Heidelberg**:** 135-151.

Debener, S., K. J. Mullinger, R. K. Niazy and R. W. Bowtell (2008). "Properties of the ballistocardiogram artefact as revealed by EEG recordings at 1.5, 3 and 7 T static magnetic field strength." Int J Psychophysiol **67**(3): 189-199.

DeFelipe, J. (1993). "Neocortical neuronal diversity: chemical heterogeneity revealed by colocalization studies of classic neurotransmitters, neuropeptides, calcium-binding proteins, and cell surface molecules." Cereb Cortex **3**(4): 273-289.

Deng, Z.-D., S. H. Lisanby and A. V. Peterchev (2013). "Electric field depth–focality tradeoff in transcranial magnetic stimulation: Simulation comparison of 50 coil designs." Brain Stimulation **6**(1): 1-13.

Descoteaux, M., R. Deriche, T. R. Knosche and A. Anwander (2009). "Deterministic and probabilistic tractography based on complex fibre orientation distributions." IEEE Trans Med Imaging **28**(2): 269-286.

Devanne, H., F. Cassim, C. Ethier, L. Brizzi, A. Thevenon and C. Capaday (2006). "The comparable size and overlapping nature of upper limb distal and proximal muscle representations in the human motor cortex." Eur J Neurosci **23**(9): 2467-2476.

Devor, A., P. Tian, N. Nishimura, I. C. Teng, E. M. Hillman, S. N. Narayanan, I. Ulbert, D. A. Boas, D. Kleinfeld and A. M. Dale (2007). "Suppressed neuronal activity and concurrent arteriolar vasoconstriction may explain negative blood oxygenation level-dependent signal." J Neurosci **27**(16): 4452-4459.

DeYoe, E. A., P. Bandettini, J. Neitz, D. Miller and P. Winans (1994). "Functional magnetic resonance imaging (FMRI) of the human brain." J Neurosci Methods **54**(2): 171-187.

Di Lazzaro, V., A. Oliviero, F. Pilato, E. Saturno, M. Dileone, P. Mazzone, A. Insola, P. A. Tonali and J. C. Rothwell (2004). "The physiological basis of transcranial motor cortex stimulation in conscious humans." Clin Neurophysiol **115**(2): 255-266.

Di Lazzaro, V., A. Oliviero, P. Profice, A. Insola, P. Mazzone, P. Tonali and J. C. Rothwell (1999). "Direct demonstration of interhemispheric inhibition of the human motor cortex produced by transcranial magnetic stimulation." Exp Brain Res **124**(4): 520-524.

Di Lazzaro, V., U. Ziemann and R. N. Lemon (2008). "State of the art: Physiology of transcranial motor cortex stimulation." Brain Stimul **1**(4): 345-362.

Donahue, M. J., J. Near, J. U. Blicher and P. Jezzard (2010). "Baseline GABA concentration and fMRI response." NeuroImage **53**(2): 392-398.

Duque, J., L. Labruna, S. Verset, E. Olivier and R. B. Ivry (2012). "Dissociating the role of prefrontal and premotor cortices in controlling inhibitory mechanisms during motor preparation." J Neurosci **32**(3): 806-816.

Edden, R. A., G. Oeltzschner, A. D. Harris, N. A. Puts, K. L. Chan, V. O. Boer, M. Schar and P. B. Barker (2016). "Prospective frequency correction for macromolecule-suppressed GABA editing at 3T." J Magn Reson Imaging.

Edden, R. A., N. A. Puts and P. B. Barker (2012). "Macromolecule-suppressed GABA-edited magnetic resonance spectroscopy at 3T." Magn Reson Med **68**(3): 657-661.

Edden, R. A. E., G. Oeltzschner, A. D. Harris, N. A. J. Puts, K. L. Chan, V. O. Boer, M. Schär and P. B. Barker (2016). "Prospective frequency correction for macromolecule-suppressed GABA editing at 3T." Journal of Magnetic Resonance Imaging **44**(6): 1474-1482.

Eichele, T., M. Moosmann, L. Wu, I. Gutberlet and S. Debener (2010). "Removal of MRI artifacts from EEG recordings." Simultaneous EEG and fMRI: Recording, Analysis and Application: 95-106.

Enager, P., H. Piilgaard, N. Offenhauser, A. Kocharyan, P. Fernandes, E. Hamel and M. Lauritzen (2009). "Pathway-specific variations in neurovascular and neurometabolic coupling in rat primary somatosensory cortex." J Cereb Blood Flow Metab **29**(5): 976-986.

Enzi, B., N. W. Duncan, J. Kaufmann, C. Tempelmann, C. Wiebking and G. Northoff (2012). "Glutamate modulates resting state activity in the perigenual anterior cingulate cortex - a combined fMRI-MRS study." Neuroscience **227**: 102-109.

Fabri, M., G. Polonara, U. Salvolini and T. Manzoni (2005). "Bilateral cortical representation of the trunk midline in human first somatic sensory area." Hum Brain Mapp **25**(3): 287-296.

Fair, D. A., B. L. Schlaggar, A. L. Cohen, F. M. Miezin, N. U. Dosenbach, K. K. Wenger, M. D. Fox, A. Z. Snyder, M. E. Raichle and S. E. Petersen (2007). "A method for using blocked and event-related fMRI data to study "resting state" functional connectivity." Neuroimage **35**(1): 396-405.

Feige, B., K. Scheffler, F. Esposito, F. Di Salle, J. Hennig and E. Seifritz (2005). "Cortical and subcortical correlates of electroencephalographic alpha rhythm modulation." J Neurophysiol **93**(5): 2864-2872.

Feinberg, D. A., T. G. Reese and V. J. Wedeen (2002). "Simultaneous echo refocusing in EPI." Magnetic Resonance in Medicine **48**(1): 1-5.

Ferbert, A., A. Priori, J. C. Rothwell, B. L. Day, J. G. Colebatch and C. D. Marsden (1992). "Interhemispheric inhibition of the human motor cortex." J Physiol **453**: 525-546.

Fergus, A. and K. S. Lee (1997). "GABAergic regulation of cerebral microvascular tone in the rat." J Cereb Blood Flow Metab **17**(9): 992-1003.

Figley, C. R. and P. W. Stroman (2011). "The role(s) of astrocytes and astrocyte activity in neurometabolism, neurovascular coupling, and the production of functional neuroimaging signals." Eur J Neurosci **33**(4): 577-588.

Fisher, R. J., Y. Nakamura, S. Bestmann, J. C. Rothwell and H. Bostock (2002). "Two phases of intracortical inhibition revealed by transcranial magnetic threshold tracking." Exp Brain Res **143**(2): 240-248.

Floyer-Lea, A., M. Wylezinska, T. Kincses and P. M. Matthews (2006). "Rapid modulation of GABA concentration in human sensorimotor cortex during motor learning." J Neurophysiol **95**(3): 1639-1644.

Fox, M. D., A. Z. Snyder, J. L. Vincent, M. Corbetta, D. C. Van Essen and M. E. Raichle (2005). "The human brain is intrinsically organized into dynamic, anticorrelated functional networks." Proc Natl Acad Sci U S A **102**(27): 9673-9678.

Fox, M. D., A. Z. Snyder, J. L. Vincent and M. E. Raichle (2007). "Intrinsic fluctuations within cortical systems account for intertrial variability in human behavior." Neuron **56**(1): 171-184.

Fox, P. T. and M. E. Raichle (1986). "Focal physiological uncoupling of cerebral blood flow and oxidative metabolism during somatosensory stimulation in human subjects." Proc Natl Acad Sci U S A **83**(4): 1140-1144.

Fox, P. T., M. E. Raichle, M. A. Mintun and C. Dence (1988). "Nonoxidative glucose consumption during focal physiologic neural activity." Science **241**(4864): 462-464.

Freund, T. F. and G. Buzsáki (1996). "Interneurons of the hippocampus." Hippocampus **6**(4): 347-470.

Friston, K. J., C. D. Frith, P. F. Liddle and R. S. Frackowiak (1993). "Functional connectivity: the principal-component analysis of large (PET) data sets." J Cereb Blood Flow Metab **13**(1): 5-14.

Fuchs, A. (2007). Beamforming and Its Applications to Brain Connectivity. Handbook of Brain Connectivity. V. K. Jirsa and A. R. McIntosh. Berlin, Heidelberg, Springer Berlin Heidelberg**:** 357-378.

Fuggetta, G., A. Fiaschi and P. Manganotti (2005). "Modulation of cortical oscillatory activities induced by varying single-pulse transcranial magnetic stimulation intensity over the left primary motor area: A combined EEG and TMS study." NeuroImage **27**(4): 896-908.

Garcia, D. M., G. Duhamel and D. C. Alsop (2005). "Efficiency of inversion pulses for background suppressed arterial spin labeling." Magnetic Resonance in Medicine **54**(2): 366-372.

Gauthier, C. J. and R. D. Hoge (2013). "A generalized procedure for calibrated MRI incorporating hyperoxia and hypercapnia." Hum Brain Mapp **34**(5): 1053-1069.

Gauthier, C. J., C. Madjar, F. B. Tancredi, B. Stefanovic and R. D. Hoge (2011). "Elimination of visually evoked BOLD responses during carbogen inhalation: implications for calibrated MRI." Neuroimage **54**(2): 1001-1011.

Gazzaniga, M. S., J. D. Holtzman and C. S. Smylie (1987). "Speech without conscious awareness." Neurology **37**(4): 682-685.

Genc, E., S. Ocklenburg, W. Singer and O. Gunturkun (2015). "Abnormal interhemispheric motor interactions in patients with callosal agenesis." Behav Brain Res **293**: 1-9.

Glover, G. H., T. Q. Li and D. Ress (2000). "Image-based method for retrospective correction of physiological motion effects in fMRI: RETROICOR." Magn Reson Med **44**(1): 162-167.

Goense, J., H. Merkle and N. K. Logothetis (2012). "High-Resolution fMRI Reveals Laminar Differences in Neurovascular Coupling between Positive and Negative BOLD Responses." Neuron **76**(3): 629-639.

Gordon, G. R., H. B. Choi, R. L. Rungta, G. C. Ellis-Davies and B. A. MacVicar (2008). "Brain metabolism dictates the polarity of astrocyte control over arterioles." Nature **456**(7223): 745-749.

Greicius, M. D. and V. Menon (2004). "Default-mode activity during a passive sensory task: uncoupled from deactivation but impacting activation." J Cogn Neurosci **16**(9): 1484-1492.

Greicius, M. D., K. Supekar, V. Menon and R. F. Dougherty (2009). "Resting-state functional connectivity reflects structural connectivity in the default mode network." Cereb Cortex **19**(1): 72-78.

Greve, D. N. and B. Fischl (2009). "Accurate and robust brain image alignment using boundary-based registration." Neuroimage **48**(1): 63-72.

Griffeth, V. E. M., J. E. Perthen and R. B. Buxton (2011). "Prospects for quantiative fMRI: Investigating the effects of caffine on baseline oxygen metabolism and the response to a visual stimulus in humans." Neuroimage **57**: 809-816.

Groppa, S., A. Oliviero, A. Eisen, A. Quartarone, L. G. Cohen, V. Mall, A. Kaelin-Lang, T. Mima, S. Rossi, G. W. Thickbroom, P. M. Rossini, U. Ziemann, J. Valls-Solé and H. R. Siebner (2012). "A practical guide to diagnostic transcranial magnetic stimulation: Report of an IFCN committee." Clinical neurophysiology : official journal of the International Federation of Clinical Neurophysiology **123**(5): 858-882.

Gross, J., J. Kujala, M. Hämäläinen, L. Timmermann, A. Schnitzler and R. Salmelin (2001). "Dynamic imaging of coherent sources: Studying neural interactions in the human brain." Proceedings of the National Academy of Sciences **98**(2): 694-699.

Hairston, W. D., D. A. Hodges, R. Casanova, S. Hayasaka, R. Kraft, J. A. Maldjian and J. H. Burdette (2008). "Closing the mind's eye: deactivation of visual cortex related to auditory task difficulty." Neuroreport **19**(2): 151-154.

Hallett, M. (2007). "Transcranial magnetic stimulation: a primer." Neuron **55**(2): 187-199.

Harada, M., H. Kubo, A. Nose, H. Nishitani and T. Matsuda (2011). "Measurement of variation in the human cerebral GABA level by in vivo MEGA-editing proton MR spectroscopy using a clinical 3 T instrument and its dependence on brain region and the female menstrual cycle." Hum Brain Mapp **32**(5): 828-833.

Harel, N., S.-P. Lee, T. Nagaoka, D.-S. Kim and S.-G. Kim (2002). "Origin of negative blood oxygenation level-dependent fMRI signals." J Cereb Blood Flow Metab **22**(8): 908-917.

Harris, A. D., N. A. J. Puts, B. A. Anderson, S. Yantis, J. J. Pekar, P. B. Barker and R. A. E. Edden (2015). "Multi-Regional Investigation of the Relationship between Functional MRI Blood Oxygenation Level Dependent (BOLD) Activation and GABA Concentration." PLoS ONE **10**(2): e0117531.

Harris, J. J., C. Reynell and D. Attwell (2011). "The physiology of developmental changes in BOLD functional imaging signals." Developmental Cognitive Neuroscience **1**(3): 199-216.

Harris, J. M. and J. Scott (2012). "Visual Cortex: Anatomy, Functions and Injuries." Nova Science Publishers.

Harris, R. K., E. D. Becker, S. M. De Menezes, P. Granger, R. E. Hoffman and K. W. Zilm (2008). "Further conventions for NMR shielding and chemical shifts (IUPAC Recommendations 2008)." Magn Reson Chem **46**(6): 582-598.

Hasan, A., J. M. Galea, E. P. Casula, P. Falkai, S. Bestmann and J. C. Rothwell (2013). "Muscle and timing-specific functional connectivity between the dorsolateral prefrontal cortex and the primary motor cortex." Journal of cognitive neuroscience **25**(4): 558-570.

Heeger, D. J. and D. Ress (2002). "What does fMRI tell us about neuronal activity?" Nat Rev Neurosci **3**(2): 142-151.

Hernandez-Pavon, J. C., J. Metsomaa, T. Mutanen, M. Stenroos, H. Maki, R. J. Ilmoniemi and J. Sarvas (2012). "Uncovering neural independent components from highly artifactual TMS-evoked EEG data." J Neurosci Methods **209**(1): 144-157.

Herring, J. D., G. Thut, O. Jensen and T. O. Bergmann (2015). "Attention Modulates TMS-Locked Alpha Oscillations in the Visual Cortex." The Journal of Neuroscience **35**(43): 14435-14447.

Hillebrand, A., K. D. Singh, I. E. Holliday, P. L. Furlong and G. R. Barnes (2005). "A new approach to neuroimaging with magnetoencephalography." Hum Brain Mapp **25**(2): 199-211.

Hoffmann, S. and M. Falkenstein (2008). "The Correction of Eye Blink Artefacts in the EEG: A Comparison of Two Prominent Methods." PLoS ONE **3**(8): e3004.

Holtzman, J. D. (1984). "Interactions between cortical and subcortical visual areas: evidence from human commissurotomy patients." Vision Res **24**(8): 801-813.

Honey, C. J., O. Sporns, L. Cammoun, X. Gigandet, J. P. Thiran, R. Meuli and P. Hagmann (2009). "Predicting human resting-state functional connectivity from structural connectivity." Proceedings of the National Academy of Sciences **106**(6): 2035-2040.

Hu, X., T. H. Le and K. Ugurbil (1997). "Evaluation of the early response in fMRI in individual subjects using short stimulus duration." Magn Reson Med **37**(6): 877-884.

Hu, Y., X. Chen, H. Gu and Y. Yang (2013). "Resting-state glutamate and GABA concentrations predict task-induced deactivation in the default mode network." J Neurosci **33**(47): 18566-18573.

Huang, H., J. Zhang, P. C. van Zijl and S. Mori (2004). "Analysis of noise effects on DTI-based tractography using the brute-force and multi-ROI approach." Magn Reson Med **52**(3): 559-565.

Huber, L., J. Goense, A. J. Kennerley, D. Ivanov, S. N. Krieger, J. Lepsien, R. Trampel, R. Turner and H. E. Moller (2014). "Investigation of the neurovascular coupling in positive and negative BOLD responses in human brain at 7 T." Neuroimage **97**: 349-362.

Huettel, S. A., A. W. Song and G. McCarthy (2014). Functional Magnetic Resonance Imaging, Sinauer.

Huo, X., J. Xiang, Y. Wang, E. G. Kirtman, R. Kotecha, H. Fujiwara, N. Hemasilpin, D. F. Rose and T. Degrauw (2010). "Gamma oscillations in the primary motor cortex studied with MEG." Brain Dev **32**(8): 619-624.

Ilmoniemi, R. J. and D. Kicic (2010). "Methodology for combined TMS and EEG." Brain Topogr **22**(4): 233-248.

Ismail, S. S., M. Mohamad, S. O. Syazarina and W. Y. Nafisah (2014). "Hand grips strength effect on motor function in human brain using fMRI: a pilot study." Journal of Physics: Conference Series **546**(1): 012005.

Iurilli, G., D. Ghezzi, U. Olcese, G. Lassi, C. Nazzaro, R. Tonini, V. Tucci, F. Benfenati and P. Medini (2012). "Sound-Driven Synaptic Inhibition in Primary Visual Cortex." Neuron **73**(4-2): 814-828.

Ivanov, D., A. Gardumi, R. A. M. Haast, J. Pfeuffer, B. A. Poser and K. Uludağ (2017). "Comparison of 3T and 7T ASL techniques for concurrent functional perfusion and BOLD studies." NeuroImage **156**: 363-376.

Jellison, B. J., A. S. Field, J. Medow, M. Lazar, M. S. Salamat and A. L. Alexander (2004). "Diffusion Tensor Imaging of Cerebral White Matter: A Pictorial Review of Physics, Fiber Tract Anatomy, and Tumor Imaging Patterns." American Journal of Neuroradiology **25**(3): 356-369.

Jenkinson, M., P. Bannister, M. Brady and S. Smith (2002). "Improved optimization for the robust and accurate linear registration and motion correction of brain images." Neuroimage **17**(2): 825-841.

Jenkinson, M. and S. Smith (2001). "A global optimisation method for robust affine registration of brain images." Med Image Anal **5**(2): 143-156.

Jensen, J. E., B. Frederick Bde and P. F. Renshaw (2005). "Grey and white matter GABA level differences in the human brain using two-dimensional, J-resolved spectroscopic imaging." NMR Biomed **18**(8): 570-576.

Jensen, O., J. Gelfand, J. Kounios and J. E. Lisman (2002). "Oscillations in the alpha band (9-12 Hz) increase with memory load during retention in a short-term memory task." Cereb Cortex **12**(8): 877-882.

Jensen, O. and A. Mazaheri (2010). "Shaping functional architecture by oscillatory alpha activity: gating by inhibition." Front Hum Neurosci **4**: 186.

Jensen, O. and C. D. Tesche (2002). "Frontal theta activity in humans increases with memory load in a working memory task." Eur J Neurosci **15**(8): 1395-1399.

Johansen-Berg, H., T. E. J. Behrens, M. D. Robson, I. Drobnjak, M. F. S. Rushworth, J. M. Brady, S. M. Smith, D. J. Higham and P. M. Matthews (2004). "Changes in connectivity profiles define functionally distinct regions in human medial frontal cortex." Proceedings of the National Academy of Sciences of the United States of America **101**(36): 13335-13340.

Jones, D. K., T. R. Knosche and R. Turner (2013). "White matter integrity, fiber count, and other fallacies: the do's and don'ts of diffusion MRI." Neuroimage **73**: 239-254.

Kannurpatti, S. S. and B. B. Biswal (2004). "Negative functional response to sensory stimulation and its origins." J Cereb Blood Flow Metab **24**(6): 703-712.

Kastrup, A., J. Baudewig, S. Schnaudigel, R. Huonker, L. Becker, J. M. Sohns, P. Dechent, C. Klingner and O. W. Witte (2008). "Behavioral correlates of negative BOLD signal changes in the primary somatosensory cortex." Neuroimage **41**(4): 1364-1371.

Kastrup, A., G. Kruger, T. Neumann-Haefelin, G. H. Glover and M. E. Moseley (2002). "Changes of cerebral blood flow, oxygenation, and oxidative metabolism during graded motor activation." Neuroimage **15**(1): 74-82.

Khalsa, S., S. D. Mayhew, M. Chechlacz, M. Bagary and A. P. Bagshaw (2013). "The structural and functional connectivity of the posterior cingulate cortex: Comparison between deterministic and probabilistic tractography for the investigation of structure-function relationships." Neuroimage **In Press**.

Kiers, L., D. Cros, K. H. Chiappa and J. Fang (1993). "Variability of motor potentials evoked by transcranial magnetic stimulation." Electroencephalogr Clin Neurophysiol **89**(6): 415-423.

Killackey, H. P., H. J. Gould, 3rd, C. G. Cusick, T. P. Pons and J. H. Kaas (1983). "The relation of corpus callosum connections to architectonic fields and body surface maps in sensorimotor cortex of new and old world monkeys." J Comp Neurol **219**(4): 384-419.

Kim, S. G. and S. Ogawa (2012). "Biophysical and physiological origins of blood oxygenation level-dependent fMRI signals." J Cereb Blood Flow Metab **32**(7): 1188-1206.

Klimesch, W., P. Sauseng and S. Hanslmayr (2007). "EEG alpha oscillations: the inhibition-timing hypothesis." Brain Res Rev **53**(1): 63-88.

Klingner, C. M., C. Hasler, S. Brodoehl and O. W. Witte (2010). "Dependence of the negative BOLD response on somatosensory stimulus intensity." Neuroimage **53**(1): 189-195.

Koch, G., M. F. Del Olmo, B. Cheeran, S. Schippling, C. Caltagirone, J. Driver and J. C. Rothwell (2008). "Functional interplay between posterior parietal and ipsilateral motor cortex revealed by twin-coil TMS during reach planning toward contralateral space." The Journal of neuroscience : the official journal of the Society for Neuroscience **28**(23): 5944-5953.

Koos, T. and J. M. Tepper (1999). "Inhibitory control of neostriatal projection neurons by GABAergic interneurons." Nat Neurosci **2**(5): 467-472.

Kornak, J., D. A. Hall and M. P. Haggard (2011). "Spatially Extended fMRI Signal Response to Stimulus in Non-Functionally Relevant Regions of the Human Brain: Preliminary Results." The Open Neuroimaging Journal **5**: 24-32.

Koshino, Y. and E. Niedermeyer (1975). "Enhancement of Rolandic mu-rhythm by pattern vision." Electroencephalography and Clinical Neurophysiology **38**(5): 535-538.

Krakow, K., P. J. Allen, M. R. Symms, L. Lemieux, O. Josephs and D. R. Fish (2000). "EEG recording during fMRI experiments: image quality." Hum Brain Mapp **10**(1): 10-15.

Kucukaltun-Yildirim, E., D. Pantazis and R. M. Leahy (2006). "Task-based comparison of inverse methods in magnetoencephalography." IEEE Trans Biomed Eng **53**(9): 1783-1793.

Kwong, K. K., J. W. Belliveau, D. A. Chesler, I. E. Goldberg, R. M. Weisskoff, B. P. Poncelet, D. N. Kennedy, B. E. Hoppel, M. S. Cohen and R. Turner (1992). "Dynamic magnetic resonance imaging of human brain activity during primary sensory stimulation." Proc Natl Acad Sci U S A **89**(12): 5675-5679.

Laurienti, P. J., J. H. Burdette, M. T. Wallace, Y. F. Yen, A. S. Field and B. E. Stein (2002). "Deactivation of sensory-specific cortex by cross-modal stimuli." J Cogn Neurosci **14**(3): 420-429.

Lauritzen, M., C. Mathiesen, K. Schaefer and K. J. Thomsen (2012). "Neuronal inhibition and excitation, and the dichotomic control of brain hemodynamic and oxygen responses." Neuroimage **62**(2): 1040-1050.

Leech, R., S. Kamourieh, C. F. Beckmann and D. J. Sharp (2011). "Fractionating the default mode network: distinct contributions of the ventral and dorsal posterior cingulate cortex to cognitive control." J Neurosci **31**(9): 3217-3224.

Leithner, C., G. Royl, N. Offenhauser, M. Füchtemeier, M. Kohl-Bareis, A. Villringer, U. Dirnagl and U. Lindauer (2010). "Pharmacological uncoupling of activation induced increases in CBF and CMRO(2)." Journal of Cerebral Blood Flow and Metabolism: Official Journal of the International Society of Cerebral Blood Flow and Metabolism **30**(2): 311-322.

Lepage, J. F., D. Saint-Amour and H. Theoret (2008). "EEG and neuronavigated single-pulse TMS in the study of the observation/execution matching system: are both techniques measuring the same process?" J Neurosci Methods **175**(1): 17-24.

Liang, C. L., B. M. Ances, J. E. Perthen, F. Moradi, J. Liau, G. T. Buracas, S. R. Hopkins and R. B. Buxton (2013). "Luminance contrast of a visual stimulus modulates the BOLD response more than the cerebral blood flow response in the human brain." Neuroimage **64**: 104-111.

Liepert, J., C. Dettmers, C. Terborg and C. Weiller (2001). "Inhibition of ipsilateral motor cortex during phasic generation of low force." Clin Neurophysiol **112**(1): 114-121.

Lin, A. L., P. T. Fox, J. Hardies, T. Q. Duong and J. H. Gao (2010). "Nonlinear coupling between cerebral blood flow, oxygen consumption, and ATP production in human visual cortex." Proc Natl Acad Sci U S A **107**(18): 8446-8451.

Liu, Y., H. Shen, Z. Zhou and D. Hu (2011). "Sustained negative BOLD response in human fMRI finger tapping task." PLoS One **6**(8): e23839.

Logothetis, N. K. (2003). "The underpinnings of the BOLD functional magnetic resonance imaging signal." J Neurosci **23**(10): 3963-3971.

Logothetis, N. K., J. Pauls, M. Augath, T. Trinath and A. Oeltermann (2001). "Neurophysiological investigation of the basis of the fMRI signal." Nature **412**(6843): 150-157.

Lopes da Silva, F. (1991). "Neural mechanisms underlying brain waves: from neural membranes to networks." Electroencephalogr Clin Neurophysiol **79**(2): 81-93.

Lopes da Silva, F. (2013). "EEG and MEG: Relevance to Neuroscience." Neuron **80**(5): 1112-1128.

Lowe, M. J., B. J. Mock and J. A. Sorenson (1998). "Functional connectivity in single and multislice echoplanar imaging using resting-state fluctuations." Neuroimage **7**(2): 119-132.

Maeder, P. P., R. A. Meuli, M. Adriani, A. Bellmann, E. Fornari, J.-P. Thiran, A. Pittet and S. Clarke (2001). "Distinct Pathways Involved in Sound Recognition and Localization: A Human fMRI Study." NeuroImage **14**(4): 802-816.

Maggioni, E., E. Molteni, C. Zucca, G. Reni, S. Cerutti, F. M. Triulzi, F. Arrigoni and A. M. Bianchi (2015). "Investigation of negative BOLD responses in human brain through NIRS technique. A visual stimulation study." NeuroImage **108**: 410-422.

Mandelkow, H., P. Halder, P. Boesiger and D. Brandeis (2006). "Synchronization facilitates removal of MRI artefacts from concurrent EEG recordings and increases usable bandwidth." Neuroimage **32**(3): 1120-1126.

Mandeville, J. B., J. J. Marota, B. E. Kosofsky, J. R. Keltner, R. Weissleder, B. R. Rosen and R. M. Weisskoff (1998). "Dynamic functional imaging of relative cerebral blood volume during rat forepaw stimulation." Magn Reson Med **39**(4): 615-624.

Mark, C. I., J. A. Fisher and G. B. Pike (2011). "Improved fMRI calibration: precisely controlled hyperoxic versus hypercapnic stimuli." Neuroimage **54**(2): 1102-1111.

Martin, D. L. and K. Rimvall (1993). "Regulation of gamma-aminobutyric acid synthesis in the brain." J Neurochem **60**(2): 395-407.

Mathewson, K. E., A. Lleras, D. M. Beck, M. Fabiani, T. Ro and G. Gratton (2011). "Pulsed Out of Awareness: EEG Alpha Oscillations Represent a Pulsed-Inhibition of Ongoing Cortical Processing." Frontiers in Psychology **2**.

Mayhew, S. D., N. Hylands-White, C. Porcaro, S. W. Derbyshire and A. P. Bagshaw (2013). "Intrinsic variability in the human response to pain is assembled from multiple, dynamic brain processes." Neuroimage **75**: 68-78.

Mayhew, S. D., G. D. Iannetti, M. W. Woolrich and R. G. Wise (2006). "Automated single-trial measurement of amplitude and latency of laser-evoked potentials (LEPs) using multiple linear regression." Clin Neurophysiol **117**(6): 1331-1344.

Mayhew, S. D., K. J. Mullinger, A. P. Bagshaw, R. Bowtell and S. T. Francis (2014). "Investigating intrinsic connectivity networks using simultaneous BOLD and CBF measurements." Neuroimage **99**: 111-121.

Mayhew, S. D., K. J. Mullinger, D. Ostwald, C. Porcaro, R. Bowtell, A. P. Bagshaw and S. T. Francis (2016). "Global signal modulation of single-trial fMRI response variability: Effect on positive vs negative BOLD response relationship." Neuroimage **133**: 62-74.

Mayhew, S. D., D. Ostwald, C. Porcaro and A. P. Bagshaw (2013). "Spontaneous EEG alpha oscillation interacts with positive and negative BOLD responses in the visual-auditory cortices and default-mode network." Neuroimage **76**: 362-372.

Mazaheri, A. and O. Jensen (2010). "Shaping Functional Architecture by Oscillatory Alpha Activity: Gating by Inhibition." Frontiers in Human Neuroscience **4**(4): 186.

Mazerolle, E. L., S. D. Beyea, J. R. Gawryluk, K. D. Brewer, C. V. Bowen and R. C. N. D'Arcy (2010). "Confirming white matter fMRI activation in the corpus callosum: Co-localization with DTI tractography." NeuroImage **50**(2): 616-621.

McKiernan, K. A., J. N. Kaufman, J. Kucera-Thompson and J. R. Binder (2003). "A parametric manipulation of factors affecting task-induced deactivation in functional neuroimaging." J Cogn Neurosci **15**(3): 394-408.

McRobbie, D., Moore, E., Graves, M., & Prince, M. (2017). What You Set is What You Get: Basic Image Optimization. MRI from Picture to Proton. D. W. McRobbie, E. A. Moore, M. J. Graves and M. R. Prince. Cambridge, Cambridge University Press**:** 67-80.

McRobbie, D. W., E. A. Moore, M. J. Graves and M. R. Prince (2017). Getting in Tune: Resonance and Relaxation. MRI from Picture to Proton. D. W. McRobbie, E. A. Moore, M. J. Graves and M. R. Prince. Cambridge, Cambridge University Press**:** 124-143.

Mennes, M., C. Kelly, X.-N. Zuo, A. Di Martino, B. B. Biswal, F. X. Castellanos and M. P. Milham (2010). "Inter-individual differences in resting-state functional connectivity predict task-induced BOLD activity." Neuroimage **50**(4): 1690-1701.

Menon, R. S., S. Ogawa, X. Hu, J. P. Strupp, P. Anderson and K. Uğurbil (1995). "BOLD Based Functional MRI at 4 Tesla Includes a Capillary Bed Contribution: Echo-Planar Imaging Correlates with Previous Optical Imaging Using Intrinsic Signals." Magnetic Resonance in Medicine **33**(3): 453-459.

Mescher, M., H. Merkle, J. Kirsch, M. Garwood and R. Gruetter (1998). "Simultaneous in vivo spectral editing and water suppression." NMR Biomed **11**(6): 266-272.

Meyer, B. U., S. Roricht, H. Grafin von Einsiedel, F. Kruggel and A. Weindl (1995). "Inhibitory and excitatory interhemispheric transfers between motor cortical areas in normal humans and patients with abnormalities of the corpus callosum." Brain **118 (Pt 2)**: 429-440.

Michels, L., E. Martin, P. Klaver, R. Edden, F. Zelaya, D. J. Lythgoe, R. Lüchinger, D. Brandeis and R. L. O'Gorman (2012). "Frontal GABA Levels Change during Working Memory." PLOS ONE **7**(4): e31933.

Mitchell, W. K., M. R. Baker and S. N. Baker (2007). "Muscle responses to transcranial stimulation in man depend on background oscillatory activity." J Physiol **583**(Pt 2): 567-579.

Morris, D. M., K. V. Embleton and G. J. M. Parker (2008). "Probabilistic fibre tracking: Differentiation of connections from chance events." NeuroImage **42**(4): 1329-1339.

Mozolic, J. L., D. Joyner, C. E. Hugenschmidt, A. M. Peiffer, R. A. Kraft, J. A. Maldjian and P. J. Laurienti (2008). "Cross-modal deactivations during modality-specific selective attention." BMC Neurol **8**: 35.

Muellbacher, W., S. Facchini, B. Boroojerdi and M. Hallett (2000). "Changes in motor cortex excitability during ipsilateral hand muscle activation in humans." Clin Neurophysiol **111**(2): 344-349.

Mukamel, R., H. Gelbard, A. Arieli, U. Hasson, I. Fried and R. Malach (2005). "Coupling between neuronal firing, field potentials, and FMRI in human auditory cortex." Science **309**(5736): 951-954.

Mulert, C., G. Leicht, P. Hepp, V. Kirsch, S. Karch, O. Pogarell, M. Reiser, U. Hegerl, L. Jager, H. J. Moller and R. W. McCarley (2010). "Single-trial coupling of the gamma-band response and the corresponding BOLD signal." Neuroimage **49**(3): 2238-2247.

Mulert, C. and L. Lemieux, Eds. (2010). Simultaneous EEG-fMRI, Springer-Verlag Berlin.

Mullinger, K. and R. Bowtell (2010). Influence of EEG Equipment on MR Image Quality. Simultaneous EEG and fMRI-Recording, Analysis, and Application, Oxford Univ Press.

Mullinger, K. J. and R. Bowtell (2011). "Combining EEG and FMRI." Methods in molecular biology (Clifton, N.J.) **711**: 303-326.

Mullinger, K. J., M. T. Cherukara, R. B. Buxton, S. T. Francis and S. D. Mayhew (2017). "Post-stimulus fMRI and EEG responses: Evidence for a neuronal origin hypothesised to be inhibitory." NeuroImage **157**: 388-399.

Mullinger, K. J., S. D. Mayhew, A. P. Bagshaw, R. Bowtell and S. T. Francis (2011). "Negative BOLD and CBF responses are predicted by natural variations in evoked EEG response to a median nerve stimulus in humans." Proc. Intl. Soc. Mag. Reson. Med. **19**(3497): 109.

Mullinger, K. J., S. D. Mayhew, A. P. Bagshaw, R. Bowtell and S. T. Francis (2014). "Evidence that the negative BOLD response is neuronal in origin: a simultaneous EEG-BOLD-CBF study in humans." Neuroimage **94**: 263-274.

Mullinger, K. J., P. S. Morgan and R. W. Bowtell (2008). "Improved artifact correction for combined electroencephalography/functional MRI by means of synchronization and use of vectorcardiogram recordings." J Magn Reson Imaging **27**(3): 607-616.

Mullins, P. G., D. J. McGonigle, R. L. O'Gorman, N. A. Puts, R. Vidyasagar, C. J. Evans and R. A. Edden (2014). "Current practice in the use of MEGA-PRESS spectroscopy for the detection of GABA." Neuroimage **86**: 43-52.

Muthukumaraswamy, S. D. (2010). "Functional properties of human primary motor cortex gamma oscillations." J Neurophysiol **104**(5): 2873-2885.

Muthukumaraswamy, S. D., R. A. E. Edden, D. K. Jones, J. B. Swettenham and K. D. Singh (2009). "Resting GABA concentration predicts peak gamma frequency and fMRI amplitude in response to visual stimulation in humans." Proc Natl Acad Sci U S A **106**(20): 8356-8361.

Myers, R. E. (1962). "Commissural connections between occipital lobes of the monkey." J Comp Neurol **118**: 1-16.

Neuper, C. and G. Pfurtscheller (2001). "Event-related dynamics of cortical rhythms: frequency-specific features and functional correlates." Int J Psychophysiol **43**(1): 41-58.

Northoff, G., A. Heinzel, F. Bermpohl, R. Niese, A. Pfennig, A. Pascual-Leone and G. Schlaug (2004). "Reciprocal modulation and attenuation in the prefrontal cortex: an fMRI study on emotional-cognitive interaction." Hum Brain Mapp **21**(3): 202-212.

Northoff, G., M. Walter, R. F. Schulte, J. Beck, U. Dydak, A. Henning, H. Boeker, S. Grimm and P. Boesiger (2007). "GABA concentrations in the human anterior cingulate cortex predict negative BOLD responses in fMRI." Nat Neurosci **10**(12): 1515-1517.

Oeltzschner, G., N. Hoogenboom, T. Baumgarten, H.-J. Wittsack and A. Schnitzler (2014). "Absolute GABA spectroscopy with MEGA-PRESS and watermapping in sensorimotor and visual cortex and correlation to handedness." European Journal of Medical Research **19**(Suppl 1): S28-S28.

Ogawa, S., T. M. Lee, A. R. Kay and D. W. Tank (1990). "Brain magnetic resonance imaging with contrast dependent on blood oxygenation." Proc Natl Acad Sci U S A **87**(24): 9868-9872.

Onton, J., M. Westerfield, J. Townsend and S. Makeig (2006). "Imaging human EEG dynamics using independent component analysis." Neurosci Biobehav Rev **30**(6): 808-822.

Oostenveld, R., P. Fries, E. Maris and J. M. Schoffelen (2011). "FieldTrip: Open source software for advanced analysis of MEG, EEG, and invasive electrophysiological data." Comput Intell Neurosci **2011**: 156869.

Osipova, D., D. Hermes and O. Jensen (2008). "Gamma power is phase-locked to posterior alpha activity." PLoS One **3**(12): e3990.

Pasley, B. N., B. A. Inglis and R. D. Freeman (2007). "Analysis of oxygen metabolism implies a neural origin for the negative BOLD response in human visual cortex." Neuroimage **36**(2): 269-276.

Patel, A. B., R. A. de Graaf, G. F. Mason, D. L. Rothman, R. G. Shulman and K. L. Behar (2005). "The contribution of GABA to glutamate/glutamine cycling and energy metabolism in the rat cortex in vivo." Proceedings of the National Academy of Sciences of the United States of America **102**(15): 5588-5593.

Patton, H. D. and V. E. Amassian (1954). "Single and multiple-unit analysis of cortical stage of pyramidal tract activation." J Neurophysiol **17**(4): 345-363.

Paus, T., P. K. Sipila and A. P. Strafella (2001). "Synchronization of neuronal activity in the human primary motor cortex by transcranial magnetic stimulation: an EEG study." J Neurophysiol **86**(4): 1983-1990.

Pelled, G., D. A. Bergstrom, P. L. Tierney, R. S. Conroy, K. H. Chuang, D. Yu, D. A. Leopold, J. R. Walters and A. P. Koretsky (2009). "Ipsilateral cortical fMRI responses after peripheral nerve damage in rats reflect increased interneuron activity." Proc Natl Acad Sci U S A **106**(33): 14114-14119.

Pellerin, L. and P. J. Magistretti (1994). "Glutamate uptake into astrocytes stimulates aerobic glycolysis: a mechanism coupling neuronal activity to glucose utilization." Proceedings of the National Academy of Sciences of the United States of America **91**(22): 10625-10629.

Pfurtscheller, G. (1992). "Event-related synchronization (ERS): an electrophysiological correlate of cortical areas at rest." Electroencephalogr Clin Neurophysiol **83**(1): 62-69.

Pfurtscheller, G. and W. Klimesch (1991). "Event-related desynchronization during motor behavior and visual information processing." Electroencephalogr Clin Neurophysiol Suppl **42**: 58-65.

Pfurtscheller, G. and F. H. Lopes da Silva (2005). "EEG event-related desynchronisation (ERD) and event-related synchronisation." Electroencephalography: Basic Principles, Clinical Applications and Related Fields **Lippincott Williams and Wilkins, Philadephia.**(Niedermeyer, E., Lopes da Silva, F. (Eds)): 1003-1016.

Pfurtscheller, G., C. Neuper and W. Mohl (1994). "Event-related desynchronization (ERD) during visual processing." Int J Psychophysiol **16**(2-3): 147-153.

Pfurtscheller, G., A. Stancak, Jr. and C. Neuper (1996). "Event-related synchronization (ERS) in the alpha band--an electrophysiological correlate of cortical idling: a review." Int J Psychophysiol **24**(1-2): 39-46.

Pietrasanta, M., L. Restani and M. Caleo (2012). "The corpus callosum and the visual cortex: plasticity is a game for two." Neural Plast **2012**: 838672.

Preti, M. G., N. Makris, M. M. Lagana, G. Papadimitriou, F. Baglio, L. Griffanti, R. Nemni, P. Cecconi, C. F. Westin and G. Baselli (2012). "A novel approach of fMRI-guided tractography analysis within a group: construction of an fMRI-guided tractographic atlas." Conf Proc IEEE Eng Med Biol Soc **2012**: 2283-2286.

Price, C. J., B. Cauli, E. R. Kovacs, A. Kulik, B. Lambolez, R. Shigemoto and M. Capogna (2005). "Neurogliaform neurons form a novel inhibitory network in the hippocampal CA1 area." J Neurosci **25**(29): 6775-6786.

Puckett, A. M., J. R. Mathis and E. A. DeYoe (2014). "An investigation of positive and inverted hemodynamic response functions across multiple visual areas." Hum Brain Mapp **35**(11): 5550-5564.

Puts, N. A. J. and R. A. E. Edden (2012). "In vivo magnetic resonance spectroscopy of GABA: A methodological review()." Progress in Nuclear Magnetic Resonance Spectroscopy **60**: 29-41.

Ridgway, J. P. (2010). "Cardiovascular magnetic resonance physics for clinicians: part I." Journal of Cardiovascular Magnetic Resonance **12**(1): 71.

Rigden, J. S. (1986). "Quantum states and precession: The two discoveries of NMR." Reviews of Modern Physics **58**(2): 433-448.

Rihs, T. A., C. M. Michel and G. Thut (2007). "Mechanisms of selective inhibition in visual spatial attention are indexed by alpha-band EEG synchronization." Eur J Neurosci **25**(2): 603-610.

Rihs, T. A., C. M. Michel and G. Thut (2009). "A bias for posterior alpha-band power suppression versus enhancement during shifting versus maintenance of spatial attention." Neuroimage **44**(1): 190-199.

Ritter, P., R. Becker, F. Freyer and A. Villringer (2010). EEG Quality:The Image Acquisition Artefact. EEG - fMRI: Physiological Basis, Technique, and Applications. C. Mulert and L. Lemieux. Berlin, Heidelberg, Springer Berlin Heidelberg**:** 153-171.

Rogasch, N. C., C. Sullivan, R. H. Thomson, N. S. Rose, N. W. Bailey, P. B. Fitzgerald, F. Farzan and J. C. Hernandez-Pavon (2017). "Analysing concurrent transcranial magnetic stimulation and electroencephalographic data: A review and introduction to the open-source TESA software." NeuroImage **147**(Supplement C): 934-951.

Romei, V., V. Brodbeck, C. Michel, A. Amedi, A. Pascual-Leone and G. Thut (2008). "Spontaneous fluctuations in posterior alpha-band EEG activity reflect variability in excitability of human visual areas." Cereb Cortex **18**(9): 2010-2018.

Rothwell, J. C. (1997). "Techniques and mechanisms of action of transcranial stimulation of the human motor cortex." J Neurosci Methods **74**(2): 113-122.

Roy Choudhury, K., L. Boyle, M. Burke, W. Lombard, S. Ryan and B. McNamara (2011). "Intra subject variation and correlation of motor potentials evoked by transcranial magnetic stimulation." Ir J Med Sci **180**(4): 873-880.

Ruddy, K. L., D. G. Woolley, D. Mantini, J. H. Balsters, N. Enz and N. Wenderoth (2018). "Improving the quality of combined EEG-TMS neural recordings: Introducing the coil spacer." Journal of Neuroscience Methods **294**: 34-39.

Ruff, C. C., J. Driver and S. Bestmann (2009). "Combining TMS and fMRI: From 'virtual lesions' to functional-network accounts of cognition." Cortex; a journal devoted to the study of the nervous system and behavior **45**(9): 1043-1049.

Sauseng, P., W. Klimesch, C. Gerloff and F. C. Hummel (2009). "Spontaneous locally restricted EEG alpha activity determines cortical excitability in the motor cortex." Neuropsychologia **47**(1): 284-288.

Schafer, K., F. Blankenburg, R. Kupers, J. M. Gruner, I. Law, M. Lauritzen and H. B. Larsson (2012). "Negative BOLD signal changes in ipsilateral primary somatosensory cortex are associated with perfusion decreases and behavioral evidence for functional inhibition." Neuroimage **59**(4): 3119-3127.

Scheeringa, R., P. Fries, K.-M. Petersson, R. Oostenveld, I. Grothe, D. G. Norris, P. Hagoort and M. C. M. Bastiaansen (2011). "Neuronal Dynamics Underlying High- and Low-Frequency EEG Oscillations Contribute Independently to the Human BOLD Signal." Neuron **69**(3): 572-583.

Schridde, U., M. Khubchandani, J. E. Motelow, B. G. Sanganahalli, F. Hyder and H. Blumenfeld (2008). "Negative BOLD with large increases in neuronal activity." Cereb Cortex **18**(8): 1814-1827.

Schulz, H., T. Ubelacker, J. Keil, N. Muller and N. Weisz (2014). "Now I am ready-now i am not: The influence of pre-TMS oscillations and corticomuscular coherence on motor-evoked potentials." Cereb Cortex **24**(7): 1708-1719.

Scolari, M., K. N. Seidl-Rathkopf and S. Kastner (2015). "Functions of the human frontoparietal attention network: Evidence from neuroimaging." Current Opinion in Behavioral Sciences **1**: 32-39.

Sekihara, K. and B. Scholz (1996). "Generalized Wiener estimation of three-dimensional current distribution from biomagnetic measurements." IEEE Trans Biomed Eng **43**(3): 281-291.

Shen, Q., H. Ren and T. Q. Duong (2008). "CBF, BOLD, CBV, and CMRO(2) fMRI Signal Temporal Dynamics at 500-msec Resolution." Journal of magnetic resonance imaging : JMRI **27**(3): 599-606.

Shmuel, A., M. Augath, A. Oeltermann and N. K. Logothetis (2006). "Negative functional MRI response correlates with decreases in neuronal activity in monkey visual area V1." Nat Neurosci **9**(4): 569-577.

Shmuel, A., E. Yacoub, J. Pfeuffer, P. F. Van de Moortele, G. Adriany, X. Hu and K. Ugurbil (2002). "Sustained negative BOLD, blood flow and oxygen consumption response and its coupling to the positive response in the human brain." Neuron **36**(6): 1195-1210.

Sibson, N. R., A. Dhankhar, G. F. Mason, D. L. Rothman, K. L. Behar and R. G. Shulman (1998). "Stoichiometric coupling of brain glucose metabolism and glutamatergic neuronal activity." Proc Natl Acad Sci U S A **95**(1): 316-321.

Sirotin, Y. B. and A. Das (2009). "Anticipatory haemodynamic signals in sensory cortex not predicted by local neuronal activity." Nature **457**(7228): 475-479.

Smith, A. T., K. D. Singh and M. W. Greenlee (2000). "Attentional suppression of activity in the human visual cortex." Neuroreport **11**(2): 271-277.

Smith, A. T., A. L. Williams and K. D. Singh (2004). "Negative BOLD in the visual cortex: evidence against blood stealing." Hum Brain Mapp **21**(4): 213-220.

Smith, S. M. (2002). "Fast robust automated brain extraction." Hum Brain Mapp **17**(3): 143-155.

Smith, S. M., M. Jenkinson, M. W. Woolrich, C. F. Beckmann, T. E. Behrens, H. Johansen-Berg, P. R. Bannister, M. De Luca, I. Drobnjak, D. E. Flitney, R. K. Niazy, J. Saunders, J. Vickers, Y. Zhang, N. De Stefano, J. M. Brady and P. M. Matthews (2004). "Advances in functional and structural MR image analysis and implementation as FSL." Neuroimage **23 Suppl 1**: S208-219.

Somogyi, P., G. Tamas, R. Lujan and E. H. Buhl (1998). "Salient features of synaptic organisation in the cerebral cortex." Brain Res Brain Res Rev **26**(2-3): 113-135.

Speckmann, E., Elger, C., Gorji, A. (2005). Neurophysiologic Basis of EEG and DC Potentials. Electroencephalography: Basic Principles, Clinical Applications and Related Fields. E. Niedermeyer, Lopes da Silva, F., Lippincott Williams and Wilkins, Philadephia. **5**.

Sperry, R. W., E. Zaidel and D. Zaidel (1979). "Self recognition and social awareness in the deconnected minor hemisphere." Neuropsychologia **17**(2): 153-166.

Stagg, C. J., V. Bachtiar and H. Johansen-Berg (2011). "The role of GABA in human motor learning." Curr Biol **21**(6): 480-484.

Stagg, C. J., V. Bachtiar and H. Johansen-Berg (2011). "What are we measuring with GABA magnetic resonance spectroscopy?" Commun Integr Biol **4**(5): 573-575.

Stagg, C. J., J. G. Best, M. C. Stephenson, J. O'Shea, M. Wylezinska, Z. T. Kincses, P. G. Morris, P. M. Matthews and H. Johansen-Berg (2009). "Polarity-sensitive modulation of cortical neurotransmitters by transcranial stimulation." J Neurosci **29**(16): 5202-5206.

Stefanovic, B., J. M. Warnking and G. B. Pike (2004). "Hemodynamic and metabolic responses to neuronal inhibition." Neuroimage **22**(2): 771-778.

Taylor, P. C. J., V. Walsh and M. Eimer (2008). "Combining TMS and EEG to study cognitive function and cortico-cortico interactions." Behavioural brain research **191**(2): 141-147.

Tettoni, L., F. Gheorghita-Baechler, R. Bressoud, E. Welker and G. M. Innocenti (1998). "Constant and variable aspects of axonal phenotype in cerebral cortex." Cerebral Cortex **8**(6): 543-552.

Thickbroom, G. W., M. L. Byrnes and F. L. Mastaglia (1999). "A model of the effect of MEP amplitude variation on the accuracy of TMS mapping." Clin Neurophysiol **110**(5): 941-943.

Thompson, R. F. (2000). The brain: A neuroscience primer. New York, W H Freeman/Times Books/ Henry Holt & Co.

Thut, G. and C. Miniussi (2009). "New insights into rhythmic brain activity from TMS–EEG studies." Trends in Cognitive Sciences **13**(4): 182-189.

Thut, G., A. Nietzel, S. A. Brandt and A. Pascual-Leone (2006). "Alpha-band electroencephalographic activity over occipital cortex indexes visuospatial attention bias and predicts visual target detection." J Neurosci **26**(37): 9494-9502.

Tootell, R. B., N. Hadjikhani, E. K. Hall, S. Marrett, W. Vanduffel, J. T. Vaughan and A. M. Dale (1998). "The retinotopy of visual spatial attention." Neuron **21**(6): 1409-1422.

Tung, K.-C., J. Uh, D. Mao, F. Xu, G. Xiao and H. Lu (2013). "Alterations in resting functional connectivity due to recent motor task." NeuroImage **78**: 316-324.

Uji, M., R. Wilson, S. Francis, K. Mullinger and S. Mayhew (2018). "Exploring the advantages of multiband fMRI with simultaneous EEG to investigate coupling between gamma frequency neural activity and the BOLD response in humans." Human Brain Mapping **In press**: 1-15.

Uludağ, K., D. J. Dubowitz, E. J. Yoder, K. Restom, T. T. Liu and R. B. Buxton (2004). "Coupling of cerebral blood flow and oxygen consumption during physiological activation and deactivation measured with fMRI." Neuroimage **23**(1): 148-155.

van den Bos, M. A. J., N. Geevasinga, P. Menon, D. Burke, M. C. Kiernan and S. Vucic (2017). "Physiological processes influencing motor-evoked potential duration with voluntary contraction." Journal of Neurophysiology **117**(3): 1156-1162.

van der Knaap, L. J. and I. J. M. van der Ham (2011). "How does the corpus callosum mediate interhemispheric transfer? A review." Behavioural Brain Research **223**(1): 211-221.

Van Der Werf, Y. D. and T. Paus (2006). "The neural response to transcranial magnetic stimulation of the human motor cortex. I. Intracortical and cortico-cortical contributions." Experimental Brain Research **175**(2): 231-245.

van Kerkoerle, T., M. W. Self, B. Dagnino, M.-A. Gariel-Mathis, J. Poort, C. van der Togt and P. R. Roelfsema (2014). "Alpha and gamma oscillations characterize feedback and feedforward processing in monkey visual cortex." Proceedings of the National Academy of Sciences **111**(40): 14332-14341.

Van Veen, B. D., Van Drongelen, W., Yuchtman, M., Suzuki, A. (1997). "Localisation of brain electrical activity via linearly constrained minimum variance spatial filtering." IEEE Transactions on biomedical engineering **44**(9).

Vigario, R. N. (1997). "Extraction of ocular artefacts from EEG using independent component analysis." Electroencephalogr Clin Neurophysiol **103**(3): 395-404.

Violante, I. R., M. J. Ribeiro, R. A. Edden, P. Guimaraes, I. Bernardino, J. Rebola, G. Cunha, E. Silva and M. Castelo-Branco (2013). "GABA deficit in the visual cortex of patients with neurofibromatosis type 1: genotype-phenotype correlations and functional impact." Brain **136**(Pt 3): 918-925.

Viswanathan, A. and R. D. Freeman (2007). "Neurometabolic coupling in cerebral cortex reflects synaptic more than spiking activity." Nat Neurosci **10**(10): 1308-1312.

Vorwerk, J., M. Clerc, M. Burger and C. H. Wolters (2012). "Comparison of boundary element and finite element approaches to the EEG forward problem." Biomed Tech (Berl) **57 Suppl 1**.

Wahl, M., B. Lauterbach-Soon, E. Hattingen, P. Jung, O. Singer, S. Volz, J. C. Klein, H. Steinmetz and U. Ziemann (2007). "Human Motor Corpus Callosum: Topography, Somatotopy, and Link between Microstructure and Function." The Journal of Neuroscience **27**(45): 12132-12138.

Walsh, V. and A. Cowey (2000). "Transcranial magnetic stimulation and cognitive neuroscience." Nat Rev Neurosci **1**(1): 73-79.

Williams, D. S., J. A. Detre, J. S. Leigh and A. P. Koretsky (1992). "Magnetic resonance imaging of perfusion using spin inversion of arterial water." Proc Natl Acad Sci U S A **89**(1): 212-216.

Wilson, M., G. Reynolds, R. A. Kauppinen, T. N. Arvanitis and A. C. Peet (2011). "A constrained least-squares approach to the automated quantitation of in vivo (1)H magnetic resonance spectroscopy data." Magn Reson Med **65**(1): 1-12.

Woolrich, M. W., T. E. Behrens, C. F. Beckmann, M. Jenkinson and S. M. Smith (2004). "Multilevel linear modelling for FMRI group analysis using Bayesian inference." Neuroimage **21**(4): 1732-1747.

Worden, M. S., J. J. Foxe, N. Wang and G. V. Simpson (2000). "Anticipatory biasing of visuospatial attention indexed by retinotopically specific alpha-band electroencephalography increases over occipital cortex." J Neurosci **20**(6): RC63.

Wright, P. J., M. Brookes, J. Dixon, P. Gowland and S. Francis (2008). Assessment of BOLD signal adaptation using single event fMRI at 7T and its correlation with MEG. ISMRM, Toronto.

Yang, J., S. S. Li, J. Bacher and J. Shen (2007). "Quantification of cortical GABA-glutamine cycling rate using in vivo magnetic resonance signal of [2-13C]GABA derived from glia-specific substrate [2-13C]acetate." Neurochem Int **50**(2): 371-378.

Ye, F. Q., J. A. Frank, D. R. Weinberger and A. C. McLaughlin (2000). "Noise reduction in 3D perfusion imaging by attenuating the static signal in arterial spin tagging (ASSIST)." Magn Reson Med **44**(1): 92-100.

Yuan, H., C. Perdoni, L. Yang and B. He (2011). "Differential electrophysiological coupling for positive and negative BOLD responses during unilateral hand movements." J Neurosci **31**(26): 9585-9593.

Zarkowski, P., C. J. Shin, T. Dang, J. Russo and D. Avery (2006). "EEG and the variance of motor evoked potential amplitude." Clin EEG Neurosci **37**(3): 247-251.

Zhang, Y., M. Brady and S. Smith (2001). "Segmentation of brain MR images through a hidden Markov random field model and the expectation-maximization algorithm." IEEE Trans Med Imaging **20**(1): 45-57.

Ziemann, U. and J. C. Rothwell (2000). "I-waves in motor cortex." J Clin Neurophysiol **17**(4): 397-405.

Zumer, J. M., R. Scheeringa, J. M. Schoffelen, D. G. Norris and O. Jensen (2014). "Occipital alpha activity during stimulus processing gates the information flow to object-selective cortex." PLoS Biol **12**(10): e1001965.